The development of biosorbents from agricultural waste sources for the separation of fat-based particles from water

by

Marli Swart

Thesis presented in partial fulfilment
of the requirements for the Degree

of

MASTER OF ENGINEERING
(CHEMICAL ENGINEERING)

in the Faculty of Engineering
at Stellenbosch University

The financial assistance of the National Research Foundation (NRF) towards this research is hereby acknowledged. Opinions expressed and conclusions arrived at, are those of the author and are not necessarily to be attributed to the NRF.

Supervisor

Prof. A.F.A. Chimphango

December 2020

Declaration

By submitting this thesis electronically, I declare that the entirety of the work contained therein is my own, original work, that I am the sole author thereof (save to the extent explicitly otherwise stated), that reproduction and publication thereof by Stellenbosch University will not infringe any third party rights and that I have not previously in its entirety or in part submitted it for obtaining any qualification.

Date: *December 2020*

Plagiarism Declaration

1. Plagiarism is the use of ideas, material and other intellectual property of another's work and to present it as my own.

2. I agree that plagiarism is a punishable offence because it constitutes theft.

3. I also understand that direct translations are plagiarism.

4. Accordingly, all quotations and contributions from any source whatsoever (including the internet) have been cited fully. I understand that the reproduction of text without quotation marks (even when the source is cited) is plagiarism.

5. I declare that the work contained in this assignment, except where otherwise stated, is my original work and that I have not previously (in its entirety or in part) submitted it for grading in this module/assignment or another module/assignment.

Initials and surname: M. Swart

Date: December 2020

Abstract

The presence of hydrocarbons and triglycerides in water pose a technical challenge for wastewater processing or re-use. Hydrocarbon contamination reduces the water quality for available for human consumption and marine life. The available petrochemical-based oil-removing technologies either have negative environmental impacts or are non-selective and ineffective for oil removal. However, plant-based biosorbents, tailored for selective oil removal by surface acetylation reactions can overcome some of the challenges posed by traditional petrochemical-based sorbents. Therefore, the aim of this study entailed the production of bio-based sorbents from corncob (CC) and wheat straw (WS) and their respective cellulose and nanofibrillated cellulose (NFC) constituents, which were functionalised via acetylation methods that follow the *green* chemistry principles, in order to increase selective oil sorption (OS, g/g). The functionalities of these feedstocks were critically dependant on the replacement of hydrophilic hydroxyl groups on the molecular surface with hydrophobic acetyl groups to attain oleophilicity.

The CC and WS were tuned to become oleophilic via *green* and *non-green* acetylations. The *green* modification implemented acetic anhydride and iodine, and was optimised via central composite design (CCD), by varying temperature (50 – 150 °C), time (0.6 – 7.4 h) and iodine concentration (0.7 – 7.4 % (w/w)). The optimal performances were compared to acetylations achieved by the *non-green* methodology, which replaced the *green* iodine catalyst with *non-green* N-bromosuccinimide. The *green* acetylation yielded CC and WS with a selective OS of approximately 17 – 18 g/g, while the *non-green* modified CC and WS exhibited OS of 17 – 20 g/g. These OS performances were statistically similar ($p < 0.05$).

Cellulose was extracted from unmodified biomass to improve the surface area for sorption. Oleophilic films were developed from CC and WS cellulose retrospective to surface acetylation. The *green* acetylation was catalysed by a 50 % (w/w) NaOH-solution and was optimised via CCD by varying temperature (40 – 140 °C), time (3.8 – 44.2 h) and catalyst volume (1.2 – 13.8 % (v/v) NaOH-solution). Concurrently, the *non-green* acetylation implemented H_2SO_4 as catalyst. The *green* modification yielded hydrophobic CC and WS films with OS of 12 – 13 g/g, while the *non-green* CC and WS films had OS of 20 – 21 g/g. These results revealed that CC and WS had an analogous reaction when subjected to the same type of modification (i.e. *green* or *non-green*). However, the *non-green* modifications outperformed the *green* modifications by 65 – 69 % based on selective OS.

NFC isolated from unmodified cellulose were utilised to develop oleophilic aerogels. The optimisation of the *green* NFC modification involved a combination of acetic anhydride and lipase from *Aspergillus niger* (EC 232-619-9). The CCD varied temperature (28 – 62 °C), time (28 – 68 h) and lipase (199 – 2 301 U). Moreover, the *non-green* acetylation combined acetic anhydride and pyridine. The *green* acetylation yielded NFC aerogels with OS of roughly 41 – 44 g/g, while the *non-green* NFC aerogels exhibited OS of 45 – 46 g/g. The performance accomplished by the *green* CC and WS NFC aerogels compared favourably to the performances of the *non-green* aerogels based on selective OS ($p < 0.05$). It was concluded that *green* NFC aerogels were identified as the most efficient and environmentally benign biosorbents since these materials were modified via *green* acetylations and achieved the most favourable OS.

Opsomming

Olie kontaminasie in water verminder die kwaliteit en kwantiteit beskikbaar vir menslike inname en seelewe. Ondanks huidige tegnologieë wat olie suksesvol verwyder, het sulke metodes gereeld nadelige omgewingseffekte. Sintetiese fisiese sorbense bestaan uit nie-bioafbreekbare materiale, en verwyder gereeld nie selektief olie uit water nie. Die tekortkominge van huidige tegnologieë kan oorkom word deur die toepassing van plant-gebaseerde biosorbense, aangemeet vir selektiewe verwydering van olie in 'n volhoubare manier. Die doel van hierdie studie hou in die produksie van bio-gebaseerde sorbense uit mieliestronke (CC) en koringstrooi (WS) en hul onderskeidelike sellulose en nanogefibrilleerde sellulose (NFC) bestanddele, wat funksioneel gemaak is via *groen* metodes om selektiewe oliesorbsie (OS) te verhoog. Die funksionaliteite van hierdie voermateriaal was krities afhanklik van die plaasvervanging van hidrofiliese hidroksielgroepe op die molekulêre oppervlak met hidrofobiese asetielgroepe om oleofilisiteit te bereik.

Die CC en WS is ingestel om oleofilies te word via *groen* en *nie-groen* asetilasies. Die *groen* modifikasie het asynsuuranhidried en jodium geïmplementeer, en is geoptimeer via sentrale samestelling ontwerp (CCD), deur temperature (50 – 150 °C), tyd (0.6 –7.4 h) en jodiumkonsentrasie (0.7 – 7.4%(w/w)) te varieer. Die optimale doeltreffendheid is vergelyk met asetilasies bereik deur die *nie-groen* metodologie, wat die *groen* jodiumkatalis met *nie-groen* N-broombarnsteensuurimied vervang het. Die *groen* asetilasie het CC en WS met 'n selektiewe OS van ongeveer 17 – 18 g/g gelewer, terwyl die *nie-groen* gemodifiseerde CC en WS OS van 17 –20 g/g getoon het. Hierdie OS-doeltreffendheid was statisties eenders ($p < 0.05$).

Sellulose is geëkstraheer uit ongemodifiseerde biomassa om die oppervlakarea vir sorbsie te verbeter. Oleofiliese films is ontwikkel uit CC- en WS-sellulose terugwerkend aan oppervlakasetilasie. Die *groen* asetilasie is gekataliseer deur 'n 50% (w/w) NaOH-oplossing en is geoptimeer via CCD deur temperatuur (40 – 140 °C), tyd (3.8 – 44.2 h) en katalisvolume (1.2 – 13.8% (v/v) NaOH-oplossing) te varieer. Gelyktydig het die *nie-groen* asetilasie H_2SO_4 as katalis geïmplementeer. Die *groen* modifikasie het hidrofobiese CC- en WS-films met OS van 12 – 13 g/g opgebring, terwyl die *nie-groen* CC- en WS-films OS van 20 – 21 g/g opgebring het. Die resultate het getoon dat CC en WS 'n analoë reaksie het wanneer dit onder dieselfde tipe modifikasie onderwerp word (i.e. *groen* of *nie-groen*). Die *nie-groen* modifikasies het egter die *groen* modifikasies oortref met 65 – 69% gebaseer op selektiewe OS.

NFC wat geïsoleer is van ongemodifiseerde sellulose is gebruik om oleofiliese aërojels te ontwikkel. Die optimering van die *groen* NFC modifikasie het 'n kombinasie van asynsuuranhidried en lipase van *Aspergillus niger* (EC 232-619-9) ingesluit. Die CCD het temperatuur (28 – 62 °C), tyd (28 – 68 h) en lipase (199 – 2301 U) gevarieer. Verder is die *nie-groen* asetilasie gekombineer met asynsuuranhidried en piridien. Die *groen* asetilasie het NFC-aërojels met OS van rofweg 41 – 44 g/g opgebring, terwyl die *nie-groen* NFC-aërojels OS van 45 – 46 g/g getoon het. Die doeltreffendheid bereik deur die *groen* CC- en WS-NFC-aërojels het gunstig vergelyk met die doeltreffendheid van die *nie-groen* aërojels gebaseer op selektiewe OS ($p < 0.05$). Dit is vasgestel dat *groen* NFC-aërojels geïdentifiseer is as die mees effektiewe en omgewingsvriendelike biosorbens aangesien hierdie sorbense gemodifiseer is via *groen* asetilasies en die mees gunstige OS bereik het.

Acknowledgements

I am specifically thankful to the following people for their contributions toward my research:

- Prof. Annie Chimphango for supervision and guidance throughout this study
- The National Research Foundation and the Process Engineering Department for the financial support to conduct this research
- Henry Solomon from the Department of Forestry and Wood Science for endless guidance and training, as well as the very valuable permission to use their facilities after hours
- Dr. Helen Pfukwa from the Department of Polymer Science for allowing me to use the Thermo Nicolet Fourier Transform Infrared Spectroscopy system for a vast amount of measurements
- Dr. Leigh Loots from the Department of Chemistry for training and guidance on the Bruker D2 Phaser X-ray Diffractometer
- Illana Bergh at Roediger Agencies for the training and permission to measure the water contact angles of all the developed aerogels and films
- Dr. Elrika Harmzen-Pretorius at the Central Analytical Facility for assistance with Scanning Electron Microscopy
- Jaco van Rooyen from the Analytical Facility for assistance with analyses, for always being eager to help with troubleshooting, and for fixing the freeze-drier in a very crucial time of my project
- Levine Simmers from the Analytical Facility for assistance with High Performance Liquid Chromatography
- Alvin Peterson and Oliver Jooste for invaluable technical guidance, as well as the provision of instruments and equipment for my experimental setup
- Novozymes for supplying FiberCare® for the production of nanofibrillated cellulose
- My fellow researchers Reagan Ceaser, Fatimatu Belo and Lia Bester for their academic patronage and motivation
- Mieke de Jager for all the irreplaceable emotional support and encouragement when I had to unexpectedly start working fulltime in 2018; and for the general assistance throughout my project
- My husband, Marinus, for endless sustenance and emotional support; and my friends and family for all the prayers, understanding and motivation
- Most of all, thank you God for carrying me through this journey

"Some beautiful paths cannot be discovered without getting lost" – Erol Ozan

"Never let a stumble in the road be the end of your journey" – Unknown

Table of Contents

List of Figures

List of Tables

Nomenclature

Acronym	Definition
AGU	Anhydroglucose Unit
ANOVA	Analyses of Variance
AR	Analytical Reactant Grade
CC	Corncob
CCD	Central Composite Design
CN	Commercial Nanofibrillated Cellulose
CO	Cotton
DF	Degrees of Freedom
DMF	Dimethylformamide
DMSO	Dimethyl Sulfoxide
DS	Degree of Substitution
FP	Filter Paper
FT-IR	Fourier Transform Infrared Spectroscopy
HCL	Hydrochloric Acid
HPLC	High Performance Liquid Chromatography
ICP-MS	Inductively coupled Plasma Mass Spectrometry
KOH	Potassium Hydroxide
KRQ	Key Research Questions
NaOH	Sodium Hydroxide
NBS	N-bromosuccinimide
NCC	Nanocrystalline Cellulose
NFC	Nanofibrillated Cellulose
NRF	National Research Foundation of South Africa
OS	Oil Sorption
RSM	Response Surface Methodology
SDS	Sodium Dodecyl Sulphate
SEM	Scanning Electron Microscope
WA	Water Sorption
WCA	Water Contact Angle
WPG	Weight Percent Gain
WS	Wheat Straw
XRD	X-ray Diffraction
XRF	X-ray Fluorescence

Chapter 1 – Introduction and Project Motivation

1.1 Background and Problem Statement

Due to anthropogenic activity, unplanned population growth and urbanisation, as well as a considerable increase in industrialisation and misuse of natural water resources, the water quality and quantity available for human consumption is deteriorating (De Gisi, Lofrano, Grassi, & Notarnicola, 2016). Typical domestic wastewater in South Africa contains approximately 30 - 300 mg/L oil-based constituents, such as hydrocarbons and triglycerides (Mahlobo, 2008). In order to directly utilise domestic greywater for the watering of plants, these oil-based constituents need to be removed prior to application in order to avoid blocking the pores of the plant roots meant for nutrient- and water reception (Oniosun, Harbottle, Tripathy, & Cleall, 2019). Moreover, when entering the sewage system, the presence of fats, oil and grease (FOG) are infamous for causing rigorous damage in pipes and pumping stations of wastewater treatment plants, which in turn has an adverse impact on further wastewater processing (El-gawad, 2014). An essential aspect of wastewater management, therefore, constitutes removing the oil-based molecules from the water, prior to further treatment (Mahlobo, 2008). Additionally, hydrocarbon spills in the ocean drastically impact marine life. It influences the insulating ability of marine mammals, the water repellence of feathers, it can be harmful when ingested and affects the growth and physical attributes of exposed fish and plants (National Oceanic Atmospheric Administration, 2017).

Removing oil from water presents a technical challenge. Since these molecules both occur in liquid form, simple full physical separation is difficult. The specific gravity of oil is less than that of water (J. Wang, Zheng, & Wang, 2013). Subsequently, the bulk of the oil should float on the water surface (S. Wang, Qin, & Dai, 2012). However, since these spills occur in non-static environments, many of the oil particles become emulsified in the water (Hubbe, Rojas, Fingas, & Gupta, 2013; Renuka, Rengasamy, & Das, 2016). Isolating emulsified oil spills often result in additionally removing some of the scarce water resources that humans have to their disposal.

An assortment of traditional technologies is available for the separation of oil from water. These include chemical emulsifiers, skimming and synthetic sorbents (Asadpour, Sapari, Isa, & Orji, 2014; Hubbe, Rojas, et al., 2013). Moreover, bioremediation and in-situ burning are frequently implemented (Asadpour et al., 2014). Even though some of these methods are successful at removing pollutants, these procedures frequently incur high installation, operational and maintenance costs. The methodologies are often not environmentally friendly and encompass complicated applications and procedures (De Gisi et al., 2016). The addition of chemical emulsifiers to marine life-containing water can be harmful to the living organisms and can destroy the eco-systems that it comes into contact with (Minnesota Pollution Control Agency, 2017). Bioremediation causes accelerated biodegradation of the oil, but forms carbon dioxide and fatty acids as a by-product. Lastly, synthetic sorbents and equipment utilised for skimming pose a potential for pollution if the materials are not retrieved after sorption.

In a world where petroleum-based products dominate, with many disadvantages regarding adverse environmental effects, limited fossil resources, non-biodegradable products and a consequent ever-growing increase in unmanageable waste – the demand for more environmentally friendly (*green*) systems are rapidly developing (De Gisi et al., 2016). Manufacturers in many fields are obligated to consider the environmental impact over the entire

life cycle of each product – from initiation and selection of starting materials to recycling, and eventually the end-of-life disposal (Kalia, Kaith, & Kaur, 2011). Therefore, the need arises for the development of *green* biosorbents, which can remove oil from water in a sustainable way.

The implementation of organic plant-based oil-sorbents can overcome some of the shortfalls presented by the current technologies. Biosorbents have recently become more popular due to the sustainability, biodegradability, recyclability and environmentally benign properties (She, Sun, & Jones, 2010). The use of banana fibre (Alaa El-Din, Amer, Malsh, & Hussein, 2018; Teli & Valia, 2013a), barley straw (Tijani, Aqsha, & Mahinpey, 2016), sugarcane bagasse (X. F. Sun, Sun, & Sun, 2004), corncob (Nwadiogbu, Ajiwe, & Okoye, 2016), jute fibre (Teli & Valia, 2013b) and wheat straw (Pirbazari, 2015) were recently applied as biosorbents for the removal of oil from water.

The characteristics of the agricultural waste crops, corncob (CC) and wheat straw (WS), led to a specific interest in utilising these biomass sources as plant-based biosorbents. In South Africa, these agricultural residues are burned on farms prior to ploughing in order to create space for new crops (Potgieter, 2011).

Lignocellulosic materials, such as CC and WS, can be utilised in their unmodified biomass form (She et al., 2010), or by implementing their smaller constituents – specifically, cellulose and nanofibrillated cellulose (NFC). Cellulose is a natural linear polysaccharide (C. Yin et al., 2007). It is considered as one of the most essential natural fibres on earth (Cherian et al., 2012) since it is an abundantly available, naturally occurring, biodegradable structural polymer (Salajkova, 2013). Additionally, these fibres exhibit low densities, high toughness and relatively low processing costs (Kalia et al., 2011). The structures are non-abrasive, combustible and non-toxic, and can thus be considered as a *green* alternative in many fields (Kalia, Thakur, Celli, Kiechel, & Schauer, 2013).

The NFC can be isolated from cellulose. These fibres have diameters between 1 and 100 nm (Liu, Geng, Chen, & Wang, 2017) and constitute entangled, flexible fibril bundles which form the structural units of cellulose (Chimphango, Mugwagwa, & Swart, 2020; Khalil, Bhat, & Yusra, 2012). Moreover, these molecules retain substantial amounts of hydrophilic surface hydroxyl groups (Arola, 2015; Chimphango et al., 2020).

In this way, three levels of lignocellulosic biomass can be defined for CC and WS, respectively. The fibres on each of these levels can be implemented for biosorbent development: (1) the *biomass level*, where the biomass is milled to a selected particle size and utilised while containing cellulose bound by hemicellulose, lignin and other extractives; (2) the *cellulose level*, where the cellulose particles are isolated from the biomass and hemicellulose, lignin and extractives are removed; and (3) the *NFC level*, where cellulose is subjected to further fractionation to increase the surface area of the fibres.

Biomass particles have exhibited specific surface areas of 0.03 – 0.28 m^2/g, depending on how fine these particles are milled, while cellulose has been known to have approximate specific surface areas of 0.6 – 1 m^2/g (Bismarck et al., 2004). Moreover, NFC exhibits amplified specific surface areas of roughly 70 – 280 m^2/g (Qian, Wang, Zhao, & Xu, 2018). The implementation of cellulose and NFC as biosorbents, therefore, have a greater potential for sorption due to the increased surface area of the particles. However, the prospective use of biomass, cellulose and NFC as biosorbents are critically dependent on the surface characteristics of the fibres (Marin & Perry, 2015). The partially crystalline structure of the lignocellulosic material and the presence of extensive amounts of accessible hydroxyl

groups at the external and internal fibre surfaces cause the exhibition of polar, hydrophilic behaviour (Salajkova, 2013). This property results in inadequate removal of oil from water since the particles demonstrate a higher affinity to the polar water particles than to the non-polar oil particles. In order to successfully apply these fibres, the polar surface hydroxyl molecules on the fibre surface need to be replaced by non-polar surface acetyl groups through acetylation reactions (Hatton, Malmstrom, & Carlmark, 2015). These reactions alter the chemical composition of the particles, which ensures a higher affinity towards oil and a lowered affinity towards water (Hubbe, Rojas, & Lucia, 2015). Consequently, the fibres become hydrophobic and oleophilic (She et al., 2010).

Numerous traditional surface modification methods have been developed and implemented in order to alter the surface characteristics of fibres and to subsequently extend the application possibilities. Some of these methods include acetylation of sugarcane bagasse with N-bromosuccinimide as catalyst (X. F. Sun et al., 2004), acetylation of cellulose with sulfuric acid as catalyst (Huang, Zhang, Zhang, Jiang, & Huang, 2014) and the acetylation of NFC with dimethylformamide, pyridine and toluene (Tingaut, Zimmermann, & Lopez-Suevos, 2009; Zepic, Poljansek, Oven, Skapin, & Hancic, 2015). Nevertheless, these treatments frequently involve the usage of large amounts of toxic chemicals (Kalia et al., 2011). Moreover, the treatments can, in some cases, cause the fibres to become non-biodegradable (Cherian et al., 2012).

Plant-based biosorbents are often regarded as *green* merely based on the fact that plants are implemented instead of synthetic sorbents. However, for the developed biosorbents to be truly environmentally friendly, it is also necessary to develop *green* surface modification methods that successfully alter the wettability and oleophilicity of lignocellulosic materials (Hubbe et al., 2015). This can be accomplished by following the *green* chemistry principles (American Chemistry Society, 2020).

1.2 Research Gaps in Literature

Green surface modifications utilising chemicals that are less harsh to the environment have been studied on biomass, cellulose and NFC. Some of these methods include the acetylation of cellulose in an organic solvent-free system with acetic anhydride and iodine (Li et al., 2009), the acetylation on konjac glucomannan with acetic anhydride and low concentrations of sodium hydroxide (Koroskenyi & McCarthy, 2001), and the enzymatic acetylation of NFC implementing Lipase from *Aspergillus niger* (EC Number 232-619-9) (Bozic, Vivod, Kavcic, Leitgeb, & Kokol, 2015). Nevertheless, the implementation of these methods on CC and WS, as well as CC cellulose, WS cellulose, CC NFC and WS NFC have not been studied. Furthermore, OS capacities of biosorbents developed by *green* surface modifications have not been directly compared to OS capacities attained by *non-green* methodologies on the three respective levels of biomass, cellulose and NFC.

1.3 Project Aims and Objectives

The primary aim of this study entails developing a process for the production of bio-based sorbents from CC and WS, and their respective cellulose and NFC constituents which are functionalised via different *green* methods to increase the selective sorption of oil in contaminated water.

In order for these biosorbents to qualify as materials that successfully remove oil from water in an environmentally friendly way, a list of key performance indicators needs to be met. The use of sustainable, abundantly available,

biodegradable sources (Deschamps, Caruel, Borredon, Bonnin, & Vignoles, 2003; Liu et al., 2017), such as CC and WS, need to be implemented. The fibres should be modified to obtain a selective affinity towards oil particles instead of water particles (Deschamps et al., 2003; Liu et al., 2017) and this modification should be conducted in a way that does not make use of toxic chemicals, and does not contribute to environmental pollution or increased carbon dioxide emissions. The product should remain biodegradable (Deschamps et al., 2003) and the implementation of the biosorbent should not adversely affect the living organisms that it comes into contact with. The modifications need to be conducted by following the *green* chemistry principles (see Section 2.7). Furthermore, a low density is favoured, since a buoyant sorbent allows simpler application in water treatment systems (Deschamps et al., 2003; Liu et al., 2017). Lastly, a higher porosity leads to a higher possible sorption capacity (Liu et al., 2017) since the oil particles can then be retained in the material matrix structure (Deschamps et al., 2003).

In order to compare the OS capacities of *green* plant-based biosorbents to traditional *non-green* plant-based biosorbents, a *non-green* surface modification is also applied to each source. The OS of the *green* biosorbents will thus be measured against the capacities that can be achieved by similar *non-green* alternatives.

1.4 Key Research Questions

Listed here are a selection of questions that will guide the investigation:

1. Can a *green* surface acetylation method be applied to the native biomass waste sources, CC and WS, in order to create a selective oleophilicity and hydrophobicity?
2. Does an increased surface area lead to an increased capacity for OS when isolating cellulose from the native biomass, and can a selective affinity to OS be accomplished by implementing *green* surface acetylation methodologies?
3. When additionally increasing the surface area by isolating NFC, is the capacity for OS increased and can *green* surface acetylations establish oleophilicity and hydrophobicity?
4. Can the *green* surface acetylation methods optimised in this study perform equally to traditional *non-green* surface acetylation reactions?

1.5 Expected Research Outcomes

Physical Biosorbents

For ease of application in water treatment systems, these biomass, cellulose and NFC particles need to be processed to form products that can easily be dispersed and retrieved. The biomass biosorbents are utilised as 425 – 600 µm particles, while the cellulose biosorbents are developed into films bound by konjac glucomannan. Aerogels are developed from the NFC samples.

Research Publications

A contribution was made towards a book chapter, titled “Extraction of Multiple Value-Added Compounds from Agricultural Biomass Waste: A Review“, in collaboration with Prof. A. F. A. Chimphango and L. R. Mugwagwa. The book editted by M. Daramola and A. Ayeni is titled “Valorization of Biomass to Value-Added Commodities”, and was published by Springer in 2020.

Chapter 2 – Literature Review

2.1 Plant-based Natural Fibres

Natural fibres can be derived from plant-based materials, and are often referred to as lignocellulosic biomass (Kalia et al., 2011). These rigid plant-based fibres constitute predominantly of cellulose, hemicellulose and lignin and contain other minor organic compounds consisting of phenols, terpenes, fats, proteins, resins, waxes and alcohols, which are soluble in either water or ethanol (Ceaser, 2019; Chimphango et al., 2020; Dufresne, 2012; Kalia et al., 2011; Rowell, Pettersen, & Tshabalala, 2012). The cell wall of each different lignocellulosic biomass source consists of different ratios of these constituents. The density of each component and the shape of the fibres relate to the mechanical properties of the material (Tywabi, 2015). The typical three-dimensional spatial arrangement of the cell wall is illustrated in Figure 2.1, while the molecular structures of cellulose, hemicellulose and lignin are demonstrated in Appendix D.3 (p. 155).

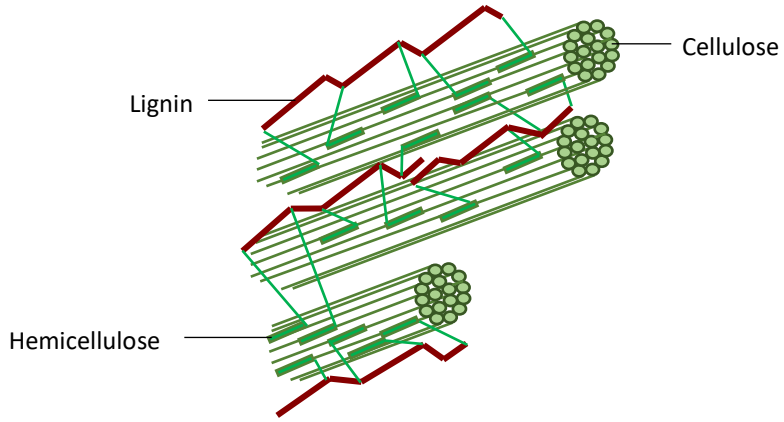

Figure 2.1 The Typical Lignocellulosic Cell Wall Spatial Arrangement, redrawn from Salimi, Nejati, Karimi, & Tavasoli (2016)

Plant-based natural fibres are categorised according to their source, and can primarily be classified as wood or non-wood fibres (Khalil et al., 2012). The general classification is presented in Figure 2.2. Furthermore, wood-based natural fibres can be classified as softwood, hardwood or recycled fibres (Khalil et al., 2012), while non-wood fibres have five classifications: (1) stem fibres, (2) straw fibres, (3) bast fibres, (4) leaf fibres, and (5) seed fibres (Hokkanen, Bhatnagar, & Sillanpää, 2016; Khalil et al., 2012). Table 2.1 summarises common examples of each non-wood biofibre category. The corncob (CC) utilised in this study is classified as a non-wood stem fibre, while the wheat straw (WS) constitutes a non-wood straw fibre.

Table 2.1 Examples of Each Non-Wood Plant-based Natural Fibre Category (Hokkanen et al., 2016; Khalil et al., 2012; Smole, Hribernik, Kleinschek, & Kreze, 2012)

Non-Wood Plant Biofibres	Examples
Stem	Bamboo, Bagasse, Corncob
Straw	Barley, Oat, Rice, Rye, Wheat, Corn Straw
Bast	Flax, Nettle, Hemp, Ramie, Kenaf, Jute
Leaf	Sisal, Manilla, Banana, Abaca
Seed	Cotton, Milkweed, Coir, Kapok

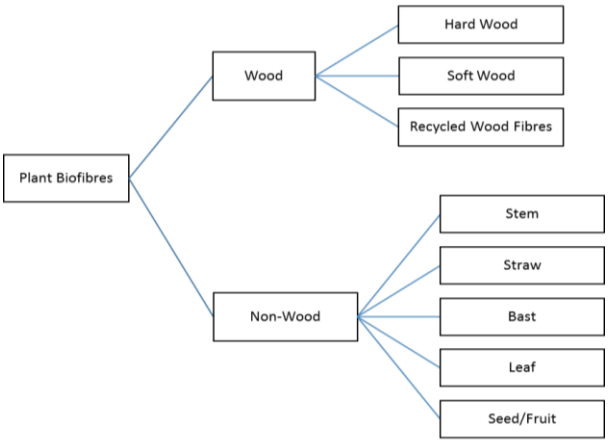

Figure 2.2 Classification of Plant-based Natural Fibres, adapted from Khalil et al. (2012)

2.2 Lignocellulosic Components of Corncob and Wheat Straw

The CC and WS consist of different molecular compositions (Table 2.2), which provide the biofibres with their distinct physical- and chemical attributes.

Table 2.2 The Biochemical Composition of Corncob and Wheat Straw

Composition	CC [a]	WS [b]	Reference
Cellulose (%)	33 – 42	35 – 40	(Ali & Arshad, 2014; Fan, Li, Zhang, Tang, & Yuan, 2014; Pasha, Saeed, Waqas, Anjum, & Arshad, 2013)
Hemicellulose (%)	15 – 36	20 – 35	(Arumugam & Anandakumar, 2016; Fan et al., 2014; Kapoor, Panwar, & Kaira, 2016; Pasha et al., 2013; Schwietzke, Kim, Ximenes, Mosier, & Ladisch, 2009)
Lignin (%)	16 – 18	10 – 19	(Fan et al., 2014; Pasha et al., 2013; Schwietzke et al., 2009; Tozluoğlu, Özyurek, Çöpür, & Özdemir, 2015)
Extractives (%)	5 – 9	8 – 9	(Ceaser, 2019; Scatolino, Silva, Mendes, & Mendes, 2013; Tozluoğlu et al., 2015)
Ash (%)	2 – 3	4 – 10	(Ceaser, 2019; Fan et al., 2014; Pasha et al., 2013; Schwietzke et al., 2009; Tozluoğlu et al., 2015)

a – Corncob abbreviated as CC; **b** – Wheat Straw abbreviated as WS

As mentioned in Section 2.1, lignocellulosic fibres also contain traces of other minor components such as starch, proteins and the phenolic compounds – ferulic acid and *p*-coumaric acid (Ceaser, 2019). These minor constituents are not considered in the current study.

2.2.1 Cellulose

Cellulose is an abundantly available, naturally occurring, biodegradable structural polymer (Salajkova, 2013; Tywabi, 2015). It mainly presents itself in the cell walls of plants as an element that provides structural support (Dufresne, 2012). Apart from plants, it can also be found in tunicates (sea animals), and in particular fungi, bacteria, algae and amoebas such as *Dictyostelium Discoideum* (Cherian et al., 2012; Riva et al., 2015). Each of these sources produces cellulose daily, and the annual production is approximated between 1×10^{10} and 1×10^{11} tonnes per year (Dufresne,

2012; Lavoine, Desloges, Dufresne, & Bras, 2012). Furthermore, it is calculated that 6 x 10^9 tonnes per year are utilised by various industries (Jawaid, Salit, & Alothman, 2017; Lavoine et al., 2012).

Cellulose is a linear polysaccharide, formed by monomers of β-D-glucopyranose units linked by β-1,4-glycosidic bonds (Arola, 2015; Ibrahim & Mondal, 2019). These β-D-glucopyranose units linked at the C-1 and C-4 atoms form a repeating dimer of glucose, known as cellobiose (Hokkanen et al., 2016; Khalil et al., 2014; Rowell et al., 2012). The number of glucose units in a single polymer molecule forms the intrinsic length of a cellulose chain (Rowell et al., 2012). This characteristic is referred to as the degree of polymerisation and differs with source and isolation methodology (Arola, 2015). R. Rowell et al. (2012) stated that cellulose is known to have typical degrees of polymerisation of 10 000 to 15 000.

The monomer β-D-glucopyranose unit is also referred to as an anhydroglucose unit (AGU), as represented in Figure 2.3. The linked AGUs are rotated at a 180° angle with respect to one another (Arola, 2015). The end-groups of a cellulose chain differ chemically since one end contains a non-reducing alcohol on C-4, and the other retains a reducing aldehyde on C-1 (Arola, 2015). Each AGU encompasses three reactive, hydrophilic hydroxyl groups (Arola, 2015; Rowell et al., 2012). These hydroxyl groups have the ability to form strong intramolecular Van der Waal's forces between glucose units, and strong intermolecular hydrogen bonds between cellulose chains (Ibrahim & Mondal, 2019; Lavoine et al., 2012). The intra- and intermolecular bonds contribute to the development of the crystalline constituencies in cellulose (Hokkanen et al., 2016; Rowell et al., 2012), and gives cellulose a highly cohesive quality (Faik, 2013; Lavoine et al., 2012).

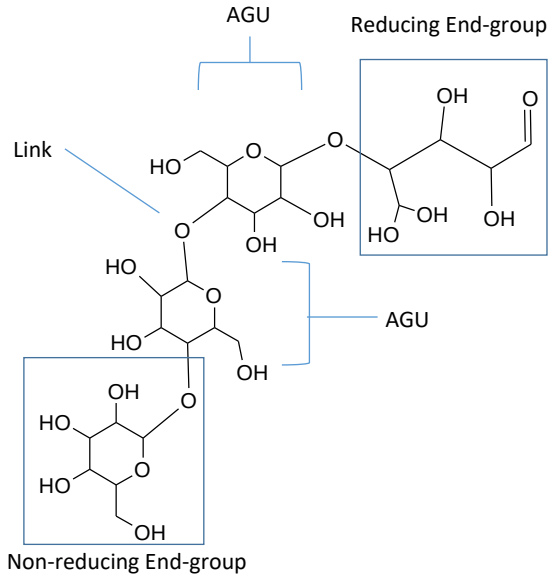

Figure 2.3 The Basic Chemical Structure of Cellulose, redrawn from Arola (2015)

The inter- and intramolecular hydrogen bonds can break at elevated temperatures, causing degradation of the cellulose chains and decomposition at temperatures exceeding 180 °C (Ceaser, 2019). Furthermore, cellulose is soluble in acid, but highly concentrated acidic environments may lead to the hydrolyses and subsequent degradation of the fibres (X. F. Sun, Sun, & Sun, 2002).

Cellulose can occur in six different polymorphs, represented in Figure 2.4: I, II, III_1, III_2, IV_1, and IV_2 (Arola, 2015; Khalil et al., 2012). Cellulose I occurs naturally as parallel-packed chains, and exists as two crystalline allomorphs,

cellulose Iα and cellulose Iβ, with different hydrogen-bonding networks (Matthews, Himmel, & Crowley, 2012). These allomorphs are present in all naturally occurring lignocellulosic materials, with the ratio differing between sources (Arola, 2015).

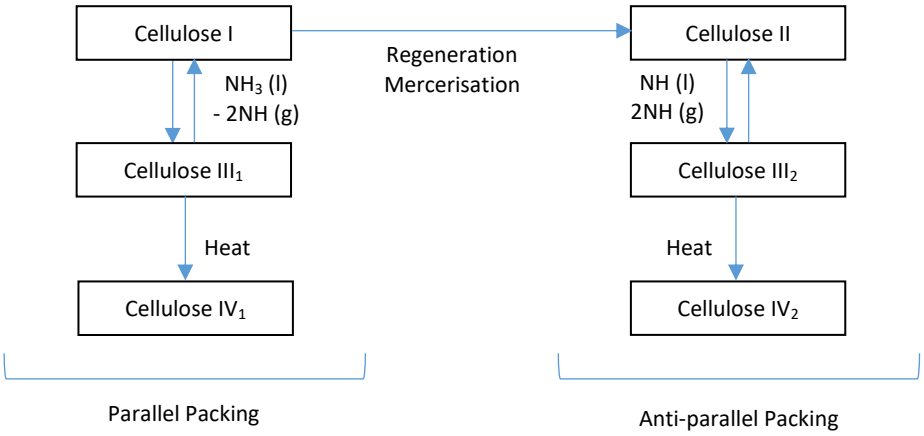

Figure 2.4 The Polymorphism of Cellulose, redrawn from Khalil et al. (2012)

Cellulose II is also referred to as regenerated cellulose. It exhibits the most stable crystalline form and has anti-parallel packing (Khalil et al., 2012; Lavoine et al., 2012). This cellulose polymorph forms if cellulose I is re-crystallised with aqueous sodium hydroxide (Lavoine et al., 2012). Ammonia treatment of cellulose I leads to cellulose III_1, while ammonia treatment of cellulose II forms cellulose III_2. The modification of cellulose III_1 and III_2 leads to cellulose IV_1 and IV_2, respectively (Lavoine et al., 2012).

Cellulose can be isolated from lignocellulosic biomass by different methods (Figure 2.5), which can be grouped into four categories: (1) physical pre-treatments, (2) physiochemical treatments, (3) chemical treatments, and (4) biological treatments (Chimphango et al., 2020). Combinations of these methods can be implemented in order to successfully isolate cellulose, and the other constituents such as hemicellulose, lignin and pectin can regularly be recovered.

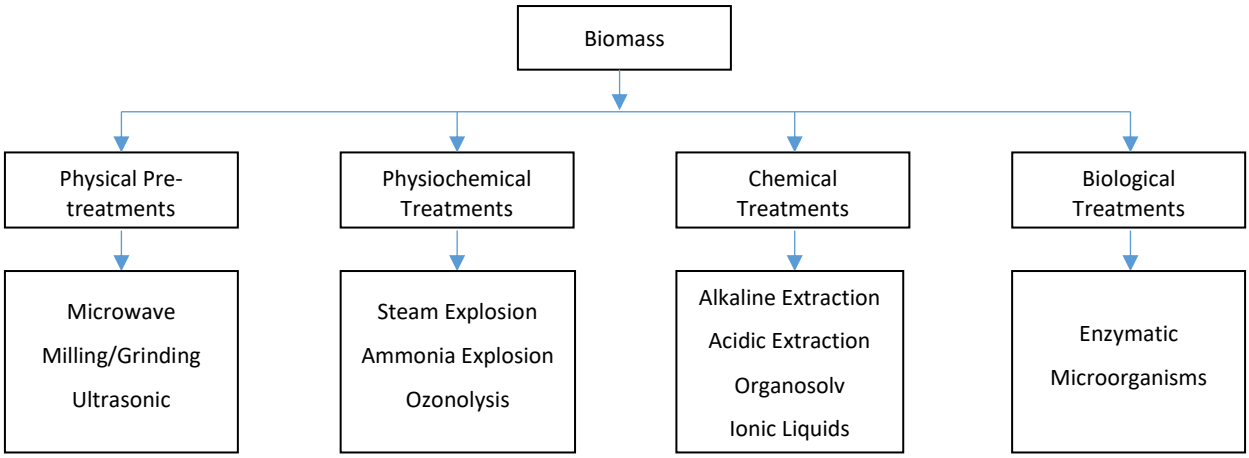

Figure 2.5 The Categorisation of Typical Treatments for Cellulose Isolation, redrawn from Chimphango et al. (2020)

The physical and physiochemical treatments often need to be implemented as a pre-treatment to the subsequent methodologies, thereby enhancing the isolation of cellulose from biomass. These physical methods frequently

involve milling, grinding, high-pressure homogenisation, microwave treatment, ozonolysis or direct or indirect ultra-sonication (16 – 100 kHz) in order to deconstruct the biomass (Chimphango et al., 2020; Khalil et al., 2012; Rehman, Kim, Chisti, & Han, 2013) prior to further treatment.

Steam explosion is a physiochemical method utilised, where saturated steam (160 – 260 °C) is pressurised to 0.69 – 4.83 MPa to deconstruct the biomass (Chimphango et al., 2020; Hoşgün & Bozan, 2019; P. Kumar, Barrett, Delwiche, & Stroeve, 2009). Upon the sudden release of pressure, the hemicellulose and lignin dissolve and the cellulose is recovered in the solid residue (Cherian et al., 2010; Hoşgün & Bozan, 2019). Alternatively, this methodology can be implemented with ammonia (70 – 200 °C) instead of steam, or acidic or alkaline chemical agents can catalyse the reaction (Carrascoa et al., 2010; Chimphango et al., 2020; J. S. Kim, Lee, & Kim, 2016).

Dilute- or concentrated acids can be implemented in an acid hydrolysis bio-fractionation method (Huntley, Crews, & Curry, 2015). Sulphuric acid, nitric acid and hydrochloric acid are commonly employed for this purpose (Ceaser, 2019). Moreover, organic acids, such as acetic acid and formic acid, are occasionally utilised (Chimphango et al., 2020). The bonds between lignin and hemicellulose are broken (Chimphango et al., 2020), and the saccharide side-branches of the hemicelluloses are hydrolysed (Kalia et al., 2013; R. C. Sun, 2010). Moreover, the non-crystalline regions in the cellulose structure can be hydrolysed in exceedingly strong acidic environments (X. F. Sun et al., 2002).

Analogous to acid hydrolyses, alkaline delignification and alkaline hydrolyses can be established by applying sodium hydroxide, ammonium salts or other base chemicals (Chimphango et al., 2020; Rosa, Rehman, De Miranda, Nachtigall, & Bica, 2012). These methods selectively remove the lignin, while preventing excessive degradation of the cellulose and hemicellulose (Chimphango et al., 2020). However, hemicelluloses are soluble in strong alkaline solutions (Tabil, Adapa, & Kashaninejad, 2011) and can also be removed under favourable conditions.

The organosolv treatment implements organic solvents such as ethanol, methanol, acetone, ethylene glycol and glycerol in order to break the linkages between hemicellulose and lignin (Vázquez, Leos, Rodríguez-Duran, & de Los Santos, 2020). Furthermore, these solvents degrade the glycosidic bonds in the hemicellulose and internal ester linkages within the lignin structure (Chimphango et al., 2020), thereby producing a pure form of cellulose.

Lastly, biological treatments such as enzymatic hydrolyses, or the utilisation of microorganisms can be applied for cellulose isolation. These microorganisms typically include fungi or bacteria, which selectively target the degradation of hemicellulose and lignin in the biomass samples (Chimphango et al., 2020). A vast array of additional alternative cellulose-isolation methods are currently studied.

2.2.2 Hemicellulose

Hemicellulose is critical component in plant-based natural fibres (Rowell et al., 2012). It comprises approximately 20 – 40 % of the total biomass for the majority of plant-based fibres (Salajkova, 2013). These molecules bind to the cellulosic surface non-covalently, and thereby functions as an auxiliary matrix to the cellulose chains (Dufresne, 2012).

The hemicellulose concentrations of plant cell walls differ between species, region and cultivation methodology (Ceaser, 2019). Hemicellulose exhibits an amorphous structure and contains saccharide side branches (Impola,

2017; Junka, 2014). These molecules comprise mainly of the repeating monomer units displayed in Figure 2.6, namely glucose, mannose, galactose, xylose, arabinose and glucuronic acid (Kalia et al., 2011; R. C. Sun, 2010). Furthermore, minor occurrences of rhamnose and fucose sugars can also be present (Rowell et al., 2012). Hemicelluloses in plant-based fibres constitute different combinations of these sugars and can be methylated or acetylated (Rowell et al., 2012; R. C. Sun, 2010).

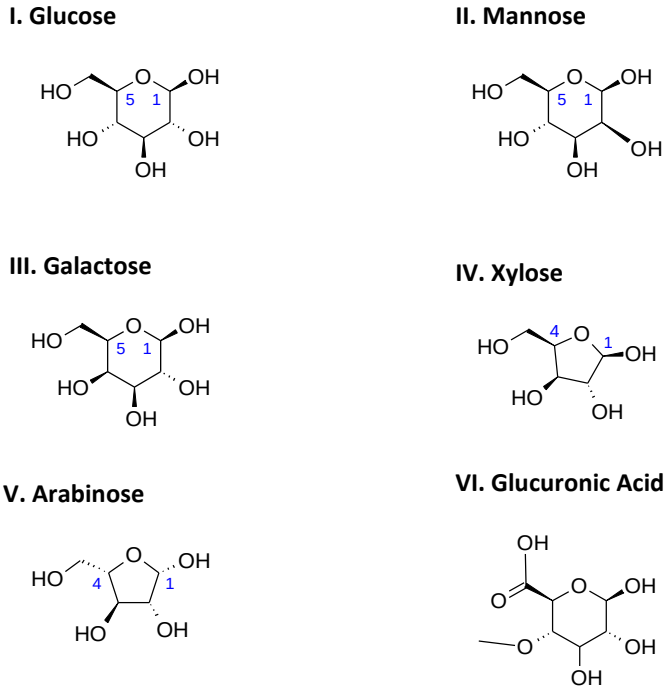

Figure 2.6 The Monomer Units of Hemicellulose **I.** β-D-glucopyranose (or β-D-glucose), **II.** β-D-mannopyranose (or β-D-mannose), **III.** β-D-galactopyranose (or β-D-galactose), **IV.** β-D-xylopyranose (or β-D-xylose), **V.** α-L-arabinofuranose (or α-L-arabinose), and **VI.** 4-O-methylglucopyranosyluronic acid (or 4-O-methylglucuronic acid), redrawn from R. Rowell et al. (2012)

Xylose and arabinose are pentoses, while glucose, mannose and galactose are hexoses (Kalia et al., 2011; Tywabi, 2015). The anomers of the molecules are indicated by the prefixes α or β in Figure 2.6, referring to the orientation of the hydroxyl on C-1 (Rowell et al., 2012). Moreover, the prefixes D or L are indicative of the hydroxyl orientation on C-4 for the pentoses and C-5 for the hexoses (Rowell et al., 2012). Hemicelluloses are commonly classified based on the monomers that the molecules are encompassed of, for example, arabinoxylan, arabinoglucuronoxylan, and arabinogalactan (Rowell et al., 2012; R. C. Sun, 2010).

The side branches of the molecules are hydrophilic, and hemicelluloses are thus hydrolysed with ease (Kalia et al., 2013; R. C. Sun, 2010). Hemicellulose has an average of two reactive hydroxyls available per sugar unit (Egüés et al., 2014). Due to the non-crystallinity of hemicellulose, these structures are more inclined to depolymerise in acidic conditions (Kalia et al., 2011). Furthermore, hemicelluloses are soluble in strong alkaline solutions (Tabil et al., 2011). These polymers have a lower molecular weight than cellulose and significantly shorter polymer chains (Salajkova, 2013). The typical degree of polymerisation could range from 50 to 300 (Kalia et al., 2011).

2.2.3 Lignin

Lignin is an amorphous, phenolic, complex network polymer (Rowell et al., 2012; Salajkova, 2013) consisting of randomly repeated units of the phenylpropanoid monomers derived from p-coumaryl alcohol, coniferyl alcohol, and sinapyl alcohol (Lu et al., 2017; Rowell et al., 2012) as indicated in Figure 2.7. Each lignocellulosic source will have a unique combination of these molecules (Lu et al., 2017), providing the lignin with a distinctive structure. Lignin molecules encompass hydroxyl groups, methoxyl groups and carbonyl groups. Additionally, small amounts of ethylenic groups and sulphur-containing constituents can be present (Kalia et al., 2011). These molecules are aromatic and highly unsaturated since it attains high carbon and low hydrogen contents.

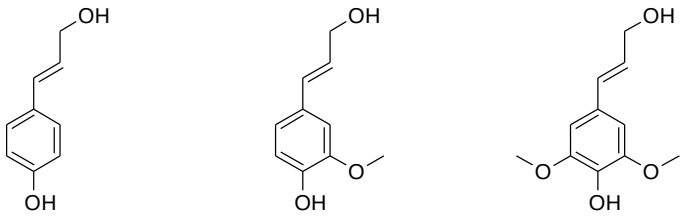

I. **II.** **III.**

Figure 2.7 I. p-Coumaryl Alcohol, **II.** Coniferyl Alcohol, and **III.** Sinapyl Alcohol, redrawn from R. Rowell et al. (2012)

Lignin functions as a structural reinforcement to plants by covalently linking to the hemicellulose molecules, thereby cross-linking the polysaccharides (Arola, 2015). In this way, lignin provides mechanical structure and rigidity to the plant (Arola, 2015; Kalia et al., 2011) and acts as a barrier to protect the plant internals from biological and physical attack (Salajkova, 2013). This strong compound demonstrates a high resistance to degradation by temperature (Kalia et al., 2011; Tabil et al., 2011).

Lignin is hydrophobic, and subsequently water-insoluble. The molecules theoretically have an average of 1.2 hydroxyl groups per nine-carbon unit (Rowell, 2014; Rowell et al., 1994). However, since there are multiple variations of the lignin structure, these will differ between sources (Lu et al., 2017).

2.3 Nanocellulosic Fibres

Nanocellulose can be classified as bacterial nanocellulose (BNC), nanocrystalline cellulose (NCC), or nanofibrillated cellulose (NFC), contingent on the source, method of preparation and structural dimensions (Chimphango et al., 2020; Hokkanen et al., 2016; Khalil et al., 2012; Liu et al., 2017).

BNC is microfibrillated nanocellulose secreted extracellularly by a family of bacteria, *Gluconoacetobacter xylinius* (Khalil et al., 2012; Lavoine et al., 2012). Although this subcategory of nanocellulose is discussed briefly, the focus of this study is on nanocellulose isolated from agricultural sources.

2.3.1 Nanofibrillated Cellulose

NFC can be isolated from cellulose. These fibres have diameters between 1 and 100 nm (Liu et al., 2017) and constitute entangled, flexible fibril bundles which form the structural units of cellulose (Chimphango et al., 2020; Khalil et al., 2012). Moreover, the molecules retain substantial amounts of hydrophilic surface hydroxyl groups (Arola, 2015; Chimphango et al., 2020). A summary of the characteristics of NFC is provided in Table 2.3.

Table 2.3 Classification of Nanofibrillated Cellulose (Khalil et al., 2012; Liu et al., 2017)

Characteristic	Nanofibrillated Cellulose
Synonym	Cellulose Nanofibres, or Cellulose Nanofibrils (CNF)
Shape	Entangled random network
Crystallinity	Relatively Low
Preparation Method	Mechanical methods, with chemical or enzymatic pre-treatment
Chemical Composition	May often contain trace amounts of hemicellulose
Typical Dimensions	Diameter: 1 – 100 nm; Length: Several Micrometres

Mechanical methods such as homogenisation and grinding can be utilised to create NFC from cellulose (Chimphango et al., 2020; Lavoine et al., 2012). However, these methods are often highly energy-intensive, since multiple fibrillations are necessary to achieve NFC of the apposite fibre diameter (Khalil et al., 2014).

Pre-treatments are frequently instilled prior to mechanical fibrillation in order to condense the fibril dimensions, thereby causing a reduction in intermolecular hydrogen bonds of the cellulose chains and ensuring less energy is required during mechanical processing (Chimphango et al., 2020; Khalil et al., 2014; Lavoine et al., 2012; Salajkova, 2013). These modifications can implement chemicals such as alkaline bleaching or carboxymethylation. The pre-treatments can also be executed with the implementation of microorganisms or enzymes (Chimphango et al., 2020).

Cellulose fibres utilised for NFC isolation must contain lignin contamination of not more than 10 %, hemicellulose contamination below 23 % and a molecular crystallinity exceeding 48 % (Ceaser, 2019; Espinosa, Sánchez, Otero, Domínguez-Robles, & Rodríguez, 2017; Teixeira et al., 2010). In order for the fibres to qualify as NFC according to ISO/TS 20477 Part 3.3.6, the diameters of the fibres should be less than 100 nm, and the fibre length can be several micrometres long (Khalil et al., 2012; Liu et al., 2017).

2.3.2 Nanocrystalline Cellulose

When cellulose is subjected to strong acid hydrolyses, the amorphous regions of the cellulose chains are hydrolysed, and the crystalline regions remain in the form of minuscule rod-like structures with fibre diameters of 2 – 20 nm (Chimphango et al., 2020; Liu et al., 2017; Salajkova, 2013). These nanowhiskers are referred to as nanocrystalline cellulose (NCC), with characteristics as summarised in Table 2.4.

Acid hydrolyses reactions are performed under strictly controlled temperature and reaction times in order to modify the amorphous, disordered sections (Chimphango et al., 2020) while maintaining the crystallinities of the samples (Arola, 2015; Lavoine et al., 2012). Sulfuric acid or hydrochloric acid is often employed (Khalil et al., 2012).

Table 2.4 Classification of Nanocrystalline Cellulose (Khalil et al., 2012; Liu et al., 2017)

Characteristic	Nanocrystalline Cellulose
Synonym	Cellulose Nanocrystals (CNC), Cellulose Nanowhiskers (CNW)
Shape	Rigid, elongated crystalline rods
Crystallinity	High (54 – 88 %)
Preparation Methods	Acid Hydrolysis
Chemical Composition	Pure Cellulose
Typical Dimensions	Diameter: 2 – 20 nm; Length: 100 nm – several micrometres

NCC has a higher degree of crystallinity when compared to NFC and BNC (Liu et al., 2017; Long, Weng, & Wang, 2018). The absence of multiple amorphous regions results in NCC exhibiting a lower degree of flexibility when compared to NFC (Khalil et al., 2014). The NCC rods are mechanically stable and can resist high tensile and shear forces (Arola, 2015).

2.3.3 Bacterial Nanocellulose

BNC is microfibrillated nanocellulose secreted extracellularly by a family of bacteria known as *Gluconoacetobacter xylinius* (Khalil et al., 2012; Lavoine et al., 2012). The bacteria feed on glucose-based sources and secretes highly crystalline cellulose microfibrils with typical diameters of 3 and 100 nm (Liu et al., 2017). These BNC fibres exhibit superior physical properties, with high crystallinity, high moduli of elasticity and high porosity (Lavoine et al., 2012). A summary of the characteristics of BNC is provided in Table 2.5.

Table 2.5 Classification of Bacterial Nanocellulose (Lavoine et al., 2012; Liu et al., 2017)

Characteristic	**Bacterial Nanocellulose**
Synonym	Bacterial Cellulose (BC), Microbial Cellulose, Biocellulose
Shape	Randomly assembled, ribbon-shaped
Crystallinity	High (84 – 89 %)
Preparation Method	Bacterial Synthesis from *Gluconoacetobacter xylinius species*
Chemical Composition	Pure cellulose (no lignin, hemicellulose, or pectin such as in plants)
Typical Dimensions	Diameter: 3 – 100 nm; Length: >100 µm

2.4 Current Systems Employed for Oil Removal

The methods currently exercised for the isolation of oil-based particles from water can be grouped into five main categories, namely: (1) mechanical methods, (2) chemical methods, (3) *in-situ* burning, (4) bioremediation, and (5) sorption (Asadpour et al., 2014; Liu et al., 2017). These methods can be employed in conjunction or individually.

Even though these techniques are often successful at cleaning oil spills and removing oil from other water sources, the procedures are frequently not environmentally friendly and often do not selectively remove oil from water. Additionally, these methods can incur large installation, operational and maintenance costs (De Gisi et al., 2016). The mechanical systems commercially applied in removing oil particles from water rely primarily on the density difference between the two liquids (Wei, Mather, & Fotheringham, 2005). Since the oil particles are less dense than water, it can predominantly be removed by the use of skimmers, fat-traps or booms (Mahlobo, 2008; She et al., 2010). The methods are highly efficient and environmentally friendly, but are time-consuming, expensive and labour intensive (Liu et al., 2017).

In wastewater, many of the oil particles are emulsified, and are therefore not found on the water surface (Hubbe, Rojas, et al., 2013; Renuka et al., 2016). Skimmers, booms and other equipment that rely on the density difference of water and oil are thus not effective in removing most of these emulsified particles (Wei et al., 2005). For this reason, some chemical methods are employed, which implement dispersants or solidifiers in order to agglomerate the oil particles (Liu et al., 2017). Solidifiers collect the emulsified particles, thereby establishing the required density difference. Physical methods can consecutively be utilised to separate the two phases. Chemical methods are

implemented to break down hydrocarbons into less harmful constituents, and can successfully treat widely polluted areas (Ifelebuegu & Johnson, 2017). However, the chemicals utilised can be harmful to the environment and can incur high capital and operating costs (Ifelebuegu & Johnson, 2017; Liu et al., 2017).

In-situ burning involves combustion of the oil particles. This method releases large quantities of ozone-depleting gasses into the atmosphere and causes vast environmental concerns (Liu et al., 2017). The process is effective and cheap, but holds a considerable safety risk and is not favourable for implementation.

Moreover, bioremediation involves degradation with the use of microorganisms. The process has a relatively low operating cost and is environmentally friendly. Unfortunately, it is ineffective and inefficient in treating large oil spills (Liu et al., 2017).

Sorbents are materials that are designed to selectively adsorb or absorb certain liquids (She et al., 2010). The use of oil sorbents is an economically beneficial and highly efficient way of removing oil particles from water (Renuka et al., 2016). These materials are applied to attract selective materials in an effective manner. The oil particles are captured and retained. The oil particles can then be recovered from the sorbents for re-application, re-use or correct, safe disposal (Hubbe, Rojas, et al., 2013). Sorbents can retrieve oil slicks of varying characteristics, viscosity and thickness, and can therefore be applied in many different water treatment situations (She et al., 2010). It can also be applied in combination with skimmers and fat-traps, in order to ensure that all trace amounts of oil particles, which cannot be reached by skimmers, are removed to a sufficient extent (Pruitt, 2017). Depending on the material of which the sorbents are fabricated, it may be classified as a *green* or *non-green* method for wastewater treatment (De Gisi et al., 2016).

2.5 Classification of Sorbents

Sorbents are generally classified according to three basic categories, namely: (1) synthetic sorbents, (2) natural inorganic sorbents and (3) natural organic sorbents (Liu et al., 2017; She et al., 2010). The most commonly employed sorbents for oil retrieval are synthetic polymer sorbents, such as polyurethane foam, polypropylene webs, nanoporous polystyrene fibres and rubber gels (Liu et al., 2017; Pruitt, 2017). These sorbents are inherently hydrophobic and oleophilic (Ifelebuegu & Johnson, 2017). According to She et al. (2010), the sorbents can retain up to 70 times their weight in oil. Even though these materials are highly effective, they are petroleum-based and non-biodegradable (Liu et al., 2017). Very often, these materials are also not reusable, and consequently, their implementation can be expensive (She et al., 2010).

Natural inorganic sorbents, such as glass, exfoliated graphite, volcanic ash, activated carbon, silica nanoparticles, organoclay, and sand are mineral-based and have a generally low sorption capacity (Adebajo, Frost, Kloprogge, Carmody, & Kokot, 2003; Liu et al., 2017). These sorbents can typically only absorb up to 20 times their weight in oil (Liu et al., 2017). Furthermore, the sorbents are highly dense and subsequently have a low buoyancy, which results in difficulty with recycling and re-use (Liu et al., 2017).

However, natural organic sorbents are environmentally friendly, biodegradable, inexpensive, sustainable, abundantly available, and have exceptional sorption properties (Asadpour, Sapari, Isa, & Kakooei, 2016; De Gisi et al., 2016; Pruitt, 2017; She et al., 2010). These materials have an extended life cycle and extended recyclability (She

et al., 2010). Accordingly, the sorbents show excellent potential for prospective application in water treatment systems (She et al., 2010). Some agricultural waste sources applied for wastewater treatment application include sugarcane bagasse (Norrihan, 2008), rice husk (Rosa et al., 2012), banana peel (Alaa El-Din et al., 2018), barley straw (Tijani et al., 2016), corncob (Nwadiogbu et al., 2016), jute fibre (Teli & Valia, 2013b) and wheat straw (Pirbazari, 2015). According to De Gisi et al. (2016), lentil shell, sunflower stalk pine sawdust, mango peel waste and orange peels are also employed. Furthermore, kapok, cotton, wood, agave, sisal, rice straw, and peat moss can be implemented (Gaballah, Goy, Allain, Kilbertus, & Thauront, 1997; Liu et al., 2017; Ngah & Hanafiah, 2008; Pruitt, 2017).

2.6 Sorbent Favourable Properties

In order for natural fibre-based sorbents to be successfully applied, specific favourable properties need to be attained. The sorbent material needs to be abundantly available and relatively inexpensive (Liu et al., 2017). Furthermore, it should be environmentally friendly and biodegradable (Deschamps et al., 2003).

It must have a selective affinity towards one material over another (Johnson, Manjreker, & Halligan, 1973). In order to remove oil particles from water, the sorbent should be oleophilic and hydrophobic (Deschamps et al., 2003). This modification will enable the material to absorb (or adsorb) oil particles instead of water. Selectivity is also influenced by pore size, capillary pressure, and whether the sorbent was exposed to oil prior to contacting the water (She et al., 2010). A high affinity to oil and a fast sorption rate, as well as a low water attraction, is preferred (Liu et al., 2017).

A low density, and consequent increased floatability is favoured since a buoyant sorbent allows simpler application in water treatment systems (Deschamps et al., 2003; Liu et al., 2017). *Porosity* is a measurement of the void volume present in a fibrous material and can be used as an indication of the amount of oil that can be absorbed by the relevant sorbent under ideal conditions (Hatton et al., 2015; Johnson et al., 1973). A higher porosity leads to a higher possible sorption capacity (Liu et al., 2017) since the oil particles can be retained in the material matrix structure (Deschamps et al., 2003).

Moreover, high oil retention, in combination with an easy release of the absorbed or adsorbed particles, ensures advantageous reusability of the sorbent (Deschamps et al., 2003; She et al., 2010). Excellent physical and chemical resistance is desired in order to ensure an extended life cycle of the product (She et al., 2010). High reusability and durability is economically beneficial.

2.7 Surface Modification of Biofibres

Agricultural waste products implemented in their natural form are cleaned, grinded, and screened until desired size ranges are achieved. Biomass particles have exhibited specific surface areas of 0.03 – 0.28 m^2/g, depending on how fine these particles are milled. In their native form, unmodified biomass can only absorb approximately 3 to 50 times their weight in oil (Liu et al., 2017; Pruitt, 2017). For this reason, the smaller constituents of the biomass, specifically cellulose and NFC, are isolated and implemented as biosorbents. In this way, the surface area available for oil sorption (OS) is increased. Cellulose has been known to have approximate specific surface areas of 0.6 – 1 m^2/g (Bismarck et al., 2004), while NFC exhibits increased specific surface areas of 70 – 280 m^2/g (Qian et al., 2018).

As described by the diagram in Figure 2.8, the presence of extensive amounts of accessible hydroxyl groups at the external and internal biomass-, cellulose- and nanocellulose molecular surfaces cause these fibres to exhibit polar, hydrophilic behaviour (Salajkova, 2013). This characteristic results in inadequate oil removal capabilities since the polar molecular surface exhibits a higher affinity to the polar water molecules rather than to the non-polar oil particles in a water-oil mixture (Hatton et al., 2015).

In order to successfully apply these fibres to remove oil from water, the polar surface hydroxyls on the fibrous surface requires replacement by non-polar surface acetyls through acetylation reactions (Pruitt, 2017; She et al., 2010). As demonstrated in Figure 2.8, this mechanism alters the chemical composition of the particles, which ensures a higher affinity towards oil and a lowered affinity towards water is achieved (Hubbe et al., 2015). Subsequently, the fibres become hydrophobic and oleophilic, and the effectivity of oil sorption dramatically increases (She et al., 2010).

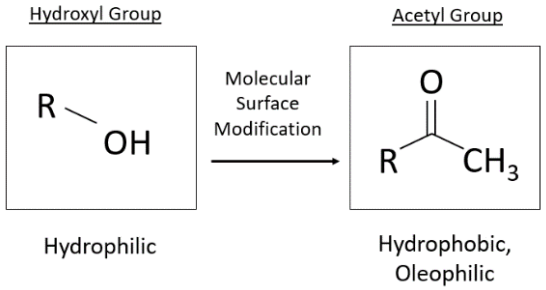

Figure 2.8 The Replacement of a Surface Hydroxyl Group with a Surface Acetyl Group through an Acetylation Reaction in order to Achieve Hydrophobicity and Oleophilicity

The chemical structures in Appendix D.3 (p. 155) reveal that all three major components of lignocellulosic biomass contain abundant hydrophilic hydroxyl groups (Onwuka, Agbaji, Ajibola, & Okibe, 2019). Conversely, since these chemical structures are interconnected in a matrix formation, some of the present hydroxyl groups are not accessible to take part in acetylation reactions of whole biomass (Rowell, 2014). These hydroxyl groups exhibit an order of reactivity (Onwuka et al., 2019). The first point of contact will occur with the protective lignin barrier (Nwadiogbu, Okoye, Ajiwe, & Nnaji, 2014; Salajkova, 2013), and the accessible phenolic, benzylic or alcoholic hydroxyls of the lignin will, therefore, be acetylated initially (Nwadiogbu et al., 2014; Rowell, 2014). Sufficient temperature and time need to be provided in order to accomplish ample diffusion of the reactants into the cell walls, thereby contacting with the reactive hydroxyls on the hemicellulose molecules (Rowell, 2014). Additional temperature and time are then required to achieve a more considerable extent of swelling to reach the hydroxyl groups of cellulose. As discussed in Section 2.2, each AGU of cellulose has three reactive hydroxyl groups (Tupa, Ramírez, Vázquez, & Foresti, 2015). Lignin theoretically provides an average of one extra hydroxyl group per unit (Rowell, 2014), while hemicellulose has an average of two hydroxyls available per sugar unit (Egüés et al., 2014).

The water contact angle (WCA) of a substance is defined as the angle that a water droplet forms when coming into contact with a surface, as presented in Figure 2.9. This contact angle can be used to determine the hydrophobicity of a sample (Zanini et al., 2017; Zhou et al., 2016). A WCA of 0 to 90 ° indicates a hydrophilic sample, while a WCA greater than 90 ° indicates a hydrophobic sample.

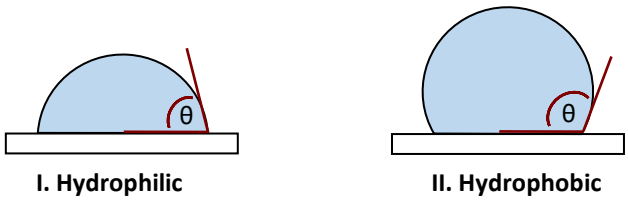

Figure 2.9 The Water Contact Angle (θ) of **I.** A Hydrophilic Sample (θ = 0 – 90 °), and **II.** A Hydrophobic Sample (θ = 90 – 180 °)

Numerous surface modification methods have been developed and implemented in order to alter the surface characteristics of fibres and to consequently extend the application possibilities. Sugarcane bagasse has been acetylated by N-bromosuccinimide as catalyst (X. F. Sun et al., 2004). Moreover, kapok fibre has been modified with hydrochloric acid, chloroform and sodium chloride, respectively (J. Wang, Zheng, & Wang, 2012). Rice straw has been acetylated with different tertiary amine catalysts, such as pyridine, N-methylpyrrolidine, and N-methylpyrrolidinone (X. F. Sun et al., 2002). Additionally, cellulose isolated from the plant *Eichhornia crassipes* was modified using methyltrimethoxysilane (T. Yin, Zhang, Liu, & Wang, 2017). Ramie cellulose has been acetylated by hydrochloric acid (Spinella et al., 2016) and cellulose was then also modified by sulfuric acid (Huang et al., 2014). Furthermore, NFC isolated from banana fibres have been modified with 3-glycidoxypropyltrimethoxysilane and 3-aminopropyltriethoxysilane, respectively (Cherian et al., 2012). Similarly, the NFC has been acetylated with dimethylformamide, pyridine and toluene (Tingaut et al., 2009; Zepic et al., 2015).

There is an extensive amount of research conducted on plant fibres via the traditional, *non-green* methods. However, these treatments often involve the usage of large amounts of toxic chemicals (Kalia et al., 2011). Plant-based biosorbents are frequently regarded as *green* merely based on the fact that plants are implemented instead of synthetic sorbents. However, for the developed biosorbents to be truly environmentally friendly, it is necessary to develop *green* surface modification methods (Hubbe et al., 2015).

The surface acetylation reactions applied in this study are evaluated based on the *green* chemistry principles (American Chemistry Society, 2020; Merck KGa, 2020), as shown in Table 2.6. The *green* chemistry principles are posted in Table 2.6a, while the scoring for each modification is presented in Table 2.6b. The modifications are classified as *green*, when most *green* chemistry principles are strived towards.

These modifications implement acetic anhydride as an acetylating agent. The use of acetic anhydride makes it possible to complete acetylation reactions without harmful organic solvents (Li et al., 2009). Less toxic by-products are produced than in a solvent-containing system (Li et al., 2009). Although acetic anhydride is a corrosive substance, it is non-carcinogenic and non-mutagenic (U.S. National Library of Medicine, 2005a). Nevertheless, it is classified as a strong irritant.

Table 2.6a The Evaluation of the Surface Acetylation Reactions against the *Green* Chemistry Principles

***Green* Chemistry Principle**		***Green* Chemistry Principle Description (American Chemistry Society, 2020; Merck KGa, 2020)**	**Evaluation Criteria**	
1	Prevention	"It is better to prevent waste than to treat or clean up waste after it has been created."	**Q1**	Does the modification aim for waste prevention?
2	Atom Economy	"Synthetic methods should be designed to maximize the incorporation of all materials used in the process into the final product."	**Q2**	Does the method aim to maximise the incorporation of all materials used in the process into the final product?
3	Less Hazardous Chemical Syntheses	"Wherever practicable, synthetic methods should be designed to use and generate substances that possess little or no toxicity to human health and the environment."	**Q3**	Is the method designed to use and generate substances that possess little or no toxicity to human health and the environment?
4	Designing Safer Chemicals	"Chemical products should be designed to affect their desired function while minimizing their toxicity"	**Q4**	Is the product designed to affect the desired function while minimizing toxicity?
5	Safer Solvents and Auxiliaries	"The use of auxiliary substances should be made unnecessary wherever possible and innocuous when used."	**Q5**	Is the use of auxiliary substances minimised wherever possible and innocuous when used?
6	Design for Energy Efficiency	"Energy requirements of chemical processes should be recognized for their environmental and economic impacts and should be minimized. If possible, synthetic methods should be conducted at ambient temperature and pressure."	**Q6**	Is energy use minimised?
7	Use of Renewable Feedstocks	"A raw material or feedstock should be renewable rather than depleting whenever technically and economically practicable."	**Q7**	Are renewable feedstocks used?
8	Reduce Derivatives	"Unnecessary derivatisation (temporary modification of physical/chemical processes) should be minimized or avoided if possible, because such steps require additional reagents and can generate waste."	**Q8**	Is unnecessary derivatisation be minimized or avoided?
9	Catalysis	"Catalytic reagents (as selective as possible) are superior to stoichiometric reagents."	**Q9**	Are catalytic reagents employed?
10	Design for Degradation	"Chemical products should be designed so that at the end of their function they break down into innocuous degradation products and do not persist in the environment."	**Q10**	Are the products designed for degradation?
11	Real-time analysis for Pollution Prevention	"Analytical methodologies need to be further developed to allow for real-time, in-process monitoring and control prior to the formation of hazardous substances."	**Q11**	Does the analytical methods allow for in-process monitoring to prevent hazardous substances from forming?
12	Inherently Safer Chemistry for Accident Prevention	"Substances and the form of a substance used in a chemical process should be chosen to minimize the potential for chemical accidents, including releases, explosions, and fires."	**Q12**	Are the applied chemical substances chosen to minimize the potential for chemical accidents, including releases, explosions, and fires?

Table 2.6b The Evaluation of the Surface Acetylation Reactions against the *Green* Chemistry Principles

Feedstock	Method	Q1	Q2	Q3	Q4	Q5	Q6	Q7	Q8	Q9	Q10	Q11	Q12	"*Green*er" in Comparison?	Comment on Chemicals
Biomass	1 [a]	Yes	No	No	No	No	No	Yes	Yes	Yes	Yes	Yes	No	No	NBS mutagenic, emits toxic fumes when heated to decomposition (U.S. National Library of Medicine, 2005b)
	2 [b]	Yes	No	Yes	Yes	Yes	No	Yes	Yes	Yes	Yes	Yes	Yes	**Yes**	Iodine non-toxic is small amounts (McGeer, 2016; Peres de Paula, Lacerda, & Frollini, 2008; S.-Y. Wang, 2004)
Cellulose	3 [c]	Yes	No	No	No	No	No	Yes	Yes	Yes	Yes	Yes	No	No	Sulfuric acid not toxic, but highly corrosive – even in small amounts; Explosion hazard; Emits toxic fumes when heated (Agency for Toxic Substances and Disease Registry, 2011)
	4 [d]	Yes	No	Yes	Yes	Yes	No	Yes	Yes	Yes	Yes	Yes	Yes	**Yes**	NaOH non-toxic in the amounts used in this study; Corrosive (Agency for Toxic Substances and Disease Registry, 2014)
NFC	5 [e]	Yes	No	No	No	No	No	Yes	Yes	Yes	Yes	Yes	No	No	Pyridine toxic, causes liver damage; Multiple carcinogens used (T. H. Kim & Kim, 2011; Yoon, Seo, Lee, Moon, & Lee, 2016; Zhang, Li, Liu, Luo, & Zhang, 2009)
	6 [f]	Yes	No	Yes	Yes	Yes	No	Yes	Yes	Yes	Yes	Yes	Yes	**Yes**	Lipase classified as environmentally friendly application, safe to use and clean; SDS is an anionic surfactant that are naturally present in coconut oil (Bondi et al., 2015; Trimukhe, Mahadik, Gokhale, & Varma, 2008; Vignes, 2000)

a – Acetylation of the corncob and wheat straw with acetic anhydride and N-bromosuccinimide (NBS) (Nagarajappa, Pandey, Shinde, & Vagdevi, 2016; X. F. Sun et al., 2004); **b** – Acetylation of the corncob and wheat straw with acetic anhydride and iodine, including the use of sodium thiosulfate (Li et al., 2009; Nwabueze, Chiaha, Ezekannagha, & Okoani, 2016); **c** – Acetylation of cellulose with acetic anhydride and sulfuric acid (Huang et al., 2014); **d** – Acetylation of cellulose with acetic anhydride and sodium hydroxide (Koroskenyi & McCarthy, 2001); **e** – Acetylation of nanofibrillated cellulose (NFC) with acetic anhydride, dimethylformamide, pyridine and toluene (Tingaut et al., 2009; Zepic et al., 2015); **f** – Acetylation of nanofibrillated cellulose with dimethyl sulphoxide, acetic anhydride and lipase from *Aspergillus niger* as washed with sodium dodecyl sulphate (SDS) (Bozic et al., 2015)

2.8 Oil Sorbent Application: Aerogels

2.8.1 Advantages of Cellulose and Nanocellulose Based Aerogels

Aerogels are highly interconnected lightweight, porous, solid materials which form when the liquid in a hydrogel is replaced by air (Liu et al., 2017). The aerogels can either be based on cellulose and its derivatives, or on modified- or unmodified nanocellulosic materials (Korhonen, Kettunen, Ras, & Ikkala, 2011).

The aerogels based on modified- and unmodified cellulose and nanocellulose combine the advantages of a robust, natural material with the favourable properties of a three-dimensional, interconnected aerogel (Liu et al., 2017). The cellulosic-base provides the aerogel with extraordinary mechanical properties, biodegradability and environmentally friendliness. Furthermore, the natural source is abundantly available and easily accessible.

By modifying the surface properties of the cellulose or nanocellulose, a high selective affinity for oil can be achieved, together with a water-repulsion characteristic. This modification can be conducted before creating the aerogel (Korhonen et al., 2011). Alternatively, the aerogel can first be created, and surface modifications can then be applied retrospectively. Surface modification can be applied with relative ease (Liu et al., 2017).

The advantages of these aerogels include high porosity, low density and large specific areas (Hubbe, Rojas, et al., 2013). These properties enable the aerogel to absorb or adsorb large amounts of oil (Figure 2.10). Aerogels often exhibit high elasticity and flexibility (Amin, Abkenar, & Zendehboudi, 2015). Moreover, the absorbed oil particles can be easily drained with simple mechanical extraction such as compression (Liu et al., 2017). The sorbent can then be re-used, and the oil particles can either be recycled or disposed of in the correct manner (Korhonen et al., 2011). Furthermore, the aerogel can be re-used until disintegration (Tarrés et al., 2016).

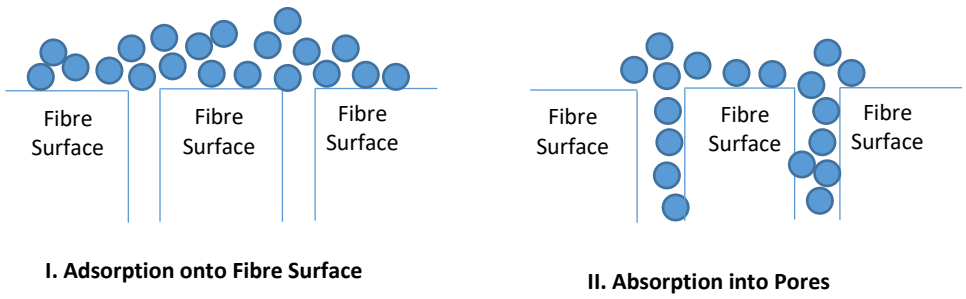

Figure 2.10 The Mechanism of **I.** Adsorption onto a Fibrous Surface and **II.** Absorption into the Fibrous Pores

2.8.2 Aerogel Formation

The first step of creating an aerogel involves producing a three-dimensional hydrogel network (Liu et al., 2017). This step is called *gelation*. If the three-dimensional network is formed without a chemical reaction, it is accomplished by a physical cross-linking mechanism (Adebajo et al., 2003). This process occurs with nanocellulose. The inter- and intramolecular hydrogen bonds present in the nanocellulosic materials, as well as the physical entanglement between the fibres, achieve the gelation effect (Ibrahim & Mondal, 2019; Liu et al., 2017).

For cellulose molecules, chemical cross-linking is necessary. This occurs if the three-dimensional network is formed by a chemical reaction between the cellulose particles and an additional cross-linking agent (Ibrahim & Mondal,

2019; Liu et al., 2017). In this case, a cross-linking agent, such as a specific resin, is necessary to induce the hydrogel formation (Adebajo et al., 2003).

A critical part of creating an aerogel for successful sorption application entails preventing the loss of the three-dimensional solid percolating network, which can occur due to shrinkage or collapsing (Arola, 2015; Hubbe, Rojas, et al., 2013). However, the desired structure can be retained by drying the sample in a specific way. The NFC fibres form a colloidal suspension in water (Afsahi et al., 2018). If the sample is dried while maintaining the bonds between the fibres, the three dimensional network of the aerogel can be retained. This can be achieved through freeze-drying, vacuum drying, or a supercritical drying process (Arola, 2015; Korhonen et al., 2011).

2.9 Conclusion

The presence of hydrocarbons and triglycerides in water pose a technical challenge for wastewater processing or re-use. Hydrocarbon contamination reduces the water quality for available for human consumption and marine life. The available petrochemical-based oil-removing technologies either have negative environmental impacts or are non-selective and ineffective for oil removal. However, plant-based biosorbents, tailored for selective oil removal by surface acetylation reactions can overcome some of the challenges posed by traditional petrochemical-based sorbents.

Therefore, bio-based sorbents can be produced from CC and WS and their respective cellulose and NFC constituents, which can be functionalised via acetylation methods that follow the *green* chemistry principles, in order to increase selective oil sorption. The functionalities of these feedstocks are critically dependant on the replacement of hydrophilic hydroxyl groups on the molecular surface with hydrophobic acetyl groups to attain oleophilicity.

Chapter 3 – Study Approach and Experimental Methodology

3.1 Research Plan, Study Approach and Thesis Layout

Figure 3.1 illustrates the experimental approach followed in this study. The feedstocks, corncob (CC) and wheat straw (WS) were selected due to the abundance of these materials in South Africa (Potgieter, 2011). WS is an agricultural waste source which can be implemented as a biosorbent in raw, milled fibre form (Ermeng, Wuyang, Mingxiao, & Yuewu, 2017). Correspondingly, CC can be applied as a treatment method for oil sorption (OS) (Nwadiogbu et al., 2016).

The OS capacities of the fibres were determined. These materials were subjected to chemical composition analyses based on the NREL/TP-510-42620 method, in order to establish the cellulose, hemicellulose and lignin constituents of the materials since these factors influence the potential utilisation in OS applications (Huntley et al., 2015). The partially crystalline structure of the lignocellulosic biomass and the presence of extensive accessible hydroxyl groups at the external and internal fibre surfaces cause the exhibition of polar, hydrophilic behaviour (Salajkova, 2013).

Two actions can be implemented to improve the OS capacities of the fibres. Firstly, the molecular surface chemistry of the feedstocks can be altered to replace the polar, hydrophilic surface hydroxyl groups with non-polar, hydrophobic acetyl groups, rendering the fibres more oleophilic (Hatton et al., 2015; Hubbe, Ayoub, Daystar, Venditti, & Pawlak, 2013; She et al., 2010). Alternatively, the OS capabilities can be increased by enlarging the specific surface areas of the fibres (Kargarzadeh et al., 2018). The surface area available for OS can be increased by removing lignin, hemicellulose and other extractives, and consequently isolating the cellulose for OS application (Wahi, Chuah, Choong, Ngaini, & Nourouzi, 2013). Furthermore, the surface area can undergo an alternative increase by fractionating the cellulose into nanofibrillated cellulose (NFC) particles (Keplinger, Wang, & Burgert, 2019). As discussed, milled biomass feedstocks have exhibited specific surface areas of 0.03 – 0.28 m^2/g, while cellulose has been known to have approximate specific surface areas of 0.6 – 1 m^2/g (Bismarck et al., 2004). NFC encompasses increased specific surface areas of roughly 70 – 280 m^2/g (Qian et al., 2018). The implementation of cellulose and NFC as biosorbents, therefore, leads to a greater potential for OS due to the increased surface areas of these substances.

Numerous traditional surface modifications have been developed and implemented to alter the surface chemistry of fibres. However, these treatments often involve the usage of toxic chemicals (Kalia et al., 2011). For this reason, *green* surface acetylations were applied to CC and WS by utilising acetic anhydride as an acetylating agent and iodine as catalyst (Li et al., 2009; Nwabueze et al., 2016). These modifications were statistically optimised by the implementation of response surface methodology (RSM) in the form of a central composite design (CCD) with the statistical software – Statistica 13.2 (Bester, 2018). The scope of this CCD was established through preliminary experiments in Appendix D.1 (p. 147). The alpha values were chosen as $[2^k]^{1/4}$, with k = 3, in order to maintain the rotatability in the CCD while including the effects of the extremities in the input parameters (Montgomery & Runger, 1994). The CCD, therefor, varied temperature (50 – 150 °C), time (0.6 – 7.4 h) and iodine concentration (0.7 – 7.4 % (w/w)) in order to maximise the degree of substitution (DS) and OS. The optimally modified WS and CC, in the form of 425 – 600 µm particles, were obtained and subjected to further analyses.

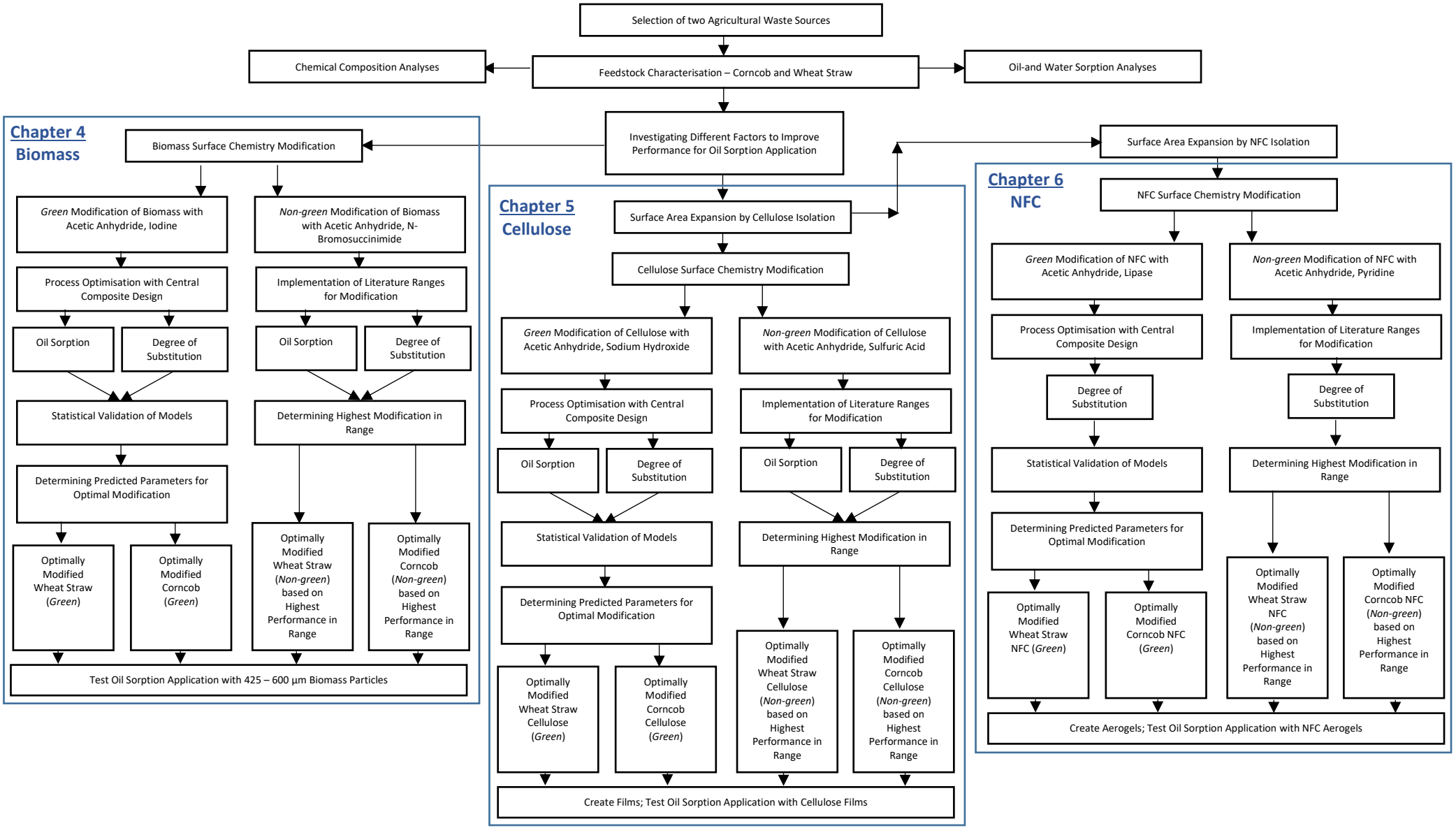

Figure 3.1 The Research Approach for the Development of Biosorbents from Corncob and Wheat Straw for the Separation of Oil Particles from Water, by the Application of Surface Acetylation Methods to the *Biomass Level*, *Cellulose Level* and *Nanofibrillated Cellulose Level* through the Implementation of Acetic Anhydride in Combination with Different *Green* and *Non-green* Catalysts

Concurrently, a traditional *non-green* modification was implemented as a reference for the OS performance. The *non-green* surface acetylation applied to CC and WS on the *biomass level* entailed the implementation of acetic anhydride and N-bromosuccinimide (NBS) as catalyst (Nagarajappa et al., 2016; X. F. Sun et al., 2004). These modifications were conducted by varying the reaction temperature (60 and 150 °C), acetylation duration (2 and 8 h) and catalyst concentration (0 and 4 % (w/v) NBS). The modifications were not statistically optimised, but the performances were rather reviewed within ranges determined from literature studies (X. F. Sun et al., 2004). The optimal modification within these ranges was selected as a benchmark for optimal performance. In this way, the OS capabilities of the unmodified, *green* and *non-green* modified plant-based biosorbents were compared.

As illustrated in Figure 3.1, the biomass was fractionated, and cellulose was isolated from CC and WS. This was achieved via an acid hydrolysis bio-fractionation method adapted from literature (Huntley et al., 2015). The bleaching step of this established method was replaced by an alkaline delignification step adapted from Rosa et al. (2012), and a pre-extraction de-waxing step adapted from J. X. Sun, Sun, Zhao, & Sun (2004) was applied. The OS capacities of these isolated, unmodified samples were determined in order to study how the surface area expansion improved the OS abilities of the fibres (Wahi et al., 2013).

Hereafter, a similar approach to the *biomass level* was followed in order to determine whether the OS of cellulose can be increased through surface modification (Ermeng et al., 2017), by rendering the fibres hydrophobic and oleophilic. The *non-green* surface modification applied on the *cellulose level* implemented acetic anhydride and sulfuric acid (Huang et al., 2014), while the *green* acetylation required acetic anhydride and low concentrations of sodium hydroxide as catalyst (Koroskenyi & McCarthy, 2001). The *green* modification was statistically optimised by implementing a CCD to maximise the DS and OS obtained through acetylation.

The scope is the CCD was established through preliminary experiments in Appendix E.1 (p. 156), and varied temperature (40 – 140 °C), time (3.8 – 44.2 h) and catalyst volume (1.2 – 13.8 % (v/v) NaOH-solution). Concurrently, the *non-green* optimal modification was determined within a range specified from literature studies (Huang et al., 2014). These *non-green* modifications were not statistically optimised, since the purpose was merely to obtain a benchmark for OS performance on the *cellulose level*. The *non-green* modifications were thus conducted by varying the reaction temperature (30 and 90 °C), the acetylation duration (2 and 4 h) and the catalyst concentration (0 and 10 % (v/v) sulfuric acid).

The CC and WS cellulose were subjected to further fractionation, and NFC was produced by implementing an adapted methodology based on pre-fibrillation, enzymatic hydrolysis with FibreCare®, followed by mechanical fibrillation (Bester, 2018; Nechyporchuk, 2015; Tarrés et al., 2016). FibreCare® is an endoglucanase which hydrolyses the amorphous regions in the cellulose chains (Arola, 2015; Ibrahim & Mondal, 2019). Consequently, microfibers are formed while preserving the crystalline regions of the cellulose (Bester, 2018).

The OS of these unmodified, isolated CC and WS NFC samples were determined in order to study how the extended surface area expansion improved the OS capacities of the fibres (Missoum, Belgacem, & Bras, 2013; Wahi et al., 2013). Subsequently, the materials underwent surface acetylations to improve the OS of the samples by the alteration of the surface chemistry. The *green* surface modification was statistically optimised by applying a CCD to

maximise the DS. This modification implemented dimethyl sulphoxide, acetic anhydride and lipase from *Aspergillus niger* (EC Number 232-619-9) (Bozic et al., 2015) and the CCD varied temperature (28 – 62 °C), time (28 – 68 h) and lipase concentration (199 – 2 301 U) for the optimisation of the modification. These ranges were established by the implementation of preliminary experiments in Appendix F.1 (p. 164).

In contrast, the *non-green* acetylation of NFC involved dimethylformamide, pyridine, acetic anhydride and toluene (Tingaut et al., 2009; Zepic et al., 2015). The *non-green* optimised modification was established within a range specified from literature studies, by varying the reaction temperature (25 and 105 °C), the acetylation duration (10 and 72 h) and the catalyst concentration (0 and 4 % (v/v) pyridine). Thereafter, NFC aerogels were created for ease of application in water treatment systems (Feng, Nguyen, Fan, & Duong, 2015).

Lastly, the biosorbents developed with CC and WS biomass, cellulose and NFC were compared based on the criteria set in Section 1.3. The sorption kinetics of the samples were then examined and the potential scale-up of the process was explored.

3.2 Materials

3.2.1 Raw Biomass, Cellulose and Nanofibrillated Cellulose Reference Feedstocks

The CC (44.50 ± 0.58 % cellulose, 20.23 ± 0.56 % hemicellulose and 15.25 ± 1.20 % lignin) and WS (37.15 ± 0.52 % cellulose, 20.75 ± 0.24 % hemicellulose and 18.42 ± 2.50 % lignin) were obtained from local farms in South Africa. These materials were thoroughly washed with distilled water in order to render the fibres of any external dirt and other extraneous impurities. Hereafter, the materials were dried in sunlight. The washed and dried biomass was cut into approximately 1 x 1 cm pieces. A Retsch 2M200 Mill was implemented to grind the biomass fibres until a particle size of 425 – 600 µm was reached for further processing.

Cotton ("100 % pure cotton rolls") was obtained from Dove®, while filter paper (3HW 90mm) was obtained from Lasec SA (Pty) Ltd. Commercial NFC (CAS No. 9004-34-6) was purchased from the University of Maine, in the form of a 98 % (w/w) freeze-dried powder with nominal fibre diameters of approximately 50 nm and a specific surface area of 31 – 33 m^2/g (BET) (University of Maine, 2020). This material was implemented as reference material on the *NFC level*. These materials were utilised as received, with no grinding, sieving, washing or drying performed prior to further processing.

3.2.2 Materials Implemented for Extraction of Cellulose and Nanofibrillated Cellulose from Raw Biomass

Glacial acetic acid (≥ 99 %, AR) and sulfuric acid (98 %, AR) were purchased from Kimix Chemicals for the isolation of cellulose from biomass sources, while sodium hydroxide pellets (≥ 97 %, AR) were procured from ScienceWorld. For the further isolation of NFC from the cellulose sources, FibreCare® (4 700 U/g enzyme) obtained from Novozymes, was utilised. Additionally, hydrochloric acid (32 %, AR) was obtained from Kimix Chemicals.

3.2.3 Materials Utilised during Surface Modification Reactions

N-bromosuccinimide (NBS, 99 %, AR) implemented for the *non-green* acetylation of biomass, was purchased from Sigma Aldrich. Furthermore, iodine (99.8 %, AR) and sodium thiosulfate (99 %, AR) was acquired from Sigma Aldrich for the *green* surface modification on the *biomass level*.

Sulfuric acid (98 %, AR) employed as a catalyst for the *non-green* surface modification of cellulose, was obtained from Kimix Chemicals. Alternatively, sodium hydroxide (≥ 97 %, AR), implemented as a catalyst for the *green* surface modification of cellulose, was purchased from Science World.

Dimethylformamide (99.8 %, AR) and pyridine (≥ 99 %, AR) applied for the *non-green* surface modification of NFC, were procured from Sigma Aldrich. Dimethyl sulphoxide (DMSO, ≥ 99 %, AR), Amano Lipase A from *Aspergillus Niger* (EC Number 232-619-9), sodium dodecyl sulphate (SDS, ≥ 99 %, AR) and a 0.1 M phosphate buffer solution (pH = 7.0) utilised for the *green* surface modification of NFC, were also procured from Sigma Aldrich. A Lipase Assay Kit was purchased from Elabscience. Lastly, the acetic anhydride (≥ 98 %, AR) used as an acetylating agent for all acetylation reactions, were purchased from Sigma Aldrich.

3.2.4 Creating Cellulose Films and Nanofibrillated Cellulose Aerogels

Sodium hydroxide pellets (≥ 97 %, AR) and urea (≥ 98 %, AR) were procured from ScienceWorld for the development of cellulose films, while konjac glucomannan powder was obtained from Health Connection Wholefoods™. Sulfuric acid (98 %, AR) was obtained from Kimix Chemicals. No extraneous chemicals were obtained for the development of NFC aerogels. These substances only employed the respective NFC samples and distilled water.

3.2.5 Other General Materials

Distilled water, implemented during all procedures, was prepared at the Chemical Engineering Faculty of Stellenbosch University. Filter Paper (3HW 90mm) utilised for the washing of the samples were obtained from Lasec SA (Pty) Ltd. The pH paper, acetone (≥ 99 %, AR), ethanol (95 %, AR) and toluene (≥ 99 %, AR) were obtained from Kimix Chemicals. The phenolphthalein indicator was acquired from ScienceWorld. Lastly, sunflower oil (extra virgin, cold-pressed) implemented during OS tests were obtained from Carbsmart®.

3.3 Experimental Setup

The experimental setup illustrated in Figure 3.2 was utilised during cellulose and NFC isolation. Similarly, this setup was applied during the *green* and *non-green* surface modifications of biomass, cellulose and NFC. A photograph of the setup can be found in Appendix A (p. 144).

This setup consisted of a 250 mL round bottom flask connected to a reflux condenser. The sample was added to the round bottom flask containing a magnetic stirring rod, which was then placed in a glycerol bath equipped with an underplate heater, complete with temperature control and magnetic stirring as demonstrated in Figure 3.2. The cooling in the condenser was accomplished with recirculating water. A submersible pump (HJ741, 600 L/h, 8 Watt) was employed for water reticulation. The condenser outlet vapours were scrubbed by passing through distilled water prior to the gas outlet into the fume hood.

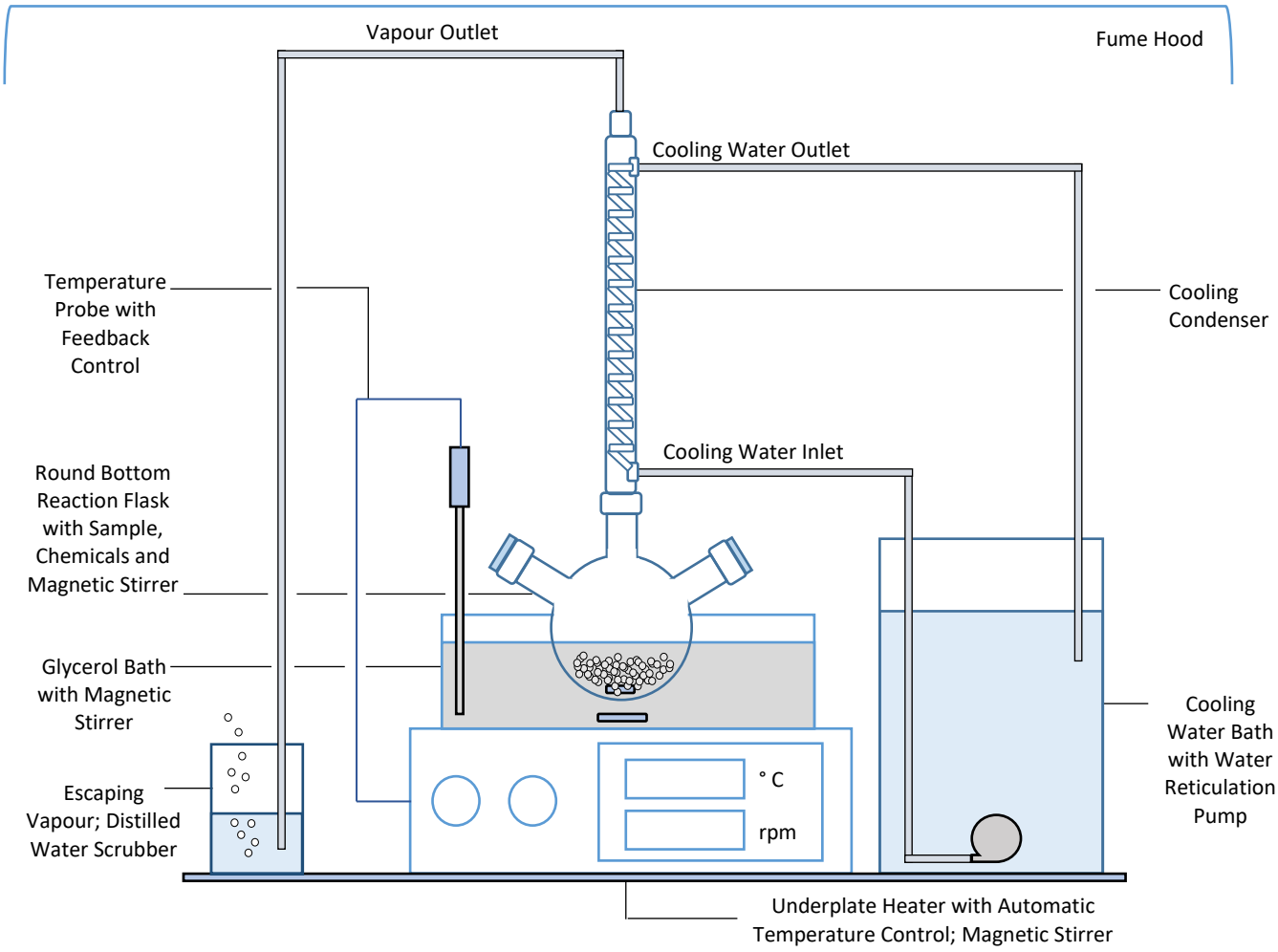

Figure 3.2 The Reflux-condenser Experimental Setup

3.4 Analytical Procedures

The general analytical procedures applied throughout the study are discussed here. Additional analyses and specific experimental procedures applied only to specific samples, are discussed within the relevant chapters.

3.4.1 Composition Analyses

The chemical compositions of the starting biomass materials were completed based on the NREL/TP-510-42620 method. This analysis method was also applied to the cellulose isolated from CC and WS for the determination of cellulose purity attained.

Each homogeneous batch was quartered. In order to achieve a well-represented sample, the opposite corners were selected, while discarding the rest to storage (Hames et al., 2008). This process was repeated until the desired sample size was retained. The samples were then stored in a controlled room with a 55 % relative humidity at 23 °C for 24 h prior to further analyses.

The moisture content of a sample was determined by drying the 2 g sample at 105 ± 3 °C for 24 h, followed by a cool-down period in a desiccator (Ceaser, 2019). The change in weight after drying relates to the moisture content of the sample (Matavire, 2018). Hereafter, the sample is discarded. In a similar manner, the ash content of the sample is determined by noting the change in weight realised after placing the sample in a furnace at 575 ± 25 °C

for 4 h (Matavire, 2018). Henceforth, the water extractives, ethanol extractives, acid-soluble and acid-insoluble lignin were determined based on the standard procedure provided by the National Renewable Energy Laboratory (NREL) (Bester, 2018). The total monomeric sugar content consisting of glucose, arabinose, cellobiose and xylose were determined by High Performance Liquid Chromatography (HPLC) by the Analytical Facility of the Process Engineering Department, Stellenbosch University. This Aminex HPx-8 HPLC column was operated at 65 °C, fitted with a cation-H Micro Guard Cartridge and a Thermo Scientific RI-101 detector (Bester, 2018). A 5 mM sulfuric acid solution was utilised at 0.6 mL/min (Matavire, 2018).

3.4.2 Fourier Transform Infrared Spectroscopy

The chemical structures of the fibres were determined by Fourier Transform Infrared Spectroscopy (FT-IR) throughout the study. This analysis was achieved by utilising a Thermo Nicolet Nexus 670 FT-IR system, which implements a Diamond Attenuated Total Reflectance (ATR) measurement tool. The data were analysed with the Thermo Scientific Omnic9 Software and the Origin60 Data Processing Package. The samples were dried at 40 °C for 24 h prior to analyses. The Smart iTR™ Diamond ATR setting was applied to collect 64 scans within the wavenumber range of 600 cm^{-1} to 4 000 cm^{-1} at every 4 cm^{-1} for each sample.

3.4.3 Crystallinity by X-ray Diffraction Spectroscopy

The isolated cellulose and NFC samples were subjected to X-ray diffraction (XRD) analyses by implementing a Bruker D2 Phaser X-ray Diffractometer calibrated to a copper tube with λ = 1.54184 Å at a voltage of 30 kV and a current of 10 mA. Sample preparation involved drying the fibres at 40 °C for 24 h. The intensities of the diffraction peaks were measured from 2θ = 3.99 ° to 2θ = 40.00 °. The molecular crystallinities of the samples were then determined by an empirical relationship, as described by Equation 3.1a (Huntley et al., 2015). I_c refers to the peak intensity at 2θ = 22.5 °, and I_a refers to the peak intensity at 2θ = 18 ° (Ceaser, 2019; Huntley et al., 2015).

$$Crystallinity\ (\%) = I_c/(I_c + I_a)\ \times\ 100 \qquad [3.1a]$$

$$Crystallinity_S\ (\%) = (I_c - I_a)/I_c\ \times\ 100 \qquad [3.1b]$$

Moreover, the Segal Equation can be applied as an additional approach to determining the crystallinity, as described in Equation 3.1b (Nam, French, Condon, & Concha, 2016). This approach delivers marginally lower estimates of the crystallinities. However, the current study only implemented the estimation described by Huntley et al. (2015).

3.4.4 Water Contact Angle Measurements

The cellulose films and nanocellulose aerogels were subjected to water contact angle (WCA) analyses in order to determine the hydrophobicity of the specimens. Sample preparation involved drying the fibres at 40 °C for 24 h. The WCA of the samples were measured at Roediger Agencies, situated at the Institute for Polymer Science of the University of Stellenbosch. The test was executed by adding a single 1 µL droplet of distilled water to the surface of an aerogel or film, and capturing high-resolution microscopic images of the response. The processing software, ImageJ, was implemented to establish the WCA from the images. A hydrophilic surface will have a WCA of 0 – 90 °, while a WCA greater than 90 ° indicates a hydrophobic substance (Zanini et al., 2017; Zhou et al., 2016).

3.4.5 Homogeneous Sorption Determinations

The OS of the samples were measured under homogeneous conditions in a static environment. This analysis was executed with either distilled water or sunflower oil, with a dynamic viscosity of 64 cP at approximately 20 °C.

The 0.1 g biomass particles, 0.1 g cellulose particles (prior to film formation) and 0.25 g NFC particles (prior to aerogel formation) were placed in centrifuge tubes with 5 g oil or 10 mL water for 20 minutes, respectively. The samples were then centrifuged for 10 minutes to remove excess oil or water. During OS, a *blank* sample, which only contained oil, was correspondingly implemented in order to correct for the oil adsorbed to the centrifuge tube surface. The OS was then determined by Equation 3.2, while the water sorption (WA) was determined by Equation 3.3:

$$OS\ (g\ oil/g\ sorbent) = \frac{w_f - w_i - w_b}{w_i} \quad [3.2]$$

$$WA\ (g\ water/g\ sorbent) = \frac{w_f - w_i}{w_i} \quad [3.3]$$

In Equation 3.2 and 3.3, the w_f is the weight of the sample after sorption; w_i is the weight of the initial sample, and w_b is the oil absorbed for the *blank* sample. The ease of application is improved by the cellulose films and NFC aerogels. These samples were simply placed in 5 g oil or 10 mL water for 20 minutes, after which the change in weight was noted as the oil- or water absorbed or adsorbed.

3.4.6 Heterogeneous Oil- and Water Sorption

The heterogeneous OS and WA of the sorbents were measured by implementing sunflower oil and distilled water. Oil emulsions were created by mixing 10 % (v/v) oil with 90 % (v/v) water. The samples were placed in these emulsions for 20 minutes. The weights of the samples were recorded. Hereafter, the samples were dried at 40 °C for 48 h in order to evaporate all the water. The heterogeneous OS and WA were determined with Equation 3.4 and Equation 3.5, where w_i is the weight of the initial sample, w_m is the weight measured directly after sorption and w_f is the final weight measured after drying for 48 h.

$$Heterogeneous\ OS\ (g\ oil/g\ sorbent) = \frac{w_f - w_i}{w_i} \quad [3.4]$$

$$Heterogeneous\ WA\ (g\ water/g\ sorbent) = \frac{w_m - w_f}{w_i} \quad [3.5]$$

This analysis was executed in order to determine whether improved selectivity for OS was accomplished by the surface modification reactions.

3.4.7 Degree of Substitution

A standard saponification method based on ASTM D871-96 (ASTM International, 2019; Tupa et al., 2015), in combination with FT-IR, was implemented to develop calibration curves for the determination of DS achieved by the acetylation reactions in this study (Tingaut et al., 2009). The step-by-step development of these calibration curves for each feedstock can be found in Appendix G (p. 173).

Five samples of a specific feedstock with different acetyl contents were selected and subjected to the test method described by ASTM D871-96: Standard Test Methods of Testing Cellulose Acetate (ASTM International, 2019;

Tingaut et al., 2009; Tupa et al., 2015), as described here. This method was also performed on an unmodified sample, referred to as the *blank* sample. In this method 8 mL of a 75 % (v/v) ethanol-solution was added to a 0.5 g fibre sample, and heated to 60 °C for 30 minutes. Furthermore, 8 mL of a 0.5 N sodium hydroxide-solution was added to the solution, and the specimen was heated to 60 °C for a further 15 minutes. The sample was then left to settle at room temperature for 72 h, after which a phenolphthalein indicator was implemented for titration with 0.5 N hydrochloric acid. Hereafter, 1 mL of the 0.5 N hydrochloric acid was added, and the sample was left to settle overnight, after which it was back titrated with 0.5 N sodium hydroxide.

The acetyl content is calculated by Equation 3.6 (ASTM International, 2019; Tingaut et al., 2009), where N_{NaOH} and N_{HCl} refer to the normality of sodium hydroxide and hydrochloric acid respectively, V_a (mL) refers to the volume of sodium hydroxide added to the sample, and V_b (mL) the volume of sodium hydroxide added to the *blank*. Furthermore, V_c (mL) is the volume of hydrochloric acid added to the sample, and V_d (mL) is the volume of hydrochloric acid added to the *blank*. Lastly, w_s refers to the weight of the sample. According to Tingaut et al. (2009), the FT-IR spectra of these samples can then be used to retrieve the following measurements summarised in Table 3.1.

$$Acetyl\ Content\ (\%) = (N_{HCl}(V_d - V_c) + N_{NaOH}(V_a - V_b)) \times \frac{4.305}{W_s} \quad [3.6]$$

Table 3.1 Measurements of Interest for Degree of Substitution Calibration Curve Development from Fourier Transform Infrared Spectroscopy, as Identified by Tingaut et al. (2009)

Peak Name	Wavenumber (cm^{-1})	Baseline constructed to Normalise Spectra	Type of Measurement	Symbol
Methyl peak	1 370	1 500 – 860 cm^{-1}	Height	H_{1370}
C-O stretching vibration of the glucopyranose ring	1 060	1 500 – 860 cm^{-1}	Height	H_{1060}
Carbonyl peak	1 740	1 790 – 1 690 cm^{-1}	Area	A_{1740}
Methyl peak	1 370	1 394 – 1 347 cm^{-1}	Area	A_{1370}

In this study, Thermo Scientific Omnic9 Software was utilised to determine these values. Four calibration curves were then determined by plotting the experimentally calculated acetyl contents against the following four ratios: (A_{1370} / H_{1060}), (H_{1740} / H_{1060}), (A_{1740} / H_{1060}) and (H_{1370} / H_{1060}) (Tingaut et al., 2009). These curves were validated by applying the saponification method based on ASTM D871-96 and evaluating if the values obtained by the FT-IR curves were within 10 % of the values reached by the saponification method. The DS is defined by Tupa et al. (2015) as the number of hydroxyl groups substituted by an acetyl group per anhydroglucose unit and can be calculated by Equation 3.7.

$$DS = \frac{(M_{AGU} \times A_c)}{\left((100 \times M_{acetyl}) - \left((M_{acetyl} - 1) \times A_c\right)\right)} \quad [3.7]$$

A_c is the acetyl content (%) as determined in Equation 3.6, while M_{acetyl} refers to the molecular weight of 43 $g.mol^{-1}$ of an acetyl group. M_{AGU} is the molecular weight of 162 $g.mol^{-1}$ of an anhydroglucose unit.

3.4.8 Density and Porosity

The bulk density of a sample, ρ_b, is defined according to Equation 3.8, where the weight of the sample is represented by w_s and the volume of the sample is shown by v_s . The volumes of the films were approximated by implementing an Elcometer ®, while the aerogel thicknesses were measured with a Vernier Calliper. The bulk density of the 425 – 600 µm biomass particles could not be measured, since these materials are implemented as particles, which do not display a bulk volume measurable with these devices.

$$\rho_b\ (g/cm^3) = w_s/v_s \qquad [3.8]$$

The porosities of the cellulose films and NFC aerogels were then calculated with Equation 3.9 (Hossen, Talbot, Kennard, Bousfield, & Mason, 2020). The particle densities, ρ_c, were assumed as 1.54 g/cm^3 for cellulose, based on the density of cotton (Barnhardt Manufacturing Company Inc., 2020), while the ρ_c was estimated as 1.5 g/cm^3 for NFC particles (Hossen et al., 2020).

$$Porosity\ (\%) = (1 - \rho_b/\rho_c) \times 100 \qquad [3.9]$$

3.4.9 Thermogravimetric Analyses

Thermogravimetric analyses (TGA) was executed with a Mettler Toledo TGA500 analyser by the Analytical Facility of the Process Engineering Department, Stellenbosch University. The samples were systematically heated to 900 °C, and subsequently cooled to 50 °C within eight process steps, as described in Table 3.2. This operation was executed in an inert environment under nitrogen flow, in order to prevent thermo-oxidative degradation from occurring (Ceaser, 2019).

Table 3.2 The Heating and Cooling Steps applied during Thermogravimetric Analyses

Step No.	Process Details	Step No.	Process Details
1	Hold isothermally at 50 °C for 1 min	**5**	Hold isothermally at 900 °C for 5 min
2	Ramp to 110 °C at 50 °C/min	**6**	Cool to 550 °C at 50 °C/min
3	Hold isothermally at 110 °C for 7 min	**7**	Hold isothermally at 550 °C for 10 min
4	Ramp to 900 °C at 100 °C/min	**8**	Equilibrate to 50 °C

3.5 Central Composite Design for *Green* Modifications

A three-factor face-centred CCD based on response surface methodology (RSM) was implemented during the *green* surface modifications, in order to establish empirical relationships relating the degree of substitution (DS, Y_1) and oil sorption (Y_2, OS) of the modified products to the varying reaction conditions, namely temperature (X_1), time (X_2) and catalyst concentration (X_3).

The scope for each CCD was established through preliminary experiments in Appendix D.1 (p. 147) for the *biomass level*, Appendix E.1 (p. 156) for the *cellulose level*, and Appendix F.1 (p. 164) for the *NFC level*, respectively. The alpha values were chosen as $[2^k]^{1/4}$, with k = 3, in order to maintain the rotatability in the CCD while including the effects of the extremities in the input parameters (Montgomery & Runger, 1994). In this way, main and combined

effects of the specific process acetylation conditions on the modified products were determined. Furthermore, the *green* acetylations (on the *biomass*, *cellulose* and *NFC levels*) were optimised by implementing the statistical software, Statistica 13.2. The combination of parameters which lead to the highest DS and OS achieved by the *green* modifications were hereby determined. The developed polynomial models are represented by Equation 3.10 – 3.12 (Hamid, Chowdhury, & Karim, 2014; Montgomery & Runger, 1994).

$$Y_i = b_0 + \sum_{i=1}^{k} b_i X_i + \sum_{i=1}^{k} b_{ii} X_i^2 + \sum_{i=1}^{k-1} \sum_{j>i}^{k} b_{ij} X_i X_j \quad [3.10]$$

$$Y_1 = b_0 + b_1 X_1 + b_2 X_2 + b_3 X_3 + b_{11} X_1^2 + b_{22} X_2^2 + b_{33} X_3^2 + b_{12} X_1 X_2 + b_{13} X_1 X_3 + b_{23} X_2 X_3 \quad [3.11]$$

$$Y_2 = b_0 + b_1 X_1 + b_2 X_2 + b_3 X_3 + b_{11} X_1^2 + b_{22} X_2^2 + b_{33} X_3^2 + b_{12} X_1 X_2 + b_{13} X_1 X_3 + b_{23} X_2 X_3 \quad [3.12]$$

In these models, b_0 represents the constant-coefficient, known as the error-term; b_1 and b_{11} are the linear and quadratic effects of temperature (X_1); b_2 and b_{22} represent the linear and quadratic effects of time (X_2); while b_3 and b_{33} depict the linear and quadratic effects of the catalyst concentration (X_3). The interaction between temperature and time is represented by b_{12}, while the interaction between temperature and catalyst concentration is shown by b_{13}. The coefficient of interaction between time and catalyst concentration is shown by b_{23}. ANOVA analyses were applied to the developed models in order to determine the regression coefficients and analyse the fit of the models to the experimental data.

Chapter 4 – The Surface Modification of Corncob and Wheat Straw for the Optimisation of Oil Sorption

Abstract

Wheat straw (WS) and corncob (CC) were altered to become hydrophobic and oleophilic via *green* and *non-green* molecular surface acetylations for selective oil removal from water. The *green* modification yielded hydrophobic CC and WS with a heterogeneous, selective oil sorption (OS) of 18.37 ± 0.12 g/g and 16.91 ± 0.42 g/g, and degree of substitutions (DS) of 2.14 ± 0.19 and 2.38 ± 0.09, respectively. The *non-green* modified CC and WS rendered OS of 20.46 ± 1.42 g/g and 17.12 ± 1.95 g/g, and DS of 2.76 ± 0.48 and 2.19 ± 0.05. Although the DS attained by these modifications differ, the OS achieved by the *green* and *non-green* acetylated CC were statistically similar. The OS realised by the *green* and *non-green* modified WS were correspondingly not significantly different. However, the sorption achieved by these plant-based biosorbents did not compare well to the commercially implemented petrochemical-based sorbents and it was recommended to additionally investigate whether cellulose-based sorbents can be considered as a worthy competitor for the *non-green* industrial alternatives.

4.1 Introduction

This chapter addresses Questions 1 and 4 of the list of *Key Research Questions* developed in Chapter 1, Section 1.4.

1. Can a *green* surface acetylation method be applied to the native biomass waste sources, CC and WS, in order to create a selective oleophilicity and hydrophobicity?
4. Can the *green* surface acetylation methods optimised in this study perform equally to traditional *non-green* surface acetylation reactions?

In order to answer these research questions, the molecular surfaces of the feedstocks were acetylated by the implementation of *green* and *non-green* surface modification reactions. The *green* acetylation implemented acetic anhydride and iodine, while the *non-green* methodology replaced the *green* iodine catalyst with *non-green* N-bromosuccinimide (NBS). The optimal performances accomplished by the feedstocks through these acetylations were compared based on DS and OS in order to determine whether sorption reached by the modernised, *green* acetylations can compete favourably with the traditional, *non-green* surface acetylation reactions.

4.2 Experimental Methodology

4.2.1 General Definitions of Biomass Modifications

In order to discern between experimental runs for the modification of CC and WS, by applying *green* and *non-green* methodologies, the experimental runs were encrypted based on the identifications displayed in Table 4.1. The biomass particles were utilised in the form of 425 – 600 µm particles (Figure 4.1).

Table 4.1 The Encryptions Utilised for the Identification of Biomass Surface Modifications

Biomass	**Modification Identification**	
	Non-green Methodology [a]	*Green* Methodology [b]
Corncob [c]	CC-B1-X	CC-B2-X
Wheat Straw [d]	WS-B1-X	WS-B2-X

a – Runs marked with B1 as suffix represents a *non-green* modification on the *biomass level*; **b** – Runs marked with B2 as suffix represents a *green* modification on the *biomass level*; **c** – Corncob is abbreviated as CC; **d** – Wheat straw is abbreviated as WS; **X** represents the number of the experimental run

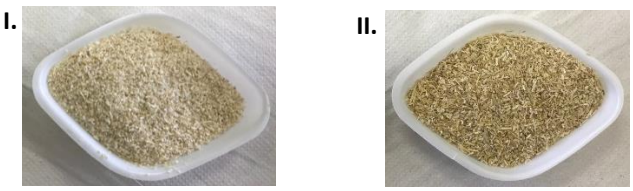

Figure 4.1 I. Unmodified Corncob, Dried and Milled to 425 – 600 µm; **II.** Unmodified Wheat Straw, Dried and Milled to 425 – 600 µm

4.2.2 The *Green* Acetylation of Corncob and Wheat Straw by Acetic Anhydride and Iodine

4.2.2.1 The Chemical Reaction

The WS and CC were modified by applying acetic anhydride as an acetylating agent and specified amounts of iodine as a catalyst (Li et al., 2009; Nwabueze et al., 2016). The chemical reaction achieved by the *green* modification is displayed in Figure 4.2. According to Li et al. (2009), this system produces less-toxic by-products, since the use of acetic anhydride enables the reaction to be organic solvent-free.

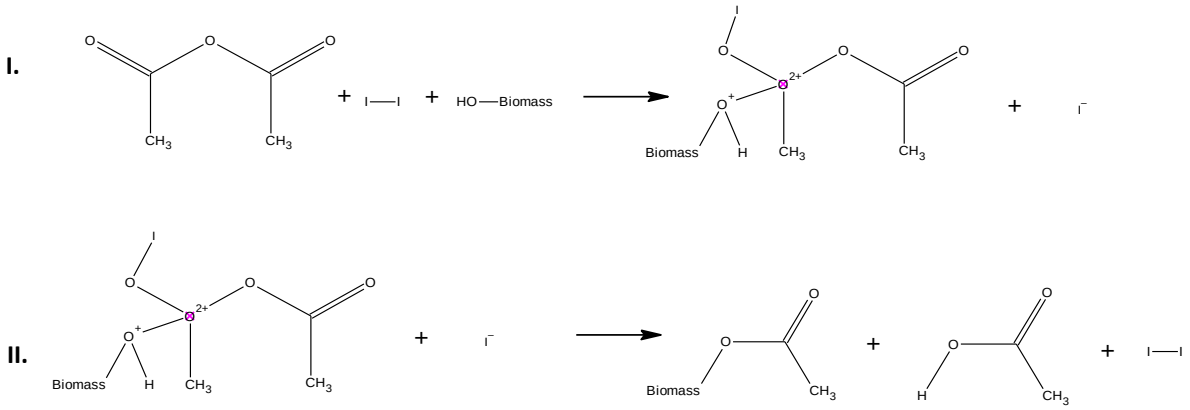

Figure 4.2 The *Green* Reaction Mechanism for Iodine-catalysed Acetylation of Biomass, redrawn from Li et al. (2009)

The two-step reaction occurs, as illustrated in Figure 4.2. Firstly, the iodine acts as a Lewis-acid catalyst and a nucleophilic attack by the I^+-donor occurs in order to activate the carbonyl group of acetic anhydride (Li et al., 2009). Instantaneously, the activated acetic anhydride reacts with the surface hydroxyl groups of the biomass (Reaction I, Figure 4.2). In the second step, the acetylated biomass is formed, the iodine-catalyst is recovered, and acetic acid is formed as a by-product (Reaction II, Figure 4.2).

4.2.2.2 The Central Composite Design and Scope Establishment

A three-factor central composite design (CCD), based on response surface methodology (RSM), was implemented in order to establish empirical relationships relating the DS (Y_1) and OS (Y_2) of the modified product to the varying reaction conditions, namely temperature (X_1), time (X_2) and catalyst concentration (X_3), as described in Chapter 3, Section 3.5. The execution was applied to CC and WS. The combination of parameters leading to the highest DS and OS were determined. The complete CCD design matrix applied to CC and WS during the *green* acetylation is displayed in Table 4.2. The temperature was varied between 50 – 150 °C, time from 0.6 – 7.4 h, and the iodine concentration was ranged from 0.7 – 7.4 % (w/w). Five identical experiments were conducted at the centre point

(Table 4.2, Run CC-B2-15 to CC-B2-19 and WS-B2-15 to WS-B2-19) to calculate the repeatability of the data (Hamid et al., 2014).

The ranges of the input variables were determined based on preliminary studies, which are detailed in Appendix D.1 (p. 147). These preliminary experiments were accomplished with WS by varying the reaction temperature from 50 – 150 °C, acetylation duration between 2 – 7.5 h and catalyst concentration from 2 – 7.5 % (w/w) iodine, in single-factor experiments. A significant escalation in DS occurred when increasing the temperature from 50 °C to 100 °C ($p = 1.40 \times 10^{-4}$) and 130 °C ($p = 2.24 \times 10^{-5}$) at a constant time and catalyst concentration (2 h, 5 % (w/w) iodine). A further ascent to 150 °C transpired in a significantly reduced DS ($p = 6.90 \times 10^{-4}$). In order to study the interactions between temperature, time and catalyst concentration, a temperature range of 50 °C to 150 °C (with $\alpha = 2^{3/4}$) was selected for the CCD.

Table 4.2 The Central Composite Design Matrix and Experimental Conditions for the *Green* Modification of Corncob and Wheat Straw in order to Improve the Hydrophobicity for Oil Sorption Applications

Factor	Symbol	Range	Coded Levels				
			-α	**-1**	**0**	**1**	**α**
Temperature	X_1	50 – 150 °C	50	70	100	130	150
Time	X_2	0.6 – 7.4 h	0.6	2	4	6	7.4
Catalyst Concentration [c]	X_3	0.6 – 7.4 % (w/w)	0.6	2	4	6	7.4

Run ID [a, b]		Type of Point	Level (Coded Factors)			Reaction Variables (Actual Factors)		
						Temperature (°C)	Time (h)	Catalyst Loading [c] (%)
CC-B2-0 [d]	**WS-B2-0** [d]	-	-	-	-	-	-	-
CC-B2-1	**WS-B2-1**	Fact	- 1	- 1	- 1	70	2	2
CC-B2-2	**WS-B2-2**	Fact	- 1	- 1	1	70	2	6
CC-B2-3	**WS-B2-3**	Fact	- 1	1	- 1	70	6	2
CC-B2-4	**WS-B2-4**	Fact	- 1	1	1	70	6	6
CC-B2-5	**WS-B2-5**	Fact	1	- 1	- 1	130	2	2
CC-B2-6	**WS-B2-6**	Fact	1	- 1	1	130	2	6
CC-B2-7	**WS-B2-7**	Fact	1	1	- 1	130	6	2
CC-B2-8	**WS-B2-8**	Fact	1	1	1	130	6	6
CC-B2-9	**WS-B2-9**	Axial	- α	0	0	50	4	4
CC-B2-10	**WS-B2-10**	Axial	+ α	0	0	150	4	4
CC-B2-11	**WS-B2-11**	Axial	0	- α	0	100	0.6	4
CC-B2-12	**WS-B2-12**	Axial	0	+ α	0	100	7.4	4
CC-B2-13	**WS-B2-13**	Axial	0	0	- α	100	4	0.6
CC-B2-14	**WS-B2-14**	Axial	0	0	+ α	100	4	7.4
CC-B2-15	**WS-B2-15**	Centre	0	0	0	100	4	4
CC-B2-16	**WS-B2-16**	Centre	0	0	0	100	4	4
CC-B2-17	**WS-B2-17**	Centre	0	0	0	100	4	4
CC-B2-18	**WS-B2-18**	Centre	0	0	0	100	4	4
CC-B2-19	**WS-B2-19**	Centre	0	0	0	100	4	4

a – Run identification for corncob (CC) and wheat straw (WS), where B2 as suffix represents a *green* modification; **b** – Each run performed with a constant acetic anhydride loading of 25:1 (25 mL acetic anhydride to 1 g biomass); **c** – Target iodine as a weight percentage of biomass; **d** – Unmodified CC and WS samples for reference

A statistically significant incline in DS ($p = 2.00 \times 10^{-4}$) was perceived when increasing the reaction time from 2 h to 6 h (at 130 °C, 5 % (w/w) iodine). The DS at 7.5 h was significantly decreased ($p = 3.94 \times 10^{-6}$). In order to study the

interactions between the input parameters, a time range of 0.6 to 7.4 h was selected for the CCD study. This designation ensured the alpha values of $\alpha = 2^{3/4}$ to maintain the statistical rotatability of the experimental design.

A significant increase in DS ($p = 7.81 \times 10^{-5}$) occurred when escalating the iodine percentage from 2 % (w/w) to 5 % (w/w) at 130 °C and a 2 h reaction time. A statistically higher DS was reached at 5 % (w/w) iodine ($p = 2.12 \times 10^{-4}$). Therefore, a testing range of 0.6 to 7.4 % (w/w) iodine was implemented (with $\alpha = 2^{3/4}$).

4.2.2.3 The Experimental Details

This modification was executed by combining 1 g of the relevant biomass and 25 mL of acetic anhydride (25 % (w/v) acetic anhydride) in a 250 mL round bottom flask. The applicable amount of iodine was added (from 0.6 % (w/w) to 0.74 % (w/w), as presented in Table 4.2). The specimens were inserted into the reflux-condenser setup (defined in Chapter 3), and the samples were maintained at the required reaction temperatures (between 50 °C and 150 °C, Table 4.2) for stipulated reaction times (between 0.6 h and 7.4 h, Table 4.2).

The samples were cooled to room temperature at approximately 25 °C, and 1 – 2 mL of a saturated sodium thiosulfate solution was added to the specimen under constant magnetic stirring of 300 rpm. This addition resulted in the mixture turning from brown to colourless, indicating that the iodine was converted to iodide (Li et al., 2009). The modified biomass was Buchner-filtered, and the retentate was washed with 100 mL acetone and 100 mL ethanol to remove unreacted constituents. It was then washed with hot distilled water until the filtrate attained a neutral pH (Chowdhury & Hamid, 2016), and oven-dried at 40 °C for 24 h.

4.2.3 The *Non-green* Acetylation of Corncob and Wheat Straw by Acetic Anhydride and N-Bromosuccinimide

4.2.3.1 The Chemical Reaction

A *non-green* acetylation performed on sugarcane bagasse was adapted for the surface modification of CC and WS (X. F. Sun et al., 2004).

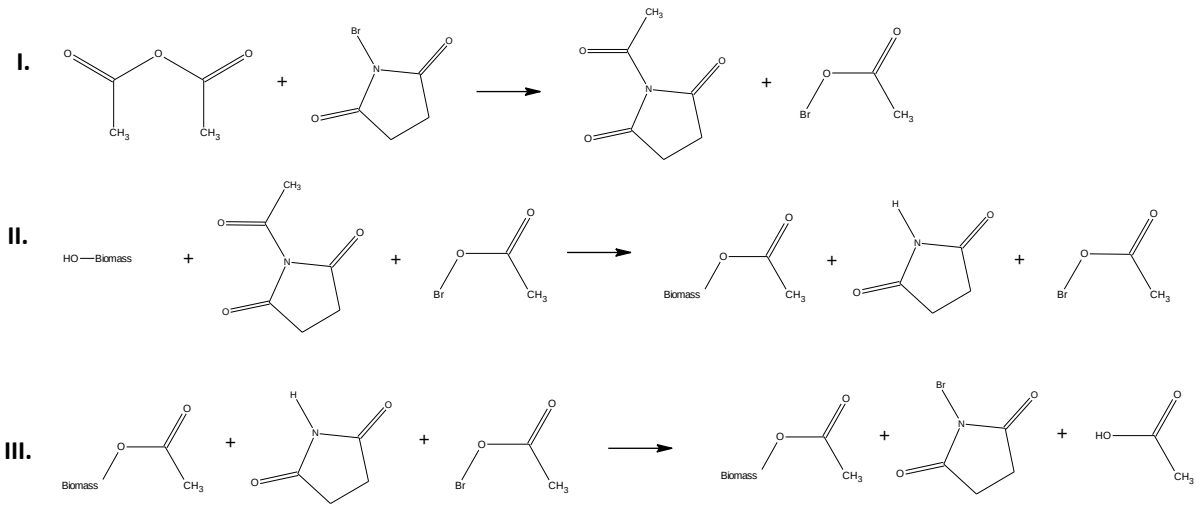

Figure 4.3 The *Non-green* Reaction Mechanism for NBS-catalysed Acetylation of Biomass, redrawn from Sun et al. (2004)

This experimental procedure involved the acetylation of biomass with acetic anhydride by implementing N-bromosuccinimide (NBS) as a catalyst. A three-step reaction achieved this acetylation. According to Sun et al. (2004), the NBS acts as Br^+-donor in order to activate the carbonyl groups of acetic anhydride (Reaction I, Figure 4.3). The highly active acetylation agent, $CH_3—CO—N—(OCCH_2CH_2CO—)$, is formed (X. F. Sun et al., 2004). This compound then reacts with the surface hydroxyl groups of the biomass (Reaction II, Figure 4.3) to produce the acetylated biomass (X. F. Sun et al., 2004). In the final step, the NBS-catalyst is recovered, and acetic acid is formed as a by-product (Reaction III, Figure 4.3).

4.2.3.2 The Experimental Details

The *non-green* biomass acetylation was carried out on CC and WS. These modifications were not statistically optimised, but the performances were instead reviewed within ranges determined from literature. The highest acetylations within this scope were selected as a reference for the optimal performance for comparison to the *green* modified samples. These modifications were conducted by varying reaction temperature between 60 and 150 °C, acetylation duration between 2 and 8 h and catalyst concentration between 0 and 4 % (w/v) NBS. Table 4.3 summarises the details specific to each experimental run.

Table 4.3 Experimental Conditions for the *Non-green* Surface Modification of Corncob and Wheat Straw in order to Improve the Hydrophobicity for Oil Sorption Applications

Run ID [a, c]	Run ID [b, c]	Temperature (°C)	Time (h)	Catalyst Concentration [d] (%)
CC-B1-0 [e]	**WS-B1-0** [e]	n/a	n/a	n/a
CC-B1-1	**WS-B1-1**	120	6	1
CC-B1-2	**WS-B1-2**	150	6	1
CC-B1-3	**WS-B1-3**	90	6	1
CC-B1-4	**WS-B1-4**	60	6	1
CC-B1-5	**WS-B1-5**	120	4	1
CC-B1-6	**WS-B1-6**	120	2	1
CC-B1-7	**WS-B1-7**	120	8	1
CC-B1-8	**WS-B1-8**	120	6	0
CC-B1-9	**WS-B1-9**	120	6	2
CC-B1-10	**WS-B1-10**	120	6	4

a – Run identification for corncob (CC), where B1 as suffix represents a *non-green* modification; **b** – Run identification for wheat straw (WS), where B1 as suffix represents a *non-green* modification; **c** – Each run performed with a constant acetic anhydride loading of 25:1 (25 mL acetic anhydride to 1 g biomass); **d** – Target N-bromosuccinimide as a mass percentage of acetic anhydride volume; **e** – Unmodified CC and WS samples for reference

In this modification, 2 g of the relevant biomass was added to 50 mL acetic anhydride (25 % (w/v) acetic anhydride) in a 250 mL round bottom flask. The appropriate amount of NBS was added (between 0 % (w/v) NBS and 4 % (w/v) NBS, as presented in Table 4.3). The specimens were added to the reflux-condenser experimental setup (defined in Chapter 3), and the samples were maintained at the required reaction temperatures (between 60 °C and 150 °C, Table 4.3) for stipulated reaction times (between 2 h and 8 h, Table 4.3).

The hot reagent was decanted, and a Buchner filter was employed to wash the retentate with 100 mL acetone and 100 mL ethanol to remove all unreacted constituents. It was then washed with hot distilled water until the filtrate attained a neutral pH (Chowdhury & Hamid, 2016), and oven-dried at 40 °C for 24 h.

4.3 Results and Discussion

4.3.1 The Characterisation of Unmodified Biomass for Oil Sorption Characterisation

The CC and WS are polymeric composites, which primarily consist of cellulose, hemicellulose and lignin (Nwadiogbu et al., 2014). The composition analyses of the starting materials (Table 4.4) were completed based on the NREL/TP-510-42620 method in order to quantify the amount of these constituents present in the samples. This composition is responsible for the physical and chemical behaviour of these feedstocks (Nwadiogbu et al., 2014). The Fourier Transform Infrared Spectroscopy (FT-IR) of the CC and WS (Figure 4.4) were studied in conjunction with the composition analyses. A summary of the assigned FT-IR peaks can be found in Appendix B (p. 145).

Table 4.4 The Composition Analyses for Corncob and Wheat Straw, compared to the Literature Biochemical Composition

Composition [a] (%)	CC	CC Literature	WS	WS Literature	Reference
Cellulose [b]	44.50 ± 0.58	33 – 42	37.15 ± 0.52	35 – 40	(Ali & Arshad, 2014; Fan et al., 2014; Pasha et al., 2013)
Hemicellulose [c]	20.23 ± 0.56	15 – 36	20.75 ± 0.24	20 – 35	(Arumugam & Anandakumar, 2016; Fan et al., 2014; Kapoor et al., 2016; Pasha et al., 2013)
Lignin [d]	15.25 ± 1.20	16 – 18	18.42 ± 2.50	10 – 19	(Fan et al., 2014; Pasha et al., 2013; Schwietzke et al., 2009; Tozluoğlu et al., 2015)
Extractives [e]	9.84 ± 0.87	5 – 9	13.83 ± 0.76	8 – 9	(Ceaser, 2019; Scatolino et al., 2013; Tozluoğlu et al., 2015)
Ash	3.09 ± 0.21	2 – 3	4.19 ± 1.56	4 – 10	(Ceaser, 2019; Fan et al., 2014; Pasha et al., 2013; Schwietzke et al., 2009; Tozluoğlu et al., 2015)
Moisture	7.05 ± 0.09	- [f]	5.37 ± 1.63	- [f]	- [f]

a – Completed based on the NREL/TP-510-42620 method for corncob (CC) and wheat straw (WS); **b –** Cellulose accounting for glucose sugars; **c –** Hemicellulose accounting for arabinose and xylose sugars; **d –** Acid-soluble and acid-insoluble lignin; **e –** Water- and ethanol extractives; **f –** Moisture content not compared to literature, since this will vary greatly between cultivation regions

Cellulose is a linear polysaccharide, formed by monomers of β-D-glucopyranose units linked by β-1,4-glycosidic bonds (Arola, 2015; Chimphango et al., 2020; Ibrahim & Mondal, 2019). These units form a repeating dimer of glucose, known as cellobiose (Hokkanen et al., 2016; Khalil et al., 2014). Strong hydrogen bonding occurs between the cellulose chains, which provides the molecules with a crystalline structure (Faik, 2013). Table 4.4 revealed that CC contained a 20 % higher fraction of cellulose when compared to WS. Additionally, the CC cellulose exceeded the typical cellulose content found in literature, as indicated in Table 4.4.

The FT-IR (Figure 4.4) confirms the presence of cellulose for both CC and WS. The peak at 1 367 cm^{-1} depicts the bending vibrations of $-CH_2$ in cellulose, and the peak at 1 027 cm^{-1} signifies the hydroxyl groups in cellulose (Hospodarova, Singovszka, & Stevulova, 2018). The C-H vibrations of cellulose occur at 1 334 cm^{-1} (Hospodarova et

al., 2018), while the stretching of the C–O–C glycosidic linkages in cellulose is shown at 1 159 cm^{-1} (Cintrón & Hinchliffe, 2015). The FT-IR peak at 896 cm^{-1} is representative of the amorphous β-glycosidic linkages in the cellulose molecules (Hospodarova et al., 2018; Reddy, Maheswari, Muzenda, Shukla, & Rajulu, 2016), while the crystalline structures of cellulose are shown at 1 430 cm^{-1}, representing the CH_2 stretching vibrations (Hospodarova et al., 2018).

The composition analyses (Table 4.4) showed that CC and WS contain equal amounts of hemicellulose. Hemicellulose exhibits an amorphous structure and contains hydrophilic saccharide side branches (Arumugam & Anandakumar, 2016; Junka, 2014). These molecules bind to the cellulosic surface non-covalently, and thereby act as an auxiliary matrix for the cellulose chains (Dufresne, 2012). The hemicellulose concentrations of the plant cell walls differ between species, region and cultivation methodology (Ceaser, 2019). However, these molecules consist mainly of repeating units of xylose, arabinose, mannose, glucose, galactose and glucuronic acid (Rowell et al., 2012). Minor occurrences of rhamnose and fucose sugars can also be present (Rowell et al., 2012). Hemicelluloses are vastly heterogeneous molecules which typically have β-1,4-D-glycan backbones named xylan, mannan and xyloglucan (Faik, 2013).

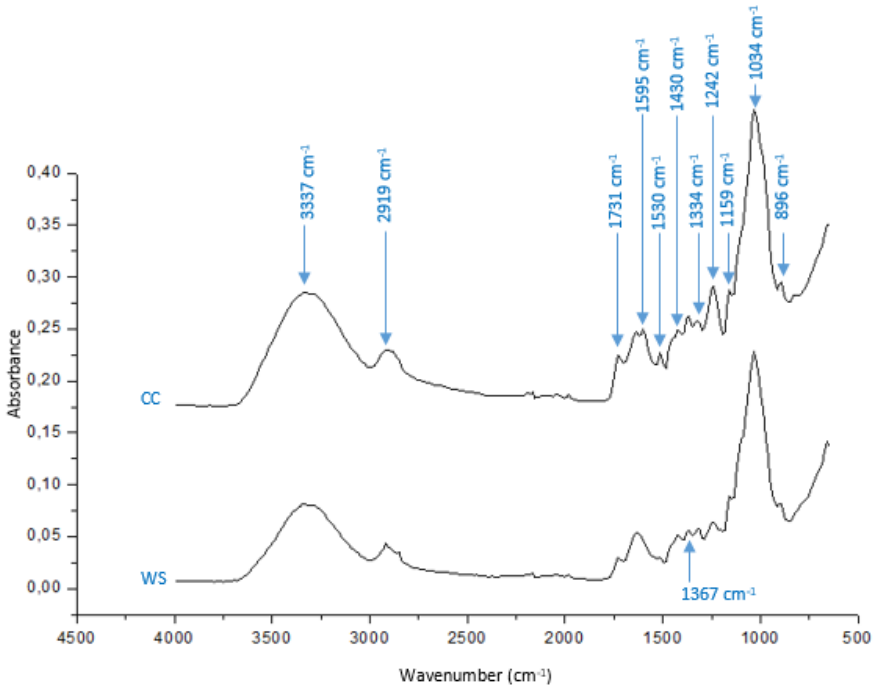

Figure 4.4 The Fourier Transform Infrared Spectra of Corncob (CC) and Wheat Straw (WS), indicating the presence of Cellulose, Hemicellulose, Lignin, Moisture and Proteins

CC and WS hemicelluloses are rich in arabinoxylans, which means the molecules have a xylan backbone with arabinose side chains (Hromádková & Ebringerová, 1995; R. C. Sun, Lawther, & Banks, 1996). Arumugam & Anandakumar (2016) correspondingly found that CC contained up to 6.0 % galactose and up to 16.0 % glucuronic acid.

WS contained up to 6.7 % galactose and 4.1 % glucuronic acid (R. C. Sun et al., 1996). Moreover, some of these monomers might be acetylated and may contain methyl-groups (Rowell et al., 2012). It is important to note that the CC and WS hemicellulose chemistry might differ in the current study. As previously mentioned, the linkages and organisation of each side chain will differ with species, climate and cultivation (Ceaser, 2019) and every individual

CC and WS will thus have a slightly different, heterogeneous sugar composition. Nevertheless, since extensive investigations and elaborate studies are necessary to isolate and determine the exact composition, the current study will assume that the hemicellulose compositions of CC and WS consist mainly of arabinoglucoronoxylan (Egüés et al., 2014; Ma et al., 2016; Schmidt, Tenkanen, Thomsen, & Woidemann, 1998) with CC having a marginally higher glucuronic acid content than WS (Arumugam & Anandakumar, 2016; R. C. Sun, 2010).

The arabinose side chains of hemicellulose are shown at 985 cm^{-1} (X. F. Sun, Sun, Fowler, & Baird, 2005), while the xylan peak of hemicellulose is represented at 1 034 cm^{-1} (Ceaser, 2019). These marginally more prominent peaks suggest that CC has slightly more arabinoxylan than WS. The linkages between lignin and hemicellulose are also depicted at 1 242 cm^{-1} (Luzi et al., 2019). This peak is higher for CC, indicating that the CC hemicellulose structures are more branched than the WS hemicellulose structures. These side branches are typically hydrophilic and are, therefore, hydrolysed with ease (Kalia et al., 2013). WS is reported to have a more linear, less-branched structure (Ceaser, 2019; X. F. Sun et al., 2005).

Lignin is an amorphous, phenolic, complex network polymer (Salajkova, 2013). It functions as structural reinforcement in plants by acting as a binder between the cellulosic and hemicellulosic fibres. It thereby provides rigidity to the plant structure (Kalia et al., 2011). Lignin protects the plant internals from external biological and physical attack and acts as a protective barrier (Salajkova, 2013). The composition analyses (Table 4.4) revealed that WS had approximately 21 % more lignin than CC, providing the WS with marginally more rigidity. The lignin structure encompasses hydroxyl groups, methoxyl groups and carbonyl groups (Kalia et al., 2011). The aromatic ring peak of lignin is shown at 1 595 cm^{-1} (Ceaser, 2019). The peak at 2 919 cm^{-1} designates the CH_2 stretching of lignin (Zheng et al., 2018) and C-H stretching of hemicellulose (Farhat et al., 2017), signifying the bonds between hemicellulose and lignin present in these samples (Rabetafika, Bchir, Blecker, Paquot, & Wathelet, 2014).

The hydroxyl stretching vibration of cellulose and hemicellulose is represented between 3 200 cm^{-1} and 3 345 cm^{-1} (Buranov & Mazza, 2010; Halal et al., 2015; Rosa et al., 2012), while the greatest peak at 3 337 cm^{-1} exemplified the inter- and intramolecular hydroxyl molecules of cellulose (Hospodarova et al., 2018; Zepic et al., 2015). The CC depicted higher hydroxyl peaks, indicating a higher potential for acetylation. The water in biomass is shown at a wavenumber of 1 633 cm^{-1} (Hospodarova et al., 2018), contributing to the moisture content of the biomass samples.

The extractives (Table 4.4) refer to other minor organic compounds consisting of phenols, terpenes, fats, resins, alcohols, and other minor constituents (Rowell et al., 2012) which can be isolated by ethanol- or water extraction. The peak at 1 530 cm^{-1} represents an amide band (Bozic et al., 2015), indicating the presence of proteins in these samples. Furthermore, the peak at 1 731 cm^{-1} indicates the presence of the ester linkages belonging to the phenolic compounds, ferulic and *p*-coumaric acids (A. Kumar, Negi, Choudhary, & Bhardwaj, 2014). The investigation of these constituents is excluded from the current study.

4.3.2 The *Green* Acetylation of Corncob and Wheat Straw by Acetic Anhydride and Iodine

4.3.2.1 The Model Development of the Degree of Substitution and Oil Sorption of the *Green* Modification of Corncob and Wheat Straw

The *green* modification was optimised on CC and WS, by implementing the CCD as determined in Section 4.2.2. The DS and OS of the CC samples are represented by runs CC-B2-1 to CC-B2-19 (Table 4.6, p. 42). Moreover, the

responses of the WS runs are denoted by WS-B2-1 to WS-B2-19. The polynomial equations predicted by Statistica 13.2 in order to model these responses are shown in Table 4.5. ANOVA analyses (Appendix D.2, p. 150) were applied to the developed models to determine the regression coefficients and analyse the statistical fit to the experimental data. These analyses indicated a regression coefficient of $R^2 = 0.7004$ for the model predicting DS of CC (Equation 4.1) and $R^2 = 0.6492$ for the model predicting OS of CC (Equation 4.2). Additionally, $R^2 = 0.7684$ was achieved for the model predicting DS of WS (Equation 4.3) and $R^2 = 0.6998$ for the model predicting OS of WS (Equation 4.4). Even though marginally low regression coefficients were accomplished, the models held an insignificant *Lack of Fit* (Table D.4 and Table D.5), indicating that the DS and OS could accurately be predicted by the developed models for both CC and WS.

Table 4.5 The Mathematical Models, Developed to Describe the Response of Degree of Substitution and Oil Sorption to the Input Parameters – Temperature, Time, and Catalyst Concentration, for the *Green* Surface Modification of Corncob and Wheat Straw

Biomass [a]	Mathematical Model [b, c]	Equation	R^2	*Lack of Fit*
CC	$Y_1 = (-2.75078) + (0.05014)X_1 + (0.23577)X_2 + (0.24658)X_3 + (-0.00018)X_1^2 + (-0.02650)X_2^2 + (-0.01164)X_3^2 + (0.00081)X_1X_2 + (-0.00131)X_1X_3 + (-0.01537)X_2X_3$	[4.1]	0.7004	Insignificant
	$Y_2 = (-27.1737) + (0.4713)X_1 + (1.8204)X_2 + (3.0979)X_3 + (-0.0017)X_1^2 + (-0.1957)X_2^2 + (-0.1870)X_3^2 + (0.0032)X_1X_2 + (-0.0130)X_1X_3 + (-0.1070)X_2X_3$	[4.2]	0.6492	Insignificant
WS	$Y_1 = (-0.755423) + (0.037821)X_1 + (-0.022567)X_2 + (0.078398)X_3 + (-0.000171)X_1^2 + (-0.024136)X_2^2 + (-0.021383)X_3^2 + (0.001619)X_1X_2 + (-0.000022)X_1X_3 + (0.025023)X_2X_3$	[4.3]	0.7684	Insignificant
	$Y_2 = (-10.9324) + (0.3738)X_1 + (-0.2611)X_2 + (1.5416)X_3 + (-0.0017)X_1^2 + (-0.2654)X_2^2 + (-0.2491)X_3^2 + (0.0186)X_1X_2 + (-0.0027)X_1X_3 + (0.1987)X_2X_3$	[4.4]	0.6998	Insignificant

a – Corncob is abbreviated as CC, while wheat straw is abbreviated as WS; **b –** Temperature (X_1), Time (X_2) and Catalyst Concentration (X_3) as input variables; **c –** Degree of Substitution (Y_1) and Oil Sorption (Y_2) as model responses

In comparison to the statistical validation, the adjusted models were experimentally validated at three random conditions (CC-B2-V1, CC-B2-V2 and CC-B2-V3 in Table 4.7 and WS-B2-V1, WS-B2-V2 and WS-B2-V3 in Table 4.8). Even though the OS values differ from the predicted values with more than 10 %, the obtained DS and OS quantities were within the 95 % confidence interval ($\alpha = 0.05$) for all validation runs. The models were, therefore, deemed acceptable to predict the DS and OS of CC and WS. The models were accepted for this purpose, but it is recommended that further tests are executed in order to attain the desired accuracy. A narrower OS prediction range is required, and higher regression coefficients should be obtained.

Table 4.6 The Degree of Substitution and Oil Sorption achieved through the *Green* Acetylation of Corncob and Wheat Straw with the Implementation of a Central Composite Design in order to Improve the Hydrophobicity for Oil Sorption Applications

Temp (°C)	Time (h)	Catalyst Loading [a, b] (%)	*Green* CC Modification			*Green* WS Modification		
			Run ID [c]	DS [d]	OS [e] (g oil /g sorbent)	Run ID [c]	DS [d]	OS [e] (g oil /g sorbent)
X_1	X_2	X_3	-	Y_1	Y_2	-	Y_1	Y_2
n/a	n/a	n/a	CC-B2-0 [f]	n/a	6.53 ± 0.47	WS-B2-0 [f]	n/a	5.90 ± 0.16
70	2	2	CC-B2-1	0.56 ± 0.09	4.16 ± 0.23	WS-B2-1	1.18 ± 0.06	8.80 ± 0.53
70	2	6	CC-B2-2	0.67 ± 0.08	5.25 ± 0.17	WS-B2-2	1.20 ± 0.06	9.38 ± 0.81
70	6	2	CC-B2-3	0.68 ± 0.08	5.10 ± 0.16	WS-B2-3	1.15 ± 0.01	8.21 ± 0.17
70	6	6	CC-B2-4	0.70 ± 0.08	5.67 ± 0.21	WS-B2-4	1.34 ± 0.05	9.87 ± 0.32
130	2	2	CC-B2-5	1.53 ± 0.11	12.59 ± 0.37	WS-B2-5	1.91 ± 0.10	15.65 ± 0.32
130	2	6	CC-B2-6	1.49 ± 0.04	11.76 ± 0.33	WS-B2-6	1.69 ± 0.13	13.49 ± 0.43
130	6	2	CC-B2-7	1.98 ± 0.31	15.49 ± 0.51	WS-B2-7	2.04 ± 0.03	17.43 ± 0.11
130	6	6	CC-B2-8	1.55 ± 0.10	11.75 ± 0.57	WS-B2-8	2.46 ± 0.02	20.55 ± 0.78
50	4	4	CC-B2-9	0.37 ± 0.01	2.99 ± 0.01	WS-B2-9	1.01 ± 0.01	7.83 ± 0.87
150	4	4	CC-B2-10	0.89 ± 0.40	6.00 ± 0.09	WS-B2-10	1.53 ± 0.16	10.97 ± 0.03
100	0.6	4	CC-B2-11	0.63 ± 0.11	6.72 ± 0.28	WS-B2-11	1.36 ± 0.09	11.22 ± 0.24
100	7.4	4	CC-B2-12	0.96 ± 0.14	6.58 ± 0.07	WS-B2-12	1.51 ± 0.08	10.46 ± 0.85
100	4	0.6	CC-B2-13	1.19 ± 0.18	6.87 ± 0.21	WS-B2-13	1.54 ± 0.04	11.36 ± 0.33
100	4	7.4	CC-B2-14	0.74 ± 0.12	6.63 ± 0.13	WS-B2-14	1.39 ± 0.16	10.70 ± 0.12
100	4	4	CC-B2-15	1.61 ± 0.06	13.42 ± 0.42	WS-B2-15	1.75 ± 0.04	15.20 ± 0.77
100	4	4	CC-B2-16	1.38 ± 0.12	11.48 ± 0.31	WS-B2-16	1.87 ± 0.10	15.58 ± 0.97
100	4	4	CC-B2-17	1.32 ± 0.07	10.05 ± 0.08	WS-B2-17	1.88 ± 0.04	15.65 ± 0.56
100	4	4	CC-B2-18	1.10 ± 0.02	9.00 ± 0.17	WS-B2-18	2.10 ± 0.02	17.63 ± 1.58
100	4	4	CC-B2-19	1.23 ± 0.09	10.32 ± 0.28	WS-B2-19	1.73 ± 0.05	13.65 ± 0.50

a – Each run performed with a constant acetic anhydride loading of 25:1 (25 mL acetic anhydride to 1 g biomass); **b –** Target iodine as a weight percentage of biomass; **c –** Run identification for corncob (CC) and wheat straw (WS), where B2 as suffix represents a *green* modification; **d –** Degree of Substitution is abbreviated as DS; **e –** Oil Sorption is abbreviated as OS; **f –** Unmodified CC and WS samples for reference

Table 4.7 A Comparison of the Predicted and Experimental Values of Degree of Substitution and Oil Sorption for the Model Validation of the *Green* Corncob Surface Modification

Run [a]	Temperature (°C)	Time (h)	Catalyst Concentration [b, c] (%)	Model Prediction	Experimental Value	Error (%)
DS (Equation 4.1)						
CC-B2-V1	80	2	3	0.82 [d]	0.76 ± 0.07	7.39
CC-B2-V2	100	8	5	0.95 [e]	0.93 ± 0.09	2.05
CC-B2-V3	130	5	1	1.72 [f]	1.56 ± 0.17	8.87
OS (g oil/g sorbent) (Equation 4.2)						
CC-B2-V1	80	2	3	6.77 [g]	5.38 ± 0.48	20.58
CC-B2-V2	100	8	5	7.45 [h]	6.36 ± 0.20	14.58
CC-B2-V3	130	5	1	12.07 [i]	15.33 ± 0.45	27.03

a – Run identification for corncob (CC), where B2 as suffix represents a *green* modification
b – Each run performed with a constant acetic anhydride loading of 25:1 (25 mL acetic anhydride to 1 g biomass)
c – Target iodine as a weight percentage of biomass
d – Predicted that degree of substitution (DS) could range from 0.53 to 1.11 at these conditions with 95 % confidence
e – Predicted that DS could range from 0.36 to 1.54 at these conditions with 95 % confidence
f – Predicted that DS could range from 1.22 to 2.21 at these conditions with 95 % confidence
g – Predicted that oil sorption (OS) could range from 4.20 to 9.35 g oil/g sorbent at these conditions with 95 % confidence
h – Predicted that OS could range from 2.21 to 12.68 g oil/g sorbent at these conditions with 95 % confidence
i – Predicted that OS could range from 7.69 to 16.44 g oil/g sorbent at these conditions with 95 % confidence

Table 4.8 A Comparison of the Predicted and Experimental Values of Degree of Substitution and Oil Sorption for the Model Validation of the *Green* Wheat Straw Surface Modification

Run [a]	Temperature (°C)	Time (h)	Catalyst Concentration [b, c] (%)	Model Prediction	Experimental Value	Error (%)
DS (Equation 4.3)						
WS-B2-V1	40	2	2	0.64 [d]	0.62 ± 0.16	3.96
WS-B2-V2	95	1	1	1.48 [e]	1.45 ± 0.09	2.44
WS-B2-V3	100	2	1	1.61 [f]	1.47 ± 0.10	8.76
OS (g oil/g sorbent) (Equation 4.4)						
WS-B2-V1	40	2	2	3.80 [g]	4.63 ± 0.36	21.93
WS-B2-V2	95	1	1	11.29 [h]	11.36 ± 0.15	0.57
WS-B2-V3	100	2	1	12.54 [i]	13.72 ± 0.66	9.34

a – Run identification for wheat straw (WS), where B2 as suffix represents a *green* modification
b – Each run performed with a constant acetic anhydride loading of 25:1 (25 mL acetic anhydride to 1 g biomass)
c – Target iodine as a weight percentage of biomass
d – Predicted that degree of substitution (DS) could range from 0.01 to 1.28 at these conditions with 95 % confidence
e – Predicted that DS could range from 1.00 to 1.97 at these conditions with 95 % confidence
f – Predicted that DS could range from 1.25 to 1.96 at these conditions with 95 % confidence
g – Predicted that oil sorption (OS) could range from 0 to 9.99 g oil/g sorbent at these conditions with 95 % confidence
h – Predicted that OS could range from 6.59 to 15.99 g oil/g sorbent at these conditions with 95 % confidence
i – Predicted that OS could range from 9.08 to 16.01 g oil/g sorbent at these conditions with 95 % confidence

4.3.2.2 The Effect of Temperature, Time and Catalyst Concentration on the Degree of Substitution and Oil Sorption of the *Green* Modification of Corncob and Wheat Straw

Due to the complex nature of the CC and WS, variations in acetylation occurred at different combinations of reaction conditions (Nwadiogbu et al., 2014). The linear- and quadratic effects of temperature, time and catalyst concentration on the DS and OS of CC and WS via the *green* surface modification were examined by studying the ANOVA analyses (Appendix D.2, p. 150), the Pareto charts (Figure 4.5) and the response surface plots (Figure 4.6 and Figure 4.7). The DS and OS for the definitive feedstocks demonstrate analogous trends. This occurrence is expected, since the increased acetyl content achieved through acetylation should result in an amplified non-polarity of the fibre surface, leading to an enhanced affinity for non-polar oil particles (Pruitt, 2017; She et al., 2010).

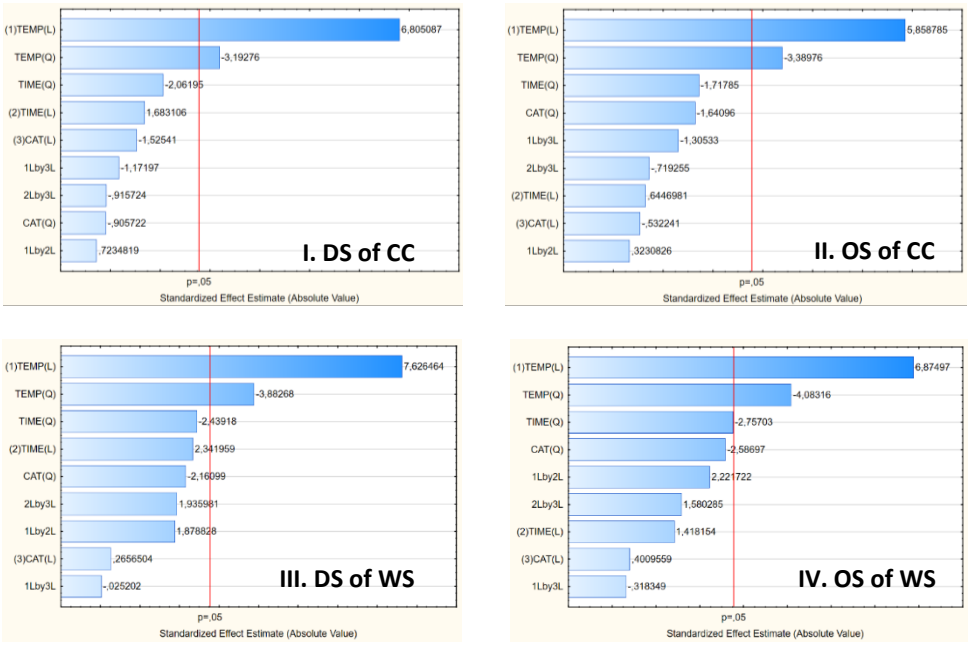

Figure 4.5 The Pareto Charts of Standardised Linear (L) and Quadratic (Q) Effects of Temperature (1), Time (2) and Catalyst Concentration (3) on the Degree of Substitution (DS) and Oil Sorption (OS) of Corncob (CC) and Wheat Straw (WS) via the *Green* Surface Modification Reaction

The effects of temperature and time have been investigated at a constant catalyst concentration (4 % (w/w) iodine) in Figure 4.6 I – II for CC and Figure 4.7 I – II for WS. These response surface plots reflect the relationship between the parameters established by the ANOVA analyses (Appendix D.2, p. 150) and Pareto charts (Figure 4.5). The Pareto charts depicted that the linear- and quadratic effects of temperature had significant effects on the DS ($p = 2.44 \times 10^{-3}$ and $p = 3.31 \times 10^{-2}$) and OS ($p = 4.24 \times 10^{-3}$ and $p = 2.75 \times 10^{-2}$) of CC. Moreover, the linear- and quadratic effects of temperature exhibited significant influences on the DS ($p = 1.59 \times 10^{-3}$ and $p = 0.02$) and OS ($p = 2.35 \times 10^{-3}$ and $p = 1.51 \times 10^{-2}$) of WS. This assertion was confirmed in the study conducted by Li et al. (2009), where an increase in temperature demonstrated the greatest effect on the degree of acetylation of cellulose at a reaction time of 15 minutes, under 400 W microwave irradiation and 5 mol % iodine.

I. (at 4 % (w/w) Iodine)

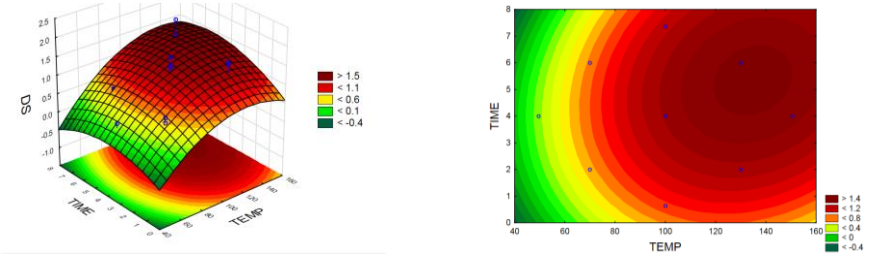

II. (at 4 % (w/w) Iodine)

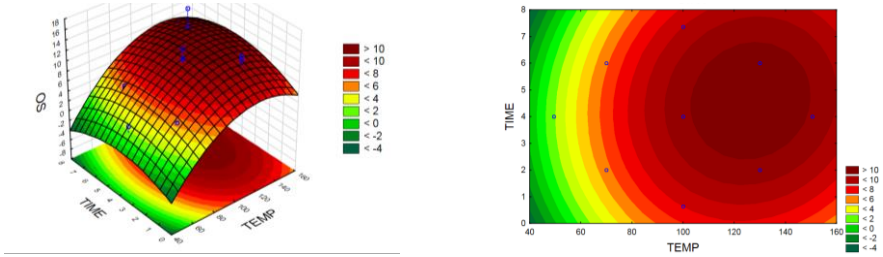

III. (at 4 h)

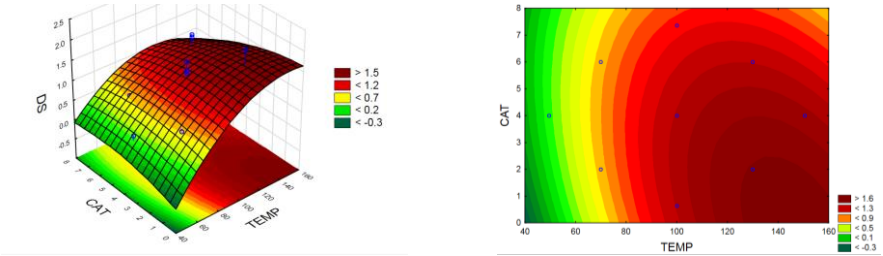

IV. (at 4 h)

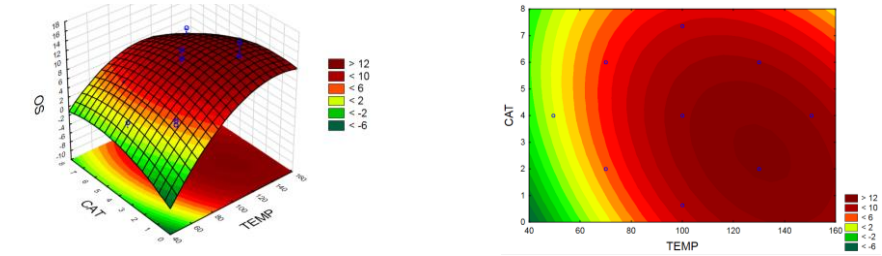

V. (at 100 °C)

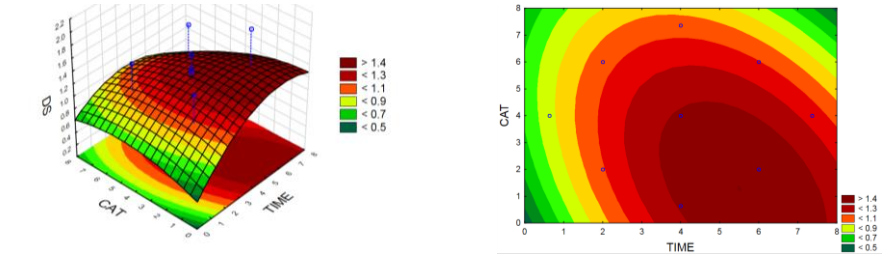

VI. (at 100 °C)

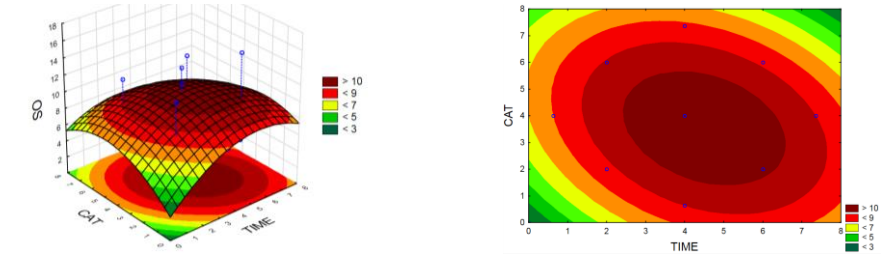

Figure 4.6 The 2-Dimensional and 3-Dimensional Response Surface Plots for the Effects of Temperature (°C), Time (h) and Iodine Catalyst Concentration (% (w/w)) on the Degree of Substitution (DS) and Oil Sorption (OS) of Corncob via the *Green* Surface Acetylation

I. (at 4 % (w/w) Iodine)

II. (at 4 % (w/w) Iodine)

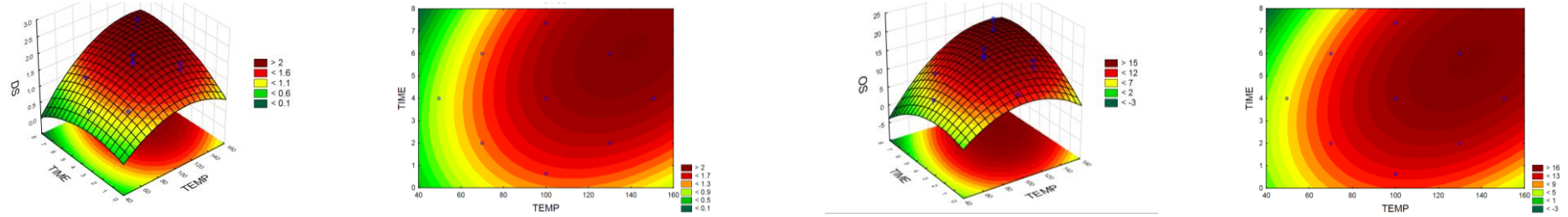

III. (at 4 h)

IV. (at 4 h)

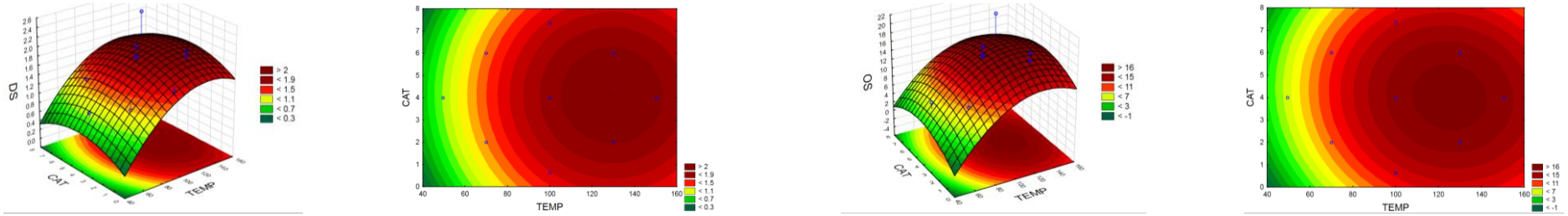

V. (at 100 °C)

VI. (at 100 °C)

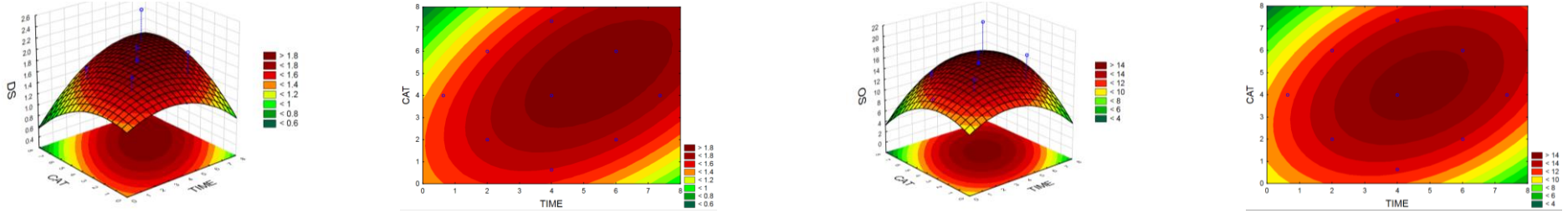

Figure 4.7 The 2-Dimensional and 3-Dimensional Response Surface Plots for the Effects of Temperature (°C), Time (h) and Iodine Catalyst Concentration (% (w/w)) on the Degree of Substitution (DS) and Oil Sorption (OS) of Wheat Straw via the *Green* Surface Acetylation

The linear- and quadratic effects of time were determined to have a negligible influence on the DS ($p = 0.17$ and $p = 0.11$) and OS ($p = 0.55$ and $p = 0.16$) of CC. These effects correspondingly depicted an insignificant impact on the DS ($p = 0.08$ and $p = 0.07$) and OS ($p = 0.23$ and $p = 0.05$) of WS.

When studying Figure 4.6 I – II and Figure 4.7 I – II, it is apparent that low DS and OS values were reached by WS and CC, irrespective of reaction time at temperatures lower than 70 °C. An escalation in temperature in excess of 70 °C resulted in the initiation of increasing acetylation. Both feedstocks favoured higher reaction temperatures and extended reaction durations for this acetylation methodology. For CC, the highest peak in DS was reached at approximately 120 °C to 150 °C for reaction times of roughly 4 h to 7 h at a catalyst concentration of 4 % (w/w) iodine. However, it can be noted that WS required slightly higher reaction temperatures of approximately 130 °C to 150 °C, and marginally longer reaction times, from 6 h to 7 h, in order to achieve the optimal DS with this feedstock.

The chemical structures in Appendix D.3 (p. 155) reveal that all three major components of lignocellulosic biomass, namely cellulose, hemicellulose and lignin, contain abundant hydrophilic hydroxyl groups (Onwuka et al., 2019). Conversely, since these chemical structures are interconnected in a matrix, some of the present hydroxyl groups are not accessible to take part in acetylation reactions (Rowell, 2014). The hydroxyl groups exhibit an order of reactivity (Onwuka et al., 2019). The first point of contact will occur with the protective lignin barrier (Nwadiogbu et al., 2014; Salajkova, 2013), and the accessible phenolic, benzylic or alcoholic hydroxyls of the lignin will, therefore, be acetylated initially (Nwadiogbu et al., 2014; Rowell, 2014). Lignin theoretically provides an average of 1.2 hydroxyl groups per nine-carbon unit available for acetylation (Rowell, 2014; Rowell et al., 1994). However, since there are multiple variations of the lignin structure, these will differ between sources (Lu et al., 2017). Sufficient temperature and time need to be provided in order to achieve ample diffusion of the reactants into the cell walls, thereby coming into contact with the reactive hydroxyls on the hemicellulose molecules (Rowell, 2014). Hemicellulose has an average of two reactive hydroxyls available per sugar unit (Egüés et al., 2014).

The composition analyses (Table 4.4) revealed that WS contains approximately 21 % more lignin than CC, providing the WS with marginally more rigidity. The WS thus requires slightly higher reaction temperatures and longer reaction times to reach significant diffusion and molecular swelling in order to make contact with the hydroxyl groups in the hemicellulose. Additional temperature and time are then required to attain a more considerable extent of swelling to reach the hydroxyl groups of cellulose. Each AGU of cellulose has three reactive hydroxyl groups (Tupa et al., 2015). Due to the crystallinity of these cellulose chains, provided by the linear packing and very strong intermolecular Van der Waal's forces (Faik, 2013), the hydroxyls in the crystalline regions of cellulose are not typically available for acetylation (Rowell, 2014). Only the hydroxyls in the non-crystalline, amorphous regions are characteristically available, provided that enough molecular swelling is achieved to make them accessible by the reactants (Rowell et al., 2012).

Table 4.4 revealed that CC contained a 20 % higher fraction of cellulose when compared to WS. Additionally, the FT-IR analyses (Figure 4.4) exposed that CC cellulose had a higher amorphous peak at 896 cm^{-1}, indicating that the cellulose in CC will be easier to acetylate, provided that enough reactants are present and ample swelling has occurred to bring the reactive hydroxyl groups in contact with the acetylation chemicals.

Figure 4.6 III – IV and Figure 4.7 III – IV suggests that exceedingly high temperatures are favourable for sufficient diffusion and consequently higher acetylation. However, the cooling in the condenser was accomplished by recirculating water at room temperature. It is unknown whether the current experimental setup will be able to condense the vapours at amplified temperatures exceeding 150 °C since a chemical coolant is not employed in the condenser.

The ANOVA analyses (Appendix D.2, p. 150) disclosed that the linear- and quadratic effects of the catalyst concentration were determined to have an inconsequential influence on the DS ($p = 0.20$ and $p = 0.42$) and OS ($p = 0.62$ and $p = 0.18$) of CC. These effects also depicted a negligible impact on the DS ($p = 0.80$ and $p = 0.10$) and OS ($p = 0.71$ and $p = 0.06$) of WS. Moreover, no significant interactions occurred between temperature, time and catalyst concentration ($p > 0.05$).

The effects of the catalyst concentration and temperature have been investigated at a constant time of 4 h in Figure 4.6 III – IV for CC and Figure 4.7 III – IV for WS. Furthermore, the influences of the catalyst concentration and time have been displayed at a constant temperature of 100 °C in Figure 4.6 V – VI for CC and Figure 4.7 V – VI for WS. These analyses revealed that CC required a lower catalyst concentration than WS. Higher catalyst concentrations resulted in lower performances for CC. When considering the acetylation reaction in Figure 4.2, it can be noted that an acetic acid molecule is produced for each hydroxyl that is replaced by an acetyl (Li et al., 2009). Therefore, as the reaction commences, the concentration of acid in the reaction environment becomes continuously increased. If this acidic concentration becomes too high, the cellulose backbone and hemicellulose constituents of the biomass will start to degrade (Li et al., 2009).

The composition analyses (Table 4.4) depicted that CC and WS contain equal amounts of hemicellulose. The linkages between lignin and hemicellulose are illustrated at 1 242 cm^{-1} (Luzi et al., 2019) in the FT-IR spectra (Figure 4.4). As mentioned in Section 4.3.1, this peak is higher for CC, indicating that the CC hemicellulose structures are more branched than the WS hemicellulose structures. These side branches are typically hydrophilic and are thus hydrolysed with ease (Kalia et al., 2013). WS is reported to have a more linear, less-branched structure (Ceaser, 2019; X. F. Sun et al., 2005). For this reason, CC will be more easily hydrolysed in a rapidly increasing acidic environment. The CC, therefore, requires lower amounts of catalyst and shorter reaction times, in order to maintain a slower acetylation rate than WS, thereby preventing acid hydrolyses. Moreover, the 21 % extra lignin possessed by WS (Table 4.4) provides this feedstock with more rigidity and protection against acid hydrolyses.

In conclusion, CC has a higher potential for acetylation due to the higher cellulose content and a more prominent occurrence of amorphous cellulose molecules. Conversely, CC possesses an exceedingly branched hemicellulose structure and less protective lignin. The CC is subsequently more vulnerable to acid hydrolyses and consequent degradation. The CC thus requires a lower catalyst concentration and shorter reaction times for sufficient acetylation without degradation.

4.3.2.3 The Optimal *Green* Modification of Corncob and Wheat Straw

Statistica 13.2 was implemented to develop desirability plots (Figure 4.8) in order to determine at which combination of reaction conditions the highest DS and OS can be achieved for CC and WS, respectively. The reaction

conditions for the optimal modification of CC was established as 150.5 °C, 5.7 h and 0.6 % (w/w) iodine. Conversely, the reaction conditions for the optimal modification of WS was predicted as 150.5 °C, 7.4 h and 5.7 % (w/w) iodine.

I.

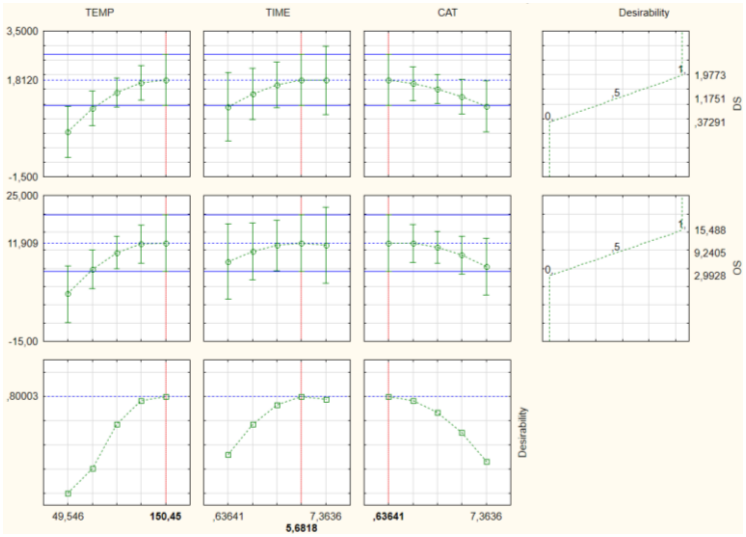

II.

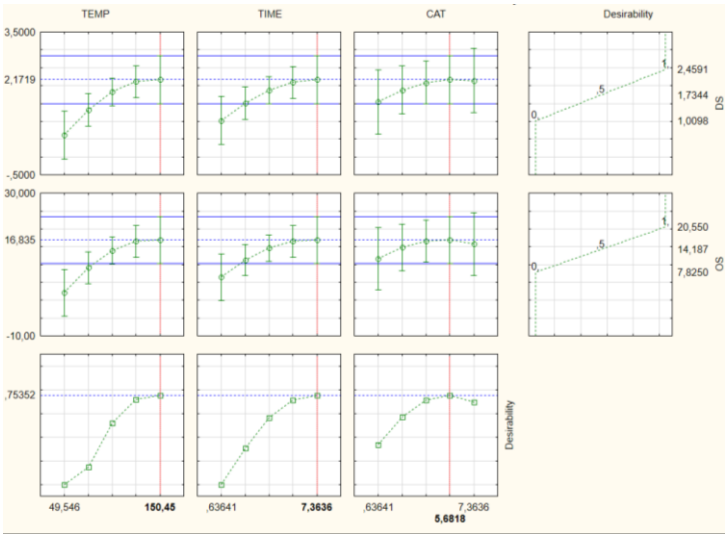

Figure 4.8 Profiles for the Predicted Values and Desirability Plots of the *Green* Modification of **I.** Corncob and **II.** Wheat Straw

These reaction conditions were applied to CC and WS to compare the optimal experimental performance to the DS and OS values predicted by the regression models. The results depicted in Table 4.9 demonstrate that the values for the DS and OS of CC and WS fall within the 95 % confidence interval ($\alpha = 0.05$) of the values predicted by the models.

As with the validation experiments completed on the models (Table 4.7 and Table 4.8), it can be noted that the models predict extensively wide ranges for the optimal OS and DS for both CC and WS. In order to develop more robust models, more experiments are recommended for future investigations.

Table 4.9 A Comparison of the Predicted and Experimental Degree of Substitution and Oil Sorption for the Optimal *Green* Modification of Corncob and Wheat Straw

Run [a]	Temperature (°C)	Time (h)	Catalyst Concentration [b, c] (%)	Model Prediction	Experimental Value	95 % Confidence Interval
DS						
CC-B2-OPT	150.5	5.7	0.6	1.81 [d]	2.14 ± 0.19	Within
WS-B2-OPT	150.5	7.4	5.7	2.17 [e]	2.38 ± 0.09	Within
OS (g oil/g sorbent)						
CC-B2-OPT	150.5	5.7	0.6	11.93 [f]	19.25 ± 0.23	Within
WS-B2-OPT	150.5	7.4	5.7	16.84 [g]	18.99 ± 1.50	Within

a – Run identification for corncob (CC) and wheat straw (WS), where B2 as suffix represents a *green* modification
b – Each run performed with a constant acetic anhydride loading of 25:1 (25 mL acetic anhydride to 1 g biomass)
c – Target iodine as a weight percentage of biomass
d – The 95 % confidence interval for the prediction of degree of substitution (DS) at these conditions is 0.94 – 2.68 for CC
e – The 95 % confidence interval for the prediction of DS at these conditions is 1.50 – 2.85 for WS
f – The 95 % confidence interval for the prediction of oil sorption (OS) at these conditions is 4.26 – 19.60 g oil/g sorbent for CC
g – The 95 % confidence interval for the prediction of OS at these conditions is 10.17 – 23.48 g oil/g sorbent for WS

The optimal DS of 2.14 ± 0.19 and optimal OS of 19.25 ± 0.23 g/g achieved for CC at 150.5 °C, 5.7 h and 0.6 % (w/w) iodine is compared to the optimal DS of 2.38 ± 0.09 and optimal OS of 18.99 ± 1.50 g/g accomplished for WS at 150.5 °C, 7.4 h and 5.7 % (w/w) iodine, in Figure 4.9. This *green* modification attained statistically similar DS ($p = 0.06$) and OS ($p = 0.88$) for CC and WS despite the different reaction conditions for each sample. The OS prior to modification was also not statistically different ($p = 0.21$) for CC and WS. A significant increase ($p = 2.15 \times 10^{-4}$) in OS was achieved by the implementation of these acetylations.

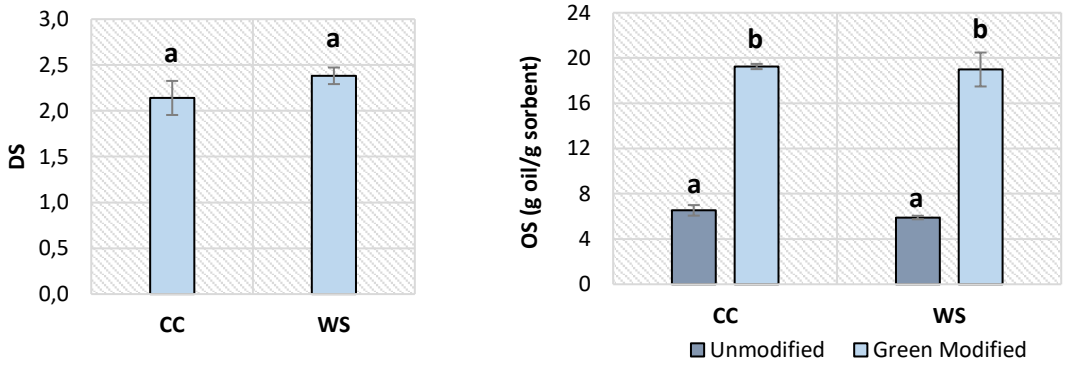

Figure 4.9 The Degree of Substitution (DS) and Oil Sorption (OS) achieved via the Optimised *Green* Surface Modification at 150.5 °C, 5.7 h and 0.6 % (w/w) Iodine for Corncob (CC) at 150.5 °C, 7.4 h and 5.7 % (w/w) Iodine for Wheat Straw (WS)

In the study conducted by Li et al. (2009) on cellulose, optimisation was not performed, but the DS attained at different single-factor conditions were instead tested. The highest results within their tested range were reached at 130 °C, 40 minutes, 400 W microwave irradiation and 5 mol % iodine, where a DS of 1.9 was achieved (Li et al., 2009). By implementing a CCD in order to include the effects of interaction between temperature, time and catalyst concentration, the current study managed to increase the DS by 13 – 25 % for this *green* surface modification (Table 4.10).

Table 4.10 The Degree of Substitution Attained by Li et al. (2009) on Cellulose under Microwave Irradiation, Compared to the Optimised Acetylation Achieved with Corncob and Wheat Straw

Feedstock [a]	Temp (°C)	Time (min)	Iodine (%)	Microwave (W)	DS [d]	Reference
Cellulose	130	40	5 [b]	400	1.9	(Li et al., 2009)
CC	150.5	5.7	0.6 [c]	-	2.14 ± 0.19	Table 4.9
WS	150.5	7.4	5.7 [c]	-	2.38 ± 0.09	Table 4.9

a – Corncob is abbreviated as CC, and wheat straw is abbreviated as WS; **b** – Performed with a 5 mol % iodine concentration; **c** – Target iodine as a weight percentage of biomass; **d** – Degree of Substitution is abbreviated as DS

When comparing the reaction conditions utilised by Li et al. (2009) on cellulose, it can be noted that the acetylation on the CC and WS biomass incurred higher reaction temperatures and longer reaction times for the optimal modification (Table 4.10). As previously discussed, the cellulose in lignocellulosic biomass is protected by an auxiliary matrix of hemicellulose and lignin, which provides rigidity to the biomass and protects the cells from physical decay (Dufresne, 2012; Salajkova, 2013). Therefore, in order to expose the reactive hydroxyl groups on the hemicellulose and cellulose surface and to consequently make them available to take place in acetylation reactions, longer reaction times and higher temperatures are required to accomplish significant swelling of the fibres and diffusion of the reactants into the plant internals (Huang et al., 2014). The protective lignin layer needs to be overcome. Moreover, the higher DS attained with the lignocellulosic biomass can be attributed to the additional hydroxyl groups provided by the lignin and hemicellulose molecules available for acetylation (Nwadiogbu et al., 2014). The potential for acetylation of biomass is, therefore, greater than the individual cellulose molecules acetylated by Li et al. (2009).

4.3.3 The *Non-green* Acetylation of Corncob and Wheat Straw by Acetic Anhydride and N-Bromosuccinimide

4.3.3.1 The Degree of Substitution and Oil Sorption of Modified and Unmodified Corncob and Wheat Straw

The responses of DS and OS achieved by the traditional *non-green* modification at the specified reaction conditions are displayed in Table 4.11. These experiments were accomplished by varying the reaction temperature between 60 and 150 °C, acetylation duration from 2 to 8 h and the catalyst concentration between 0 and 4 % (w/v) NBS. Figure 4.10 and Figure 4.11 depict the DS and FT-IR spectra of each experimental run.

The effect of temperature was investigated by performing reactions on CC (CC-B1-1, CC-B1-2, CC-B1-3 and CC-B1-4) and WS (WS-B1-1, WS-B1-2, WS-B1-3 and WS-B1-4) at a set time of 6 h and a constant catalyst concentration of 1 % (w/v) NBS. According to Zepic et al. (2015), three primary ester bands can be identified, namely the carbonyl C=O stretching of the ester at 1 740 cm^{-1}; the C-H band in $–O(C=O)-CH_3$ at 1 369 cm^{-1} and the C-O stretching band of the acetyl group at 1 234 cm^{-1}. The hydroxyl stretching band and hydroxyl in-plane bending bands of the samples are shown at 3 337 cm^{-1}, 1 337 cm^{-1} and 1 310 cm^{-1} (Zepic et al., 2015). The CC and WS demonstrated comparable reactions to a variation in temperature. The FT-IR for CC and WS (Figure 4.10 II and Figure 4.11 II) illustrate intensifying ester peak intensities when increasing the temperature from 60 °C to 120 °C, with an accompanied drastic reduction in hydroxyl peaks, indicating successful acetylation. A further escalation to 150 °C transpired in lowered ester peaks. Analogously, CC and WS showed a significant escalation in DS ($p = 5.65 \times 10^{-4}$ and $p = 1.52 \times 10^{-6}$) when increasing the temperature from 60 °C to 90 °C (Figure 4.10 I and Figure 4.11 I). A further escalation to

120 °C revealed a significant incline ($p = 3.15 \times 10^{-4}$ and $p = 7.46 \times 10^{-6}$) in DS for both CC and WS. Nevertheless, the DS achieved at 150 °C was lower ($p = 0.01$ and $p = 1.06 \times 10^{-5}$) than the DS attained at 120 °C for these feedstocks.

It was established in the discussion about the *green* acetylation (Section 4.3.2.2) that cellulose, hemicellulose and lignin contain abundant hydrophilic hydroxyl groups (Onwuka et al., 2019) as demonstrated in Appendix D.3 (p. 155). These chemical structures are interconnected in a matrix, resulting in some of the hydroxyl groups being inaccessible (Rowell, 2014) to the reactants during the acetylation reaction. The first point of contact between the reactants and the biomass occurs with the lignin, and these hydroxyls are thus acetylated first (Nwadiogbu et al., 2014; Rowell, 2014). In order for the reactants to reach the hydroxyls on the hemicellulose embedded in the lignin, sufficient temperature and time need to be provided in order to realise ample diffusion of the reactants into the cell walls (Rowell, 2014). Increasing diffusion is necessary to ensure contact of the reactants with the hydroxyl groups on the cellulose molecules (Rowell et al., 2012). Subsequently, sufficient diffusion occurred at 120 °C for both CC and WS. However, when considering the acetylation reaction in Figure 4.3, it can be noted that an acetic acid molecule is produced for each hydroxyl that is replaced by an acetyl (X. F. Sun et al., 2004). It was established that the cellulose backbone and hemicellulose constituents of the biomass undergo hydrolysis in increasingly acidic environments (Li et al., 2009). The acetic acid overcomes the protective lignin layer and hydrolyses the β-D-glucopyranose units, which form the cellulose backbone (Hokkanen et al., 2016; Khalil et al., 2014).

Table 4.11 The Degree of Substitution and Oil Sorption of Modified and Unmodified Corncob and Wheat Straw achieved though the *Non-green* Acetylation by Acetic Anhydride and NBS in order to Improve the Hydrophobicity for Oil Sorption Applications

			***Non-green* CC Acetylation**			***Non-green* WS Acetylation**		
Temp (°C)	**Time (h)**	**Catalyst Loading [a, b] (%)**	**Run ID [c]**	**DS [d]**	**OS [e] (g oil /g sorbent)**	**Run ID [c]**	**DS [d]**	**OS [e] (g oil /g sorbent)**
n/a	n/a	n/a	CC-B1-0 [f]	n/a	6.53 ± 0.47	WS-B1-0 [f]	n/a	5.90 ± 0.16
120	6	1	CC-B1-1	2.76 ± 0.48	20.93 ± 0.81	WS-B1-1	2.19 ± 0.05	18.12 ± 0.18
150	6	1	CC-B1-2	1.87 ± 0.13	16.51 ± 0.44	WS-B1-2	1.74 ± 0.05	14.45 ± 0.64
90	6	1	CC-B1-3	0.96 ± 0.07	8.01 ± 0.12	WS-B1-3	1.62 ± 0.06	13.72 ± 0.18
60	6	1	CC-B1-4	0.36 ± 0.17	6.29 ± 0.55	WS-B1-4	0.96 ± 0.03	7.00 ± 0.22
120	4	1	CC-B1-5	1.81 ± 0.07	14.26 ± 0.74	WS-B1-5	1.91 ± 0.06	15.53 ± 0.59
120	2	1	CC-B1-6	0.41 ± 0.14	6.77 ± 1.24	WS-B1-6	0.97 ± 0.10	7.28 ± 0.40
120	8	1	CC-B1-7	1.90 ± 0.07	16.66 ± 0.48	WS-B1-7	1.93 ± 0.06	15.88 ± 0.31
120	6	0	CC-B1-8	0.54 ± 0.11	4.74 ± 0.87	WS-B1-8	1.33 ± 0.08	9.07 ± 0.12
120	6	2	CC-B1-9	2.48 ± 0.31	19.28 ± 0.37	WS-B1-9	2.06 ± 0.08	16.70 ± 0.57
120	6	4	CC-B1-10	0.66 ± 0.15	5.61 ± 0.27	WS-B1-10	1.55 ± 0.09	12.55 ± 0.78

a – Each run performed with a constant acetic anhydride loading of 25:1 (25 mL acetic anhydride to 1 g biomass)
b – Target N-bromosuccinimide as a mass percentage of acetic anhydride volume
c – Run identification for corncob (CC) and wheat straw (WS), where B1 as suffix represents a *non-green* modification
d – Degree of Substitution is abbreviated as DS
e – Oil Sorption is abbreviated as OS
f – Unmodified CC and WS samples for reference

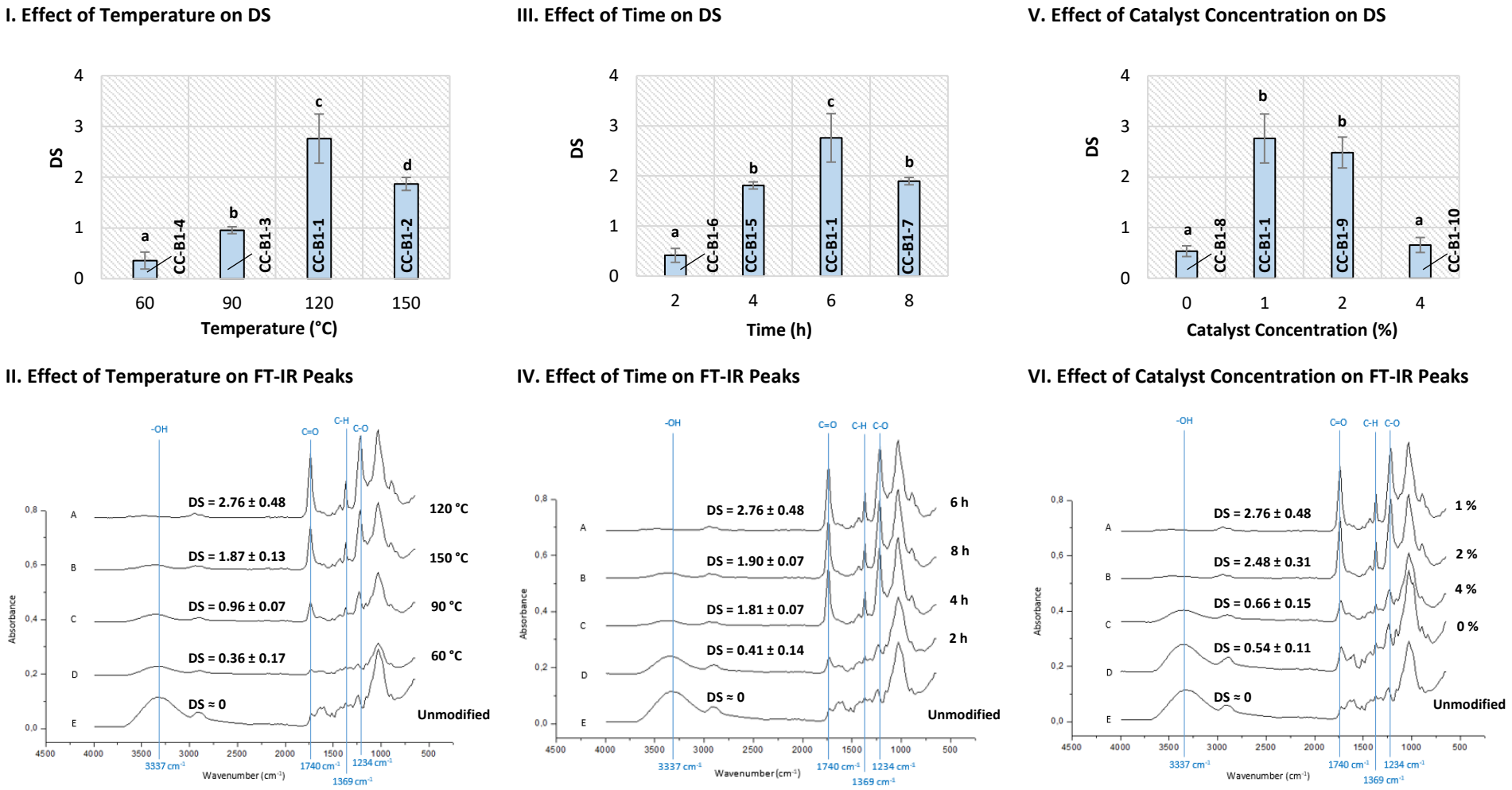

Figure 4.10 The Effects of Temperature, Time and Catalyst Concentration on the Degree of Substitution (DS) and Fourier Transform Infrared (FT-IR) Spectra of the *Non-green* Acetylated Corncob at **I., II.** Constant Time and Catalyst Concentration (6 h, 1 % (w/v) NBS); **III., IV.** Constant Temperature and Catalyst Concentration (120 °C, 1 % (w/v) NBS); **V., VI.** Constant Temperature and Reaction Time (120 °C, 6 h)

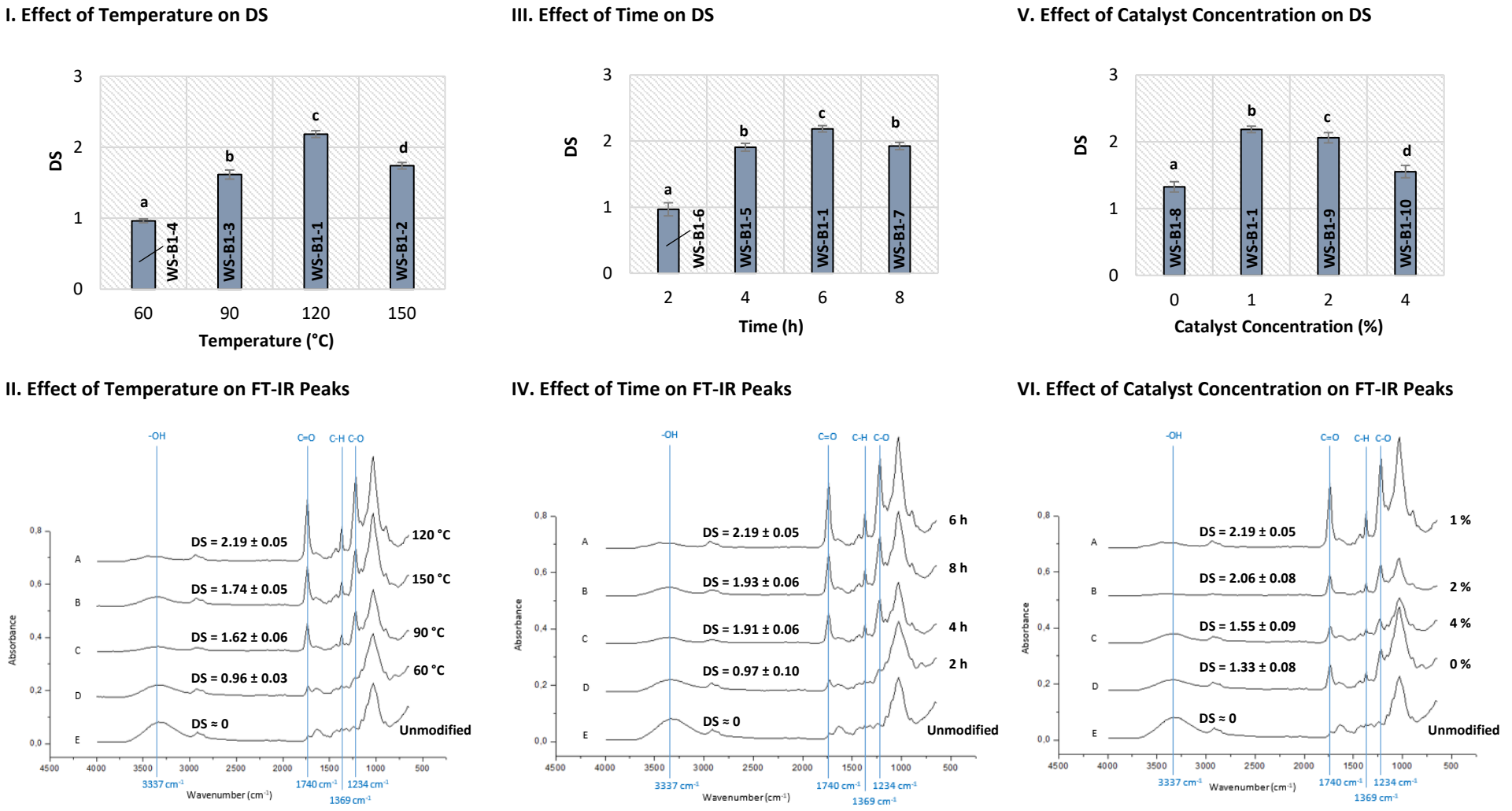

Figure 4.11 The Effects of Temperature, Time and Catalyst Concentration on the Degree of Substitution (DS) and Fourier Transform Infrared (FT-IR) Spectra of the *Non-green* Acetylated Wheat Straw at **I., II.** Constant Time and Catalyst Concentration (6 h, 1 % (w/v) NBS); **III., IV.** Constant Temperature and Catalyst Concentration (120 °C, 1 % (w/v) NBS); **V., VI.** Constant Temperature and Reaction Time (120 °C, 6 h)

The intramolecular Van der Waal's forces between glucose units in the cellulose molecules are then broken, and the hemicellulose structures undergo acid degradation (Kalia et al., 2013). Since cellulose and hemicellulose provide the biomass fibres with their three-dimensional structure (Dufresne, 2012), the samples will have a lowered OS capacity if these molecules are hydrolysed. This phenomenon started occurring at 150 °C for both CC and WS.

WS presented a marginally higher DS at 150 °C when compared to CC (Figure 4.10 I and Figure 4.11 I). Although CC and WS were determined to contain similar amounts of hemicellulose (Table 4.4), it was established that the WS hemicelluloses had a more linear, less-branched structure (Ceaser, 2019; X. F. Sun et al., 2005). The branched nature of the CC hemicelluloses provided this feedstock with a greater vulnerability towards acid hydrolyses (Kalia et al., 2013). Furthermore, WS contained a 21 % higher lignin portion (Table 4.4), which rendered this feedstock with higher rigidity.

The effect of time was studied by performing reactions on CC (CC-B1-1, CC-B1-5, CC-B1-6 and CC-B1-7) and WS (WS-B1-1, WS-B1-5, WS-B1-6 and WS-B1-7) at a set temperature of 120 °C and a constant catalyst concentration of 1 % (w/v) NBS. The duration was varied between 2 h and 8 h. For CC and WS, a significant incline ($p = 1.99 \times 10^{-6}$ and $p = 3.46 \times 10^{-6}$) in DS occurred when increasing the reaction time from 2 h to 4 h (Figure 4.10 III and Figure 4.11 III). Moreover, a further inclination to 6 h led to a significant increase ($p = 8.09 \times 10^{-3}$ and $p = 3.28 \times 10^{-4}$) for CC and WS. These escalations were accompanied by improved ester peaks and decreased hydroxyl-bands (Figure 4.10 IV and Figure 4.11 IV). Prolonging the reaction time intensifies the contact between the fibres and the reactants, thereby achieving more swelling and consequently more acetylation. However, a further increase towards 8 h transpired in the occurrence of acid hydrolyses, which resulted in a significant reduction in DS ($p = 0.01$ and $p = 3.88 \times 10^{-4}$) for CC and WS.

The effect of the NBS catalyst concentration was investigated by performing reactions on CC (CC-B1-1, CC-B1-8, CC-B1-9 and CC-B1-10) and WS (WS-B1-1, WS-B1-8, WS-B1-9 and WS-B1-10) at a set temperature of 120 °C and a set reaction time of 6 h. The NBS concentration was varied between 0 % (w/v) and 4 % (w/v) based on the weight of NBS to the volume of acetic anhydride added to the reaction. The experiments conducted without a catalyst demonstrated marginally decreased hydroxyl peaks achieved for CC and WS (Figure 4.10 VI and Figure 4.11 VI). Acetyl peaks were furthermore already present at these conditions without the catalyst present. However, the rate of reaction was significantly inclined ($p = 1.06 \times 10^{-4}$ and $p = 1.37 \times 10^{-6}$) when introducing 1 % (w/v) NBS for both CC and WS. This occurrence was accompanied by affectedly increased ester peaks and considerably decreased hydroxyl peaks. The study conducted by Nwadiogbu et al. (2014) on CC confirmed that the presence of the NBS catalyst had a significant influence on the rate of acetylation.

A statistically similar ($p = 0.37$) DS was accomplished with 2 % (w/v) NBS, while the DS achieved on WS at 2 % (w/v) NBS was marginally lower ($p = 0.03$) than when implementing 1 % (w/v) NBS. Conversely, a considerably decreased ($p = 3.78 \times 10^{-5}$ and $p = 1.53 \times 10^{-4}$) DS and ester peaks were observed when using 4 % (w/v) NBS for both CC and WS. When the concentration of NBS becomes too high, a large amount of undecomposed NBS can be absorbed on the active sites of the CC and WS biomass (X. F. Sun et al., 2004). This occurrence can lead to a decrease in the contact area between the active sites and the chemical reagents and can cause a decrease in acetylation.

Additionally, the rapid rate of reaction achieved is accompanied by a rapid acid build-up, which leads to degradation of the biomass. For CC, the OS of run CC-B1-10 (4 % (w/v) NBS) (Table 4.11) was less than that of the unmodified sample (CC-B1-0), indicating the occurrence of significant fibre degradation. This phenomenon did not occur in WS, since the 21 % higher lignin content and less-branched hemicellulose structure provided this feedstock with higher resistance to structural degradation by acid hydrolyses.

An interaction might likely occur between temperature, time and catalyst concentration. An efficient catalyst can shorten the reaction time, which can prevent degradation due to acetic acid build-up. This occurrence will have an improved OS to effect. Conversely, too much catalyst can increase the rate of reaction to such a great extent, that acetic acid is built-up too fast, which can, in turn, increase the occurrence of acid hydrolyses. It is recommended that a full CCD is completed in future studies in order to determine the interactions between these input parameters.

4.3.3.2 The Comparison between Unmodified Biomass and Biomass Optimally Modified with Acetic Anhydride and N-bromosuccinimide via *Non-green* Acetylation Reactions

From the single-factor experiments concluded in Table 4.11, it was ascertained that the optimal performance from the set of conditions tested were found to occur at 120 °C, 6 h and 1 % (w/v) NBS – relating to specifications examined in the experimental runs identified by CC-B1-1 and WS-B1-1.

Table 4.12 The Degree of Substitution and Oil Sorption for the Optimal *Non-green* Acetylation of Corncob and Wheat Straw

Run [a]	Temperature (°C)	Time (h)	Catalyst Concentration [b, c] (%)	DS [d]	OS [e] (g oil /g sorbent)
CC-B1-OPT	120	6	1	2.76 ± 0.48	20.93 ± 0.81
WS-B1-OPT	120	6	1	2.19 ± 0.05	18.12 ± 0.18

a – Run identification for corncob (CC) and wheat straw (WS), where B1 as suffix represents a *non-green* modification; **b** – Each run performed with a constant acetic anhydride loading of 25:1 (25 mL acetic anhydride to 1 g biomass); **c** – Target N-bromosuccinimide as a mass percentage of acetic anhydride volume; **d** – Degree of Substitution is abbreviated as DS; **e** – Oil Sorption is abbreviated as OS

The optimal DS of 2.76 ± 0.48 and optimal OS of 20.93 ± 0.81 g/g achieved for CC is compared to the optimal DS of 2.19 ± 0.05 and optimal OS of 18.12 ± 0.18 g/g attained for WS at 120 °C, 6 h and 1 % (m/v) NBS, in Figure 4.12. This *non-green* acetylation accomplished statistically comparable DS ($p = 0.06$) for CC and WS. However, the OS accomplished by the CC sample was marginally higher ($p = 0.04$) than the OS reached by WS, despite having the same DS. Nevertheless, a significant increase ($p = 1.22 \times 10^{-5}$) in OS was attained by the implementation of these acetylations for both feedstocks.

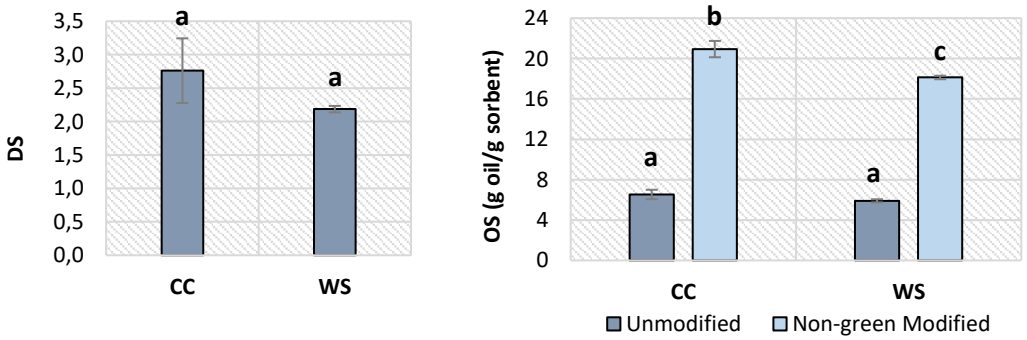

Figure 4.12 The Degree of Substitution (DS) and Oil Sorption (OS) achieved via the Optimal *Non-green* Surface Acetylation of Corncob (CC) and Wheat Straw (WS) at 120 °C, 6 h and 1 % (w/v) NBS

4.3.4 The Comparison between the *Green* Acetylation and the *Non-green* Acetylation of Corncob and Wheat Straw

4.3.4.1 Extent of Acetylation

The successes of acetylation achieved by the *green* and *non-green* modifications of CC and WS were compared in this section, based on FT-IR (Figure 4.13) and DS (Figure 4.14). The molecular changes brought about by the *green* and *non-green* acetylation reactions are evident, since substantial increases in the three major ester bands at 1 740 cm^{-1}, 1 369 cm^{-1} and 1 234 cm^{-1} were present. Moreover, the hydroxyl bands at 3 337 cm^{-1}, 1 337 cm^{-1} and 1 310 cm^{-1} were drastically reduced by the acetylations.

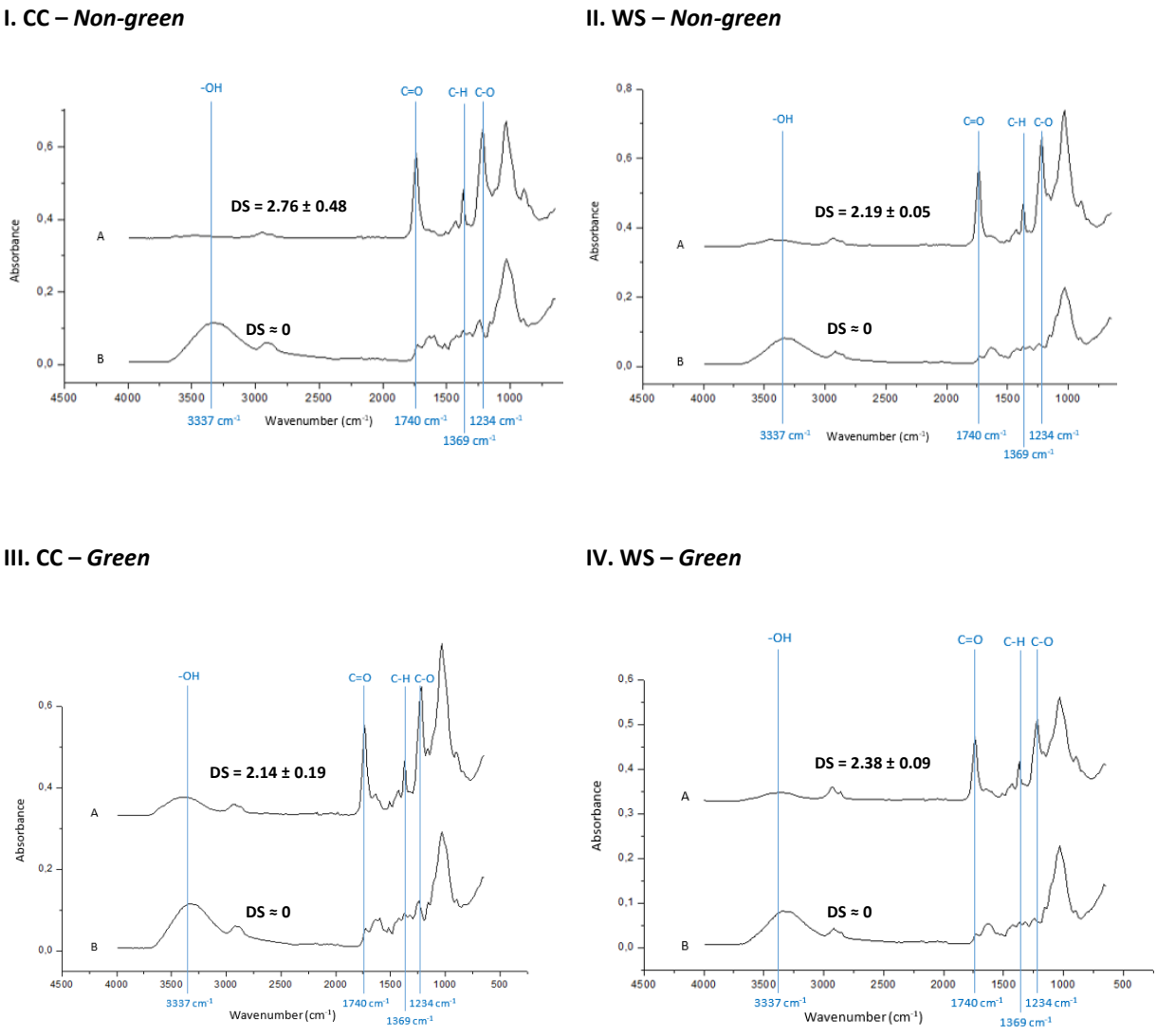

Figure 4.13 The Degree of Substitution (DS) and Fourier Transform Infrared Spectra of Corncob (CC) and Wheat Straw (WS), where ***A*** depicts an Optimally Modified Sample (*Green* at 150.5 °C, 5.7 h and 0.6 % (w/w) Iodine for CC and 150.5 °C, 7.4 h and 5.7 % Iodine for WS; *Non-green* at 120 °C, 6 h and 1 % (w/v) NBS for CC and WS). ***B*** represents an Unmodified Sample.

The *green* and *non-green* modifications accomplished statistically similar DS for CC ($p = 0.05$), while the *green* acetylation was marginally more successful than the *non-green* acetylation of WS ($p = 0.01$) (Figure 4.14). From

Section 4.3.1 it is known that cellulose, hemicellulose and lignin, contain abundant hydrophilic hydroxyl groups (Onwuka et al., 2019), which are not necessarily accessible to take part in acetylation reactions (Rowell, 2014).

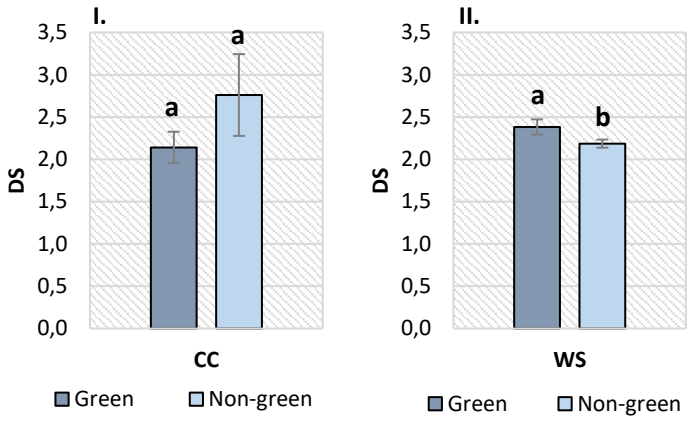

Figure 4.14 The Degree of Substitution (DS) achieved via the Optimised *Green* and *Non-green* Surface Acetylations of **I.** Corncob (CC) and **II.** Wheat Straw (WS)

The average of 1.2 hydroxyls on the molecular surface of the lignin is the most accessible and will, therefore, be acetylated first (Rowell, 2014). When comparing the FT-IR of the unmodified WS and CC to the *green* and *non-green* modified samples, an apparent reduction can be observed in the aromatic ring peak of lignin (shown at 1 595 cm^{-1}) with modification. This phenomenon confirms that the lignin present in the CC and WS samples were acetylated through these reactions.

As discussed in Section 4.3.1 and 4.3.3, the hemicellulose provides an average of two reactive hydroxyls per sugar unit (Egüés et al., 2014), while the cellulose has three reactive hydroxyl groups per AGU (Tupa et al., 2015). However, these hydroxyls are inaccessible to acetylation, unless ample diffusion of the reactants into the cell walls are achieved (Rowell, 2014). Therefore, the DS values of approximately equal to, or smaller than three reached by the *green* and *non-green* acetylations are indicative that the lignin and hemicellulose of CC and WS have been acetylated. However, insignificant swelling has been accomplished to reach the internal hydroxyl groups of the cellulose constituents.

4.3.4.2 Heterogeneous Oil Sorptions of Biomass Particles

The heterogeneous OS of the CC and WS particles were qualitatively investigated (Figure 4.15) by placing the biomass particles in a mixture of artificial seawater (3.5 % (w/w) sodium chloride in distilled water) and motor oil (Shell Helix Ultra, 5W-40) (Alaa El-Din et al., 2018). The extensive hydrophilic hydroxyl groups belonging to the lignin, cellulose and hemicellulose (Salajkova, 2013) cause the unmodified WS and CC to demonstrate an affinity for the sorption of the water in a heterogeneous environment (Figure 4.15 I and IV).

Subsequently, an affinity for non-polar oil particles is established by replacing the hydrophilic hydroxyl groups with hydrophobic acetyl groups (Hatton et al., 2015; Hubbe, Ayoub, et al., 2013) by the implementation of the *green* and *non-green* surface acetylation reactions applied to CC and WS (Figure 4.15 II, III and V, VI).

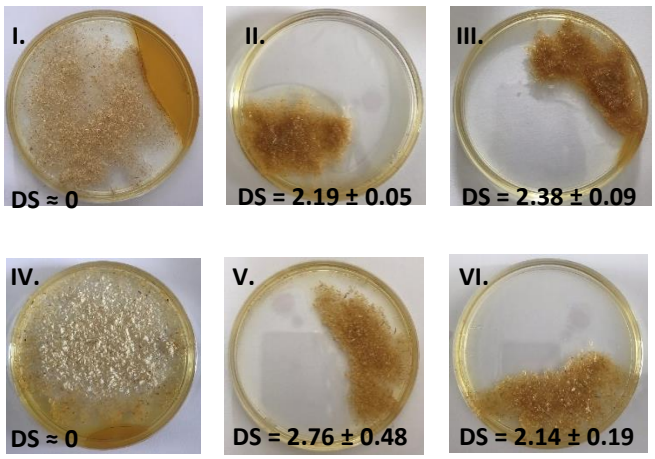

Figure 4.15 The Degree of Substitution (DS) and Qualitative Heterogeneous Oil Sorption of Motor Oil in Artificial Seawater for **I.** Unmodified Wheat Straw (WS); **II.** WS Modified via the *Non-green* Acetylation; **III.** WS Modified via the *Green* Acetylation; **IV.** Unmodified Corncob (CC); **V.** CC Modified via the *Non-green* Acetylation and **VI.** CC Modified via the *Green* Acetylation

As an additional analysis, the heterogeneous oil- and water sorptions (OS and WA) were quantitatively determined with sunflower oil and distilled water (Figure 4.16). The unmodified CC and WS demonstrated an affinity towards WA with 14.59 ± 0.27 g/g and 13.03 ± 0.47 g/g retained. In conjunction, only 6.82 ± 2.30 g/g and 8.52 ± 0.12 g/g was removed with these sorbents Since unmodified CC and WS often contain minor acetyl constituents on the hemicellulose (Rowell, 2014), these samples do demonstrate some sorption of oil.

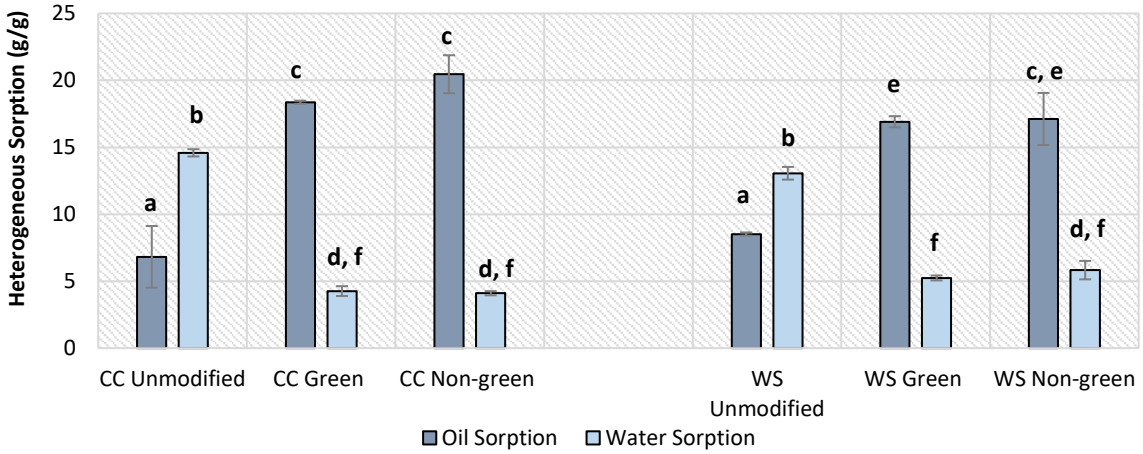

Figure 4.16 The Heterogeneous Oil- and Water Sorptions determined with Sunflower Oil and Distilled Water at Room Temperature (± 20 °C) for Modified and Unmodified Corncob (CC) and Wheat Straw (WS)

The affinity for OS was significantly amplified by the *green* and *non-green* surface modification reactions for both CC and WS. The *green* and *non-green* modifications of CC accomplished statistically comparable ($p = 0.17$) OS of 18.37 ± 0.12 g/g and 20.46 ± 1.42 g/g. These samples had reduced WA of 4.26 ± 0.37 g/g and 4.10 ± 0.16 g/g. Moreover, the OS attained by the *green* and *non-green* WS samples were not significantly different ($p = 0.90$), with values of 16.91 ± 0.42 g/g and 17.12 ± 1.95 g/g. These *green* and *non-green* modified WS samples exhibited reduced WA of 5.24 ± 0.19 g/g and 5.83 ± 0.69 g/g. Figure 4.16 depicts that the OS for modified CC and WS are significantly higher than the WA, regardless of the type of modification. This proves that a selective affinity towards OS is achieved through the surface acetylations in this study.

However, the traditional petrochemical-based sorbents, such as polyurethane foam, polypropylene webs, nanoporous polystyrene fibres, and rubber gels are known to retain approximately 60 – 70 g/g motor oil (Nyankson, Rodene, & Gupta, 2016; She et al., 2010). The biosorbents developed from CC and WS on this level can, therefore, not compete with the performances achieved by the petrochemical-based sorbents. Subsequently, the study was shifted to the *cellulose level* (Chapter 5) in order to establish whether the CC and WS cellulose-based sorbents can exhibit increased sorption capacities in order to be considered as a worthy competitor for the *non-green* alternatives.

Chapter 5 – The Isolation and Modification of Cellulose from Corncob and Wheat Straw for the Optimisation of Oil Sorption

Abstract

Hydrophobic, oleophilic films were developed from corncob (CC) cellulose and wheat straw (WS) cellulose, which were modified via *green* and *non-green* molecular surface acetylation methods for selective oil removal from water. The *green* acetylation yielded hydrophobic CC and WS cellulose films with water contact angles (WCA) of 103.1 ± 0.6 ° and 106.1 ± 0.4 °, heterogeneous selective oil sorption (OS) values of 12.09 ± 0.45 g/g and 12.77 ± 1.15 g/g, and degree of substitutions (DS) of 0.89 ± 0.05 and 0.91 ± 0.04, respectively. The *non-green* modified CC and WS cellulose films had WCA of 113.5 ± 1.0 ° and 114.8 ± 1.5 °, with OS of 20.39 ± 0.62 g/g and 21.03 ± 1.69 g/g and DS of 1.54 ± 0.05 and 1.55 ± 0.05. From these results, it was evident that the CC and WS cellulose fibres react similarly when subjected to the same type of acetylation (i.e. *green* or *non-green*). However, the *non-green* acetylations outperformed the *green* acetylations by approximately 65 – 69 % based on OS. Additionally, the sorption achieved by these plant-based biosorbents did not compare well to the commercially implemented petrochemical-based sorbents and it was recommended to additionally investigate whether nanofibrillated cellulose-based sorbents can be considered as a worthy competitor for the *non-green* industrial alternatives.

5.1 Introduction

The surface area available for OS was enhanced by isolating cellulose from the unmodified CC and WS. The molecular surfaces of the cellulose particles were modified to become hydrophobic and oleophilic via *green* and *non-green* surface acetylation reactions. Acetic anhydride was implemented as an acetylating agent. The *green* acetylation was catalysed by a 50 % (w/w) NaOH-solution, while the *non-green* acetylation implemented H_2SO_4 as the catalyst.

It was investigated whether an increase in OS was achieved by the increase in surface area available for OS with the cellulose powder obtained. For ease of application, the cellulose samples were then packaged as films for sorption. This chapter addresses Questions 2 and 4 of the list of *Key Research Questions* developed in Chapter 1, Section 1.4.

2. Does an increased surface area lead to an increased capacity for OS when isolating cellulose from the native biomass, and can a selective affinity to OS be accomplished by implementing *green* surface acetylation methodologies?
4. Can the *green* surface acetylation methods optimised in this study perform equally to traditional *non-green* surface acetylation reactions?

5.2 Experimental Methodology

5.2.1 General Definitions of Cellulose Modifications

The *green* and *non-green* cellulose molecular surface acetylations were optimised by implementing cotton since this feedstock was more readily available than the isolated CC cellulose and WS cellulose, and was expected to achieve more consistent results since it possesses a consistent composition. The optimised acetylation parameters were then applied to the CC and WS cellulose fibres to determine how these feedstocks react to the surface

modifications. The optimised acetylation conditions, as determined on cotton, were correspondingly also applied to filter paper. In order to discern between these acetylations, the experimental runs were encrypted based on the identifications displayed in Table 5.1.

Table 5.1 The Encryptions Utilised for the Identification of Cellulose Surface Modifications

Cellulose Type [a]	**Modification Identification**	
	Non-green Methodology [b]	*Green* Methodology [c]
Cotton	CO-C1-X	CO-C2-X
Wheat Straw Cellulose	WS-C1-X	WS-C2-X
Corncob Cellulose	CC-C1-X	CC-C2-X
Filter Paper	FP-C1-X	FP-C2-X

a – Cotton is abbreviated as CO, wheat straw as WS; corncob as CC and filter paper is abbreviated as FP; **b** – Runs marked with C1 as suffix represents a *non-green* modification on the *cellulose level*; **c** – Runs marked with C2 as suffix represents a *green* modification on the *cellulose level*; **X** represents the number of the experimental run

5.2.2 Extracting Cellulose from Biomass

Cellulose was isolated from CC and WS via an acid hydrolysis bio-fractionation method (Huntley et al., 2015). The bleaching step of this established method was replaced by an alkaline delignification adapted from Rosa et al. (2012) and a pre-extraction de-waxing step adapted from Sun et al. (2004) was applied. The procedure (Figure 5.1) was employed on CC and WS, respectively.

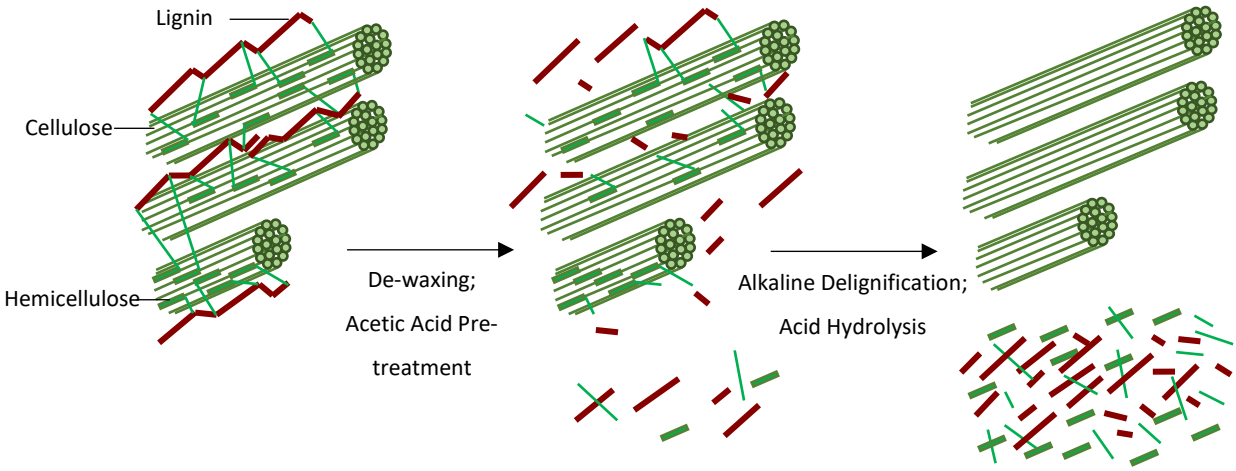

Figure 5.1 The Methodology for Extracting Cellulose from Raw Biomass, through De-waxing and Acetic Acid Pre-treatment, followed by Alkaline Delignification and Acid Hydrolysis

The CC and WS were milled (Retch 2M200) to achieve a finer particle size distribution of 200 – 425 µm. The samples were then de-waxed in a Soxhlet extraction device with a toluene-ethanol (2:1, v/v) solution for 6 h (J. X. Sun, Sun, Zhao, & Sun, 2004). Hereafter it was filtered with a Buchner filter and washed with hot distilled water until the filtrate attained a neutral pH (Chowdhury & Hamid, 2016). The samples were oven-dried at 40 °C for 24 h.

Phenolic- and hemicellulose hydrolysis was facilitated by adding 200 mL of a 90 % (v/v) acetic acid solution to 5 g of the de-waxed CC and WS. The reflux-condenser experimental setup (defined in Chapter 3) was implemented to heat these solutions to 120 °C for 2 h (Huntley et al., 2015).

The hydrolysed compounds were separated from the cellulose-containing filtrate by implementing a Buchner filter. The retentate was washed with hot distilled water until the permeate achieved a neutral pH (Chowdhury & Hamid, 2016), indicating that all the unreacted, residual acids were removed. The samples were subsequently oven-dried at 40 °C for 24 h.

Delignification was accomplished by placing the biomass and a 5 % (w/w) aqueous NaOH-solution into an autoclave (Eastern EA-630 Vertical Autoclave) with a 1:30 biomass to liquid ratio at 121 °C for 30 minutes (Rosa et al., 2012). The sample was allowed to cool for 1 hour, after which it was homogenised at 10 000 rpm (Hand-held Homogeniser PRO250, Pro-Scientific, USA) for 1 minute. The Buchner filtration step was repeated, and acid hydrolysis was performed for 24 h at room temperature with a 32 % (v/v) sulfuric acid solution (Huntley et al., 2015). Lastly, the filtration step was repeated for a final time, and the sample was oven-dried at 40 °C for 24 h.

5.2.3 The *Green* Acetylation of Cotton, Corncob Cellulose and Wheat Straw Cellulose by Acetic Anhydride and Sodium Hydroxide

5.2.3.1 The Chemical Reaction

Cellulose was modified by applying acetic anhydride and specified volumes of a 50 % (w/w) sodium hydroxide (NaOH) solution as catalyst (Koroskenyi & McCarthy, 2001). The chemical reaction achieved by the modification is depicted in Figure 5.2

In the first step, NaOH acts as Na^+-donor in order to activate the carbonyl groups of acetic anhydride (Reaction I, Figure 5.2). Na—O—CO—CH_3 and acetic acid are formed. The acetic acid acts as the acetylating agent and consequently reacts with the surface hydroxyl groups of the cellulose (Reaction II, Figure 5.2) to produce the acetylated compound, Cellulose—O—CO—CH_3. Water is formed. In the final step, the water molecules react with the Na—O—CO—CH_3 (Reaction III, Figure 5.2). In this way, the NaOH-catalyst is recovered, and acetic acid is formed as a by-product.

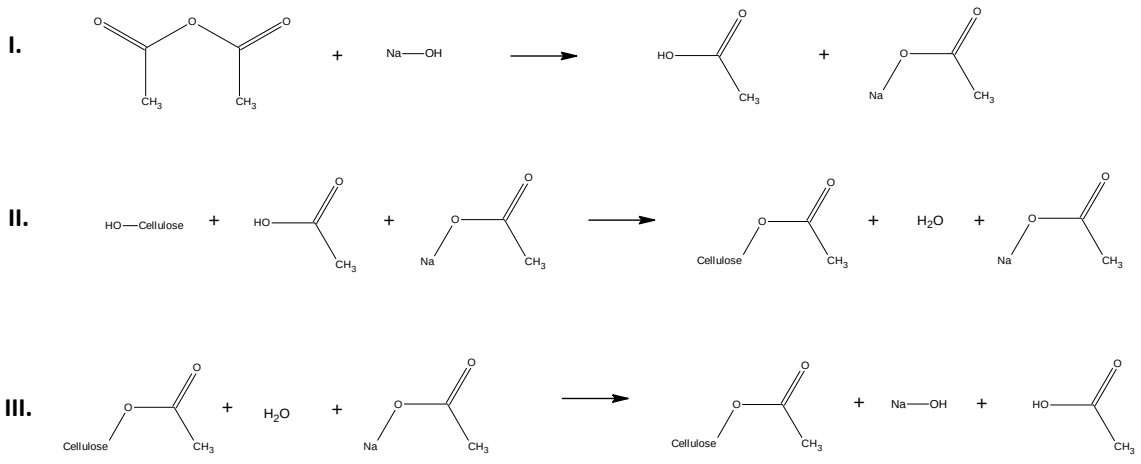

Figure 5.2 The *Green* Reaction Mechanism for NaOH-catalysed Acetylation of Cellulose, redrawn from Koroskenyi & McCarthy (2001)

5.2.3.2 The Central Composite Design and Scope Establishment

The three-factor central composite design (CCD), based on response surface methodology (RSM), was implemented in order to establish empirical relationships relating the DS (Y_1) and OS (Y_2) of the modified product to the varying reaction conditions, namely temperature (X_1), time (X_2) and catalyst concentration (X_3), as described in Chapter 3, Section 3.5. This optimisation was executed with cotton. In this way, the *green* acetylation of cellulose could be optimised by implementing the statistical software, Statistica 13.2. The combination of parameters determined to achieve the highest DS and OS of cotton was applied to CC cellulose, WS cellulose and filter paper for comparison with the *non-green* modified samples.

The complete CCD design matrix applied to cotton during the *green* acetylation is displayed in Table 5.2. The temperature was varied between 40 – 140 °C, time was ranged from 3.8 – 44.2 h, and the catalyst concentration was fluctuated between 1.2 – 13.8 % (v/v) NaOH-solution. Five identical experiments were conducted at the centre point (Table 5.2, Run CO-C2-15 to CO-C2-19) to calculate the repeatability of the data (Hamid et al., 2014).

Table 5.2 The Central Composite Design Matrix and Experimental Conditions for the *Green* Modification of Cotton in order to Improve the Hydrophobicity for Oil Sorption Applications

Factor	Symbol	Range	Coded Levels				
			-α	**-1**	**0**	**1**	**α**
Temperature	X_1	40 – 140 °C	40	60	90	120	140
Time	X_2	3.8 – 44.2 h	3.8	12	24	36	44.2
Catalyst Concentration [c]	X_3	1.2 – 13.8 % (v/v)	1.2	3.75	7.5	11.25	13.8

Run ID [a, b]	Type of Point	Level (Coded Factors)			Reaction Variables (Actual Factors)		
					Temperature (°C)	Time (h)	Catalyst Loading [c] (%)
CO-C2-0 [d]	-	-	-	-	-	-	-
CO-C2-1	Fact	- 1	- 1	- 1	60	12	3.8
CO-C2-2	Fact	- 1	- 1	1	60	12	11.3
CO-C2-3	Fact	- 1	1	- 1	60	36	3.8
CO-C2-4	Fact	- 1	1	1	60	36	11.3
CO-C2-5	Fact	1	- 1	- 1	120	12	3.8
CO-C2-6	Fact	1	- 1	1	120	12	11.3
CO-C2-7	Fact	1	1	- 1	120	36	3.8
CO-C2-8	Fact	1	1	1	120	36	11.3
CO-C2-9	Axial	- α	0	0	40	24	7.5
CO-C2-10	Axial	+ α	0	0	140	24	7.5
CO-C2-11	Axial	0	- α	0	90	3.8	7.5
CO-C2-12	Axial	0	+ α	0	90	44.2	7.5
CO-C2-13	Axial	0	0	- α	90	24	1.2
CO-C2-14	Axial	0	0	+ α	90	24	13.8
CO-C2-15	Centre	0	0	0	90	24	7.5
CO-C2-16	Centre	0	0	0	90	24	7.5
CO-C2-17	Centre	0	0	0	90	24	7.5
CO-C2-18	Centre	0	0	0	90	24	7.5
CO-C2-19	Centre	0	0	0	90	24	7.5

a – Run identification for cotton (CO), where C2 as suffix represents a *green* modification; **b** – Each run performed with a constant acetic anhydride loading of 30:1 (30 mL acetic anhydride to 1 g CO); **c** – Target sodium hydroxide (50 % (w/w) NaOH-solution) percentage, based on volume to volume ratio of acetic anhydride; **d** – Unmodified CO sample for reference

The ranges of the input variables were based on preliminary studies, which are detailed in Appendix E.1 (p. 156). These preliminary experiments were accomplished by varying the reaction temperature between 40 – 120 °C, the acetylation duration from 2 – 24 h and the catalyst concentration between 0 – 14 % (v/v) NaOH-solution, in single-factor experiments.

Increasing the temperature from 40 °C to 90 °C (at 2 h and 7.5 % (v/v) NaOH-solution) resulted in a significant incline in DS ($p = 5.47 \times 10^{-4}$), while a further escalation to 120 °C had no significant effect ($p = 0.06$) on the acetylation. Nevertheless, the DS reached at 120 °C was marginally higher (though not statistically significant) than the DS achieved at 90 °C. The temperature range of 40 °C to 140 °C was consequently selected for the CCD investigation (with $\alpha = 2^{3/4}$) in order to study the effects of interaction between the input parameters. It is important to note that the temperature should not be escalated above 140 °C. A 50 % (v/v) NaOH-solution becomes volatile above 143 °C, and the current experimental setup cannot condense the vapours at these amplified temperatures, since a chemical coolant is not employed in the condenser.

An increase in reaction time from 2 to 24 h (at 90 °C and 7.5 % (v/v) NaOH-solution) produced a significant amplification in acetylation ($p = 2.78 \times 10^{-5}$), which indicated that the optimal reaction duration might only occur in excess of 24 h. In the study performed by Thakur (2013), comparable experiments were conducted with rice and wheat husks at room temperature for up to 48 h at different NaOH-concentrations. In order for the experimental design to maintain rotatability, the alpha values of $\alpha = 2^{3/4}$ were selected, and the range of reaction time of 3.8 – 44.2 h was utilised for the CCD.

Increasing the catalyst concentration from 0 % (v/v) NaOH-solution to 3.75 % (v/v) NaOH-solution had a significantly heightened ($p = 4.42 \times 10^{-6}$) DS to effect at a constant temperature of 90 °C and a constant reaction time of 2 h. However, a further incline to 7.5 % (v/v) NaOH-solution had no significant effect ($p = 0.32$) and a reduced DS ($p = 2.26 \times 10^{-5}$) was achieved at 14 % (v/v) NaOH-solution. It was decided to test the entire range of catalyst concentration in the CCD (with $\alpha = 2^{3/4}$) in order to determine any interactions that might occur between temperature, time and catalyst concentration.

5.2.3.3 The Experimental Details

A 30 % (w/v) acetic anhydride solution was created in a 250 mL round bottom flask by dispersing 0.5 g of cotton in 15 mL of acetic anhydride. Additionally, a 50 % (w/w) NaOH-solution was produced by adding 20 g NaOH to 20 g water. This suspension (referred to as the NaOH-solution) was stored at 4 ± 1 °C until use. During the experimental runs, the specified volumes of the NaOH-solution (between 1.2 and 13.8 % (v/v), Table 5.2) was included, based on the volume of acetic anhydride added to the cellulose.

The specimens were introduced into the reflux-condenser experimental setup (defined in Chapter 3), and the samples were maintained at the required reaction temperatures (between 40 °C and 140 °C, Table 5.2) for stipulated reaction times (between 3.8 h and 44.2 h, Table 5.2). The hot reagent was decanted, and a Buchner filter was employed to wash the retentate with 100 mL acetone and 100 mL ethanol to remove all unreacted constituents. The samples were then washed with hot distilled water until the filtrate attained a neutral pH (Chowdhury & Hamid, 2016), and oven-dried at 40 °C for 24 h.

5.2.4 The *Non-green* Acetylation of Cotton, Corncob Cellulose, Wheat Straw Cellulose and Filter Paper by Acetic Anhydride and Sulfuric Acid

5.2.4.1 The Chemical Reaction

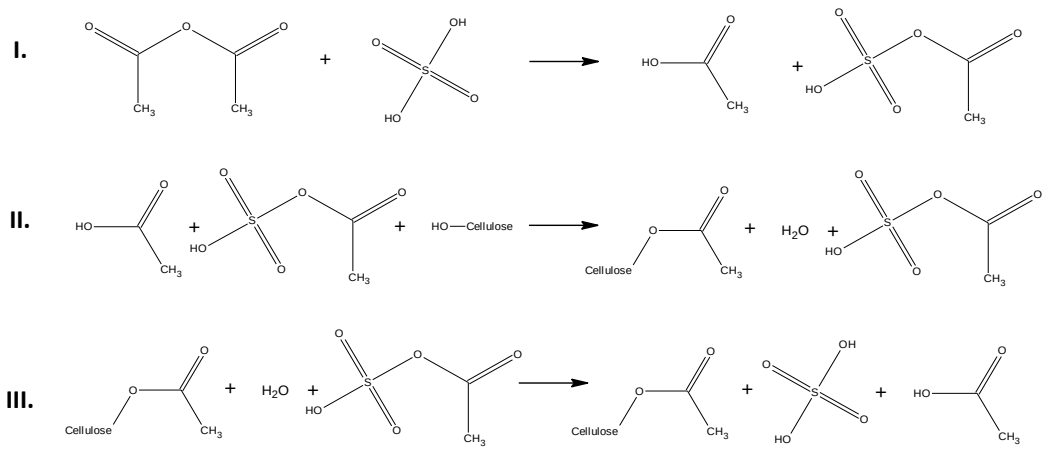

Figure 5.3 The *Non-green* Reaction Mechanism for Sulfuric Acid-catalysed Acetylation of Cellulose, redrawn from Huang et al. (2014)

A *non-green* acetylation, which implements acetic anhydride as an acetylating agent and sulfuric acid as a catalyst (Huang et al., 2014), was applied to cellulose as a reference for the performance of acetylation. This method is largely commercially used to produce cellulose acetate (Li et al., 2009). However, cellulose degradation and hydrolyses of cellulose acetate can easily occur if the acid catalyst is not present in the correct amount, or if this catalyst is not completely removed after the acetylation (Li et al., 2009). The chemical reaction achieved by this modification is displayed in Figure 5.3.

5.2.4.2 The Experimental Details

The *non-green* methodology was firstly executed on cotton. These modifications were not statistically optimised, but the performances were rather reviewed within ranges determined from literature studies. The highest acetylation within the scope was selected as a reference for the optimal performance. The combination of parameters determined to achieve the highest DS and OS of cotton was applied to the isolated CC cellulose, WS cellulose and filter paper for comparison to the *green* modified samples.

These modifications were conducted by varying the reaction temperature between 30 and 90 °C, the acetylation duration from 2 to 4 h and the catalyst concentration between 0 and 10 % (v/v) sulfuric acid. Table 5.3 summarises the details specific to each experimental run.

The specified volume of sulfuric acid (as stipulated in Table 5.3) was added to 5 mL acetic anhydride, and this mixture was pre-cooled to 4 ± 1 °C. A 250 mL round bottom flask was prepared with 20 mL of acetic anhydride and 1 g cotton, whereafter the pre-cooled mixture of acetic anhydride and sulfuric acid was added. The specimens were introduced to the reflux-condenser experimental setup (defined in Chapter 3), and the samples were maintained at the required reaction temperatures (from 30 °C to 90 °C, Table 5.3) for stipulated reaction durations (between 2 h and 4 h, Table 5.3). The hot reagent was decanted, and a Buchner filter was employed to wash the retentate with 100 mL acetone and 100 mL ethanol to remove all unreacted constituents. Furthermore, the samples were washed

with hot distilled water until the filtrate achieved a neutral pH (Chowdhury & Hamid, 2016), and subsequently oven-dried at 40 °C for 24 h.

Table 5.3 Experimental Conditions for the *Non-green* Acetylation of Cotton in order to Improve the Hydrophobicity for Oil Sorption Applications

Run ID [a, b]	Temperature (°C)	Time (h)	Catalyst Loading [c] (%)
CO-C1-0 [d]	n/a	n/a	n/a
CO-C1-1	30	2	5
CO-C1-2	60	2	5
CO-C1-3	90	2	5
CO-C1-4	60	4	5
CO-C1-5	60	2	10
CO-C1-6	60	2	0
CO-C1-7 [e]	60	2	9

a – Run identification for cotton (CO), where C1 as suffix represents a *non-green* modification; **b** – Each run performed with a constant acetic anhydride loading of 25:1 (25 mL acetic anhydride to 1 g CO); **c** – Target sulfuric acid percentage, based on volume to the mass of CO; **d** – Unmodified CO sample for reference; **e** – Literature optimal determined at 60 °C, 2 h and 9 % sulfuric acid (Huang et al., 2014)

5.2.5 Creating Cellulose Films

A method adapted from Nel (2017) was applied for cellulose film formation (Figure 5.4). An aqueous NaOH-urea solution was prepared in the mass ratio of 7:12:81 for distilled water to NaOH and urea. This solution was stored at 4 ± 1 °C until utilisation.

A 2 % (w/w) cellulose-solution was prepared by mixing cellulose with the aqueous NaOH-urea solution through the implementation of a 900 W Nutribullet for 5 minutes. Additionally, a 1 % (w/w) konjac glucomannan solution was formulated by mixing konjac glucomannan with the aqueous NaOH-urea solution. The cellulose-solution and konjac glucomannan solution were then blended with the 900 W Nutribullet for 5 minutes in an 80:20 mass ratio (80 g cellulose-solution to 20 g konjac glucomannan solution).

The samples were divided into moulds for individual films and allowed to settle for 60 minutes under ambient temperatures. The films were submerged into a 5 % (w/w) sulfuric acid coagulation bath for 5 minutes. This immersion aids the bond-formation between the molecules (Nel, 2017). The samples were thoroughly washed with distilled water and left to air-dry for 10 days, after which analyses could take place.

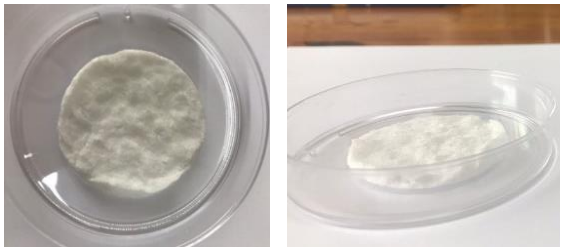

Figure 5.4 Films Created from Cellulose for Ease of Application in Oil Sorption

5.3 Results and Discussion

5.3.1 The Isolation and Characterisation of Unmodified Cellulose from Corncob and Wheat Straw, and the Characterisation of Reference Cotton and Filter Paper

The composition analyses of CC biomass, CC cellulose, WS biomass and WS cellulose are compared in Table 5.4, in order to determine the success of cellulose isolation. The chemical compositions of cotton and filter paper are additionally displayed as references.

The cellulose isolation methodology (Section 5.2.2) resulted in an approximate 75 % decrease in lignin for the CC sample, while an 80 % lignin-reduction was accomplished for WS (Table 5.4). Concurrently, the CC cellulose exhibited an estimated 53 % lower hemicellulose concentration, while the WS cellulose had a 63 % reduction in hemicellulose. Furthermore, this isolation method achieved increased cellulose concentrations by approximately 23 % and 62 % for CC cellulose and WS cellulose, respectively.

Table 5.4 The Composition Analyses for Cotton, Filter Paper, Corncob Biomass and -Cellulose, and Wheat Straw Biomass and -Cellulose

Composition [a] (%)	CO	FP	Unmodified CC Biomass	Isolated CC Cellulose	Unmodified WS Biomass	Isolated WS Cellulose
Lignin [b]	1.10 ± 0.04	3.66 ± 0.33	15.25 ± 1.20	3.81 ± 0.83	18.42 ± 2.50	3.64 ± 0.67
Cellulose [c]	82.00 ± 5.94	61.16 ± 3.92	44.50 ± 0.58	54.88 ± 1.60	37.15 ± 0.52	60.17 ± 4.06
Hemi-cellulose [d]	0.00 [f]	10.72 ± 1.13	20.23 ± 0.56	9.40 ± 0.81	20.75 ± 0.24	7.68 ± 0.65
Extractives [e]	2.59 ± 0.59	6.81 ± 1.63	9.84 ± 0.87	3.14 ± 0.35	13.83 ± 0.76	6.45 ± 0.51
Moisture	9.80 ± 0.19	10.10 ± 0.71	7.05 ± 0.09	12.76 ± 0.72	5.37 ± 1.63	11.81 ± 1.40
Ash	2.00 ± 0.42	5.83 ± 1.04	3.09 ± 0.21	6.97 ± 0.62	4.19 ± 1.56	6.06 ± 0.86

a – Completed based on NREL/TP-510-42620 method for cotton (CO), filter paper (FP), corncob (CC) and wheat straw (WS); **b** – Acid-soluble and acid-insoluble lignin; **c** – Cellulose accounting for glucose sugars; **d** – Hemicellulose accounting for arabinose and xylose sugars; **e** – Water- and ethanol extractives; **f** – Zero hemicelluloses detected with HPLC

The isolated CC and WS cellulose samples contained comparative cellulose, hemicellulose, lignin, and ash constituents when compared to filter paper. However, the cotton samples retained an affectedly increased cellulose purity and considerably lower hemicellulose, lignin and ash contaminants. This phenomenon occurred because cotton is a naturally occurring source of pure cellulose (Hsieh, 2007), while the filter paper cellulose, WS cellulose and CC cellulose are isolated from different biomass sources. The original cellulose content of the sources, therefore, limit the cellulose purity of the extracted samples (Ceaser, 2019). In order to achieve less lignin and hemicellulose contamination, bleaching with *non-green* chemicals will be necessary (Rabetafika et al., 2014).

The ash content of the CC and WS cellulose might be amplified by the precipitation of neutralised salts caused by non-extensive washing (Ceaser, 2019). Additionally, the acid-insoluble lignin can re-condensate and attribute to the lignin-content if not adequately washed and removed from the samples (Ceaser, 2019).

The Fourier Transform Infrared (FT-IR) Spectroscopy of the cellulose (Figure 5.5) demonstrates the presence of lignin and hemicellulose for CC cellulose, WS cellulose, cotton and filter paper. The absence of the aromatic ring peak of

lignin at 1 595 cm^{-1} suggests a substantial reduction in lignin molecules, which is coherent with the NREL/TP-510-42620 composition analyses (Table 5.4). However, the minor peak at 1 242 cm^{-1} indicates linkages between lignin and hemicellulose (Luzi et al., 2019). Furthermore, the peak at 2 919 cm^{-1} designates the CH_2 stretching of lignin (Zheng et al., 2018) and C-H stretching of hemicellulose (Farhat et al., 2017), signifying the incomplete cleavage of the bonds between hemicellulose and lignin (Rabetafika et al., 2014).

The arabinose side chains of hemicellulose are shown at 985 cm^{-1} (X. F. Sun et al., 2005), while the xylan peak of hemicellulose is represented at 1 034 cm^{-1} (Ceaser, 2019). The absence of the peak at 1 731 cm^{-1} designates the absence of the phenolic compounds, ferulic and *p*-coumaric acids (Ceaser, 2019; A. Kumar et al., 2014). This analysis is in coherence with the composition analysis, indicating the presence of hemicellulose with minor contamination of lignin.

The hydroxyl stretching vibration of cellulose and hemicellulose is represented between 3 200 cm^{-1} and 3 345 cm^{-1} (Buranov & Mazza, 2010; Halal et al., 2015; Rosa et al., 2012), while the greatest peak at 3 337 cm^{-1} exemplifies the inter- and intramolecular hydroxyl molecules of cellulose (Hospodarova et al., 2018; Zepic et al., 2015). Additionally, the peak at 1 027 cm^{-1} signifies the hydroxyl groups in cellulose (Hospodarova et al., 2018). The C-H vibrations occur at 1 334 cm^{-1} (Hospodarova et al., 2018). Moreover, the peak at 1 633 cm^{-1} represents the moisture present in the samples (Hospodarova et al., 2018), which is coherent with the 10 to 13 % moisture detected with the NREL/TP-510-42620 method.

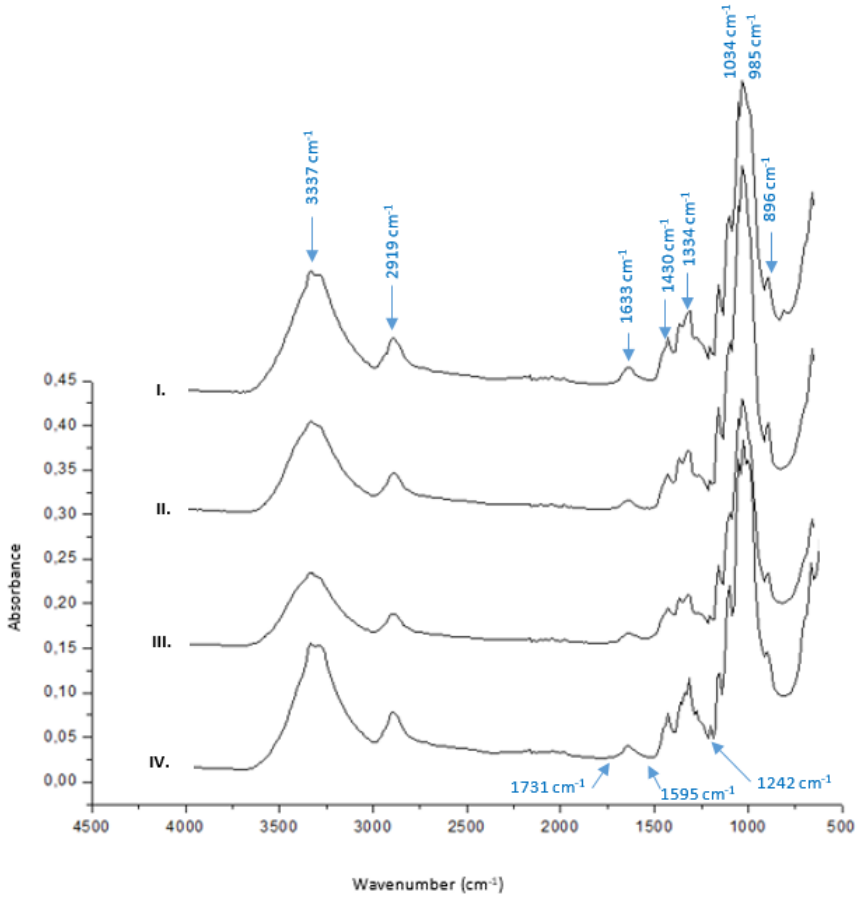

Figure 5.5 The Fourier Transform Infrared Spectra of **I.** Filter Paper; **II.** Extracted Corncob Cellulose; **III.** Extracted Wheat Straw Cellulose; and **IV.** Unmodified Cotton

The marginal presence of lignin and hemicellulose in the isolated CC and WS cellulose specimens indicate the need for an increase in cellulose purity. Conversely, since the focus of this study was not on the success of cellulose isolation, the achieved purity of cellulose is accepted, and a recommendation is made for further investigation in future studies.

The molecular crystallinities of the cellulose samples determined with a Bruker D2 Phaser X-ray Diffractometer are displayed in Table 5.5. The X-ray diffraction (XRD) spectra are available in Appendix E.3 (p. 163). As previously discussed, each AGU in a cellulose chain has three reactive, hydrophilic hydroxyl groups (Arola, 2015). These hydroxyl groups have the ability to form strong intra- and intermolecular bonds (Lavoine et al., 2012), which is responsible for the crystalline nature of cellulose (Hokkanen et al., 2016).

Table 5.5 The Molecular Crystallinities of Cotton, Wheat Straw Cellulose, Corncob Cellulose and Filter Paper

Feedstock [a]	Crystallinity [b] (%)
CO	75.49 ± 3.67
WS Cellulose	72.47 ± 1.04
CC Cellulose	68.81 ± 1.02
FP	79.99 ± 0.21

a – The molecular crystallinities of cotton (CO), corncob (CC) cellulose, wheat straw (WS) cellulose and filter paper (FP), determined by a Bruker D2 Phaser X-ray Diffractometer; **b** – Determined with the method defined by Huntley et al. (2015) in Equation 3.1a

The crystallinities of cotton, CC cellulose and WS cellulose were found to be statistically similar ($p = 0.13$), while filter paper had a significantly higher crystallinity ($p = 0.02$). The FT-IR peak (Figure 5.5) at 896 cm^{-1} is representative of the amorphous β-glycosidic linkages in the cellulose molecules (Hospodarova et al., 2018; Reddy et al., 2016), while the crystalline structures of cellulose are shown between 1 420 cm^{-1} and 1 430 cm^{-1}, representing the CH_2 stretching vibrations (Hospodarova et al., 2018). In coherence with this XRD analyses, the FT-IR demonstrates marginally sharper crystalline peaks for cotton and filter paper, while more prominent amorphous peaks occurred for CC cellulose and WS cellulose.

Table 5.6 The Elemental Composition of Filter Paper as Determined by X-ray Fluorescence and Inductively Coupled Plasma Mass Spectrometry

Element	Concentration (mg/kg)	Element	Concentration (mg/kg)
Calcium	430.25	**Aluminium**	6.85
Magnesium	57.10	**Strontium**	4.67
Sodium	43.16	**Barium**	2.49
Potassium	27.62	**Phosphorus**	2.06
Iron	22.73	**Copper**	1.62
Silicon	20.35	**Zinc**	1.61

X-ray Fluorescence (XRF) and Inductively Coupled Plasma Mass Spectrometry (ICP-MS) were completed (Table 5.6) by the Central Analytical Facility of Stellenbosch University in order to determine the composition of the binding materials present in the filter paper specimens. The high calcium content of filter paper suggests that a calcium-based substance is used as a binder material between the cellulose fibres. Calcium carbonate is often implemented as a strengthening agent in filter paper (Chen, Qian, & An, 2011) and frequently occurs as a contaminant in this

application (Meakin, 1973). Furthermore, calcium carbonate is a crystalline molecule (Chen et al., 2011; U.S. National Library of Medicine, 2004), which can contribute to the augmented crystallinity of filter paper.

5.3.2 The *Green* Acetylation of Cotton, Corncob Cellulose, Wheat Straw Cellulose and Filter Paper by Acetic Anhydride and Sodium Hydroxide

5.3.2.1 The Model Development of the Degree of Substitution and Oil Sorption of the *Green* Modification of Cotton

The *green* acetylation was statistically optimised on cotton by implementing the CCD as determined in Section 5.2.3. The DS and OS of these samples are represented by run CO-C2-1 to CO-C2-19 (Table 5.8, p. 73), and the polynomial models predicted by Statistica 13.2 are shown in Table 5.7.

Table 5.7 The Mathematical Models, Developed to Describe the Response of Degree of Substitution and Oil Sorption to the Input Parameters – Temperature, Time, and Catalyst Concentration, for the *Green* Surface Modification of Cotton

Model	Mathematical Model [a, b]	Equation	R^2	*Lack of Fit*
Original Prediction	$Y_1 = (0.011108) + (0.007908)X_1 + (0.011896)X_2 + (0.016003)X_3 + (-0.000043)X_1^2 + (-0.000222)X_2^2 + (-0.000941)X_3^2 + (0.000062)X_1X_2 + (0.000040)X_1X_3 + (-0.000227)X_2X_3$	[5.1]	0.5061	Significant
	$Y_2 = (12.27558) + (0.09164)X_1 + (0.13447)X_2 + (0.19750)X_3 + (-0.00052)X_1^2 + (-0.00280)X_2^2 + (-0.01397)X_3^2 + (0.00087)X_1X_2 + (0.00075)X_1X_3 + (-0.00239)X_2X_3$	[5.2]	0.5045	Significant
Adapted Prediction	$Y_1 = (-0.043582) + (0.009318)X_1 + (0.015160)X_2 + (-0.000041)X_1^2 + (-0.000209)X_2^2$	[5.3]	0.4779	Significant
	$Y_2 = (11.29168) + (0.11229)X_1 + (0.18490)X_2 + (-0.00049)X_1^2 + (-0.00260)X_2^2$	[5.4]	0.4678	Significant

a – Temperature (X_1), Time (X_2) and Catalyst Concentration (X_3) as input variables; **b** – Degree of Substitution (Y_1) and Oil Sorption (Y_2) as model responses

ANOVA analyses (Appendix E.2, p. 159) were applied to the developed models to determine the regression coefficients and analyse the statistical fit of the models to the experimental data. These analyses indicated a regression coefficient of R^2 = 0.5061 for the model predicting DS (Equation 5.1) and R^2 = 0.5045 for the model predicting OS (Equation 5.2). The significant *Lack of Fit* for both models designated that the DS and OS cannot be accurately predicted by these obtained models.

In an attempt to improve the statistical fit of the models, the insignificant effects were pooled into the error-terms (b_0 in Equation 3.12, Section 3.5). The inconsequential effects on the DS included the linear and quadratic effects of the catalyst (p = 0.98 and p = 0.28), as well as the interactions between temperature and time (p = 0.18), interactions between temperature and catalyst concentration (p = 0.76) and interactions between catalyst concentration and time (p = 0.50). Equivalently, the linear and quadratic effects of the catalyst (p = 0.96 and p = 0.23) and interactions between input parameters (p = 0.16, p = 0.67 and p = 0.59, respectively) also had negligible effects on the OS of the samples. The adjusted models are signified by Equation 5.3 and Equation 5.4 (Table 5.7).

Table 5.8 The Degree of Substitution and Oil Sorption achieved through the *Green* Acetylation of Cotton with the Implementation of a Central Composite Design in order to Improve the Hydrophobicity for Oil Sorption Applications

Run ID [a, b]	Temp (°C)	Time (h)	Catalyst Loading [c] (%)	DS Model Prediction	DS	DS Error (%)	OS Model Prediction	OS (g oil/g sorbent)	OS Error (%)
Central Composite Design									
CO-C2-1	60	12	3.8	-	0.56 ± 0.04	-	-	18.72 ± 0.67	-
CO-C2-2	60	12	11.3	-	0.55 ± 0.11	-	-	18.29 ± 0.59	-
CO-C2-3	60	36	3.8	-	0.58 ± 0.03	-	-	18.75 ± 0.07	-
CO-C2-4	60	36	11.3	-	0.54 ± 0.03	-	-	18.47 ± 0.26	-
CO-C2-5	120	12	3.8	-	0.73 ± 0.03	-	-	20.56 ± 0.05	-
CO-C2-6	120	12	11.3	-	0.75 ± 0.07	-	-	21.05 ± 0.25	-
CO-C2-7	120	36	3.8	-	0.86 ± 0.06	-	-	22.42 ± 0.03	-
CO-C2-8	120	36	11.3	-	0.82 ± 0.05	-	-	21.89 ± 1.05	-
CO-C2-9	40	24	7.5	-	0.60 ± 0.03	-	-	19.02 ± 0.26	-
CO-C2-10	140	24	7.5	-	0.51 ± 0.02	-	-	17.99 ± 0.05	-
CO-C2-11	90	3.8	7.5	-	0.39 ± 0.09	-	-	16.62 ± 0.18	-
CO-C2-12	90	44.2	7.5	-	0.76 ± 0.07	-	-	20.76 ± 0.09	-
CO-C2-13	90	24	1.2	-	0.60 ± 0.02	-	-	19.08 ± 0.64	-
CO-C2-14	90	24	13.8	-	0.65 ± 0.03	-	-	19.46 ± 0.02	-
CO-C2-15	90	24	7.5	-	0.74 ± 0.04	-	-	21.01 ± 0.28	-
CO-C2-16	90	24	7.5	-	0.71 ± 0.04	-	-	20.46 ± 0.47	-
CO-C2-17	90	24	7.5	-	0.77 ± 0.08	-	-	21.23 ± 0.20	-
CO-C2-18	90	24	7.5	-	0.73 ± 0.08	-	-	20.47 ± 0.08	-
CO-C2-19	90	24	7.5	-	0.67 ± 0.03	-	-	19.91 ± 0.21	-
Experimental Validation of Model									
CO-C2-V1	60	14	7.5	0.54 [d]	0.63 ± 0.02	16.49	18.35 [g]	16.57 ± 0.39	9.71
CO-C2-V2	100	36	5	0.75 [e]	0.83 ± 0.06	10.63	20.93 [h]	20.31 ± 0.56	2.95
CO-C2-V3	120	24	3.75	0.73 [f]	0.83 ± 0.04	13.49	20.67 [i]	21.94 ± 0.80	6.14

a – Run identification for cotton (CO), where C2 as suffix represents a *green* modification and validation runs are depicted by V1, V2 and V3
b – Each run performed with a constant acetic anhydride loading of 30:1 (30 mL acetic anhydride to 1 g CO)
c – Target sodium hydroxide (50 % (w/w) NaOH-solution) percentage, based on volume to volume ratio of acetic anhydride
d – Predicted that degree of substitution (DS) could range from 0.42 to 0.66 at these conditions with 95 % confidence
e – Predicted that DS could range from 0.64 to 0.87 at these conditions with 95 % confidence
f – Predicted that DS could range from 0.61 to 0.84 at these conditions with 95 % confidence
g – Predicted that oil sorption (OS) could range from 16.79 to 19.91 g oil/g sorbent at these conditions with 95 % confidence
h – Predicted that OS could range from 19.38 to 22.47 g oil/g sorbent at these conditions with 95 % confidence
i – Predicted that OS could range from 19.13 to 22.22 g oil/g sorbent at these conditions with 95 % confidence

The ANOVA analyses of the adjusted models (Appendix E.2, p. 159) indicated that the *Lack of Fit* was improved, but remained significant (Table 5.7). The fit of the experimental data remained suboptimal, and marginally lower regression coefficients were obtained. These consisted of R^2 = 0.4779 for the model predicting DS (Equation 5.3) and R^2 = 0.4678 for the model predicting OS (Equation 5.4).

In comparison to the statistical validation, the adjusted models were experimentally validated at three random conditions (CO-C2-V1, CO-C2-V2 and CO-C2-V3 in Table 5.8). Even though the DS values differ from the predicted values with more than 10 %, the obtained DS and OS values were within the 95 % confidence interval (α = 0.05) for all three validation runs. The developed models were, therefore, deemed acceptable for predicting the DS and OS of cellulose. The models were accepted for this purpose, but it is recommended that further tests are executed in order to improve the accuracy of the models.

5.3.2.2 The Effect of Temperature, Time and Catalyst Concentration of the Degree of Substitution and Oil Sorption of the *Green* Modification of Cotton

The linear- and quadratic effects of temperature, time and catalyst concentration on the DS and OS of cotton via the *green* surface modification were surveyed by studying the ANOVA analyses (Appendix E.2, p. 159), the Pareto charts (Figure 5.6) and the response surface plots (Figure 5.7).

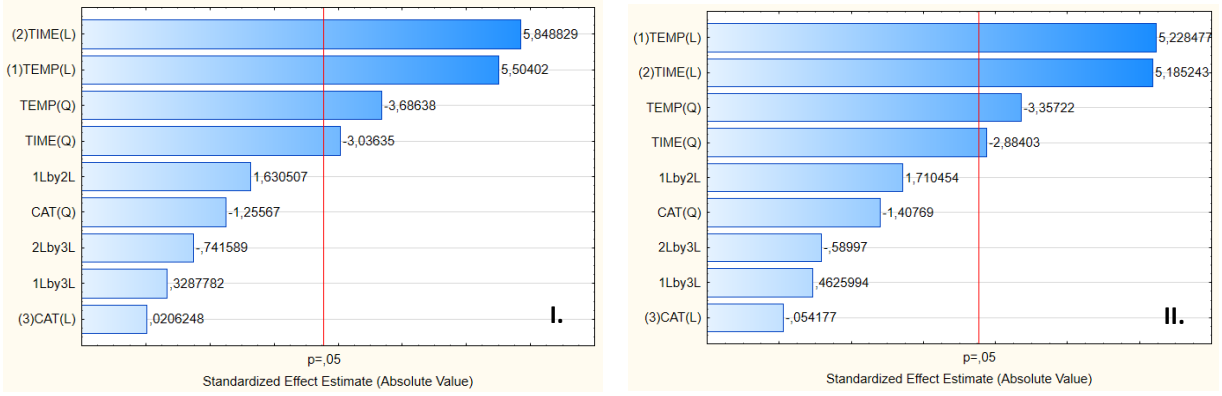

Figure 5.6 The Pareto Charts of Standardised Linear (L) and Quadratic (Q) Effects of Temperature (1), Time (2) and Catalyst Concentration (3) on **I.** The Degree of Substitution and **II.** The Oil Sorption of Cotton via the *Green* Surface Modification Reaction

The effects of temperature and time have been investigated at a constant catalyst concentration (7.5 % (v/v) NaOH-solution) in Figure 5.7 I and II. These response surfaces reflect the relationship between the parameters established by the ANOVA analyses and Pareto charts. The linear- and quadratic effects of the reaction temperature exhibited significant influences on the DS ($p = 5.31 \times 10^{-3}$ and $p = 2.11 \times 10^{-2}$) and OS ($p = 6.39 \times 10^{-3}$ and $p = 2.84 \times 10^{-2}$) accomplished by the acetylation reactions. This finding was confirmed by Koroskenyi & McCarthy (2001), where the temperature of the reaction demonstrated a significant influence on the acetylation of konjac glucomannan at 4 h with a 2 % (v/v) NaOH-solution.

I. (at 7.5 % (v/v) NaOH-solution)

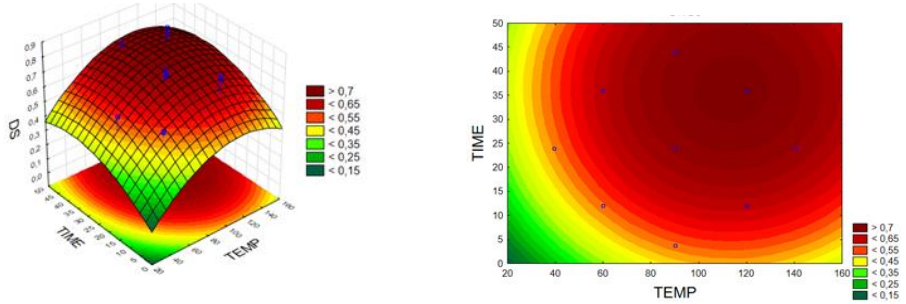

II. (at 7.5 % (v/v) NaOH-solution)

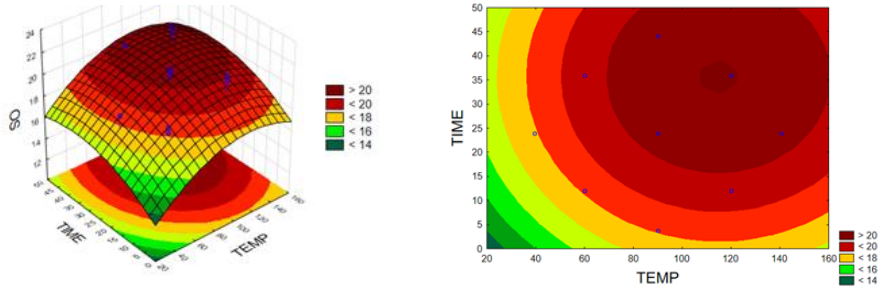

III. (at 24 h)

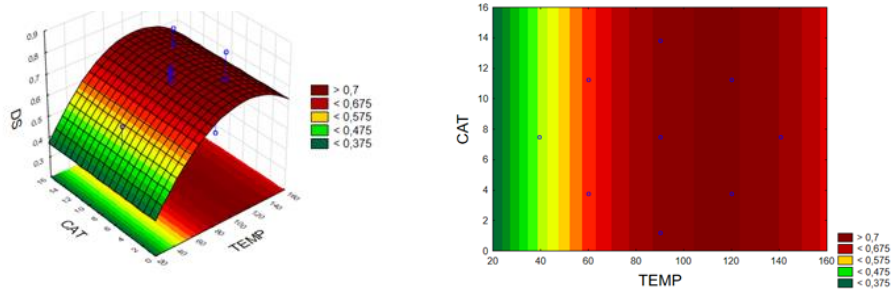

IV. (at 24 h)

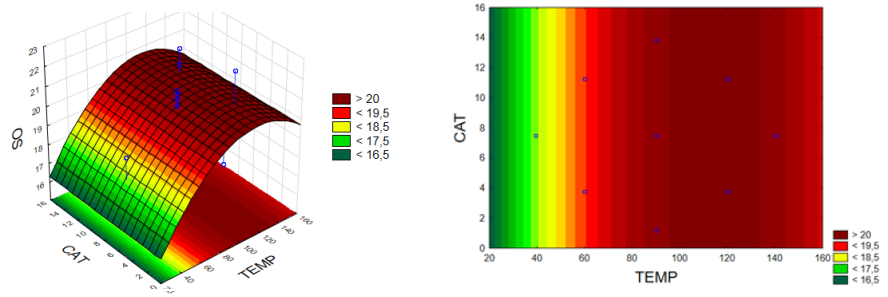

V. (at 90 °C)

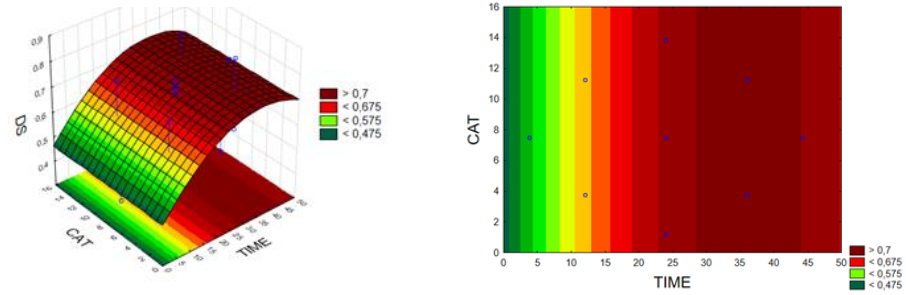

VI. (at 90 °C)

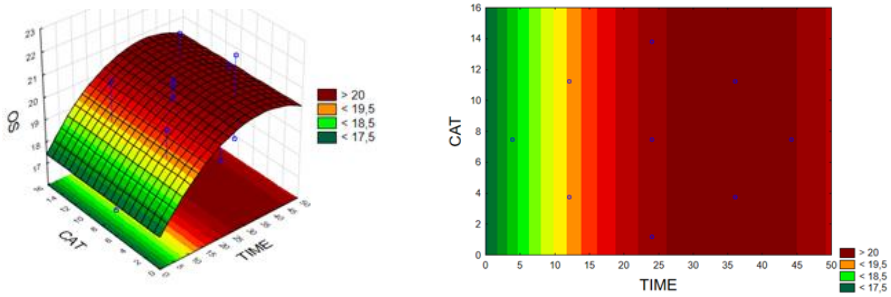

Figure 5.7 The 2-Dimensional and 3-Dimensional Response Surface Plots for the Effects of Temperature (°C), Time (h) and Lipase Concentration (U) on the Degree of Substitution (DS) and Oil Sorption (OS) of Cotton via the *Green* Surface Acetylation

Additionally, the linear- and quadratic effects of time established a significant influence on the DS ($p = 4.26 \times 10^{-3}$ and $p = 3.85 \times 10^{-2}$) and OS ($p = 6.58 \times 10^{-3}$ and $p = 4.48 \times 10^{-2}$) of the samples. From Figure 5.7 I and II it is clear that the highest peak in DS was reached at temperatures of approximately 100 °C to 130 °C and times of 30 h to roughly 45 h at a catalyst concentration of 7.5 % (v/v) NaOH-solution. However, Figure 5.7 III reveals that the highest DS values can be reached between 115 °C and 120 °C, with a contact time of 24 h.

It is noted that this reaction favours higher reaction temperatures. Conversely, at these extended durations, an increase to 140 °C leads to a decreased DS. It is important to note that the temperature should not be escalated above 140 °C, since a 50 % (w/w) NaOH-solution becomes volatile above 143 °C. The current experimental setup cannot condense the vapours at these amplified temperatures, as a chemical coolant is not employed in the condenser.

The peaks of performance for OS appear more robust, with the apex of performance reached at 115 °C to 120 °C and 35 h to 40 h. Nevertheless, the performance of DS and OS remained high for a wide range of temperature and reaction duration. High values of OS are predicted between 80 °C and 160 °C for reaction times of 20 h to 50 h.

According to the Pareto chart, no significant interactions occurred between temperature, time and catalyst concentration. This effect is visually evident in the response surface plots, where Figure 5.7 III to VI indicate that the linear and quadratic effects of the catalyst had negligible effects on the DS and OS of cotton via the *green* surface modification. This assertion stands in contrast to the outcome of the preliminary experiments (Appendix E.1, p. 156), where it was determined that the presence of the catalyst does improve the acetylation of the reaction. Furthermore, according to Koroskenyi & McCarthy (2001), a significant amount of acetylation of konjac glucomannan had taken place without the catalyst present. However, in their findings, the DS increased substantially when the catalyst was included (Koroskenyi & McCarthy, 2001). This occurrence indicates that the incorrect catalyst range was implemented in this study and that the NaOH-catalyst was not sufficient to facilitate the acetylation reaction (Figure 5.2). The NaOH acts as a Na^+-donor to activate the carbonyl groups in the acetic anhydride reactant. However, as the acetic acid by-product is formed, it will react with the NaOH catalyst in an acid-base reaction. Consequently, catalyst quenching will occur. If insufficient NaOH is present, this reaction step will limit the rate of reaction, and less acetylation will be able to take place. The study completed by Halal et al. (2014) implemented up to 23 % (v/v) NaOH-solution in the acetylation of barley starches. Future experiments should be completed to establish whether a higher concentration of NaOH will be sufficient to catalyse this reaction.

5.3.2.3 Application of the Optimal Conditions for the *Green* Acetylation of Cotton in the Modification of Cellulose from Corncob, Wheat Straw and Filter Paper

Statistica 13.2 was implemented to develop desirability plots, in order to predict at which combination of reaction conditions the highest DS and OS can be accomplished with this reaction. The acetylation conditions for the optimal modification of cotton was stipulated as 115.2 °C and 34.1 h (Figure 5.8). However, these desirability plots depicted that the presence of the NaOH-solution between 1.2 % (v/v) and 13.8 % (v/v) had the same acetylation to effect. Nevertheless, 13.8 % (v/v) NaOH-solution was implemented as the optimal catalyst concentration in order to provide an excess of catalyst to the reaction, thereby ensuring that no unintended influences were caused.

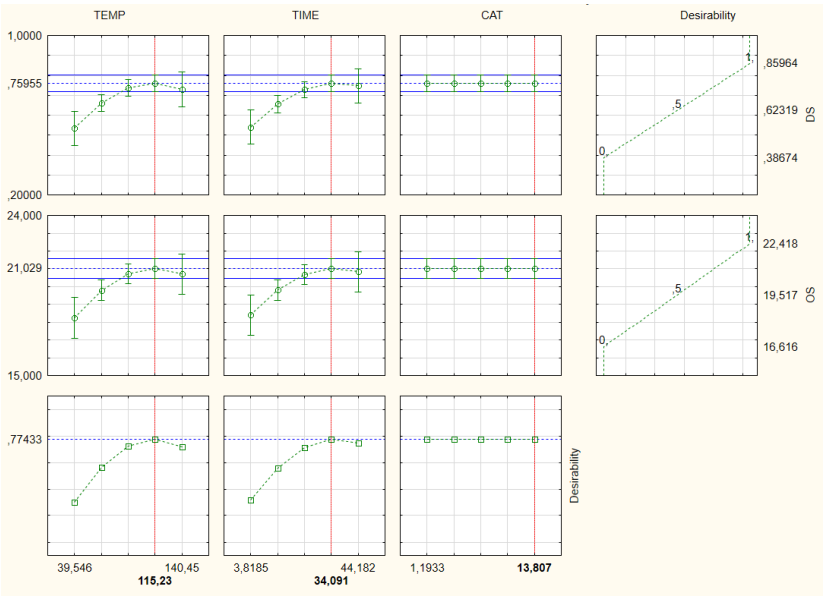

Figure 5.8 Profiles for the Predicted Values and Desirability Plots of the *Green* Modification of Cotton

These predicted reaction conditions were applied to cotton, CC cellulose, WS cellulose and filter paper to compare the actual experimental performance to the predicted DS of 0.76 and OS of 21.0 g/g. The results illustrated in Table 5.9 show that multiple feedstocks exceeded the 95 % confidence interval (α = 0.05) of the model predicted DS and OS values. This occurrence is a confirmation that the developed DS and OS models do not accurately predict the behaviour of this reaction, and additional experiments are advised to develop more robust statistical models. Nevertheless, since these DS and OS values exceed the expected results, the reaction conditions were accepted as the optimal operating conditions for this study.

Table 5.9 A Comparison of the Predicted and Experimental Degree of Substitution and Oil Sorption for the Optimal *Green* Modification of Cotton, Corncob Cellulose, Wheat Straw Cellulose and Filter Paper

Run [a]	Temperature (°C)	Time (h)	Catalyst Concentration [b, c] (%)	Model Prediction	Experimental Value	95 % Confidence Interval
DS						
CO-C2-OPT	115	34.1	13.8	0.76 [d]	1.25 ± 0.08	Exceeding
CC-C2-OPT	115	34.1	13.8	0.76 [d]	0.89 ± 0.05	Exceeding
WS-C2-OPT	115	34.1	13.8	0.76 [d]	0.91 ± 0.04	Exceeding
FP-C2-OPT	115	34.1	13.8	0.76 [d]	1.63 ± 0.14	Exceeding
OS (g oil/g sorbent)						
CO-C2-OPT	115	34.1	13.8	21.03 [e]	27.97 ± 0.71	Exceeding
CC-C2-OPT	115	34.1	13.8	21.03 [e]	21.80 ± 1.44	Within
WS-C2-OPT	115	34.1	13.8	21.03 [e]	21.04 ± 1.70	Within
FP-C2-OPT	115	34.1	13.8	21.03 [e]	26.85 ± 1.56	Exceeding

a – Run identification for cotton (CO), filter paper (FP), corncob (CC) cellulose and wheat straw (WS) cellulose, where C2 as suffix represents a *green* modification; **b** – Each run performed with a constant acetic anhydride loading of 30:1 (30 mL acetic anhydride to 1 g cellulose); **c** – Target sodium hydroxide (50 % (w/w) NaOH-solution) percentage, based on volume to volume ratio of acetic anhydride; **d** – The 95 % confidence interval for the prediction of degree of substitution (DS) at these conditions is 0.64 – 0.88, based on CO; **e** – The 95 % confidence interval for the prediction of oil sorption (OS) at these conditions is 19.49 – 22.57 g oil/g sorbent, based on CO

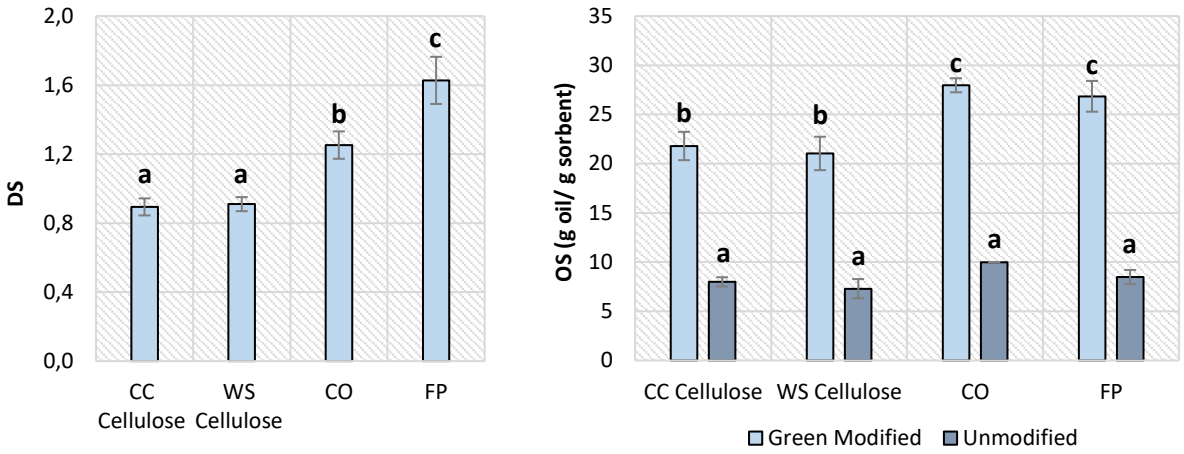

Figure 5.9 The Degree of Substitution (DS) and Oil Sorption (OS) achieved via the Optimised *Green* Surface Modifications of Cotton (CO), Corncob (CC) Cellulose, Wheat Straw (WS) Cellulose and Filter Paper (FP) at 115.2 °C, 34.1 h and 13.8 % (v/v) NaOH-solution

The *green* acetylation attained statistically comparable DS ($p = 0.63$) and OS ($p = 0.68$) for CC and WS cellulose, while a significantly amplified DS ($p = 1.68 \times 10^{-5}$) and OS ($p = 0.03$) were achieved with cotton (Figure 5.9). It is known that the molecular crystallinity of a sample can influence the potential for surface acetylation reactions since a higher crystallinity indicates more exposed hydroxyl groups on the fibre surface (Huntley et al., 2015). However, the cotton was acetylated to a greater extent than the CC and WS cellulose, despite retaining a statistically analogous molecular crystallinity (Table 5.5). This characteristic can be attributed to the 24 % to 33 % higher cellulose content of the cotton (Table 5.4), leading to more accessible hydroxyl groups available to take part in the acetylation reaction. The presence of lignin and hemicellulose contamination in the CC and WS cellulose resulted in fewer hydroxyl groups available for acetylation.

Furthermore, filter paper demonstrated a statistically similar OS ($p = 0.54$) to that of cotton while achieving a significantly higher DS ($p = 3.17 \times 10^{-3}$). The increased crystallinity of filter paper could contribute to the higher acetylations achieved for this feedstock. Additionally, the calcium carbonate binding material could potentially interfere with the chemical acetylation reaction (Figure 5.2) or the method of determining DS in this project (Section 3.4.7), leading to a false result. Even though the highest DS was attained by the filter paper, the modification only resulted in a 23 – 28 % higher OS when compared to CC and WS cellulose. Furthermore, despite attaining a 30 % lower DS, cotton still retained a similar OS to that of filter paper. The lack of three-dimensional structure of the filter paper disadvantages this feedstock for OS (Figure 5.10). Adsorption onto the acetylated surface can occur due to the high DS, but the two-dimensional structure does not allow for ample absorption into the fibrous surface.

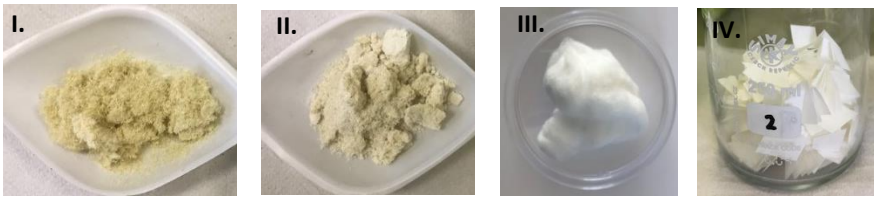

Figure 5.10 I. Unmodified, Isolated Wheat Straw Cellulose; **II.** Unmodified, Isolated Corncob Cellulose; **III.** Unmodified Cotton and **IV.** Unmodified Filter Paper for an Additional Reference Test

All modified feedstocks demonstrated significantly augmented OS ($p = 1.49 \times 10^{-7}$) when compared to the unmodified samples (Figure 5.9), indicating that the affinity toward OS was accomplished through the surface acetylation reactions. Specifically, the *green* acetylation of the CC cellulose and WS cellulose improved the OS by 63 to 65 %.

5.3.3 The *Non-green* Acetylation of Cotton, Corncob Cellulose, Wheat Straw Cellulose and Filter Paper by Acetic Anhydride and Sulfuric Acid

5.3.3.1 The Degree of Substitution and Oil Sorption of Modified and Unmodified Cotton Cellulose

The responses of DS and OS achieved by the traditional *non-green* modification at the specified reaction conditions are displayed in Table 5.10. These experiments were accomplished by varying the reaction temperature between 30 °C and 90 °C, the acetylation duration from 2 to 4 h and the catalyst concentration between 0 and 10 % (v/w) sulfuric acid. Figure 5.11 depicts the DS and Fourier Transform Infrared (FT-IR) spectra of each experimental run, while the OS values are presented in Figure 5.12.

Table 5.10 The Degree of Substitution and Oil Sorption of Modified and Unmodified Cotton achieved through the *Non-green* Acetylation by Acetic Anhydride and Sulfuric Acid for Hydrophobicity Improvement

Run ID [a, b]	Temp (°C)	Time (h)	Catalyst Loading [c] (%)	DS [d]	OS [e] (g/g)
CO-C1-0 [f]	n/a	n/a	n/a	n/a	9.99 ± 0.01
CO-C1-1	30	2	5	0.98 ± 0.06	16.87 ± 0.92
CO-C1-2	60	2	5	2.19 ± 0.04	36.73 ± 0.58
CO-C1-3	90	2	5	1.83 ± 0.08	30.63 ± 0.68
CO-C1-4	60	4	5	2.09 ± 0.11	33.96 ± 0.90
CO-C1-5	60	2	10	1.29 ± 0.05	22.58 ± 0.38
CO-C1-6	60	2	0	0.42 ± 0.04	10.41 ± 0.12
CO-C1-7	60	2	9	2.04 ± 0.12	34.41 ± 0.56

a – Run identification for cotton (CO), where C1 as suffix represents a *non-green* modification; **b** – Each run performed with a constant acetic anhydride loading of 25:1 (25 mL acetic anhydride to 1 g CO); **c** – Target sulfuric acid percentage, based on volume to the mass of CO; **d** – Degree of Substitution is abbreviated as DS; **e** – Oil Sorption is abbreviated as OS; **f** – Unmodified CO sample for reference

The effect of temperature was investigated by performing the reactions identified by CO-C1-1, CO-C1-2 and CO-C1-3 at a set time of 2 h and a constant catalyst concentration of 5 % (v/w) sulfuric acid. The temperature was varied between 30 and 90 °C. The FT-IR in Figure 5.11 II illustrates the intensifying ester peaks at 1 740 cm^{-1}, 1 369 cm^{-1} and 1 234 cm^{-1} when increasing the temperature from 30 °C to 60 °C, with an accompanied drastic reduction in hydroxyl peaks at 3 337 cm^{-1}, 1 337 cm^{-1} and 1 310 cm^{-1}. This phenomenon indicates successful acetylation. Analogously, a significant increase in DS ($p = 3.67 \times 10^{-8}$) and OS ($p = 1.50 \times 10^{-3}$) occurred when escalating the temperature from 30 °C to 60 °C (Figure 5.11 and Figure 5.12). A further escalation to 90 °C transpired in lowered ester peaks and a significantly reduced DS ($p = 1.56 \times 10^{-4}$) and OS ($p = 1.05 \times 10^{-2}$).

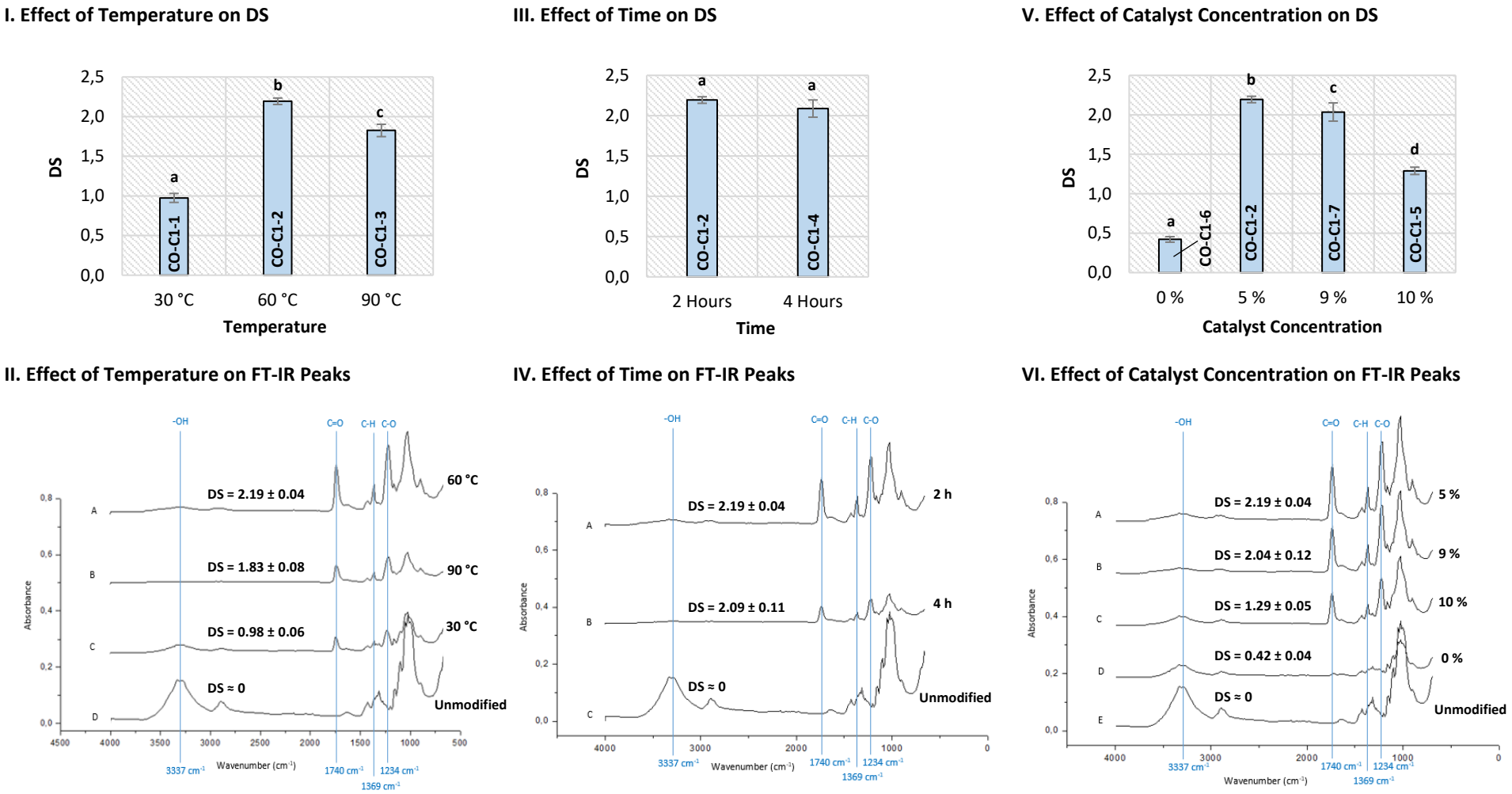

Figure 5.11 The Effects of Temperature, Time and Catalyst Concentration on the Degree of Substitution (DS) and Fourier Transform Infrared (FT-IR) Spectra of the *Non-green* Acetylated Cotton at **I., II.** Constant Time and Catalyst Concentration (2 h, 5 % (v/w) Sulfuric Acid); **III., IV.** Constant Temperature and Catalyst Concentration (60 °C, 5 % (v/w) Sulfuric Acid); **V., VI.** Constant Temperature and Reaction Time (60 °C, 2 h)

I.

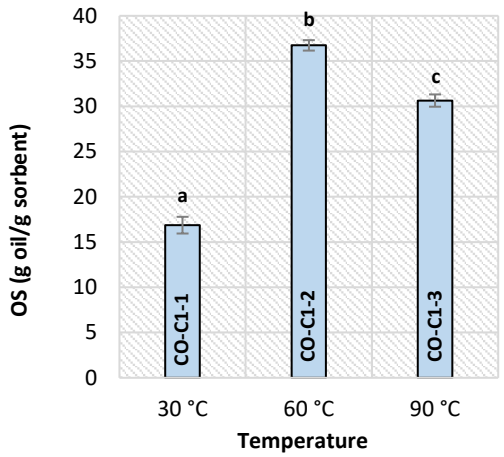

II.

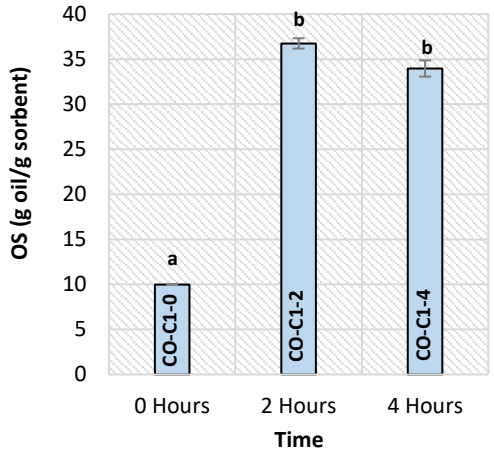

III.

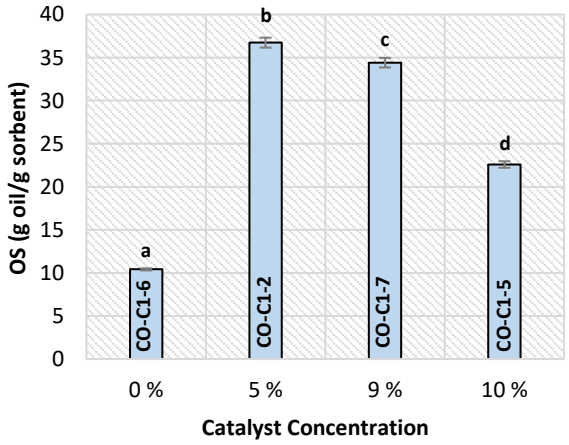

Figure 5.12 I. The Effect of Temperature on the Oil Sorption (OS) of Cotton during *Non-green* Acetylation at a Constant Time and Catalyst Concentration (2 h, 5 % (v/w) Sulfuric Acid); **II.** The Effect of Time on the OS of Cotton during *Non-green* Acetylation at a Constant Temperature and Catalyst Concentration (60 °C, 5 % (v/w) Sulfuric Acid); **III.** The Effect of Catalyst Concentration on the OS of Cotton during *Non-green* Acetylation at a Constant Reaction Temperature and Time (60 °C, 2 h)

These results suggest that higher reaction temperatures lead to improved diffusion of acetic anhydride into the fibre surface, achieving substantial molecular swelling, which exposes the internal hydroxyl groups for acetylation (Huang et al., 2014). However, the reaction rate is increased by elevated temperatures. As the acetylation reaction

occurs, acetic acid is formed as a by-product, as indicated in Figure 5.3. Increased fibre exposure to the acidic by-product, in combination with the acidic reactant, leads to acid hydrolyses of the glycosidic oxygen bond in the cellulose structure (Bozic et al., 2015). Consequently, the fibres undergo chemical degradation.

The runs CO-C1-0, CO-C1-2 and CO-C1-4 were employed to study the effects of reaction duration on the extent of acetylation at a constant temperature (60 °C) and constant catalyst concentration (5 % (v/w) sulfuric acid). Figure 5.12 II demonstrates a significant incline in OS ($p = 2.33 \times 10^{-4}$) achieved when comparing the sample modified for 2 h to the unmodified cotton sample. This was accompanied by a substantial increase in ester peak intensities, as indicated in Figure 5.11 IV. Amplifying the reaction time increases the contact between the fibres and the reactants, thereby achieving more acetylation (X. F. Sun et al., 2002).

Figure 5.11 III and Figure 5.12 II depict that a performance plateau was reached when increasing the reaction time from 2 h to 4 h at 60 °C and a 5 % (v/w) sulfuric acid concentration. A statistically similar DS ($p = 0.11$) and OS ($p = 0.07$) were attained for the reaction duration of 2 h and 4 h. This plateau was supplemented by considerably lowered ester peak intensities a 4 h (Figure 5.11 IV), indicating that the reaction at 2 h accomplished a higher acetylation extent than the reaction conducted for 4 h. After longer reaction times, the easily accessible hydroxyl groups are already acetylated, and only the more inaccessible hydroxyls remain. The rate of reaction consequently slows down since these hydroxyls are harder to access and replace (Tingaut et al., 2009). An experiment was conducted at 6 h, 60 °C and 5 % (v/w) sulfuric acid (Figure 5.13) in order to establish whether a longer reaction time will overcome the performance plateau by augmented molecular swelling, resulting in the availability of more exposed hydroxyl groups available for reaction. However, the cotton was degraded by acid hydrolyses at these conditions, indicating that the reaction duration could not be increased to 6 h for improved acetylation.

I.  **II.** 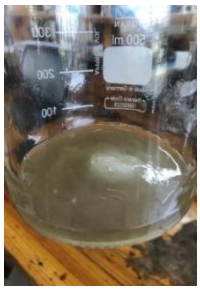

Figure 5.13 I. Non-degraded Cotton, Acetylated at 2 h, 60 °C and 5 % (v/w) Sulfuric Acid, and **II.** Cotton showing Signs of Degradation by Acid Hydrolyses, Modified at 6 h, 60 °C and 5 % (v/w) Sulfuric Acid

The effect of the sulfuric acid catalyst was investigated by performing reactions identified by CO-C1-2, CO-C1-5, CO-C1-6 and CO-C1-7 at a set temperature of 60 °C and a constant reaction time of 2 h. The sulfuric acid concentration was varied between 0 % (v/w) and 10 % (v/w). The reaction conducted without the catalyst demonstrated marginally decreased hydroxyl peaks, but substantial acetyl peaks did not form at these conditions (Figure 5.11 VI). The absence of the acetyl peaks indicates that the rate of reaction is too slow to achieve significant acetylation without the sulfuric acid catalyst.

Increasing the sulfuric acid concentration to 5 % (v/w) accomplished a significant incline in DS ($p = 8.11 \times 10^{-10}$) and OS ($p = 2.51 \times 10^{-4}$), accompanied by dramatically amplified ester peaks and considerably decreased hydroxyl peaks (Figure 5.11 VI). Conversely, a further increase to 9 % (v/w) resulted in a marginally declined DS ($p = 0.04$) and OS

($p = 0.04$). Moreover, a further escalation to 10 % (v/w) sulfuric acid resulted in a substantial decrease in ester peaks, DS ($p = 2.07 \times 10^{-5}$) and OS ($p = 1.62 \times 10^{-3}$).

Therefore, increasing the catalyst concentration above 5 % (v/w) demonstrated comparable effects to increasing the temperature above 60 °C and the reaction time above 4 h. The highly acidic environment caused by the catalyst and acidic by-product instigated fibre hydrolyses, which led to a decrease in DS. Since the fibres are hydrolysed, the decline in three-dimensional molecular structure leads to decreased sorption. The completion of a full CCD is recommended for future studies in order to determine the interactions between temperature, time and sulfuric acid concentration.

5.3.3.2 Application of the Optimal Conditions for the *Non-green* Acetylation of Cotton in the Modification of Cellulose from Corncob, Wheat Straw and Filter Paper

From the single-factor experiments concluded in Table 5.10, it was determined that the optimal performance from the set of conditions tested were found to occur at 60 °C, 2 h and 5 % (v/w) sulfuric acid – relating to specifications examined in the experimental run identified by CO-C1-2. These parameters were applied to CC cellulose, WS cellulose and filter paper. The results are displayed in Table 5.11.

Table 5.11 The Degree of Substitution and Oil Sorption for the Optimal *Non-green* Modification of Cotton, Corncob Cellulose, Wheat Straw Cellulose and Filter Paper

Run [a]	Temperature (°C)	Time (h)	Catalyst Concentration [b, c] (%)	DS [d]	OS [e] (g oil /g sorbent)
CO-C1-OPT	60	2	5	2.19 ± 0.04	36.73 ± 0.58
CC-C1-OPT	60	2	5	1.54 ± 0.05	30.79 ± 2.08
WS-C1-OPT	60	2	5	1.55 ± 0.05	29.51 ± 0.93
FP-C1-OPT	60	2	5	2.75 ± 0.21	33.27 ± 0.89

a – Run identification for cotton (CO), filter paper (FP), corncob (CC) cellulose and wheat straw (WS) cellulose, where C1 as suffix represents a *non-green* modification
b – Each run performed with a constant acetic anhydride loading of 25:1 (25 mL acetic anhydride to 1 g cellulose)
c – Target sulfuric acid percentage, based on volume to the mass of cellulose
d – Degree of Substitution is abbreviated as DS
e – Oil Sorption is abbreviated as OS

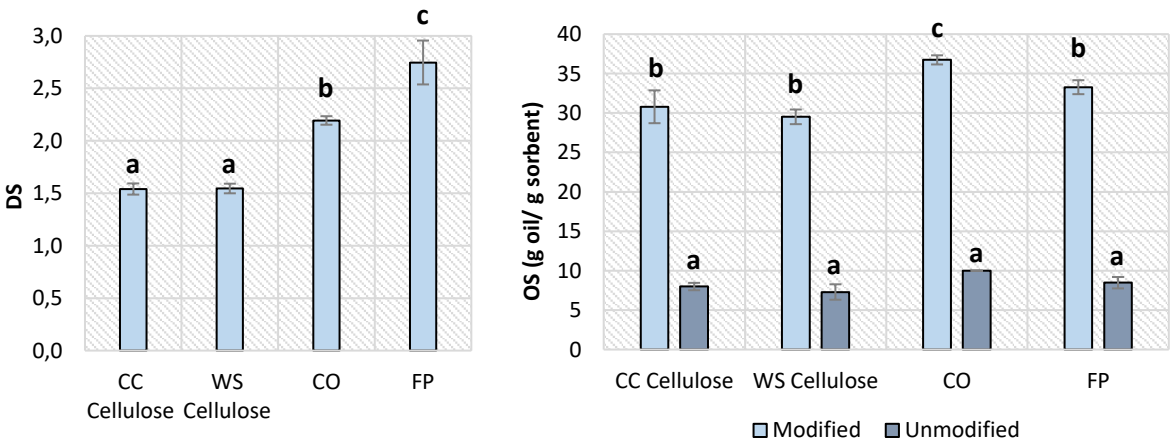

Figure 5.14 The Degree of Substitution (DS) and Oil Sorption (OS) achieved via the Optimised *Non-green* Surface Acetylation of Cotton (CO), Corncob (CC) Cellulose, Wheat Straw (WS) Cellulose and Filter Paper (FP) at 60 °C, 2 h and 5 % (v/w) Sulfuric Acid

This *non-green* acetylation achieved a statistically similar DS ($p = 0.89$) for CC and WS cellulose, while a significantly amplified DS ($p = 1.14 \times 10^{-8}$) was realised with cotton (Figure 5.14). As with the *green* modification (Section 5.3.2), filter paper exhibited the highest DS ($p = 2.04 \times 10^{-3}$), while maintaining an OS statistically analogous to CC and WS cellulose ($p = 0.16$). Cotton had a significantly improved OS ($p = 0.02$). This trend was in-line with the conclusions reached with the optimal *green* surface modification reaction. It was established that the higher cellulose purity of cotton led to a higher potential for acetylation, while the contaminants in the isolated CC and WS cellulose resulted in fewer hydroxyl groups available for the reaction. This phenomenon occurred despite these sources exhibiting statistically similar molecular crystallinities. Furthermore, it was indicated that the amplified crystallinity of filter paper could contribute to the augmented DS attained. However, even though the highest DS was reached by the filter paper, the lack of a three-dimensional structure resulted in a disadvantage of absorption into the acetylated surface.

All modified feedstocks demonstrated significantly increased OS values ($p = 2.89 \times 10^{-9}$) when compared to the unmodified samples (Figure 5.14), indicating that the affinity toward OS was achieved through the surface acetylation reactions. Specifically, the *non-green* acetylation of the CC and WS cellulose improved the OS by roughly 75 %.

In the study conducted by Huang et al. (2014), a related acetylation reaction was performed on rice straw fibre instead of cellulose (Table 5.12). Huang et al. (2014) did not determine the DS or OS reached by the surface modifications, and the reactions were not statistically optimised. The success of acetylation in their study was rather based on the weight percent gain (WPG) achieved at different reaction conditions in single-factor experiments. A WPG will theoretically be established with modification since an acetyl group attains a higher molecular weight than a hydroxyl group (X. F. Sun et al., 2004). Replacing the surface hydroxyls with acetyls will, therefore, lead to an increased weight of the sample.

Table 5.12 The Degree of Substitution Attained by Huang et al. (2014) on Rice Straw Fibre, Compared to the Acetylation Achieved with Corncob Cellulose and Wheat Straw Cellulose

Feedstock [a]	Temp (°C)	Time (min)	Sulfuric Acid [b] (%)	DS [c]	Reference
Rice Straw Fibre	50	2	9	- [d]	(Huang et al., 2014)
CC Cellulose	60	2	5	1.54 ± 0.05	Table 5.11
WS Cellulose	60	2	5	1.55 ± 0.05	Table 5.11

a – Corncob is abbreviated as CC, and wheat straw is abbreviated as WS; **b** – Target sulfuric acid percentage, based on volume to the mass of feedstock; **c** – Degree of Substitution is abbreviated as DS; **d** – DS not determined, but rather a weight percent gain of 40.1 % was achieved (Huang et al., 2014)

As indicated in Table 5.12, the highest acetylation of rice straw occurred at 50 °C, 2 h and 9 % (v/w) sulfuric acid (Huang et al., 2014). However, the current study conducted on CC and WS cellulose determined 60 °C, 2 h and 5 % (v/w) sulfuric acid as the optimal *non-green* reaction conditions (Table 5.11). Contrary to the CC and WS cellulose samples, rice straw fibre possesses a defensive lignin barrier that protects the biomass from acid hydrolyses (Salajkova, 2013). Consequently, the optimal results on cellulose require less acidic conditions than the rice straw fibre, since reduced protective lignin structures are present to shield the fibres from degradation.

5.3.4 The Comparison between the *Green* Acetylation and the *Non-green* Acetylation of Corncob Cellulose and Wheat Straw Cellulose Films

5.3.4.1 Extent of Acetylation

The successes of acetylation achieved by the *green* and *non-green* modifications of CC and WS cellulose were compared in this section, based on DS, FT-IR and Water Contact Angles (WCA). The FT-IR spectra (Figure 5.16) indicate the molecular changes brought about by the acetylations of the samples. The three main ester bands are designated at 1 740 cm^{-1}, 1 369 cm^{-1} and 1 234 cm^{-1}, signifying the C=O stretching of the ester, the –O(C=O)-CH_3 and C-H bands, respectively (Zepic et al., 2015). The intensification of these peaks in the *green* and *non-green* modified samples indicate the addition of surface acetyl groups by modification. Figure 5.17 depicts the significantly higher DS ($p = 5.33 \times 10^{-11}$) attained by the *non-green* acetylations of both CC and WS cellulose. This assertion is confirmed by higher ester bands in Figure 5.16 II and III when compared to the *green* modified samples in Figure 5.16 V and VI.

In conjunction, the hydroxyl bands at 3 337 cm^{-1}, 1 337 cm^{-1} and 1 310 cm^{-1} were reduced by the modifications. Conversely, these hydroxyl peaks were not completely obliterated, indicating incomplete acetylation via the *green* and *non-green* acetylations.

As discussed in Section 2.2.1, cellulose consists of linked chains of AGUs, which make up the glucose units forming the cellulose backbone (Arola, 2015). The hydroxyl groups form strong intramolecular forces between glucose units and strong intermolecular hydrogen bonds between cellulose chains, as depicted in Figure 5.15 (Ibrahim & Mondal, 2019; Lavoine et al., 2012). Since each AGU has three reactive hydroxyl groups, a maximum DS of three can be accomplished. The attained DS values of lower than three (Figure 5.17), accompanied by the presence of hydroxyl peaks on the FT-IR (Figure 5.16), suggest that the acetylation predominantly occurred on the most exposed, exterior hydroxyl groups. In contrast, the internal hydroxyl groups were left unacetylated (Bozic et al., 2015). Supplementary reaction steps which promote more molecular swelling to expose the internal hydroxyl groups might be necessary to facilitate the additional acetylation.

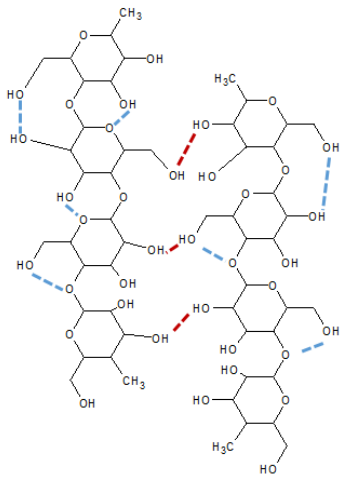

Figure 5.15 The Inter- (Red) and Intramolecular (Blue) Bonding of Cellulose Chains, redrawn from Rowell et al. (2012)

I. CO – *Non-green*

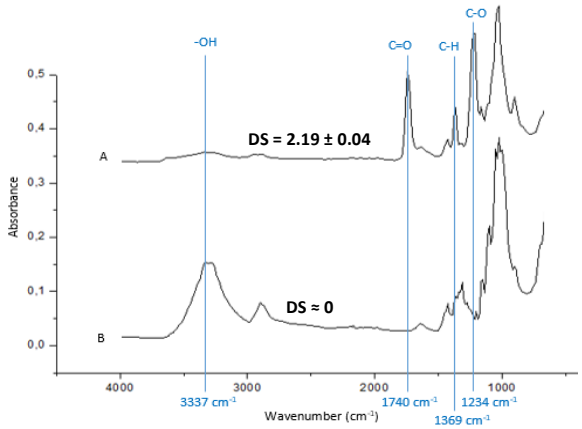

II. CC Cellulose – *Non-green*

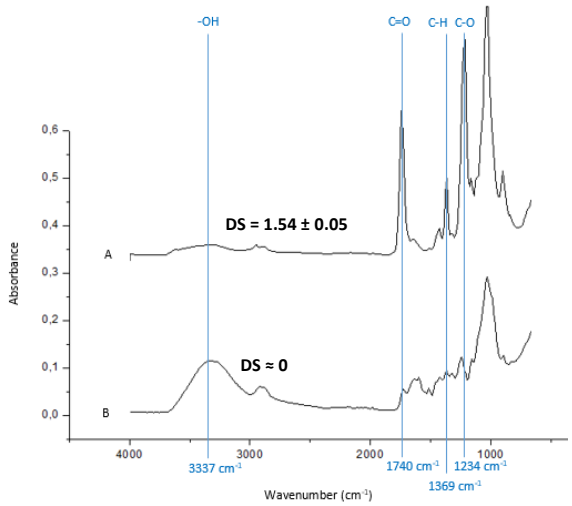

III. WS Cellulose – *Non-green*

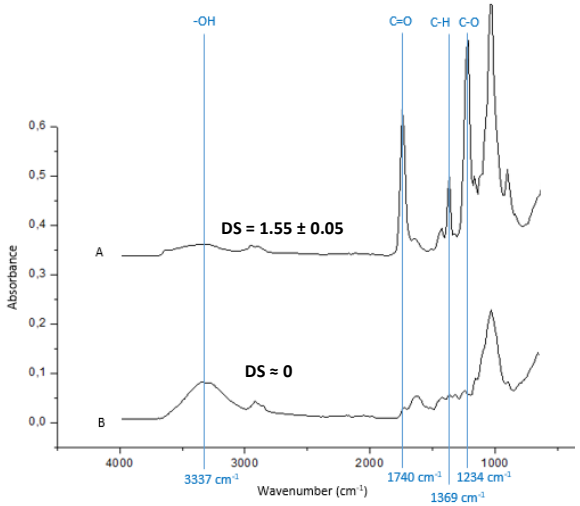

IV. CO – *Green*

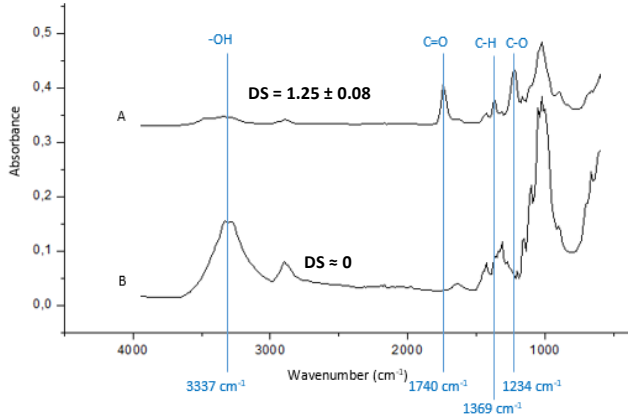

V. CC Cellulose – *Green*

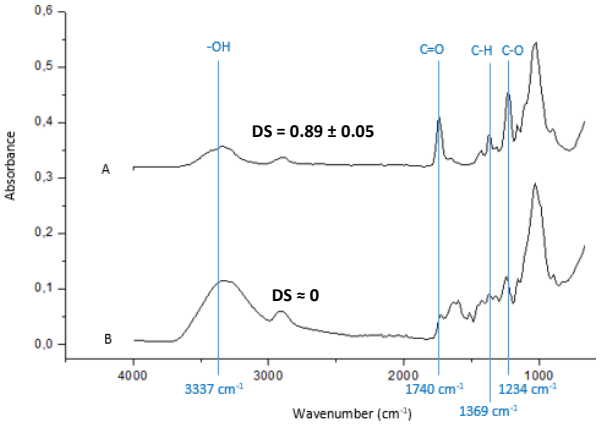

VI. WS Cellulose – *Green*

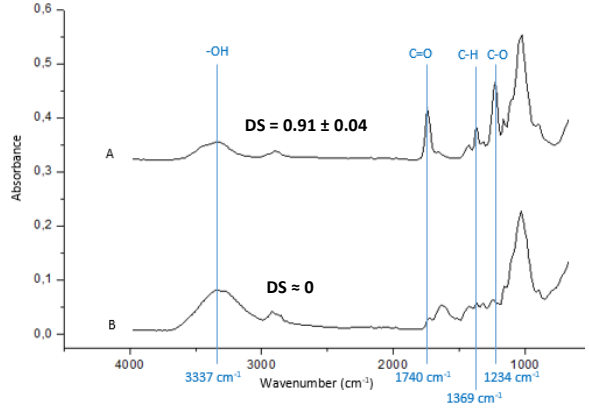

Figure 5.16 The Degree of Substitution (DS) and Fourier Transform Infrared Spectra of Cotton (CO), Corncob (CC) Cellulose and Wheat Straw (WS) Cellulose, where ***A*** depicts an Optimally Modified Sample (*Green* at 115.2 °C, 34.1 h and 13.8 % (v/v) NaOH-solution; *Non-green* at 60 °C, 2 h and 5 % (v/w) Sulfuric Acid). ***B*** represents an Unmodified Sample.

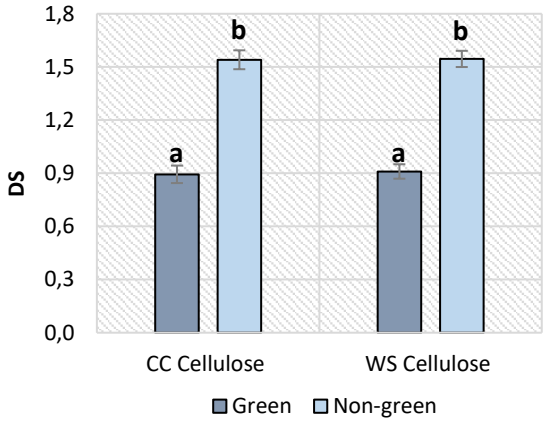

Figure 5.17 The Degree of Substitutions (DS) achieved via the Optimised *Green* and *Non-green* Surface Modifications of Corncob (CC) Cellulose and Wheat Straw (WS) Cellulose

The low DS values achieved via the *green* acetylation can correspondingly be indicative that the NaOH-catalyst was not able to facilitate the acetylation reaction. As established in Section 5.3.2.2, the NaOH acts as a Na^+-donor to activate the carbonyl groups in the acetic anhydride reactant. However, as the acetic acid by-product is formed, it will react with the NaOH catalyst in an acid-base reaction. Consequently, catalyst quenching will occur. If an insufficient amount of NaOH is present for the reaction, this reaction step will limit the rate of reaction, and lower acetylation will be able to take place. Concurrently, the low DS attained by the *non-green* acetylation can be indicative of undetected minor molecular destruction by acid hydrolyses. If the AGUs are hydrolysed by an acidic environment, fewer hydroxyl groups can be replaced by acetyl groups, which will be detected as a lower DS.

The hemicellulose and lignin contamination in the unmodified cellulose can also have an impact on the acetylation of these samples since the molecular crystallinities of the fibres are influenced by these molecules. Subsequent purification using methods such as bleaching with sodium chloride would improve the quality of the cellulose (Shamsabadi, Behzad, & Bagheri, 2015). Nevertheless, this step is regarded as *non-green* and was thus not included in this study.

5.3.4.2 The Water Contact Angles and Heterogeneous Oil Sorption of Cellulose Films

Cellulose films were created from CC and WS cellulose via the methodology described in Section 5.2.5. The heterogeneous OS values of the films were qualitatively investigated (Figure 5.18) by placing the films in a mixture of artificial seawater (3.5 % (w/w) sodium chloride in distilled water) and motor oil (Shell Helix Ultra, 5W-40) (Alaa El-Din et al., 2018). The water contact angles (WCA, θ) of the films are also indicated in Figure 5.18.

The unmodified CC cellulose (Figure 5.18 I) and unmodified WS cellulose (Figure 5.18 II) retained 0 ° WCA, with immediate penetration of the water droplets into the fibrous surface. The presence of extensive amounts of accessible hydroxyl groups at the external and internal molecular cellulose surfaces of the unmodified samples causes the exhibition of polar, hydrophilic behaviour (Salajkova, 2013). This characteristic resulted in inadequate removal of the oil from the water since the cellulose sources demonstrate a higher affinity to the polar water particles than to the non-polar oil particles.

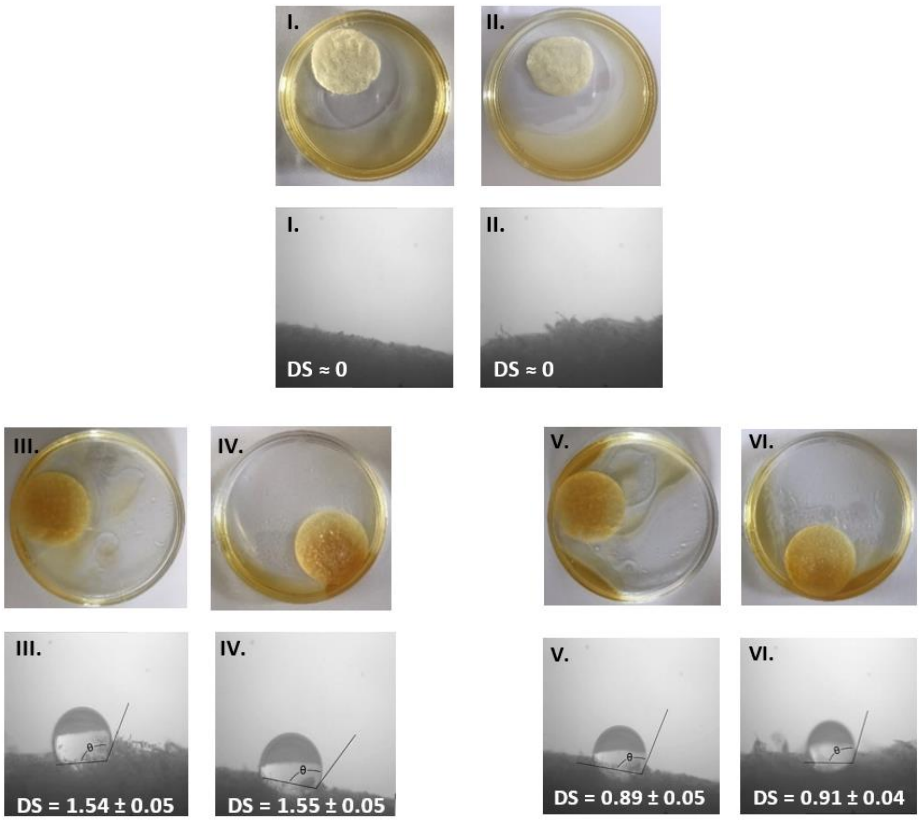

Figure 5.18 The Degree of Substitution (DS) and Qualitative Heterogeneous Oil Sorption of Motor Oil in Artificial Seawater and the Water Contact Angle (θ) for **I.** Unmodified Corncob (CC) Cellulose (θ = 0 °) and **II.** Unmodified Wheat Straw (WS) Cellulose (θ = 0 °); **III.** Optimal *Non-green* Modified CC Cellulose (θ = 113.5 ± 1.0 °) and **IV.** Optimal *Non-green* Modified WS Cellulose (θ = 114.8 ± 1.5 °); **V.** Optimal *Green* Modified CC Cellulose (θ = 103.1 ± 0.6 °) and **VI.** Optimal *Green* Modified WS Cellulose (θ = 106.1 ± 0.4 °)

However, when these polar hydroxyl molecules were replaced by non-polar acetyl groups, a higher affinity towards oil was achieved (Hatton et al., 2015; Hubbe, Ayoub, et al., 2013). Consequently, the fibres became hydrophobic and oleophilic (She et al., 2010). This attribute is demonstrated by the *green* and *non-green* modified films (Figure 5.18 III – VI), where an improved affinity to OS can be visually noted. The *non-green* acetylated films reached improved WCA of 113.5 ± 1.0 ° for CC cellulose and 114.8 ± 1.5 ° for WS cellulose. In conjunction, the *green* acetylated films reached WCA of 103.1 ± 0.6 ° for CC cellulose and 106.1 ± 0.4 ° for WS cellulose. Since these values exceed 90 °, the *green* and *non-green* modified films were classified as hydrophobic and therefore, oleophilic (Zanini et al., 2017; Zhou et al., 2016). The marginally lower WCA, in combination with the higher quantities of visible residual oil for the *green* modified samples (Figure 5.18 V – VI), reiterates that the *non-green* films had a higher acetyl content and therefore exhibited slightly more hydrophobic behaviour.

As an additional analysis, the heterogeneous oil- and water sorptions (OS and WA) were quantitatively determined with sunflower oil and distilled water, as displayed in Figure 5.19. The unmodified CC and WS cellulose films demonstrated an affinity towards WA with 16.75 ± 0.23 g/g and 15.14 ± 0.11 g/g retained. In conjunction, only 4.88 ± 0.77 g/g and 4.72 ± 0.43 g/g oil were removed with these films.

The affinity for OS was significantly augmented by the *green* and *non-green* surface acetylation reactions for both CC and WS cellulose. The *green* modifications achieved significantly higher OS ($p = 6.95 \times 10^{-4}$) of 12.09 ± 0.45 g/g and 12.77 ± 1.15 g/g when compared to the unmodified samples. However, the *non-green* modified CC and WS cellulose films significantly outperformed the *green* films ($p = 2.07 \times 10^{-3}$) with OS of 20.39 ± 0.62 g/g and 21.03 ± 1.69 g/g, respectively.

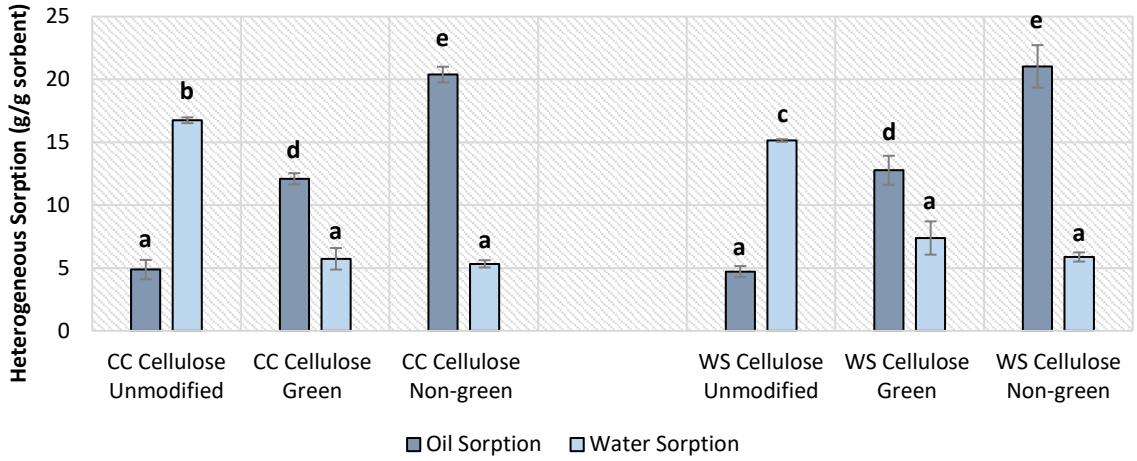

Figure 5.19 The Heterogeneous Oil- and Water Sorptions determined with Sunflower Oil and Distilled Water at Room Temperature (± 20 °C) for Modified and Unmodified Corncob (CC) Cellulose and Wheat Straw (WS) Cellulose

Figure 5.19 depicts that the OS for the modified CC and WS cellulose films were significantly higher than the WA, regardless of the type of modification. This occurrence proves that a selective affinity towards OS was accomplished through the surface modifications in this study. Nevertheless, even though the *green* acetylations are favoured due to their environmentally benign properties, the *green* films merely achieved approximately 60 % of the performance of the *non-green* films, based on OS. The higher performance of the *non-green* films will need to be sacrificed for environmental gain.

5.3.4.3 The Homogeneous Oil Sorption of Cellulose Films and Cellulose Particles

The homogeneous OS was quantitatively determined with sunflower oil, as displayed in Figure 5.20. These measurements were completed for the cellulose particles and compared to the measurements conducted with the cellulose films.

The OS analyses indicated that the sorptions achieved by the individual cellulose particles were significantly higher than that of cellulose films for each sample. The presence of the konjac glucomannan binding material in the cellulose films adversely affected the OS ability. In order to act as binding material, the konjac glucomannan cross-linked with some of the active chemical sites of the cellulose molecules (Ibrahim & Mondal, 2019; Liu et al., 2017). These konjac glucomannan fibres have abundant surface hydroxyl groups (Koroskenyi & McCarthy, 2001), which render the fibres highly hydrophilic. Utilising this substance as binding material for the cellulose films essentially reverses some of the effects brought about by surface modification. It is necessary to apply additional surface acetylation methods to the konjac glucomannan fibres post-film formation, or an alternative, less-hydrophilic binding material needs to be implemented.

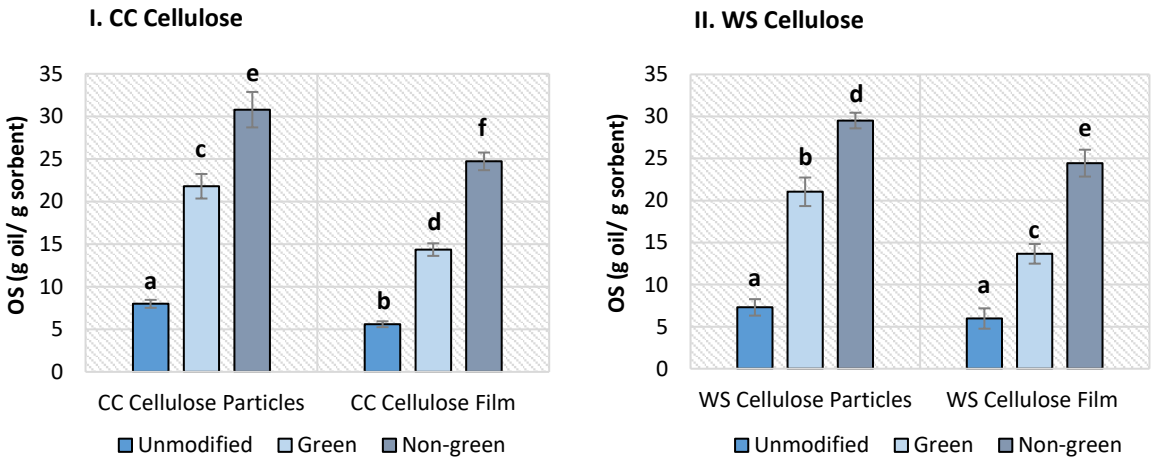

Figure 5.20 The Homogeneous Oil Sorption (OS) of Sunflower Oil at Room Temperature (± 20 °C) for the Modified and Unmodified Cellulose Samples as Particles, Compared to the Samples Packaged as Films for **I.** Corncob (CC) Cellulose and **II.** Wheat Straw (WS) Cellulose

However, the traditional petrochemical-based sorbents, such as polyurethane foam, polypropylene webs, nanoporous polystyrene fibres, and rubber gels are known to retain approximately 60 – 70 g/g motor oil (Nyankson, Rodene, & Gupta, 2016; She et al., 2010). The biosorbents developed from CC and WS cellulose can, therefore, not compete with the performances achieved by the petrochemical-based sorbents. Subsequently, the study was shifted to the *nanofibrillated cellulose (NFC) level* (Chapter 6) in order to establish whether the CC and WS NFC-based sorbents can exhibit increased sorption capacities in order to be considered as a worthy competitor for the *non-green* alternatives.

Chapter 6 – The Isolation and Modification of Nanofibrillated Cellulose from Corncob and Wheat Straw for the Optimisation of Oil Sorption

Abstract

Aerogels tuned to be oleophilic and hydrophobic were developed from corncob (CC) and wheat straw (WS) nanofibrillated cellulose (NFC), which were modified via *green* and *non-green* acetylations in order to increase hydrophobicity and oleophilicity for selective oil removal from water. The *green* modification yielded hydrophobic CC and WS NFC aerogels with water contact angles (WCA) of 117.2 ± 0.4 ° and 115.2 ± 2.8 °, heterogeneous selective oil sorption (OS) of 41.48 ± 3.25 g/g and 41.60 ± 2.32 g/g, and degree of substitution (DS) of 1.01 ± 0.12 and 0.85 ± 0.15. The *non-green* modified CC and WS NFC aerogels had WCA of 123.7 ± 2.5 ° and 121.9 ± 4.0 °, with OS of 46.23 ± 0.45 g/g and 45.12 ± 0.90 g/g, and DS of 1.32 ± 0.06 and 1.15 ± 0.05. From these results, it was apparent that the CC and WS NFC reacted analogously to the *green* acetylation. Additionally, these feedstocks responded similarly to the *non-green* acetylation, and corresponding results were achieved with the different feedstocks by each method. Lastly, the performance by the *green* CC and WS NFC aerogels compared favourably to the performance achieved by the *non-green* aerogels, and motor oil sorptions of 71 – 74 g/g were achieved which were comparable to the commercially implemented petrochemical-based sorbents.

6.1 Introduction

The surface area available for OS was amplified by isolating NFC from the unmodified CC and WS cellulose segregated in Chapter 5. The molecular surfaces of the NFC particles were modified to become hydrophobic and oleophilic via *green* and *non-green* surface acetylation reactions. The *green* NFC modification involved a combination of acetic anhydride, dimethyl sulphoxide (DMSO) and lipase from *Aspergillus niger* (EC 232-619-9), while the *non-green* NFC acetylation combined acetic anhydride, dimethylformamide (DMF) and pyridine.

An investigation was launched to determine whether an increase in the surface area related to a higher OS capacity. For ease of application, the NFC fibres were packaged as aerogels for sorption. This chapter addresses Questions 3 and 4 of the list of *Key Research Questions* developed in Chapter 1, Section 1.4.

3. When additionally increasing the surface area by isolating NFC, is the capacity for OS increased and can *green* surface acetylations establish oleophilicity and hydrophobicity?
4. Can the *green* surface acetylation methods optimised in this study perform equally to traditional *non-green* surface acetylation reactions?

6.2 Experimental Methodology

6.2.1 General Definitions for Nanofibrillated Cellulose Modifications

Commercial NFC (CAS No. 9004-34-6), implemented as reference material, was purchased from the University of Maine, in the form of a 98 % (w/w) freeze-dried powder with nominal fibre diameters of approximately 50 nm and a specific surface area of 31 – 33 m^2/g (BET) (University of Maine, 2020). Subsequently, the *green* and *non-green* NFC molecular surface acetylations were optimised by implementing the commercial NFC since this feedstock was more readily available than the isolated CC and WS NFC. Subsequently, the optimised modification parameters were applied to the CC and WS NFC fibres to determine how these feedstocks react to the surface chemistry reactions.

In order to discern between the acetylations, the experimental runs were encrypted based on the identifications displayed in Table 6.1.

Table 6.1 The Encryptions Utilised for the Identification of Nanofibrillated Cellulose Surface Modifications

Nanocellulose Type [a]	**Modification Identification**	
	Non-green Methodology [b]	*Green* Methodology [c]
Commercial NFC	CN-N1-X	CN-N2-X
Wheat Straw NFC	WS-N1-X	WS-N2-X
Corncob NFC	CC-N1-X	CC-N2-X

a – Commercial nanofibrillated cellulose (NFC) is abbreviated as CN, wheat straw as WS and corncob as CC; **b** – Runs marked with N1 as suffix represents a *non-green* modification on the *NFC level*; **c** – Runs marked with N2 as suffix represents a *green* modification on the *NFC level*; **X** represents the number of the experimental run

6.2.2 Extracting Corncob and Wheat Straw Nanofibrillated Cellulose

NFC was isolated from both WS cellulose and CC cellulose by implementing methodology adapted from Nechyporchuk (2015) and Tarrés, Oliver-Ortega, Llop, M. Àngels Pèlach et al. (2016). The isolation method consisted of pre-fibrillation and enzymatic hydrolysis with FibreCare®, followed by mechanical fibrillation. FibreCare® was obtained from Novozymes, Denmark. This enzyme is produced from *Humicola insolens* and a cellulose-binding domain which assists with adsorption onto the fibrous surface (Bester, 2018).

The CC and WS cellulose were dispersed at 5 % (w/w) in distilled water. The pre-fibrillation step was executed by homogenising the specimens at 20 000 rpm for 5 minutes (PRO250 Homogeniser, Pro-Scientific, USA), repeated five times. Thereafter, 0.1 N HCl was added dropwise until a pH of 5 was reached.

FibreCare® exhibits a stable enzymatic activity at pH 5 to 9 and at temperatures of 45 °C to 50 °C (Bester, 2018). The reflux-condenser experimental setup (defined in Chapter 3) was therefore implemented. The suspension was heated to 50 °C under constant magnetic stirring at 600 rpm. When 50 °C was reached, 315 U/g FibreCare® was added, and the mixture was continually magnetically stirred at 600 rpm and 50 °C for 4 h. After the time had commenced, the temperature was raised to 80 °C for 15 minutes in order to stop the activity of the enzyme. The suspension was centrifuged (Labotec, Universal 320R electric benchtop centrifuge) at 6 000 rpm for 5 minutes. Hereafter, the supernatant was drained and replaced with distilled water, while the retentate was additionally centrifuged at 6 000 rpm for 5 minutes. This washing step was repeated five times. Thereafter, final fibrillation was accomplished by dispersing the washed pellets in an unmeasured amount of distilled water and homogenising the samples at 20 000 rpm for 5 minutes. This final fibrillation step was also repeated five times. The obtained CC and WS NFC were then pre-freezed in an ultra-low freezer (-80 °C), and freeze-dried with a VirTis Bench Top 6K freeze drier, at 80 mTorr and -55 °C for 72 h, until further analyses.

6.2.3 The *Green* Acetylation of Nanofibrillated Cellulose by Acetic Anhydride, Dimethyl Sulphoxide and Amano Lipase A from Aspergillus Niger

6.2.3.1 The Chemical Reaction

NFC was enzymatically modified by applying acetic anhydride, DMSO and Amano Lipase A from *Aspergillus niger*, as adapted from Bozic et al. (2015). The optimal operating conditions of the lipase is typically 45 °C at pH 6.5 (Sigma-Aldrich, 2020), while the enzyme deactivates at approximately 60 °C (Bozic et al., 2015). The chemical reaction

achieved by the modification is displayed in Figure 6.1. In this reaction, enzymatic acetylation is executed by attaching an acyl-enzyme complex on the surface of the NFC molecules (Bozic et al., 2015). The enzymatic acetylations accomplished in organic solvents are found to be 50 times greater than the enzymatic acetylation in aqueous media, due to the lower presence of bulk water and the amplified solubility of the substrate (Yang & Wang, 2003).

According to Yang & Wang (2003), an acyl-enzyme intermediate pathway occurs in order to acetylate the NFC with an activated ester within an organic medium. A surface hydroxyl group on the active centre is firstly acetylated by acetic anhydride, which causes a nucleophilic attack of the hydroxyls on the NFC surface (Yang & Wang, 2003). In this way, the NFC acts as an acyl acceptor – releasing the enzyme, acetic acid and DMSO as by-products.

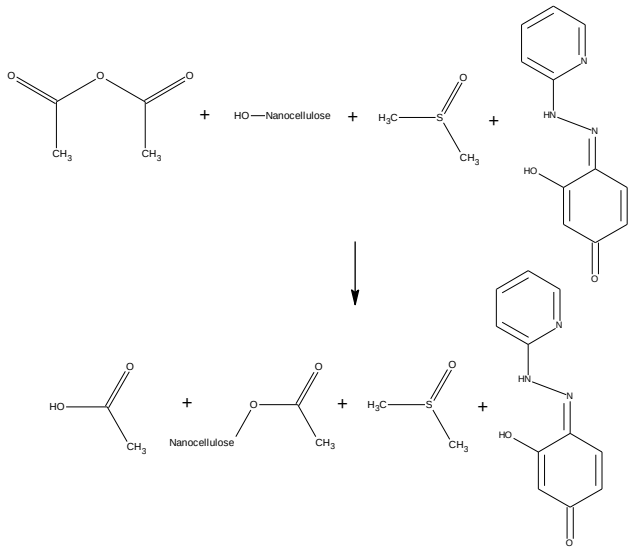

Figure 6.1 The *Green* Reaction Mechanism for Lipase-catalysed Acetylation of Nanofibrillated Cellulose, redrawn from Bozic et al. (2015)

6.2.3.2 The Central Composite Design and Scope Establishment

As with Chapter 4 and Chapter 5, a three-factor central composite design (CCD) based on response surface methodology (RSM), was applied in order to establish an empirical relationship relating the DS (Y_1) of the modified product to the varying reaction conditions, namely temperature (X_1), time (X_2) and catalyst concentration (X_3). This optimisation was executed with commercial NFC. In this way, the enzymatic acetylation of NFC could be optimised by implementing the statistical software, Statistica 13.2. The combination of parameters determined to achieve the highest DS of commercial NFC was applied to the isolated CC and WS NFC for comparison to the *non-green* modified samples.

The complete CCD design matrix applied to commercial NFC during the *green* acetylation is displayed in Table 6.2. The temperature was varied between 28 – 62 °C, time was fluctuated from 28 – 68 h, and the catalyst concentration was adapted from 199 – 2 301 units (U) of lipase. Five identical experiments were conducted at the centre point (Table 6.2, Run CN-N2-15 to CN-N2-19) to calculate the repeatability of the data (Hamid et al., 2014).

The scope of the input variables were based on preliminary studies, which are detailed in Appendix F.1 (p. 164). These preliminary experiments were completed by varying the reaction temperature from 25 °C to 60 °C, the

acetylation duration between 12 h and 72 h and the catalyst concentration from 200 U to 2 250 U of lipase, in single-factor experiments. No significant increase transpired when escalating the temperature from 25 °C to 30 °C ($p = 0.31$) or 30 °C to 45 °C ($p = 0.93$) at 24 h and 1 250 U lipase. However, a significant decline in DS occurred when increasing the temperature from 45 °C to 60 °C ($p = 6.70 \times 10^{-3}$) at these conditions. In order for the experimental design to maintain rotatability, the alpha values of $\alpha = 2^{3/4}$ were transcribed, and the range of temperature tested was selected as 28 °C to 62 °C.

Correspondingly, an incline in reaction time from 12 to 24 h (at 45 °C and 1 250 U lipase) led to a significant increase in acetylation ($p = 2.64 \times 10^{-3}$), while a further escalation to 48 h had no significant effect ($p = 0.09$). Moreover, a significant decrease occurred when increasing the reaction time to 72 h ($p = 0.02$), and a testing range of 28 – 68 h was therefore utilised for the CCD. Cumulating the lipase concentration from 200 U to 2 250 U had no significant influence ($p = 0.10$) on the DS at the specified temperature and reaction time of 45 °C and 24 h. It was decided to test the entire range of catalyst concentration in the CCD in order to determine any chemical interactions that might occur between the input parameters.

Table 6.2 The Central Composite Design Matrix and Experimental Conditions for the *Green* Modification of Commercial Nanofibrillated Cellulose in order to Improve the Hydrophobicity for Oil Sorption Applications

Factor	Symbol	Range	Coded Levels				
			-α	**-1**	**0**	**1**	**α**
Temperature	X_1	28 – 62 °C	28	35	45	55	62
Time	X_2	28 – 68 h	28	36	48	60	68
Catalyst Concentration [c]	X_3	199 – 2 301 U	199	625	1 250	1 875	2 301

Run ID [a, b]	Type of Point	Level (Coded Factors)			Reaction Variables (Actual Factors)		
					Temperature (°C)	**Time (h)**	**Catalyst Loading [c] (U)**
CN-N2-1	Fact	- 1	- 1	- 1	35	36	625
CN-N2-2	Fact	- 1	- 1	1	35	36	1 875
CN-N2-3	Fact	- 1	1	- 1	35	60	625
CN-N2-4	Fact	- 1	1	1	35	60	1 875
CN-N2-5	Fact	1	- 1	- 1	55	36	625
CN-N2-6	Fact	1	- 1	1	55	36	1 875
CN-N2-7	Fact	1	1	- 1	55	60	625
CN-N2-8	Fact	1	1	1	55	60	1 875
CN-N2-9	Axial	- α	0	0	28	48	1 250
CN-N2-10	Axial	+ α	0	0	62	48	1 250
CN-N2-11	Axial	0	- α	0	45	28	1 250
CN-N2-12	Axial	0	+ α	0	45	68	1 250
CN-N2-13	Axial	0	0	- α	45	48	199
CN-N2-14	Axial	0	0	+ α	45	48	2 301
CN-N2-15	Centre	0	0	0	45	48	1 250
CN-N2-16	Centre	0	0	0	45	48	1 250
CN-N2-17	Centre	0	0	0	45	48	1 250
CN-N2-18	Centre	0	0	0	45	48	1 250
CN-N2-19	Centre	0	0	0	45	48	1 250

a – Run identification for commercial nanofibrillated cellulose (CN), where N2 as suffix represents a *green* modification; **b** – Each run performed with a constant acetic anhydride loading of 6.1 M; **c** – Target concentration of Amano Lipase A from *Aspergillus niger* based on the Units (U) of enzyme added

The effect of the acetic anhydride application was not tested in this study. Instead, a constant acetic anhydride concentration of 6.1 M was utilised for each experiment. Bozic et al. (2015) found that a concentration exceeding this value resulted in declined acetylation due to an increasingly acidic environment. Nevertheless, it is recommended that the interactions of this acetylating agent with the other input parameters are established in future studies.

6.2.3.3 The Experimental Details

The experiment was executed in a 0.5 % (w/v) suspension, with 90 % (v/v) of DMSO (≥ 99 %, AR) and 10 % (v/v) of a 0.1 M phosphate buffer solution (pH = 7.0) (Bozic et al., 2015). This was accomplished by firstly dispersing 0.05 g of freeze-dried commercial NFC from the University of Maine in 9 mL of DMSO by homogenisation at 10 000 rpm for 30 seconds. The sample was left to stand overnight, after which it was homogenised at 10 000 rpm for 30 seconds. The specified amount of lipase (between 199 U and 2 301 U, Table 6.2) was diluted in 1 mL of the 0.1 M phosphate buffer solution and added to the NFC-DMSO mixture. The activity of the Amano Lipase A was determined to be 4 625 U/g, based on the Elabscience Lipase Assay Kit. Hereafter, 5.8 mL of acetic anhydride (equivalent to 6.1 M) was added to the reaction flask (Bozic et al., 2015).

The reflux-condenser experimental setup (defined in Chapter 3) was implemented to heat the mixture for a specific duration (from 28 h and 68 h, Table 6.2) at the specified reaction temperature (between 28 °C and 62 °C, Table 6.2). After refluxing was complete, the suspension was cooled to room temperature and centrifuged at 6 000 rpm for 15 minutes. The supernatant was decanted, replaced with distilled water and centrifuged again at 6 000 rpm for 5 minutes. This washing step was repeated three times. The sample was re-suspended in distilled water and heated to 100 °C in the glycerol bath in order to stop any residual enzymatic activity.

The following washing steps were then executed by suspending the modified NFC in the relevant chemical and centrifuging the sample at 6 000 rpm for 5 minutes: five acetone (≥ 99 %, AR) washing steps; five washing steps with a 1 % (v/v) sodium dodecyl sulphate (SDS, ≥ 99 %, AR) solution, and five washing steps with distilled water. The modified NFC was once again dispersed in distilled water and pre-freezed in an ultra-low freezer (-80 °C), after which it was freeze-dried at 80 mTorr and -55 °C for 72 h, until further analyses (Bozic et al., 2015).

6.2.4 The *Non-green* Acetylation of Nanofibrillated Cellulose by Acetic Anhydride, Dimethylformamide and Pyridine

6.2.4.1 The Chemical Reaction

A traditional *non-green* acetylation entailing acetic anhydride, DMF and pyridine (Tingaut et al., 2009; Zepic et al., 2015) was implemented on NFC. The chemical reaction achieved by this modification is displayed in Figure 6.2.

The specimens were firstly dispersed in a highly polar aprotic DMF solvent, prior to acetylation. This step was implemented in order to prevent the flocculation of the NFC fibres that naturally occur due to the high hydrogen concentration of the samples. If this solvent exchange is not established, the intermolecular hydrogen bonding can result in steric hindrance, which can inhibit acetylation from occurring (Tingaut et al., 2009).

According to Zepic et al. (2015), pyridine acts as a highly effective chemical in this reaction since it devises a dual purpose. Firstly, this chemical contributes to the swelling of the fibres, exposing the internal hydroxyl groups to

become more accessible for acetylation. Secondly, the pyridine increases the rate of the reaction through nucleophilic mediated catalyses (Zepic et al., 2015).

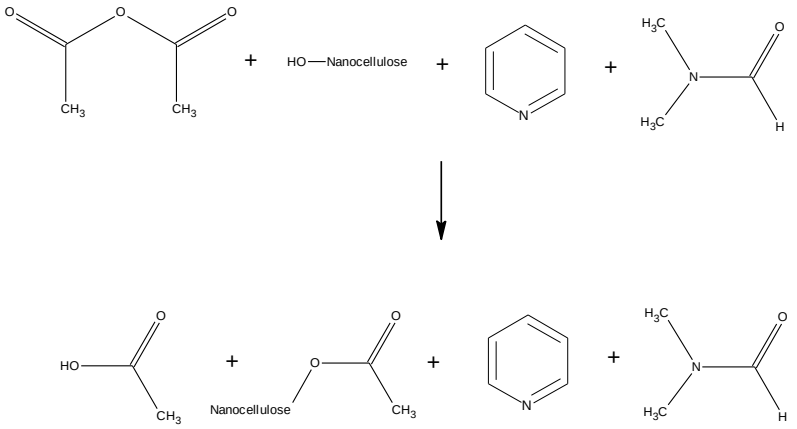

Figure 6.2 The *Non-green* Reaction Mechanism for Pyridine-catalysed Acetylation of Nanofibrillated Cellulose, redrawn from Tingaut et al. (2009)

6.2.4.2 The Experimental Details

The *non-green* methodology was initially executed on commercial NFC. These acetylations were not statistically optimised, but the performances were rather reviewed within ranges determined from literature studies. The highest modification within the selected scope was designated as the reference for the optimal performance. Subsequently, the combination of input parameters established to accomplish the highest DS of commercial NFC was applied to the isolated CC and WS NFC for comparison to the *green* modified samples.

The *non-green* experiments were conducted by varying the reaction temperature between 25 and 105 °C, the acetylation duration from 10 to 72 h and the catalyst concentration within 0 and 4 % (v/v) pyridine. Table 6.3 summarises the details specific to each experimental run.

Table 6.3 Experimental Conditions for the *Non-green* Modification of Commercial Nanofibrillated Cellulose in order to Improve the Hydrophobicity for Oil Sorption Applications

Run ID [a, b]	Temp (°C)	Time (h)	Catalyst Loading [c] (%)
CN-N1-1	105	24	3
CN-N1-2	105	48	3
CN-N1-3	105	72	3
CN-N1-4	105	10	3
CN-N1-5	90	48	3
CN-N1-6	25	48	3
CN-N1-7	105	48	0
CN-N1-8	105	48	1
CN-N1-9	105	48	4

a – Run identification for commercial nanofibrillated cellulose (CN), where N1 as suffix represents a *non-green* modification; **b** – Each run performed with a constant 1 % (w/w) DMF and 35 mL acetic anhydride (35 % (v/w) acetic anhydride volume to CN weight); **c** – Target pyridine percentage, based on volume to volume of acetic anhydride

The reaction was executed by dispersing 1 g of freeze-dried commercial NFC in DMF (99.8 %, AR) at a concentration of 1 % (w/v) by homogenisation at 10 000 rpm for 5 minutes. The NFC-DMF suspension was sonicated (PS-10A, ScienceWorld) at room temperature for 5 minutes. In conjunction, 35 mL acetic anhydride (≥ 98 %, AR) and the

relevant amount of pyridine (≥ 99 %, AR) was added. Consecutively, the suspension was homogenised at 2 000 rpm for 5 minutes. The percentage of pyridine (0 – 4 % (v/v), Table 6.3) was based on the volume of pyridine to the volume of acetic anhydride added to the NFC-DMF suspension.

The reflux-condenser setup was implemented to heat the mixture for the designated reaction time (between 24 h and 72 h, Table 6.3) at the specified temperature (from 25 to 105 °C, Table 6.3). This reaction was conducted under nitrogen flow in order to create an inert environment and prevent the pyridine from burning (Tingaut et al., 2009). Moreover, the specimens were magnetically stirred at 600 rpm. After the reaction had commenced, the suspension was cooled to room temperature and centrifuged at 6 000 rpm for 15 minutes. The supernatant was then decanted and replaced with a 4:1:1 toluene-ethanol-acetone mixture, whereafter it was homogenised at 10 000 rpm for 1 minute and centrifuged at 6 000 rpm for 15 minutes. This washing step was repeated five times with the toluene-ethanol-acetone mixture, twice with ethanol (95 %, AR) and five times with distilled water. Lastly, the modified NFC was then dispersed in distilled water, pre-freezed at -80 °C and freeze-dried at 80 mTorr and -55 °C for 72 h, until further analyses.

6.2.5 Creating Aerogels from Nanofibrillated Cellulose

A 0.25 % (w/w) hydrogel (Figure 6.3) was created by adding 0.0375 g NFC to 15 mL distilled water (Cheng et al., 2017; Feng et al., 2015). The mixture was homogenised at 20 000 rpm for 5 minutes and transferred to a mould. Each hydrogel in the relevant mould was pre-freezed at -80 °C and freeze-dried at 80 mTorr and -55 °C for 72 h. The aerogels were subsequently cured in a 105 °C oven for 90 minutes to promote cross-linking between the fibres. Furthermore, the obtained aerogels were stored in a desiccator until analyses.

Figure 6.3 Aerogel Created from Nanofibrillated Cellulose for Ease of Application in Oil Sorption

The sorption performances of the NFC particles are compared to that of the aerogels in Appendix F.3 (p. 170).

6.2.6 Scanning Electron Microscopy

Scanning Electron Microscopy (SEM) analyses were completed at the Central Analytical Facility of Stellenbosch University by employing a Zeiss Merlin Field Emission Gun. A tungsten crystal was utilised (Bester, 2018). The samples were dried at 40 °C for 24 h and coated in gold prior to analyses to ensure adequate conductivity. A voltage of 3 kV was implemented under vacuum conditions in order to capture images at 200 nm and 20 µm magnification.

6.2.7 Zeta Sizer® Nano-ZS90 Size Analyser

Diluted suspensions (< 0.01 % (w/w)) of NFC in distilled water were created. A Zeta Sizer® Nano-ZS90 Size Analyser (Malvern) was employed to determine the mean particle diameter distributions of the NFC particles. The particle

diameters were analysed by dynamic light scattering, which enables the Zeta Sizer® to determine multi-angle particle sizes up to 5 µm (Bester, 2018; Malvern Instruments Ltd, 2004). Measurements were obtained at 25 °C by utilising a helium-neon laser with a 90 ° light scattering angle and 633 nm wavelength. The Zeta Sizer® software was applied to determine the size distributions of the particles.

6.3 Results and Discussion

6.3.1 The Isolation and Characterisation of Unmodified Nanofibrillated Cellulose

The CC and WS cellulose isolated in Chapter 5 (Table 5.4) satisfied the minimum requirements for NFC production since the lignin contamination was below 10 %, the hemicellulose contamination was below 23 %, and the molecular crystallinity exceeded 48 % (Ceaser, 2019; Espinosa et al., 2017; Teixeira et al., 2010). Fibres with dimensions in the nano-range were achieved with the enzymatic hydrolyses of both CC and WS cellulose (Table 6.4). In order for the fibres to qualify as NFC according to ISO/TS 20477 Part 3.3.6, the diameters of the fibres should be less than 100 nm, and the fibre length can be several micrometres long (Khalil et al., 2012; Liu et al., 2017). A Zeta Sizer® was used to determine the particle diameter distribution attained after each isolation step (Figure 6.4), and the obtained particle diameter distributions are displayed in Appendix C (p. 146). These diagrams demonstrate a narrow size distribution.

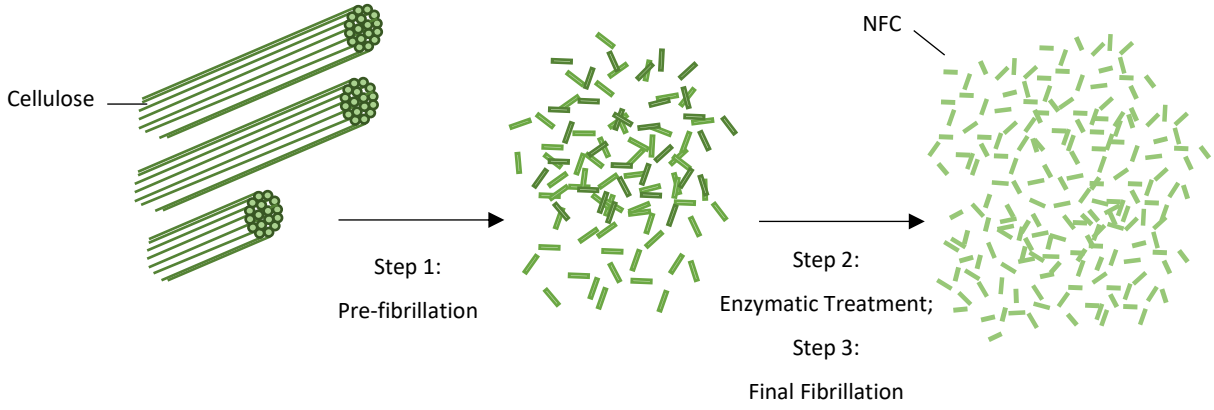

Figure 6.4 The Methodology for Extracting Nanofibrillated Cellulose (NFC) from Cellulose, through Pre-fibrillation, followed by Enzymatic Hydrolyses and Mechanical Fibrillation

The mean fibre diameters achieved after pre-fibrillation (Figure 6.4, Step 1) was 122.4 ± 6.9 nm for the treated CC cellulose and 141.8 ± 5.5 nm for the treated WS cellulose (Table 6.4). The NFC size range was accomplished for CC and WS after consecutive enzymatic treatment (Figure 6.4, Step 2), while additional fibrillation (Figure 6.4, Step 3) resulted in CC and WS NFC with diameters of 50.8 ± 3.8 nm and 37.8 ± 6.2 nm. The results in Table 6.4 indicate that the final fibrillation step is not required to obtain fibres in the nano-range.

Table 6.4 The Fibre Diameters achieved by Nanofibrillated Cellulose Isolation from Corncob Cellulose and Wheat Straw Cellulose, as determined with the Zeta Sizer® Nano-ZS90 Size Analyser

Stage	Fibre Diameter (nm)	
	CC NFC [b, c]	WS NFC [b, d]
Step 1: After Pre-fibrillation [a]	122.4 ± 6.9	141.8 ± 5.5
Step 2: After Enzymatic Treatment	68.1 ± 1.4	50.8 ± 1.3
Step 3: After Final Fibrillation	50.8 ± 3.8	37.8 ± 6.2

a – Starting material diameter approximated between 250 µm and 425 µm by sieve separation; **b** – Nanofibrillated cellulose is abbreviated as NFC; **c** – Corncob is abbreviated as CC; **d** – Wheat straw is abbreviated as WS

FibreCare® consists of endoglucanase which forms enzyme-substrate complexes by adsorbing onto the fibrous surface. The amorphous regions in the cellulose chains are then hydrolysed, and the accessible β-1,4-glycosidic bonds are consequently broken (Arola, 2015; Ibrahim & Mondal, 2019). Oligosaccharide chains are formed through this phase, referred to as the primary hydrolysis (Bester, 2018). Hereafter, secondary hydrolysis occurs when the intermolecular hydrogen bonds are broken, and microfibers are formed while preserving the crystalline regions of the cellulose (Bester, 2018).

The SEM analyses (Figure 6.5) revealed that both longer entangled fibrous bundles and shorter agglomerated fibres were present in the freeze-dried CC NFC (Figure 6.5 II and V) and WS NFC (Figure 6.5 III and VI). The shorter agglomerated fibres were prominent in these samples due to the final fibrillation process (Figure 6.4, Step 3). In order to save energy, this final fibrillation step can be eliminated, and fibre diameters in the nano-range would still be achieved. The commercial NFC (Figure 6.5 IV) appeared less fibrillated when compared to the CC NFC (Figure 6.5 V) and WS NFC (Figure 6.5 VI) at 20 µm, indicating that the method utilised for isolation of commercial NFC might have excluded additional fibrillation steps, thereby resulting in more solid fibrils. These commercial NFC fibres had declared fibre diameters of 50 nm (University of Maine, 2020).

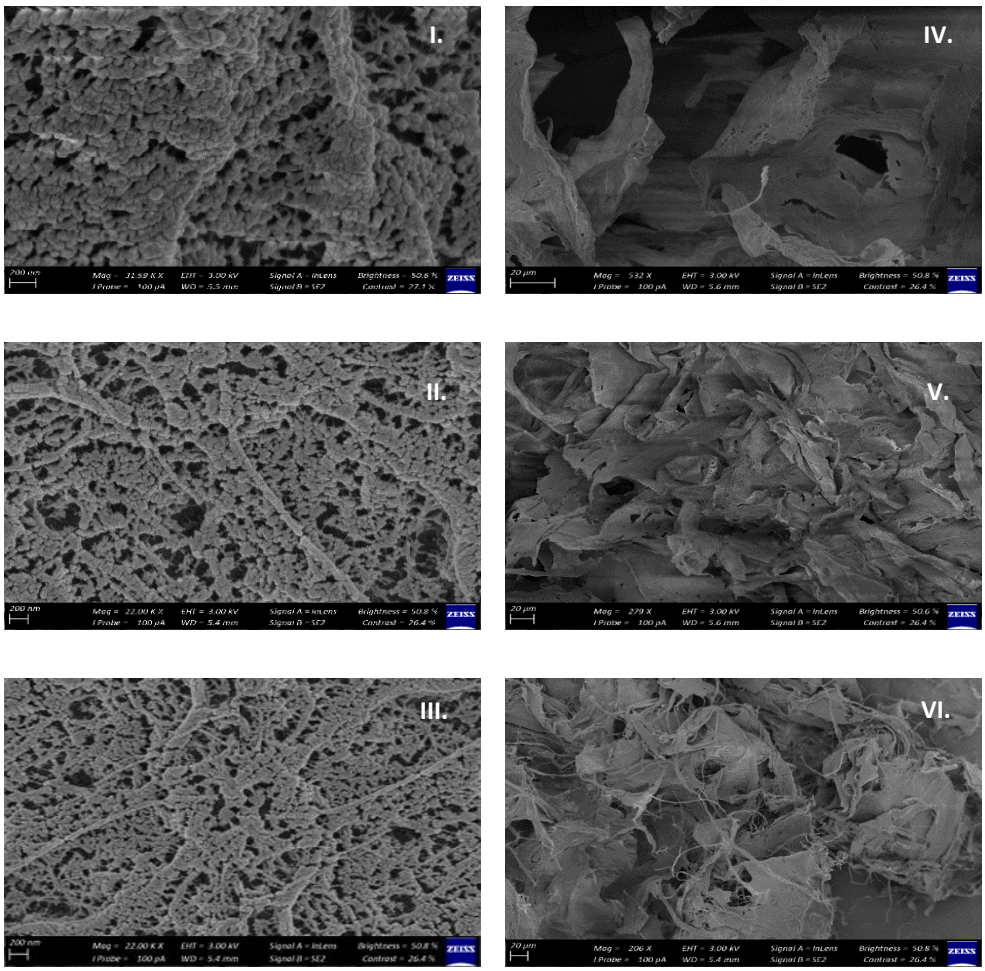

Figure 6.5 The Scanning Electron Microscopy of **I.** Commercial Nanofibrillated Cellulose (NFC) at 200 nm, **II.** Corncob (CC) NFC at 200 nm, **III.** Wheat Straw (WS) NFC at 200 nm, **IV.** Commercial NFC at 20 µm, **V.** CC NFC at 20 µm and **VI.** WS NFC at 20 µm

The molecular crystallinities of the NFC established with a Bruker D2 Phaser X-ray Diffractometer are displayed in Table 6.5, while the X-ray diffraction (XRD) spectra are displayed in Appendix F.3 (p. 170). In order to determine the effect of enzymatic hydrolyses on the molecular crystallinities of the samples, a comparison is drawn between the crystallinity of each cellulose source and NFC counterpart.

Table 6.5 The Molecular Crystallinities of Commercial Nanofibrillated Cellulose, as well as Nanofibrillated Cellulose derived from Corncob and Wheat Straw Cellulose

Feedstock [a, b]	Crystallinity (%)	
	Cellulose	NFC [a]
CN [c]	-	74.0 ± 1.3
CC	72.5 ± 1.0	75.4 ± 1.3
WS	68.8 ± 1.0	74.2 ± 0.3

a – Commercial nanofibrillated cellulose (NFC) is abbreviated as CN, wheat straw is abbreviated as WS, and corncob is abbreviated as CC; **b** – The molecular crystallinities are determined by a Bruker D2 Phaser X-ray Diffractometer; **c** – The CN is sourced from University of Maine, with original cellulose source unknown

The molecular crystallinity of a fibre is an indication of the number of exposed, accessible hydroxyl groups available for acetylation (Zanini et al., 2017) and high crystallinity is, therefore, favoured. As mentioned, the endoglucanase in FibreCare® targets the amorphous regions of cellulose through enzymatic hydrolyses (Bester, 2018), thereby leading to amplified crystallinities of CC and WS NFC, as indicated in Table 6.5. The increased crystallinity demonstrated in Table 6.5 confirms that the amorphous regions of the cellulose were predominantly targeted by the endoglucanase, while the crystalline regions were retained. Moreover, the CC NFC, WS NFC and commercial NFC exhibited statistically similar ($p = 0.34$) crystallinities and are thus expected to display analogous molecular behaviour under the same reaction conditions during surface acetylation reactions.

6.3.2 The *Green* Acetylation of Nanofibrillated Cellulose by Acetic Anhydride, Dimethyl Sulphoxide and Amano Lipase A from Aspergillus niger

6.3.2.1 The Model Development for the Degree of Substitution of the *Green* Modification of Commercial Nanofibrillated Cellulose

The *green* acetylation was optimised on commercial NFC by implementing the CCD as ascertained in Section 6.2.3. The DS of these samples are represented by run CN-N2-1 to CN-N2-19 in Table 6.6, and the polynomial model predicted by Statistica 13.2 is depicted as Equation 6.1 in Table 6.7.

The ANOVA analysis (Appendix F.2, p. 167) designated a regression coefficient of $R^2 = 0.8437$ for Equation 6.1. Conversely, the statistical *Lack of Fit* ($p = 8.43 \times 10^{-4}$) of this model was indicated to be significant, denoting that the experimental data cannot accurately be predicted by the model. The ANOVA analysis revealed that the catalyst concentration ($p = 0.65$) and the interaction between catalyst concentration and time ($p = 0.37$) had insignificant effects on the DS achieved by the acetylation reaction. In order to improve the accuracy of Equation 6.1, the negligible effects were pooled into the error term of the model (b_0 in Equation 3.12, Section 3.5). The adjusted model is signified by Equation 6.2 in Table 6.7.

Table 6.6 The Degree of Substitution achieved through the *Green* Acetylation of Commercial Nanofibrillated Cellulose with the Implementation of a Central Composite Design in order to Improve the Hydrophobicity for Oil Sorption Applications

Central Composite Design						
Run ID [a, b]	**Temp (°C)**	**Time (h)**	**Lipase Concentration [c] (U)**	**DS [d] Model Prediction**	**Experimental DS [d]**	**Error (%)**
CN-N2-1	35	36	625	-	0.72 ± 0.10	-
CN-N2-2	35	36	1 875	-	0.71 ± 0.26	-
CN-N2-3	35	60	625	-	0.59 ± 0.14	-
CN-N2-4	35	60	1 875	-	0.68 ± 0.11	-
CN-N2-5	55	36	625	-	0.64 ± 0.10	-
CN-N2-6	55	36	1 875	-	0.57 ± 0.15	-
CN-N2-7	55	60	625	-	0.47 ± 0.12	-
CN-N2-8	55	60	1 875	-	0.35 ± 0.05	-
CN-N2-9	28	48	1 250	-	1.01 ± 0.12	-
CN-N2-10	62	48	1 250	-	0.31 ± 0.09	-
CN-N2-11	45	28	1 250	-	0.61 ± 0.12	-
CN-N2-12	45	68	1 250	-	0.45 ± 0.11	-
CN-N2-13	45	48	199	-	0.47 ± 0.12	-
CN-N2-14	45	48	2 301	-	0.55 ± 0.25	-
CN-N2-15	45	48	1 250	-	0.64 ± 0.11	-
CN-N2-16	45	48	1 250	-	0.66 ± 0.12	-
CN-N2-17	45	48	1 250	-	0.65 ± 0.10	-
CN-N2-18	45	48	1 250	-	0.62 ± 0.13	-
CN-N2-19	45	48	1 250	-	0.65 ± 0.12	-
Experimental Validation of Model						
Run ID [b, d]	**Temp (°C)**	**Time (h)**	**Lipase [c] (U)**	**DS Model Prediction**	**Experimental DS**	**Error (%)**
CN-N2-V1	35	35	1 000	0.77 [e]	0.81 ± 0.16	5.35
CN-N2-V2	35	25	600	0.72 [f]	0.75 ± 0.15	4.52
CN-N2-V3	40	60	1 500	0.61 [g]	0.64 ± 0.11	5.47

a – Run identification for commercial nanofibrillated cellulose (CN), where N2 as suffix represents a *green* modification and validation runs are depicted by V1, V2 and V3; **b –** Each run is performed with a constant acetic anhydride loading of 6.1 M; **c –** Target concentration of Amano Lipase A from *Aspergillus niger* enzyme, based on the Units (U) of enzyme added; **d –** Degree of substitution is abbreviated as DS; **e –** The 95 % confidence interval for the prediction of DS at these conditions is 0.72 to 0.82; **f –** The 95 % confidence interval for the prediction of DS at these conditions is 0.65 to 0.78; **g –** The 95 % confidence interval for the prediction of DS at these conditions is 0.56 to 0.65

Although the statistical *Lack of Fit* ($p = 1.49 \times 10^{-3}$) was improved with the adjusted model, with a comparable regression coefficient of $R^2 = 0.8431$, the fit of the experimental data remained suboptimal (Appendix F.2, p. 167). Therefore, in comparison to the statistical validation, the adjusted model was also experimentally validated at random conditions. These experimental validations (CN-N2-V1, CN-N2-V2 and CN-N2-V3 in Table 6.6) indicated that DS values could be accomplished within the 95 % confidence interval ($\alpha = 0.05$) of the values predicted by the model. The experimental DS differed with less than 10 % when compared to the model predicted DS for each validation. The developed model was, therefore, deemed acceptable to predict the DS of NFC for the purpose of this study. Nevertheless, in order to develop increasingly robust models with improved accuracy of prediction, additional

experiments are recommended for future investigations. The optimal operating conditions of the lipase is typically 45 °C at pH 6.5 (Sigma-Aldrich, 2020), while this enzyme deactivates at approximately 60 °C (Bozic et al., 2015). However, the acetic acid by-product alters the pH of the system, which in turn affects the lipase performance (see Section 6.3.2.2). If this optimisation were to be repeated, it may be beneficial to test increasingly lower operating temperatures. The highest value in the CCD can also be adjusted to approximately 35 °C (Figure 6.7) in order to determine whether affectedly increased optimal DS values can be achieved.

Table 6.7 The Mathematical Models, Developed to Describe the Response of Degree of Substitution to the Input Parameters – Temperature, Time, and Catalyst Concentration, for the *Green* Surface Modification of Commercial Nanofibrillated Cellulose

Model	Mathematical Model [a, b]	Equation	R^2	*Lack of Fit*
Original Prediction	$Y_1 = (0.227015) + (-0.006184)X_1 + (0.028245)X_2 + (0.000477)X_3 + (0.000128)X_1^2 + (-0.000238)X_2^2 + (-0.0000001)X_3^2 + (-0.000252)X_1X_2 + (-0.000005)X_1X_3 + (0.000001)X_2X_3$	[6.1]	0.8437	Significant
Adapted Prediction	$Y_1 = (0.833545) + (-0.019002)X_1 + (0.026718)X_2 + (0.000164)X_1^2 + (-0.000213)X_2^2 + (0.000000)X_3^2 + (-0.000252)X_1X_2 + (0.000002)X_1X_3$	[6.2]	0.8431	Significant

a – Temperature (X_1), Time (X_2) and Catalyst Concentration (X_3) as input variables; **b** – Degree of Substitution (Y_1) as model response

6.3.2.2 The Effect of Temperature, Time and Catalyst Concentration on the Degree of Substitution of the *Green* Modification of Nanofibrillated Cellulose

The linear- and quadratic effects of temperature, time and catalyst concentration on the DS of commercial NFC via the *green* surface acetylation was determined by the ANOVA analyses (Appendix F.2, p. 167), the Pareto chart (Figure 6.6) and the response surface plots (Figure 6.7).

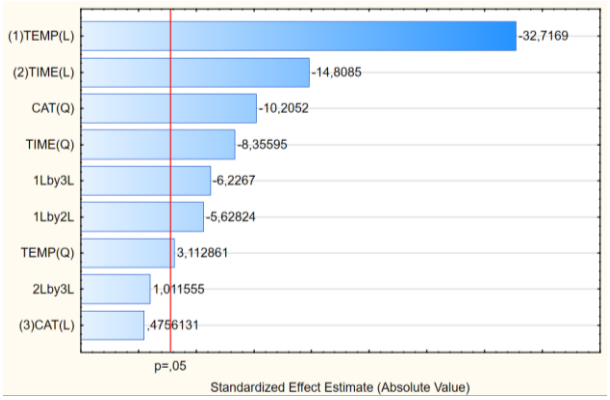

Figure 6.6 The Pareto Chart of Standardised Linear (L) and Quadratic (Q) Effects of Temperature (1), Time (2) and Catalyst Concentration (3) on the Degree of Substitution of Commercial Nanofibrillated Cellulose via the *Green* Surface Modification Reaction

I. (at 1 250 U Lipase)

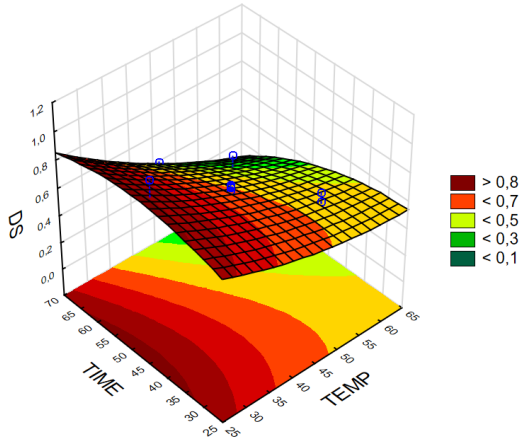

II. (at 1 250 U Lipase)

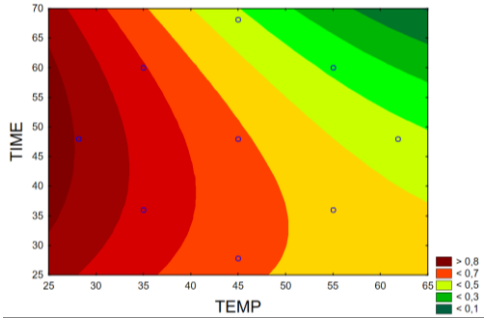

III. (at 48 h)

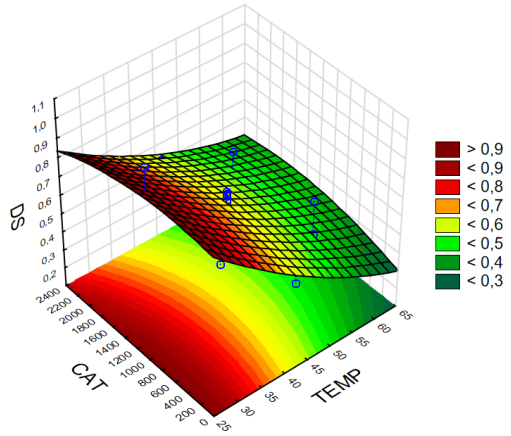

IV. (at 48 h)

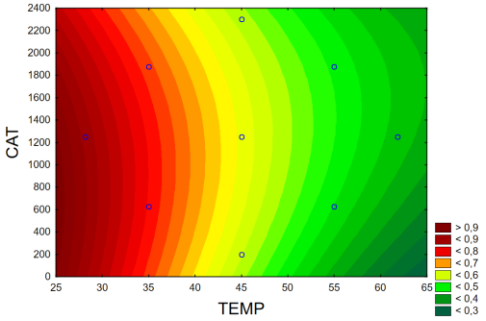

V. (at 45 °C)

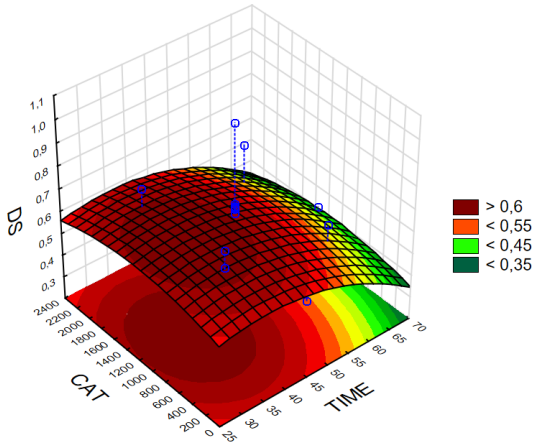

VI. (at 45 °C)

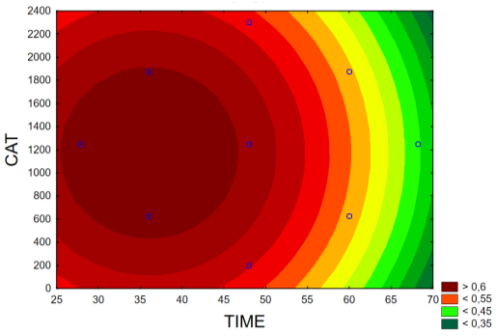

Figure 6.7 The 2-Dimensional and 3-Dimensional Response Surface Plots for the Effects of Temperature (°C), Time (h) and Lipase Concentration (U) on the Degree of Substitution (DS) of Commercial Nanofibrillated Cellulose via *Green* Surface Acetylation

The Pareto chart indicates that the linear- and quadratic effects of temperature exhibited a significant influence ($p = 5.00 \times 10^{-6}$ and $p = 3.58 \times 10^{-2}$) on the DS achieved through this *green* reaction. Similarly, the linear- and quadratic effects of time presented a significant influence ($p = 1.21 \times 10^{-4}$ and $p = 1.12 \times 10^{-3}$) and a statistically significant

interaction ($p = 4.90 \times 10^{-3}$) transpired between temperature and reaction duration. These effects were evident when studying the response surfaces in Figure 6.7 I and II. Longer reaction times from approximately 30 h to 60 h led to enhanced acetylations at lower temperatures and a constant lipase concentration of 1 250 U. These conditions provide the acetyl groups with sufficient time to interact with the reactive chemical sites, replacing the surface hydroxyl groups of the fibres until an equilibrium is reached. Moreover, these plots depict that higher reaction temperatures are theoretically required to achieve similar acetylations within shorter reaction times.

Furthermore, Figure 6.7 III and IV are utilised to consider the effects of temperature and lipase concentration on the DS at a constant reaction time of 48 h. These response surfaces indicate that an increase in lipase concentration has no influence at temperatures between 25 °C to 35 °C. Moreover, the Pareto chart denotes that the linear effects of the lipase catalyst had a statistically negligible influence ($p = 0.65$) on the DS, while the quadratic effects of the lipase concentration significantly impacted ($p = 5.19 \times 10^{-4}$) this response. Additionally, a significant interaction ($p = 3.39 \times 10^{-3}$) transpired between the reaction temperature and the lipase concentration.

According to Bozic et al. (2015), this enzyme is deactivated at 60 °C. The lipase depicts an affectedly increased activity at lowered temperatures. A high performance is noted at temperatures below 40 °C, while the paramount DS is achieved between 25 °C and 30 °C. Figure 6.7 I – IV suggests that temperatures below 25 °C may theoretically lead to higher acetylations via this reaction. Conversely, it is not possible to test temperatures below 25 °C with the current experimental setup, since a chemical coolant is not implemented. An adaption to the experimental setup is advised for future studies in order to investigate whether the performance can be augmented at affectedly lower temperatures.

The significant quadratic effects ($p = 5.19 \times 10^{-4}$) of the catalyst are apparent from the surface plots in Figure 6.7 IV and V, shown at a constant reaction temperature of 45 °C. According to the Pareto chart, the interaction between the catalyst and time had a statistically negligible effect ($p = 0.37$) on the extent of acetylation. On the contrary, from Figure 6.7 it is apparent that shorter reaction times of approximately 25 h to 45 h were necessary to achieve a greater number of acetylations if higher catalyst concentrations of roughly 500 U to 1 800 U were present at 45 °C.

6.3.2.3 The Optimal *Green* Modification of Nanofibrillated Cellulose

Statistica 13.2 was implemented to develop desirability plots in order to determine at which combination of reaction conditions the highest DS can be reached, as indicated in Figure 6.8. The reaction conditions for the optimal modification was ascertained as 28.2 °C, 48.0 h and 724.4 U of lipase. These conditions were applied to commercial NFC, CC NFC and WS NFC to compare the optimal experimental performance to the DS of 0.9 predicted by the regression model. The results depicted in Table 6.8 demonstrate that the values for commercial NFC and WS NFC fall within the 95 % confidence interval ($\alpha = 0.05$) of the values predicted by the model, while the CC NFC exhibited marginally amplified DS values which exceeded the 95 % confidence interval. However, by applying a single-factor ANOVA analyses to the three optimal DS values (0.86 ± 0.09, 1.01 ± 0.12 and 0.85 ± 0.15), it was revealed that these attributes are not statistically different ($p = 0.18$).

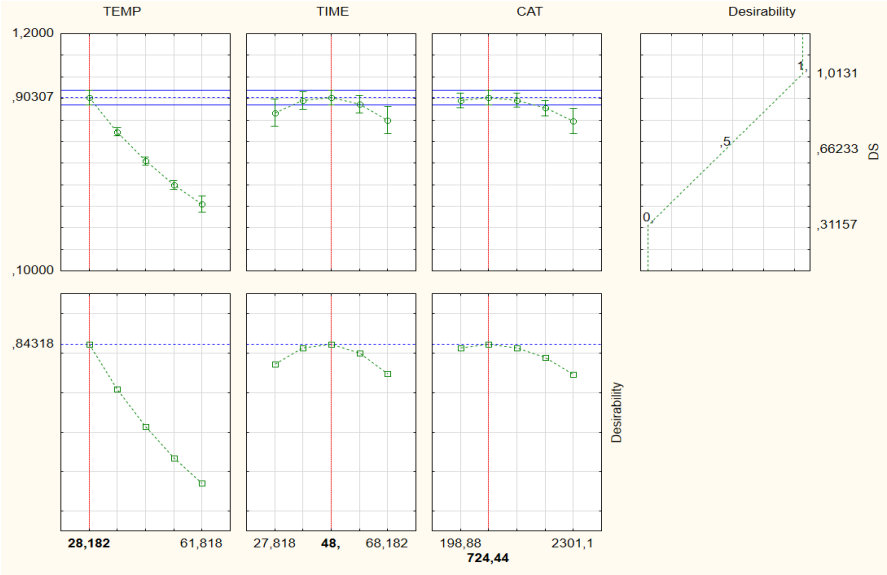

Figure 6.8 Profiles for the Predicted Values and Desirability Plots of the *Green* Modification of Commercial Nanofibrillated Cellulose

Table 6.8 A Comparison of the Predicted and Experimental Degree of Substitution for the Optimal *Green* Modification of Commercial Nanofibrillated Cellulose, as well as Corncob and Wheat Straw Nanofibrillated Cellulose

Run ID [a, b]	Temp (°C)	Time (h)	Lipase [c] (U)	DS Model Prediction [d]	Experimental DS	Error (%)
CN-N2-OPT	28.2	48	724.4	0.90	0.86 ± 0.09	- 4.44
CC-N2-OPT	28.2	48	724.4	0.90	1.01 ± 0.12	12.22
WS-N2-OPT	28.2	48	724.4	0.90	0.85 ± 0.15	- 5.56

a – Run identification commercial nanofibrillated cellulose (CN), as well as nanofibrillated cellulose derived from wheat straw (WS) and corncob (CC), where N2 as suffix represents a *green* modification; **b** – Each run is performed with a constant acetic anhydride loading of 6.1 M; **c** – Target concentration of Amano Lipase A from *Aspergillus niger* based on the Units (U) of enzyme added; **d** – The 95 % confidence interval for the prediction of degree of substitution (DS) at these conditions is 0.85 – 0.96, based on CN

It was previously established that the crystallinity of a sample could influence the potential for surface acetylation since a higher crystallinity indicates more exposed, accessible hydroxyl groups on the molecular surface. The crystallinities of these sources were determined as 74.0 ± 1.3 % for the commercial NFC, 75.4 ± 1.3 % for CC NFC and 74.2 ± 0.3 % for WS NFC in Section 6.3.1. These values were furthermore ascertained to be statistically similar ($p = 0.34$), which reiterates the assertion that the fibres had undergone analogous extents of acetylation.

In the study conducted by Bozic et al. (2015), statistical optimisation was not performed, but the ester content achieved at different single-factor conditions were rather tested. The highest results within their tested range were reached at 40.0 °C, 24.0 h and 1 250 U of lipase, where a DS of 0.15 was accomplished. By implementing a CCD in order to include the effects of interaction between temperature, time and catalyst concentration, the current study managed to increase the DS by 82 – 85 % for this *green* surface modification. The OS values attained by these modified samples are investigated in Section 6.3.4.

6.3.3 The *Non-green* Acetylation of Nanofibrillated Cellulose by Acetic Anhydride, Dimethylformamide and Pyridine

6.3.3.1 The Effect of Temperature, Time and Catalyst Concentration on the Degree of Substitution of the *Non-green* Modification of Nanofibrillated Cellulose

The responses of DS, achieved by the traditional *non-green* modification at the specified reaction conditions, are displayed in Table 6.9. These experiments were accomplished by fluctuating the reaction temperature between 25 and 105 °C, the acetylation duration between 10 and 72 h and the catalyst concentration between 0 and 4 % (v/v) pyridine. Figure 6.9 depicts the DS and Fourier Transform Infrared (FT-IR) spectra of each experimental run.

Table 6.9 The Degree of Substitution achieved through the *Non-green* Acetylation of Commercial Nanofibrillated Cellulose in order to Improve the Hydrophobicity for Oil Sorption Applications

Run ID [a, b]	Temp (°C)	Time (h)	Catalyst Loading [c] (%)	DS [d]
CN-N1-1	105	24	3	1.13 ± 0.02
CN-N1-2	105	48	3	0.90 ± 0.03
CN-N1-3	105	72	3	0.62 ± 0.02
CN-N1-4	105	10	3	1.03 ± 0.04
CN-N1-5	90	48	3	0.87 ± 0.02
CN-N1-6	25	48	3	0.68 ± 0.02
CN-N1-7	105	48	0	0.74 ± 0.03
CN-N1-8	105	48	1	1.07 ± 0.06
CN-N1-9	105	48	4	0.50 ± 0.02

a – Run identification for commercial nanofibrillated cellulose (CN), where N1 as suffix represents a *non-green* modification; **b** – Each run performed with a constant 1 % (w/w) DMF and 35 mL acetic anhydride (35 % (v/w) acetic anhydride volume to CN weight); **c** – Target pyridine percentage, based on volume to volume of acetic anhydride; **d** – Degree of Substitution is abbreviated as DS

The effect of temperature was investigated in Figure 6.9 by performing reactions CN-N1-2, CN-N1-5 and CN-N1-6 at a constant reaction duration of 48 h and a set pyridine concentration of 3 % (v/v) to the volume of acetic anhydride added. A significant amplification in DS occurred when increasing the temperature from 25 °C to 90 °C ($p = 4.09 \times 10^{-5}$). However, a further incline to 105 °C had no significant effect ($p = 0.15$). A higher reaction temperature causes superior diffusion of acetic anhydride into the cells, and thus enables acetic anhydride to improve the swelling of the fibres. This mechanism exposes the reactive chemical sites, making them more accessible to take part in the acetylation reaction (Huang et al., 2014). A performance plateau was reached between 90 °C to 105 °C, when most of the easily accessible surface hydroxyl groups were replaced by acetyl groups (Tingaut et al., 2009).

I. Effect of Temperature on DS

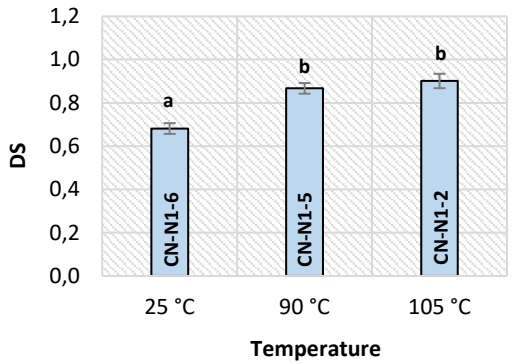

III. Effect of Time on DS

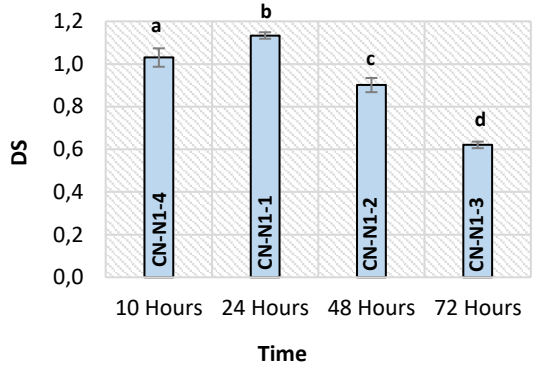

V. Effect of Catalyst Concentration on DS

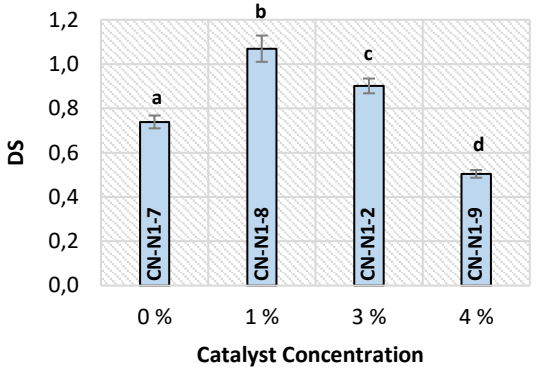

II. Effect of Temperature on FT-IR Peaks

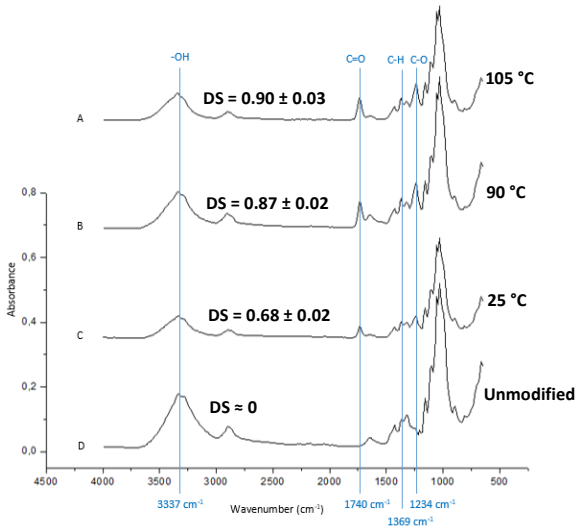

IV. Effect of Time on FT-IR Peaks

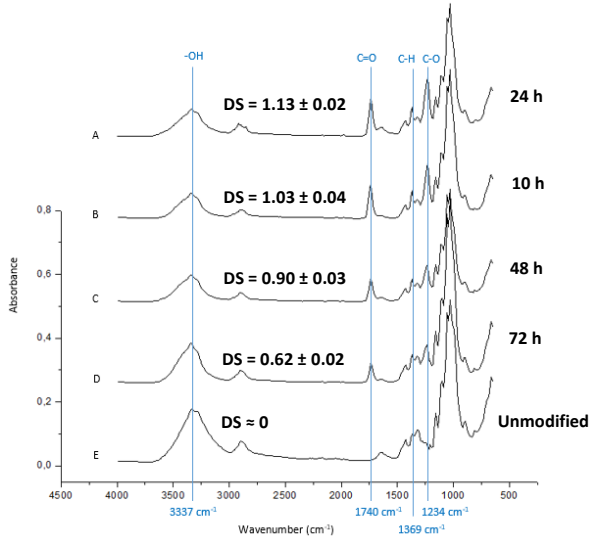

VI. Effect of Catalyst Concentration on FT-IR Peaks

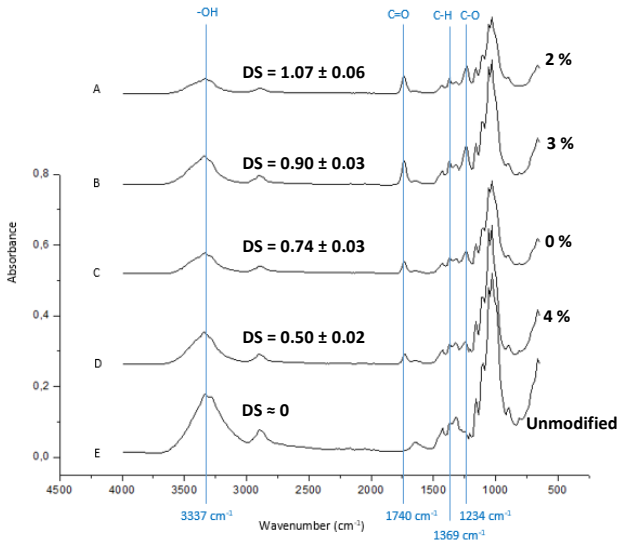

Figure 6.9 The Effects of Temperature, Time and Catalyst Concentration on the Degree of Substitution (DS) and Fourier Transform Infrared (FT-IR) Spectra of the *Non-green* Acetylated Commercial Nanofibrillated Cellulose (CN) at **I., II.** Constant Time and Catalyst Concentration (48 h, 3 % Pyridine); **III., IV.** Constant Temperature and Catalyst Concentration (105 °C, 3 % Pyridine); **V., VI.** Constant Temperature and Reaction Time (105 °C, 48 h)

Due to safety concerns, the experimental temperature was not increased above 105 °C. This reaction was conducted under nitrogen flow in order to create an inert environment and prevent the pyridine from burning (Tingaut et al., 2009). The current experimental setup would not be able to condense the evaporated pyridine at higher temperatures, which could lead to pyridine escaping from the system and consequently catching fire.

The effect of time was investigated by performing reactions CN-N1-1, CN-N1-2, CN-N1-3 and CN-N1-4 at a constant temperature of 105 °C and a set pyridine concentration of 3 % (v/v). A significant increase in DS transpired when escalating the reaction duration from 10 h to 24 h ($p = 4.06 \times 10^{-3}$). Hereafter a significant decline in DS occurred when increasing the time to 48 h ($p = 1.47 \times 10^{-5}$) and 72 h ($p = 4.93 \times 10^{-6}$), respectively. It is presumed that the reaction firstly occurs on the most accessible hydroxyl groups during the shorter reaction times, leading to a faster rate of reaction (Tingaut et al., 2009). After longer reaction times, the rate of reaction slows down since the hydroxyl groups are harder to access and replace. The new acetyl groups on the surface of the fibres correspondingly create steric hindrance, which contributes to the inaccessibility of the hydroxyl groups located beneath the fibre surface (Tingaut et al., 2009). By extensively increasing the reaction duration to 48 h and 72 h, the acetylation decreased, which indicates that degradation of the fibres had occurred.

The effect of the pyridine catalyst concentration was investigated by performing reactions CN-N1-2, CN-N1-7, CN-N1-8 and CN-N1-9 at a set temperature of 105 °C and a set reaction time of 48 h. A significant escalation in DS ensued when increasing the catalyst concentration from 0 % (v/v) to 1 % (v/v) ($p = 5.75 \times 10^{-5}$), while a significant decrease occurred when increasing the catalyst concentration to 3 % (v/v) ($p = 2.59 \times 10^{-3}$) and 4 % (v/v) ($p = 7.37 \times 10^{-7}$). Increasing the catalyst concentration causes a very high rate of reaction, which augments the rate of acetic acid build-up. An excess of acid causes hydrolysis of the ester groups and consequent degradation of the fibres, leading to a lower acetylation performance (Zepic et al., 2015).

Moreover, when the concentration of pyridine is too high, a large amount of undecomposed pyridine can be absorbed on the active sites of the NFC. This occurrence can lead to a decline in the contact area between the hydroxyl groups and the chemical reagents. The FT-IR spectra in Figure 6.9 II, IV and VI revealed an increase in ester peak intensities (at 1 740 cm^{-1}; 1 369 cm^{-1} and at 1 234 cm^{-1}) with an increase in DS for all experimental runs. A marginal decrease in the hydroxyl peaks (at 3 337 cm^{-1}, 1 337 cm^{-1} and 1 310 cm^{-1}) was also observed, ascertaining that acetylation has taken place. It is recommended that a full CCD is completed in future studies in order to determine the interactions between temperature, time and catalyst concentration.

6.3.3.2 The Optimal *Non-green* Modification of Nanofibrillated Cellulose

From the single-factor experiments concluded in Table 6.9, it was determined that the optimal performance from the set of conditions tested were found to occur at 105 °C, 24 h and 3 % (v/v) pyridine – relating to conditions examined in the experimental run identified by CN-N1-1. These conditions were applied to CC and WS NFC, and the results are displayed in Table 6.10.

An optimal DS of 1.13 ± 0.02 was achieved for the modified commercial NFC, while DS values of 1.32 ± 0.06 and 1.15 ± 0.05 were accomplished for CC and WS NFC. These values compare well with the DS of 0.93 ± 0.08 attained by Zepic et al. (2015) under comparable reaction conditions at 105 °C, 20 h and 3 % (v/v) pyridine with freeze-dried

NFC. The slightly extended reaction time in the current study leads to a 19 – 30 % increase in DS for the *non-green* surface modification reaction.

Table 6.10 The Degree of Substitution for the Optimal *Non-green* Modification of Commercial Nanofibrillated Cellulose, as well as Corncob and Wheat Straw Nanofibrillated Cellulose

Run ID [a, b]	Temperature (°C)	Time (h)	Pyridine Catalyst [c] (% v/v)	DS [d]
CN-N1-OPT	105	24	3	1.13 ± 0.02
CC-N1-OPT	105	24	3	1.32 ± 0.06
WS-N1-OPT	105	24	3	1.15 ± 0.05

a – Run identification commercial nanofibrillated cellulose (CN), as well as nanofibrillated cellulose derived from wheat straw (WS) and corncob (CC), where N1 as suffix represents a *non-green* modification; **b** – Each run is performed with a constant 1 % (w/w) DMF and 35 mL acetic anhydride (35 % (v/w) acetic anhydride volume to NFC weight); **c** – Target pyridine percentage, based on the volume of pyridine to the volume of acetic anhydride; **d** – Degree of Substitution is abbreviated as DS

The CC NFC exhibited a marginally higher DS ($p = 5.09 \times 10^{-3}$) when compared to the commercial NFC and WS NFC ($p = 0.68$). Although the crystallinities of these feedstocks were established to be statistically similar ($p = 0.34$; Table 6.5), the marginally higher crystallinity of CC NFC could relate to slightly more exposed hydroxyl groups on the fibre surface, which can potentially contribute to the higher DS achieved by this modification.

6.3.4 The Comparison between the *Green* and the *Non-green* Acetylation of Corncob and Wheat Straw Nanofibrillated Cellulose

6.3.4.1 Extent of Acetylation

The successes of acetylation achieved through the application of the *green* and *non-green* modifications of CC and WS NFC are compared based on DS and FT-IR. The FT-IR spectra of the modified and unmodified NFC in Figure 6.10 were utilised to study the molecular changes that occur due to the acetylation reaction. According to Zepic et al. (2015), three principal ester bands can be identified, namely the C=O stretching of the ester at 1 740 cm^{-1}; the C-H band in –O(C=O)-CH_3 at 1 369 cm^{-1} and the C-O stretching band of the acetyl group at 1 234 cm^{-1}. In Figure 6.10, the heights of these peaks can be seen to intensify with the addition of acetyl groups during the modification process for each source. The absence of these bands in the unmodified samples indicate that these peaks are formed during the acetylation reaction. The higher DS values are accompanied by higher ester peak intensities, indicating that more hydroxyl groups are replaced by acetyl groups for these specimens.

Only a minor decrease can be noted in the hydroxyl stretching band and hydroxyl in-plane bending bands of the modified samples at 3 337 cm^{-1}, 1 337 cm^{-1} and 1 310 cm^{-1}. This phenomenon illustrates that molecular erosion occurs during the chemical reaction, which causes internal hydroxyl groups to become exposed. This can lead to a marginal amplification of the hydroxyl peaks (Zepic et al., 2015). Additionally, this assertion can indicate that only the most exposed surface hydroxyl groups were replaced by acetyl groups and that supplementary investigation is required to improve the success of acetylation for this reaction through molecular swelling.

The absence of absorbance peaks at 1 840 cm^{-1} and 1 760 cm^{-1} for the modified samples indicates that all the acetic acid by-products were removed after modification, and the absence of a peak at 1 700 cm^{-1} suggests that all the acetic anhydride reactant was eliminated through washing.

I. CN NFC – *Non-green*

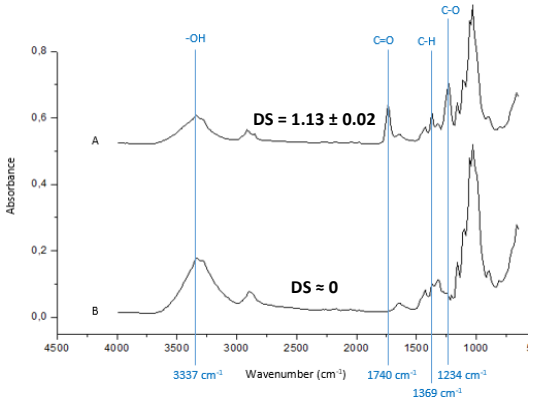

II. CC NFC – *Non-green*

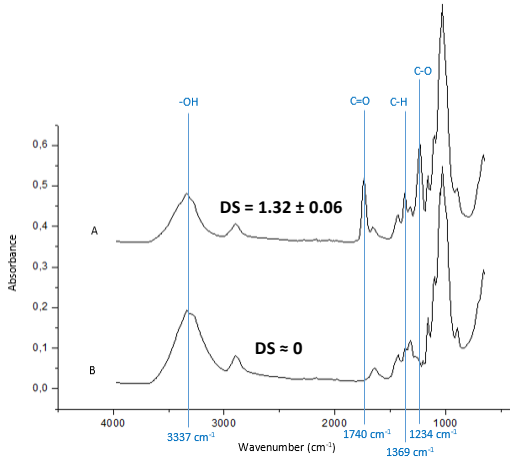

III. WS NFC – *Non-green*

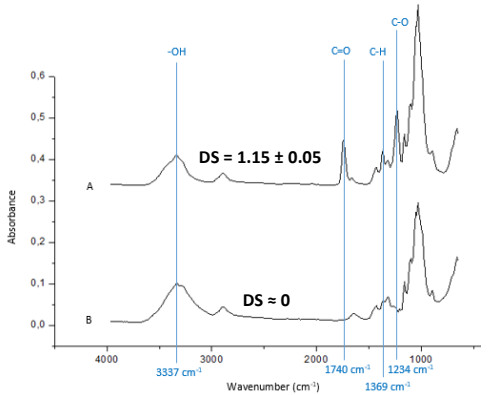

IV. CN NFC – *Green*

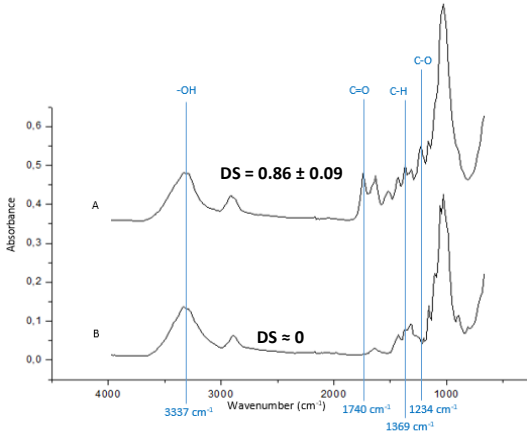

V. CC NFC – *Green*

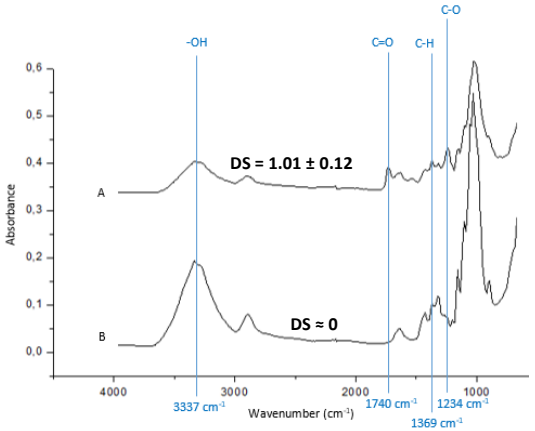

VI. WS NFC – *Green*

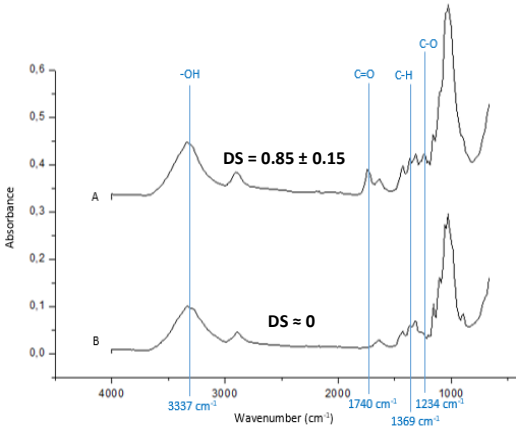

Figure 6.10 The Degree of Substitution (DS) and Fourier Transform Infrared Spectra of Commercial (CN) Nanofibrillated Cellulose (NFC), Corncob (CC) NFC and Wheat Straw (WS) NFC, where ***A*** depicts an Optimally Modified Sample (*Green* at 28.2 °C, 48.0 h and 724.4 U of Lipase; *Non-green* at 105 °C, 24 h and 3 % (v/v) Pyridine). ***B*** represents an Unmodified Sample.

Conversely, an increase in the amide I band and amide II band is observed at 1 650 cm^{-1} and 1 530 cm^{-1} for the *green* modifications in Figure 6.10 IV – VI. This incline signifies that enzymatic proteins are still present in the final washed product, which is confirmed in the study by Bozic et al. (2015) where extensive washing of the specimens did not achieve decreased amide bands after several washing cycles. This occurrence denotes that the lipase proteins have formed a stable bond with the NFC during the reaction. Moreover, Bozic et al. (2015) proved that these stable acyl-enzyme complex molecules were additionally acetylated and therefore contributed to the OS capacities of the sorbents. It can be noted that these amine peaks are greater for commercial NFC than for CC and WS NFC.

Figure 6.11 depicts that the *non-green* modification had a significantly higher DS for both CC NFC ($p = 3.24 \times 10^{-3}$) and WS NFC ($p = 0.01$). This finding is confirmed by superior ester bands at 1 740 cm^{-1}, 1 369 cm^{-1} and 1 234 cm^{-1} and lower hydroxyl-bands at 3 337 cm^{-1}, 1 337 cm^{-1} and 1 310 cm^{-1} in Figure 6.10 II and III when compared to the *green* modified samples in Figure 6.10 V and VI. According to Bozic et al. (2015), the presence of the acyl-enzyme complex, which forms during the *green* acetylation reaction, inhibits the accessibility of the internal hydroxyl groups through molecular steric hindrance.

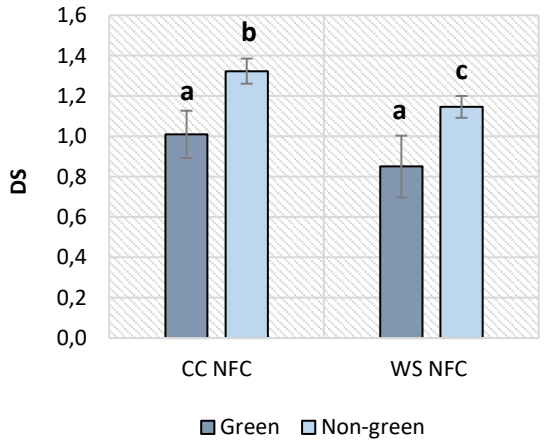

Figure 6.11 The Degree of Substitutions (DS) achieved via the Optimised *Green* and *Non-green* Surface Modifications of Corncob (CC) and Wheat Straw (WS) Nanofibrillated Cellulose (NFC)

A DS of one designates that only the most accessible hydroxyl groups are replaced by acetyl groups. Therefore, in order to achieve a higher DS, molecular erosion and swelling are necessary to expose the internal, less-accessible hydroxyl groups (Zepic et al., 2015). Freeze-drying the isolated NFC prior to acetylation establishes the formation of strong intermolecular bonds between the NFC fibres, which results in the acetylating agent experiencing difficulty in penetrating the fibres to establish the chemical reaction (Zepic et al., 2015). Consequently, a DS merely marginally higher than one was attained in this study. Supplementary reaction steps which promote more molecular swelling might be necessary to facilitate the acetylation of additional hydroxyls.

Moreover, chemical contaminants present in the CC and WS NFC can influence the ability of internal hydroxyl substitution. The cellulose particles in this study, which contain the reactive hydroxyl groups available for acetylation, are contaminated by residual lignin and hemicellulose. The composition analysis illustrates that the specimen isolated from CC contained 54.88 ± 1.60 % cellulose, 9.40 ± 0.81 % hemicellulose, and 3.81 ± 0.83 % lignin (Table 6.11). In comparison, the specimen isolated from WS contained 60.17 ± 4.06 % cellulose, 7.68 ± 0.65 %

hemicellulose, and 3.64 ± 0.67 % lignin. These samples were applied to produce the CC and WS NFC utilised during the modification reactions.

Table 6.11 The Composition Analyses of the Isolated Corncob Cellulose and Isolated Wheat Straw Cellulose utilised for Nanofibrillated Cellulose Production

Composition of Source [a]	Lignin (%) [b]	Cellulose (%) [c]	Hemi-cellulose (%) [d]	Moisture (%)	Ash (%)	Extractives (%) [e]
CC Cellulose	3.81 ± 0.83	54.88 ± 1.60	9.40 ± 0.81	12.76 ± 0.72	6.97 ± 0.62	3.14 ± 0.35
WS Cellulose	3.64 ± 0.67	60.17 ± 4.06	7.68 ± 0.65	11.81 ± 1.40	6.06 ± 0.86	6.45 ± 0.86

a – Completed based on the NREL/TP-510-42620 method for corncob (CC) cellulose and wheat straw (WS) cellulose; **b –** Acid-soluble and acid-insoluble lignin; **c –** Cellulose accounting for glucose sugars; **d –** Hemicellulose accounting for arabinose and xylose sugars; **e –** Water- and ethanol extractives

These impurities may have an impact on the quality of the NFC produced. The presence of these molecules can cause the produced NFC fibres to exhibit lower molecular crystallinities, which affects the potential success of acetylation. As previously discussed, samples with higher crystallinities are inclined to be acetylated more successfully since these materials will have more exposed, accessible surface hydroxyl groups available for substitution. The presence of lignin and hemicellulose consequently leads to longer required reaction times and higher required reaction temperatures in order to establish the sufficient molecular swelling needed for successful acetylation. Further purification using methods such as bleaching with sodium chloride (Shamsabadi et al., 2015) would improve the quality of the cellulose for NFC production. Nevertheless, this step is regarded as *non-green* and was therefore not included in this study.

6.3.4.2 The Water Contact Angles and Heterogeneous Oil Sorption of Nanofibrillated Cellulose Aerogels

NFC aerogels were created from CC and WS NFC via the methodology described in Section 6.2.5. The heterogeneous OS values of the aerogels were qualitatively investigated by placing the aerogels in a mixture of artificial seawater (3.5 % (w/w) sodium chloride in distilled water) and motor oil (Shell Helix Ultra, 5W-40) (Alaa El-Din et al., 2018). These results are displayed in Figure 6.12 for the unmodified, *green* and *non-green* modified aerogels for CC and WS NFC. The water contact angles (WCA, θ) of the aerogels are also indicated in Figure 6.12.

The unmodified CC NFC (Figure 6.12 I) and unmodified WS NFC (Figure 6.12 II) demonstrate an affinity to the sorption of the water in the heterogeneous environment. It appears as if practically no oil was removed during the addition of the unmodified aerogels to the oil-and-water mixture. These sorbents correspondingly demonstrated a 0 ° WCA, since the water droplets immediately penetrated the surfaces of these aerogels.

The *green*- and *non-green* modified specimens (Figure 6.12 III – VI) exhibited a substantial sorption of oil. These samples had WCA exceeding 90 °, indicating that these sorbents were hydrophobic and therefore, oleophilic (Zanini et al., 2017; Zhou et al., 2016). These modified sorbents exhibited an improved affinity for OS when compared to the unmodified samples. It is visually evident that the *non-green* modified CC and WS NFC aerogels (Figure 6.12 III – IV) removed more motor oil than the respective *green* modified counterparts (Figure 6.12 V – VI), as indicated by the more considerable amount of residual oil in the latter samples. Furthermore, it is evident that the *green*

modified CC and WS NFC had a marginally lower WCA than the respective *non-green* sorbents. These results demonstrate that the acetylation of the NFC improved the functionality in OS applications. It validates that a higher DS will cause a superior WCA. Consequently, the modification leads to an augmented OS since more hydrophobic acetyl groups are available for sorption.

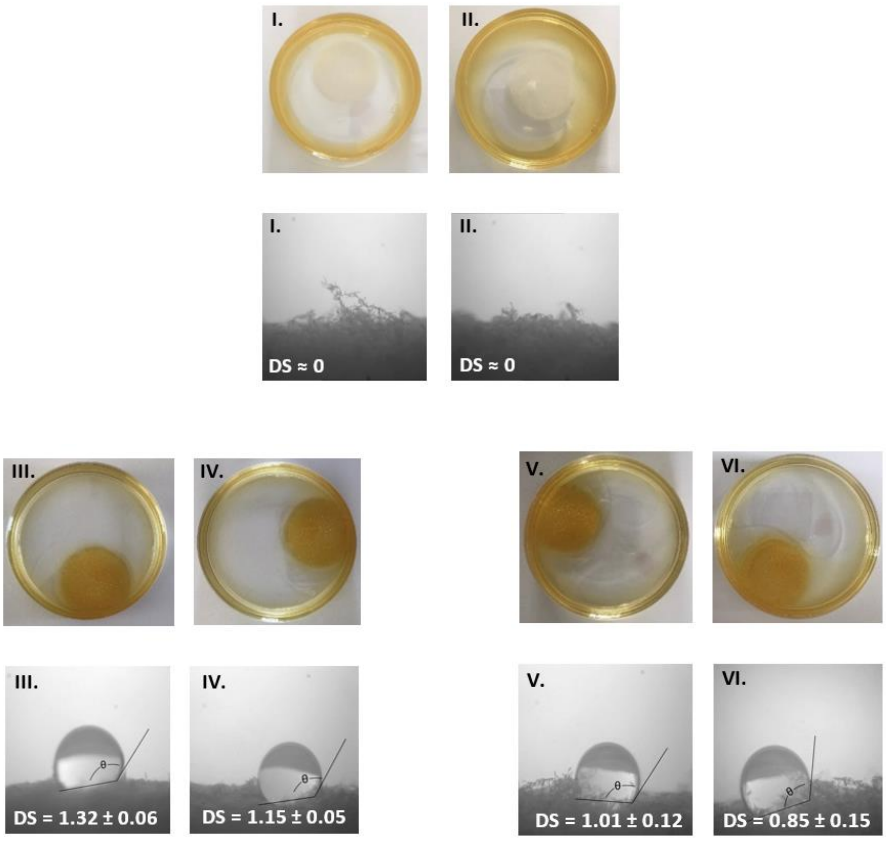

Figure 6.12 The Degree of Substitution (DS) and Qualitative Heterogeneous Oil Sorption of Motor Oil in Artificial Seawater and the Water Contact Angle (θ) for **I.** Unmodified Corncob (CC) Nanofibrillated Cellulose (NFC) (θ = 0 °) and **II.** Unmodified Wheat Straw (WS) NFC (θ = 0 °); **III.** Optimal *Non-green* Modified CC NFC (θ = 123.7 ± 2.5 °) and **IV.** Optimal *Non-green* Modified WS NFC (θ = 121.9 ± 4.0 °); **V.** Optimal *Green* Modified CC NFC (θ = 117.2 ± 0.4 °) and **VI.** Optimal *Green* Modified WS NFC (θ = 115.2 ± 2.8 °)

The *non-green* acetylated samples reached WCA of 123.7 ± 2.5 ° for CC NFC and 121.9 ± 4.0 ° for WS NFC. This result demonstrates an approximate 40 % increase in WCA when compared to the WCA of 72.8 ± 2.6 ° reached by Zepic et al. (2015) under the comparable reaction conditions of 105 °C, 20 h and 3 % (v/v) pyridine. Correspondingly, the enzymatically acetylated WCA of 117.2 ± 0.4 ° for CC NFC and 115.2 ± 2.8 ° for WS NFC is roughly 30 % higher than the 84 ± 9 ° achieved by Bozic et al. (2015).

Moreover, the heterogeneous oil- and water sorptions (OS and WA) were quantitatively determined with sunflower oil and distilled water (Figure 6.13). The unmodified CC and WS NFC exhibit an affinity for WA, with 33.93 ± 3.50 g/g and 35.44 ± 1.11 g/g retained. In conjunction, only 12.85 ± 0.93 g/g and 11.35 ± 0.95 g/g oil were removed with these aerogels. However, the affinity for OS is significantly enhanced by the *green* and *non-green* surface modification reactions for both CC and WS NFC. The OS of 41 – 46 g/g achieved by the *green* and *non-green* modified NFC were statistically similar ($p = 0.17$). In conjunction, the WA of 9 – 12 g/g reached by these samples were also not statistically different ($p = 0.11$).

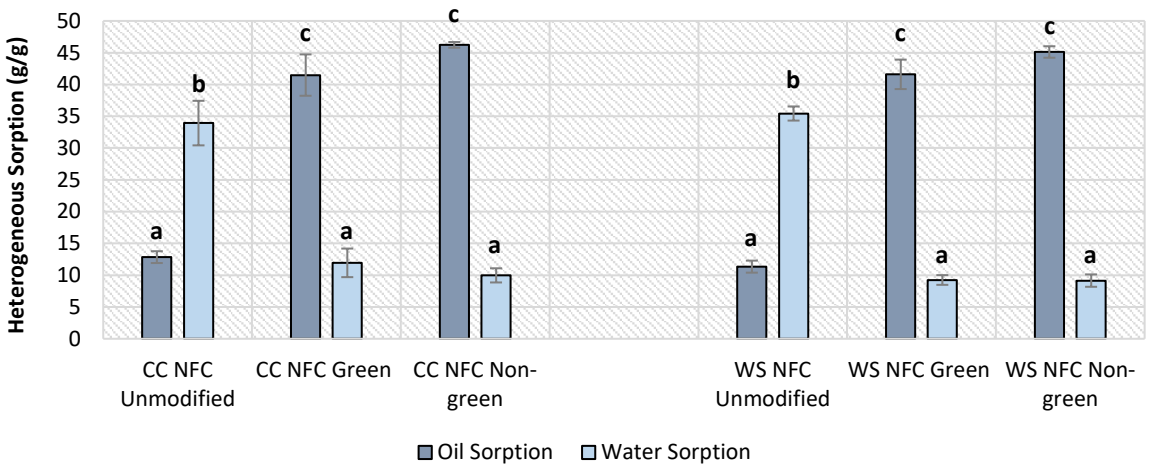

Figure 6.13 The Heterogeneous Oil- and Water Sorptions determined with Sunflower Oil and Distilled Water at Room Temperature (± 20 °C) for Modified and Unmodified Corncob (CC) and Wheat Straw (WS) Nanofibrillated Cellulose (NFC)

Figure 6.13 depicts that the OS for modified CC and WS NFC were significantly higher than the WA, regardless of the type of modification. This assertion proves that a selective affinity for OS is achieved through the surface modifications in this study and that the *green*, enzymatically acetylated NFC aerogels perform equally to the *non-green*, chemically acetylated aerogels for both CC and WS. Enzymatically catalysed modifications are favoured above chemically catalysed reactions due to their inherent environmental friendliness and chemo-selectivity or stereo-selectivity, which can potentially be instituted to target specific functional groups (Bozic et al., 2015).

The effect of viscosity on the OS of CC and WS NFC aerogels are discussed in Appendix F.3.3 (p. 171). A homogeneous motor oil sorption (Shell Helix Ultra, 5W-40) of 71 – 74 g/g was achieved with the *green* NFC aerogels. Traditional petrochemical-based sorbents, such as polyurethane foam, polypropylene webs, nanoporous polystyrene fibres, and rubber gels are known to retain approximately 60 – 70 g/g motor oil (Nyankson, Rodene, & Gupta, 2016; She et al., 2010). The biosorbents developed from CC and WS NFC can, therefore, potentially compete with the performances achieved by the petrochemical-based sorbents. However, the developed sorbents are currently single-use items since the three-dimensional aerogel matrix degenerates after the first usage cycle. The retrained oil cannot easily be extracted for re-use without the expensive separation of the oil from the loose NFC particles. More research is needed to provide the aerogels with tensile strength, thereby establishing reusability, while retaining the high sorption capacities.

Chapter 7 – The Comparison of the Sorption Properties between Corncob, Wheat Straw and their Distinctive Cellulose and Nanofibrillated Cellulose Counterparts

Abstract

The corncob (CC) and wheat straw (WS) biomass, cellulose films and nanofibrillated cellulose (NFC) aerogels – modified via *green* and *non-green* surface modifications – were compared by using the set of key performance indicators identified in Chapter 1. It was ascertained that the *green* CC NFC aerogels and *green* WS NFC aerogels most adequately satisfied the criteria. These aerogels were, therefore, designated as the optimal, lignocellulosic-based, *green* biosorbent for selective oil sorption (OS) application.

Sorption kinetic analyses were applied to the *green* NFC aerogels by utilising sunflower oil. The pseudo-second-order model accurately correlated with the experimental data for both CC and WS NFC with R^2 = 0.9963 and R^2 = 0.9958, respectively. The intra-particle diffusion model furthermore accurately predicted the sorption mechanism of these aerogels. This assertion indicated that a liquid film forms on the fibre surface and adsorption could take place (R^2 = 0.9850 for CC NFC and R^2 = 0.9887 for WS NFC). Thereafter, diffusion into the fibrous pores swiftly occurred, resulting in oil absorption (R^2 = 0.9613 for CC NFC and R^2 = 0.9761 for WS NFC).

7.1 Results and Discussion

7.1.1 Density, Porosity and Heterogeneous Oil Sorption

The bulk densities, porosities and heterogeneous OS of the CC and WS biomass, cellulose and NFC samples are displayed in Table 7.1. It is illustrated that both cellulose films and NFC aerogels have lower bulk densities than that of water and will, therefore, float on the water surface during application. These buoyant properties allow for simpler application in water treatment systems (Deschamps et al., 2003; Liu et al., 2017) since the particles could be retrieved with ease.

The bulk densities and porosities of the biomass particles were not determined since robust three-dimensional structures were not formed, and the sorption was rather achieved with 425 µm to 600 µm biomass particles. The highly interconnected, lightweight, porous structure of the NFC aerogels provides these samples with drastically decreased densities when compared to the cellulose films (Liu et al., 2017). It is clear from Table 7.1 that the *green* and *non-green* modified sorbents retained marginally higher densities than the unmodified samples on each level. This occurrence is attributed to the higher molecular weight attained by the acetyl groups compared to the weight attained by the hydroxyl groups. The acetylation reactions thus increase the overall weight of the samples (Huang et al., 2014), which influences the density.

Porosity is a measurement of the void volume present in a fibrous material and could subsequently be used as an indication of the amount of oil that can be absorbed or adsorbed by the relevant sample under ideal conditions since it provides an indication of the specific surface area available for OS (Hatton et al., 2015; Hubbe et al., 2015; Johnson et al., 1973).

Table 7.1 The Density and Porosity of the Unmodified, *Green* and *Non-green* Biosorbents produced from Corncob and Wheat Straw Biomass, Cellulose and Nanofibrillated Cellulose, compared to the Heterogeneous Oil Sorption

Source Material [a]	Status	Density (kg/m^3)	Porosity (%)	Heterogeneous OS [c] (g oil/g sorbent)
WS Biomass (425 – 600 µm)	Unmodified	n/a	n/a	8.52 ± 0.12
	Green Modified	n/a	n/a	16.91 ± 0.42
	Non-green Modified	n/a	n/a	17.12 ± 1.95
CC Biomass (425 – 600 µm)	Unmodified	n/a	n/a	6.82 ± 2.30
	Green Modified	n/a	n/a	18.37 ± 0.12
	Non-green Modified	n/a	n/a	20.46 ± 1.42
WS Cellulose Films	Unmodified	270.23 ± 19.51	82.45 ± 1.27	4.72 ± 0.43
	Green Modified	349.31 ± 17.58	77.32 ± 1.14	12.77 ± 1.15
	Non-green Modified	356.88 ± 16.75	76.83 ± 1.09	21.03 ± 1.69
CC Cellulose Films	Unmodified	273.98 ± 17.15	82.21 ± 1.11	4.88 ± 0.77
	Green Modified	354.68 ± 13.20	76.97 ± 0.86	12.09 ± 0.45
	Non-green Modified	351.39 ± 23.26	77.18 ± 1.51	20.39 ± 0.62
WS NFC [b] Aerogels	Unmodified	8.76 ± 0.15	99.42 ± 0.01	11.35 ± 0.95
	Green Modified	10.10 ± 0.80	99.33 ± 0.05	41.60 ± 2.32
	Non-green Modified	10.17 ± 0.56	99.32 ± 0.04	45.12 ± 0.90
CC NFC [b] Aerogels	Unmodified	8.29 ± 0.52	99.45 ± 0.03	12.85 ± 0.93
	Green Modified	10.91 ± 0.87	99.27 ± 0.06	41.48 ± 3.25
	Non-green Modified	11.49 ± 0.94	99.23 ± 0.06	46.23 ± 0.45

a – Corncob is abbreviated as CC, while wheat straw is abbreviated as WS; **b –** Nanofibrillated cellulose is represented as NFC; **c –** OS depicts oil sorption

The CC and WS NFC aerogels demonstrated increased porosities when compared to the cellulose films. These increased porosities achieved by the aerogels resulted in the drastically enhanced heterogeneous OS for the *green* and *non-green* modified sorbents. Conversely, the OS of the cellulose films were analogous to that of the biomass particles, despite the relatively high porosities achieved. It was determined in Chapter 5 that the presence of the konjac glucomannan binding material in the cellulose films affected OS capabilities. In order to act as binding material, the konjac glucomannan cross-linked with some of the active chemical sites of the cellulose particles (Ibrahim & Mondal, 2019; Liu et al., 2017). These konjac glucomannan fibres have abundant surface hydroxyl groups (Koroskenyi & McCarthy, 2001), which render the fibres highly hydrophilic. Utilising this substance as binding material for the cellulose films essentially reverses some of the effects brought about by surface modification.

Table 7.1 suggests that the cellulose films have the potential to achieve OS more comparable to that of the NFC samples, provided that additional surface acetylation methods are applied to the konjac glucomannan fibres, or another less-hydrophilic binding material needs to be implemented.

7.1.2 Selection of Optimal Sorbent

The primary aim of this study entailed developing a process for the production of bio-based sorbents from CC and WS, and their respective cellulose and NFC constituents which are functionalised via different *green* methods to increase the selective sorption of oil in contaminated water. In order for these biosorbents to qualify as materials that successfully remove oil from water in a *green* way, a defined list of key performance indicators needed to be met (Chapter 1, Section 1.3).

According to these criteria, sustainable, abundantly available, biodegradable sources (Deschamps et al., 2003; Liu et al., 2017) such as the agricultural waste crops, CC and WS, need to be implemented. The fibres have to be modified to develop a selective affinity for oil particles instead of water particles (Deschamps et al., 2003; Liu et al., 2017). Furthermore, this modification has to be conducted in a way that does not make use of toxic chemicals and does not contribute to environmental pollution or increased carbon dioxide emissions. A low density is favoured since a buoyant sorbent allows simpler application in water treatment systems (Deschamps et al., 2003; Liu et al., 2017). Higher porosity furthermore leads to a greater possible sorption capacity (Liu et al., 2017), since the oil particles can be retained in the material matrix structure (Deschamps et al., 2003). Lastly, the product should not become non-biodegradable with the surface modification (Deschamps et al., 2003) and the implementation of the biosorbent should not adversely affect the living organisms that it contacts. The CC and WS biomass, cellulose films and NFC aerogels modified via *green* and *non-green* surface modifications were compared based on these criteria, as set out in Appendix H (p. 193).

The *green* CC NFC aerogels and *green* WS NFC aerogels were determined to adequately satisfy these criteria. These sorbents were derived from CC and WS, and were therefore abundant and sustainable (Deschamps et al., 2003; Liu et al., 2017). *Green* surface modifications were applied to accomplish highly oleophilic, hydrophobic products (Deschamps et al., 2003; Liu et al., 2017).

Moreover, the sorbents remained biodegradable (Deschamps et al., 2003). The aerogels were adequately washed with distilled water until a filtrate pH of 7 was reached, indicating that all acetic anhydride reactants and acetic acid by-products were removed from the samples after modifications (Chowdhury & Hamid, 2016). However, the final product did contain the lipase protein applied during the surface modification reaction (Section 6.3.2). The enzyme could not be adequately removed from the final sorbent, and it was determined that the lipase proteins had formed a stable bond with the NFC during the reaction (Bozic et al., 2015). Despite this occurrence, Bozic et al. (2015) furthermore proved that these stable acyl-enzyme complex molecules were additionally acetylated and therefore contributed to the OS capacities of the particles. Since these protein molecules are bound to the biosorbent, these constituents will not be released during OS applications and therefore pose no threat to the environment.

The NFC aerogels exhibited low densities and high porosities, aiding in OS application. The *green* CC and WS NFC aerogels were therefore selected as the optimal, lignocellulosic-based, environmentally friendly biosorbent for selective OS application.

The effect of temperature and viscosity on the OS of CC and WS NFC aerogels are discussed in Appendix F.3.3 (p. 171).

7.1.3 Sorption Kinetics of *Green* Nanofibrillated Cellulose Aerogels

An evaluation of the kinetic behaviour of the *green* CC and WS NFC aerogels were performed. The OS of the samples were measured under homogeneous conditions in a static environment at different contact times (Figure 7.1). This analysis was achieved by placing the aerogels (with approximate weights of 0.025 g) in 5 g sunflower oil for times varying between 10 seconds and 20 minutes. A sharp, significant increase ensued between 0 min and 6 min for both CC NFC ($p = 2.04 \times 10^{-6}$) and WS NFC ($p = 5.94 \times 10^{-6}$). A plateau occurred after 6 minutes, indicating that equilibrium was reached for both sorbents, and no significant incline in sorption was attained hereafter for either CC NFC ($p = 0.23$) or WS NFC ($p = 0.69$). It is evident that approximately 50 – 60 % of the maximum saturation capacity was reached after 2 – 3 min of contact for both aerogels, as indicated in Figure 7.1. This is a desirable quality since it indicates efficiency (Z. Wang, Barford, Hui, & McKay, 2015).

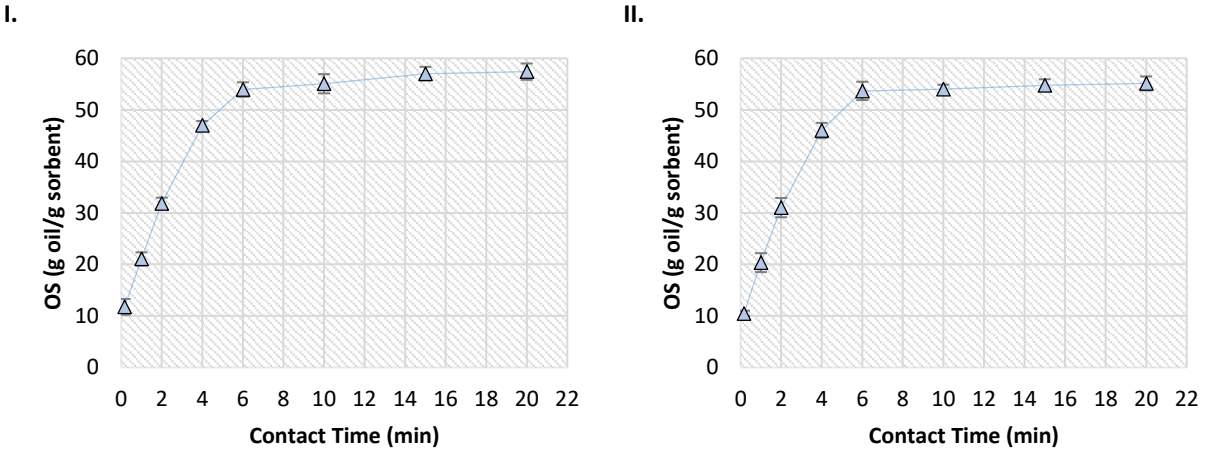

Figure 7.1 The Homogeneous Oil Sorptions (OS) determined with Sunflower Oil at Room Temperature (± 20 °C) with Different Oil-to-Sorbent Contact Times for **I.** *Green* Corncob Nanofibrillated Cellulose Aerogels and **II.** *Green* Wheat Straw Nanofibrillated Cellulose Aerogels

In order to study the sorption kinetics of the *green* NFC aerogels, kinetic models were applied to the sorption data, and the applicability of the models were evaluated (Nwadiogbu et al., 2016). These kinetic models included the pseudo-first-order kinetic model, the pseudo-second-order kinetic model, the intra-particle diffusion model and the liquid-film diffusion model. The pseudo-first-order and pseudo-second-order models were implemented to predict the OS capacity and to evaluate the rate and effectiveness of sorption, while stablishing whether physisorption or chemisorption is predominantly taking place (Z. Wang et al., 2015). Moreover, the liquid-film diffusion model and intra-particle diffusion model were utilised to study the mechanism of sorption. Hereby, the rate-limiting step was determined.

According to Wang et al. (2015), the pseudo-first-order model for sorption kinetics was developed by Lagergren and can also be referred to as the Lagergren equation (Nwadiogbu et al., 2016). This model was amongst the first to consider the mechanism of sorption between a liquid and a solid (Z. Wang et al., 2015). If the experimental data follows the pseudo-first-order model, it indicates that physisorption is predominantly occurring (Ho & McKay, 1999). In this case, the sorption is taking place through a physical exchange – diffusion into the fibrous pores (Ho & McKay,

1999). The pseudo-first-order kinetic model is represented by Equation 7.6, with k_1 (min^{-1}) as rate constant, q_t as the OS (g oil/g sorbent) at any time (t, min) and q_e as the OS (g oil/g sorbent) at equilibrium. By integrating Equation 7.6 with the boundary conditions of t = 0 and q_t = 0, the pseudo-first-order kinetic model was represented by Equation 7.7 (Al Zubaidi, Al Tamimi, & Ahmed, 2016).

$$\frac{dq_t}{dt} = k_1(q_e - q_t) \quad [7.6]$$

$$\ln(q_e - q_t) = \ln(q_e) - k_1 t \quad [7.7]$$

The experimental data (Figure 7.1) were utilised to plot a straight line of $\ln(q_e - q_t)$ as a function of time, as displayed in Figure 7.2 I and II. The slope of the straight line is equal to $-k_1$, while the intercept provided $\ln(q_e)$. The computed k_1 and model-predicted q_e values are displayed in Table 7.2, and the fit of the model was evaluated by studying the R^2 value.

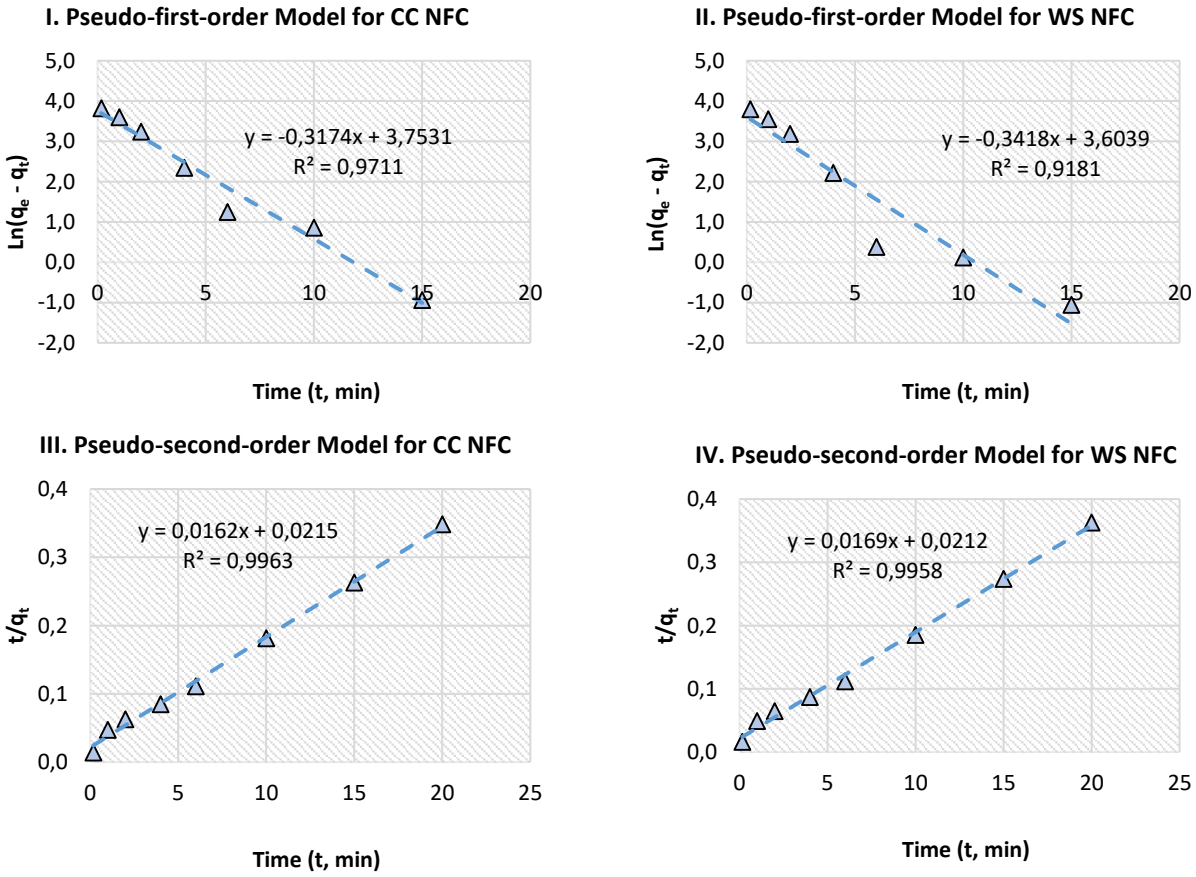

Figure 7.2 The Kinetic Sorption Profiles for Corncob (CC) and Wheat Straw (WS) Nanofibrillated Cellulose (NFC) Aerogels via the Pseudo-first-order Model and Pseudo-second-order Model

The pseudo-second-order kinetic model is depicted by Equation 7.8, with k_2 ($g.g^{-1}.min^{-1}$) as rate constant, q_t as the OS (g oil/g sorbent) at any time (t, min) and q_e as the OS (g oil/g sorbent) at equilibrium. By integrating Equation 7.8 with the boundary conditions of t = 0 and q_t = 0, the pseudo-second-order kinetic model was represented by Equation 7.9 (Al Zubaidi et al., 2016). If the experimental data follows the pseudo-second-order model, it indicates that chemisorption is predominantly taking place (Ho & McKay, 1999). In this case, the sorption is occurring through physiochemical interactions between the oil and the molecules on the fibre surface (Robati, 2013).

$$\frac{dq_t}{dt} = k_2(q_e - q_t)^2 \quad [7.8]$$

$$\frac{t}{q_t} = \frac{1}{k_2 q_e^2} + \frac{1}{q_e} \quad [7.9]$$

The experimental data (Figure 7.1) can be utilised to plot t/q_t as a function of time, as shown in Figure 7.2 III and IV. The slope of the straight line is equal to $1/q_e$, while the intercept computes to $1/(k_2.q_e^2)$. The k_2 and model-predicted q_e values are displayed in Table 7.2, and the fit of the model was evaluated by studying the R^2 value.

Table 7.2 Comparison of Kinetic Sorption Profiles for Corncob and Wheat Straw Nanofibrillated Cellulose Aerogels via the Pseudo-first-order Model, Pseudo-second-order Model, Intra-particle Diffusion Model and Liquid-film Diffusion Model

Kinetic Model	Source [a, b]		Slope	Intercept	Model Parameters [c]	R^2
Pseudo-first-order Model	**CC NFC**		- 0.3174	3.7531	k_1 = 0.3174 min^{-1} q_e = 42.6531 g/g	0.9711
	WS NFC		- 0.3418	3.6039	k_1 = 0.3418 min^{-1} q_e = 36.7412 g/g	0.9181
Pseudo-second-order Model	**CC NFC**		0.0162	0.0215	k_2 = 0.0122 $g.g^{-1}.min^{-1}$ q_e = 61.7284 g/g	0.9963
	WS NFC		0.0169	0.0212	k_2 = 0.0135 $g.g^{-1}.min^{-1}$ q_e = 59.1716 g/g	0.9958
Liquid-film Diffusion Model	**CC NFC**		0.3471	-	k_f = 0.3471 $g.g^{-1}.min^{-0.5}$	0.9555
	WS NFC		0.3823	-	k_f = 0.3823 $g.g^{-1}.min^{-0.5}$	0.8944
Intra-particle Diffusion Model	**CC NFC**	Part 1	22.3780	0.9369	$k_{i,1}$ = 22.378 $g.g^{-1}.min^{-0.5}$ $C_{i,1}$ = 0.9369	0.9850
		Part 2	1.8361	49.4600	$k_{i,2}$ = 1.8361 $g.g^{-1}.min^{-0.5}$ $C_{i,2}$ = 49.4600	0.9613
	WS NFC	Part 1	22.5210	- 0.1902	$k_{i,1}$ = 22.5210 $g.g^{-1}.min^{-0.5}$ $C_{i,1}$ = - 0.1902	0.9887
		Part 2	0.7627	51.7400	$k_{i,2}$ = 0.7627 $g.g^{-1}.min^{-0.5}$ $C_{i,2}$ = 51.7400	0.9761

a – Corncob is abbreviated as CC, while wheat straw is abbreviated as WS; **b –** Nanofibrillated cellulose is represented as NFC; **c –** k_1 is the rate constant for the Pseudo-first-order Model, k_2 is the rate constant for the Pseudo-second-order Model, k_i is the rate constant for the Intra-particle Diffusion Model, C_i is the intercept for the Intra-particle Diffusion Model, k_f is the rate constant for the Liquid-film Diffusion Model, and q_e is the model-predicted equilibrium OS (g oil/g sorbent)

The pseudo-second-order model accurately correlates with the experimental data for both CC and WS NFC, with higher R^2 values of 0.9963 and 0.9958, respectively. This model can be applied to accurately predict the OS capacity of the *green* NFC aerogels at different times. The sorption kinetics of the *green* CC and WS NFC aerogels thus follow

pseudo-second-order kinetics. Chemisorption is, therefore, predominantly taking place through physiochemical interactions between the oil particles and the acetylated molecular surface.

The liquid-film diffusion model and intra-particle diffusion model were used to study how the oil is transported to the fibrous surface of the sorbent. These models have diffusion mass transport dependant terms, which contribute to the description of the behaviour of porous sorbents (Z. Wang et al., 2015). The mechanism of oil adsorption and absorption is depicted in Figure 7.3. Initially, a film is formed, covering the oleophilic, non-polar external surface of the aerogel (Pruitt, 2017; She et al., 2010). The film thickness will here be dependent on the intermolecular acetyl groups on the fibre surface attracting the polar oil particles, causing adhesion of the oil particles to the fibre surface (Z. Wang et al., 2015). Subsequently, adsorption takes place (Figure 7.3 II).

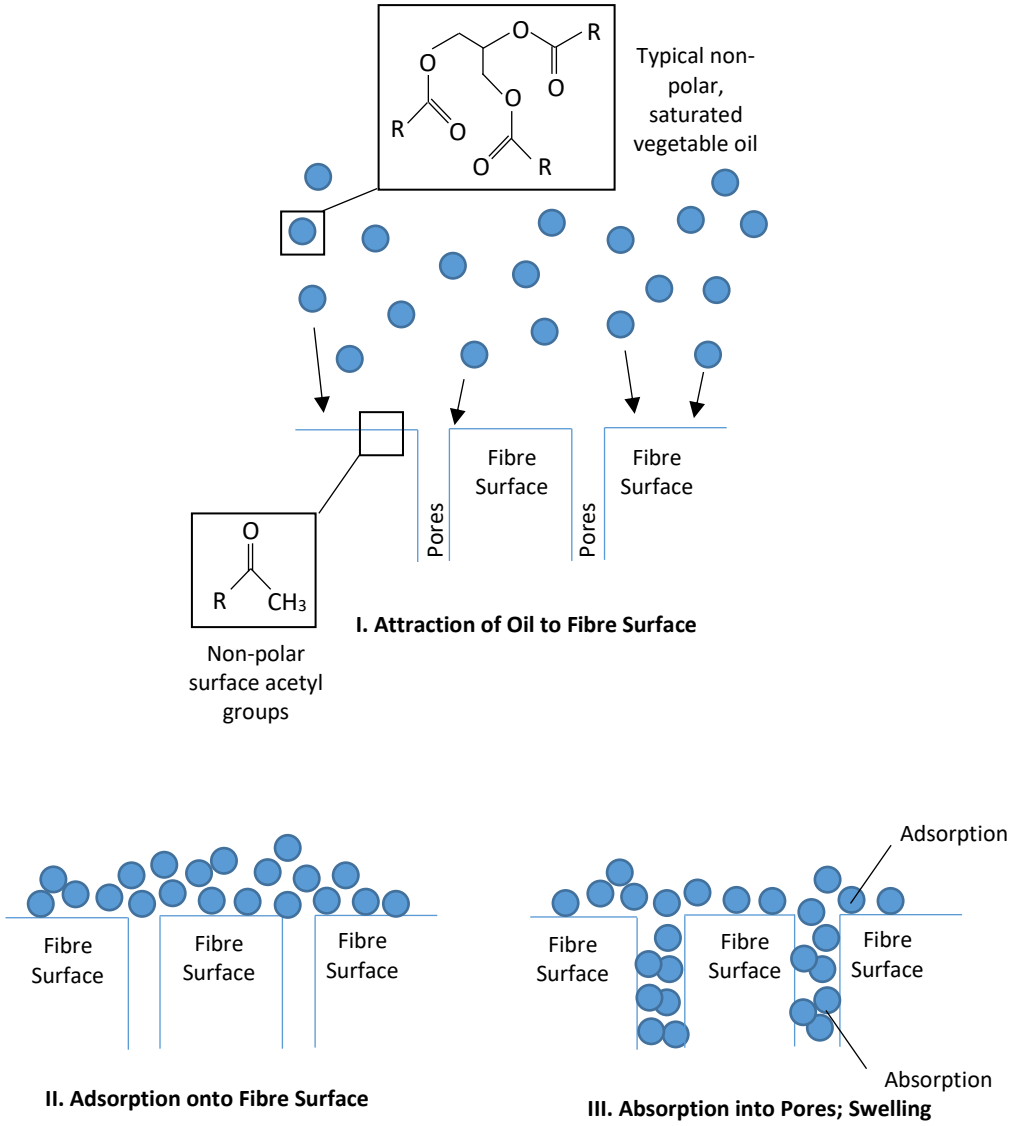

Figure 7.3 The Mechanism of Adsorption onto the Fibre Surface and Absorption into the Fibrous Pores of the Nanofibrillated Cellulose Biosorbent

As time progresses, the oil particles will be attracted to the intramolecular acetyl groups, and the internal voids of the aerogel will be penetrated with oil (Z. Wang et al., 2015) via the absorption mechanism (Figure 7.3 III). Cohesion and capillary forces then cause the oil to be retained in the aerogel matrix (Z. Wang et al., 2015).

The rate of sorption is influenced by the chemical and physical characteristics of the oil and sorbent (Z. Wang et al., 2015). The pore structure and number of acetyl groups on the external fibre surface will influence the sorption capacity of the fibre. The liquid-film diffusion model and intra-particle diffusion model were evaluated and compared based on this mechanism. If the liquid-film diffusion model is identified as the superior fit, then step II (Figure 7.3) is the rate-limiting factor, and adsorption onto the external fibre surface predominantly occurs. However, if the intra-particle diffusion model has a higher R^2, then the diffusion of oil particles into the fibrous pores is the rate-limiting step of the mechanism.

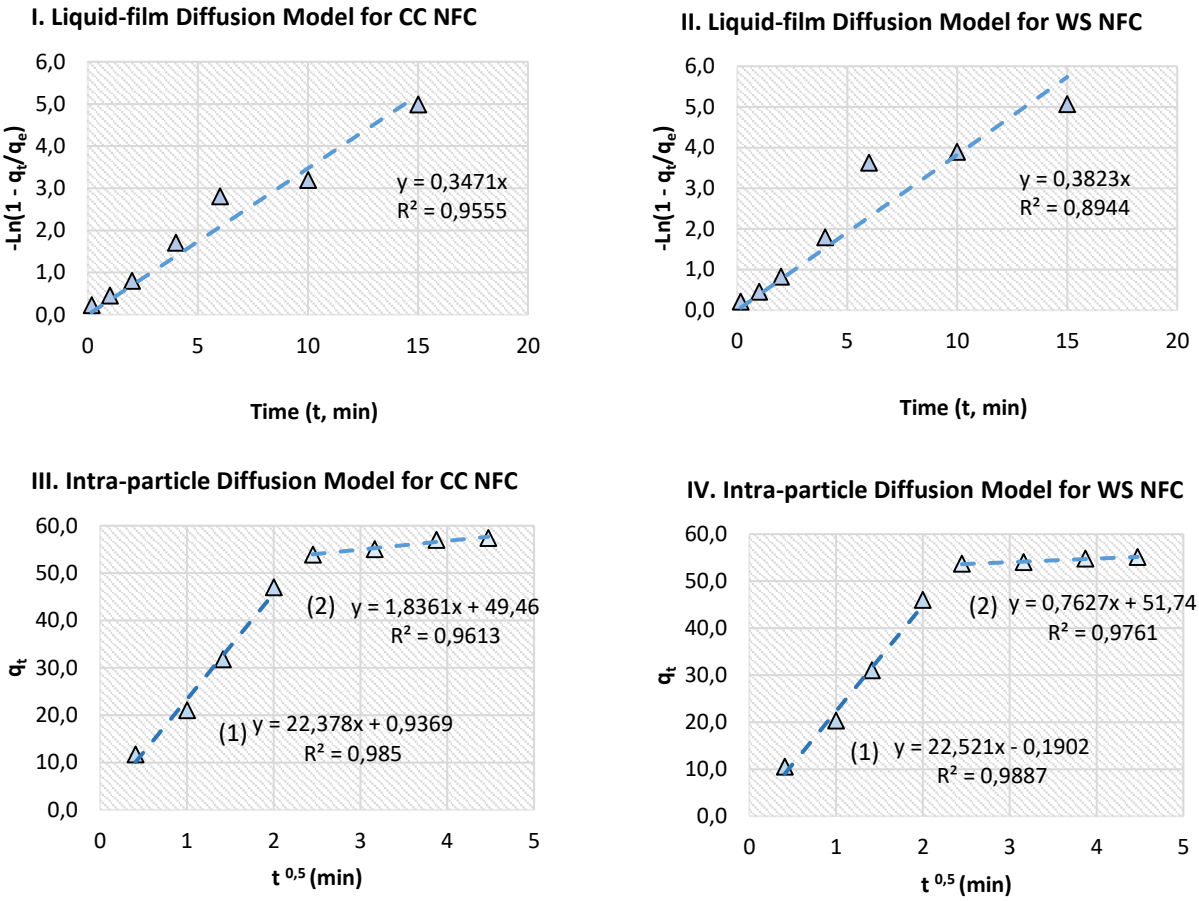

Figure 7.4 The Kinetic Sorption Profiles for Corncob (CC) and Wheat Straw (WS) Nanofibrillated Cellulose (NFC) Aerogels via the Intra-particle Diffusion Model and Liquid-film Diffusion Model

The liquid-film diffusion model is represented in Equation 7.10, with k_f ($g.g^{-1}.min^{-0.5}$) as rate constant, q_t as the OS (g oil/g sorbent) at any time (t, min) and q_e as the OS (g oil/g sorbent) at equilibrium (Nwadiogbu et al., 2016).

$$\ln\left(1-\frac{q_t}{q_e}\right) = -k_f t \qquad [7.10]$$

The experimental data (Figure 7.1) can be utilised to plot a linear graph of $-\ln(1 - q_t/q_e)$ as a function of time, with a zero intercept. These graphs have a slope of k_f (Figure 7.4 I and II). The k_f values are displayed in Table 7.2, and the fit of the model is evaluated by studying the R^2 value.

The intra-particle diffusion model is outlined in Equation 7.11, where k_i ($g.g^{-1}.min^{-0.5}$) represents the intra-particle diffusion rate constant and q_t denotes the OS (g oil/g sorbent) at any time (t, min). Moreover, the experimental data

(Figure 7.1) can be utilised to plot q_t as a function of $t^{0.5}$, where C_i represents the intercept of the linear graph (Figure 7.4 III and IV).

$$q_t = k_i t^{0.5} + C_i \quad [7.11]$$

The intra-particle diffusion model presents a graph that can be fragmented into two parts. An initial steep rise in the curve is followed by a plateau after $t^{0.5}$ exceeds 2 min (Figure 7.4 III and IV). These data points can be fragmented into two groups, and two separate trend lines can be attributed. The initial steep incline is accredited to external adsorption by adhesion and cohesion of the oil on the fibre surface (Figure 7.3 II), while the second group represents the internal absorption of the oil into the fibrous pores (Figure 7.3 III) (Z. Wang et al., 2015).

The steep incline in the first group indicates that surface adsorption occurs swiftly and that this is not the rate-limiting step. However, the low incline observed in the second group for both CC and WS NFC designates that the penetration into the pores is the rate-limiting step. The C_i value (Equation 7.11) can be used as an indication of resistance created by the liquid layer on the fibre surface (Z. Wang et al., 2015). Initially, the C_i value is low, demonstrating that little resistance is created by the liquid film forming on the fibre surface. As time progresses, this C_i value increases – signifying that a boundary layer has formed around the fibre surface.

When comparing the liquid-film diffusion model with the intra-particle diffusion model, it can be noted that both models retained high regression coefficients, with marginally higher R^2 values achieved by the intra-particle diffusion model for both CC and WS NFC. This occurrence ascertains that a liquid film does form on the fibre surface, but that diffusion into the pores can swiftly occur. It can, therefore, be concluded that surface adsorption is not the rate-limiting step and that penetration into the fibrous pores occurred more predominantly. This mechanism is demonstrated in Figure 7.5, where surface adhesion occurs rapidly on the initiation of contact between the oil and the sorbent (Figure 7.5 I). The oil then correspondingly penetrates into the pores of the sorbent, causing swelling (Figure 7.5 II – IV). This mechanism will occur until all the internal pores are saturated. Finally, a liquid layer will then form around the sorbent through cohesion (Figure 7.5 V).

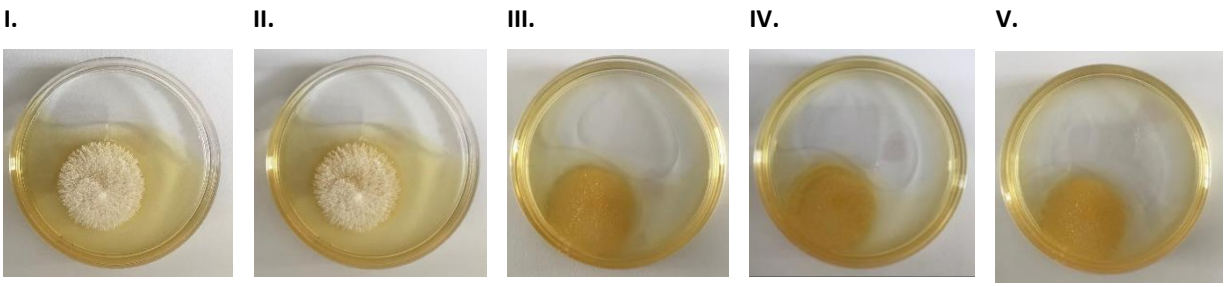

Figure 7.5 Demonstration of the Oil Sorption Mechanism of a *Green* Nanofibrillated Cellulose Aerogel, with **I.** Surface Adhesion Occurring Rapidly on Initial Contact; **II.** Initiation of Absorption into Fibre Pores; **III.** and **IV.** Swelling and Additional Absorption into Fibre Pores, and **V.** Saturated Sorbent with Liquid Layer Surrounding Sorbent through Cohesion

7.1.4 Thermogravimetric Analyses of *Green* Nanofibrillated Cellulose Aerogels

The thermal stabilities of lignocellulosic fibres are integral to their application possibilities (Ceaser, 2019). Therefore, TGA was applied in order to study the degradation temperatures of the CC and WS NFC aerogels, by the methodology described in Chapter 3, Section 3.4.9. The responses to the analyses are displayed in Figure 7.6.

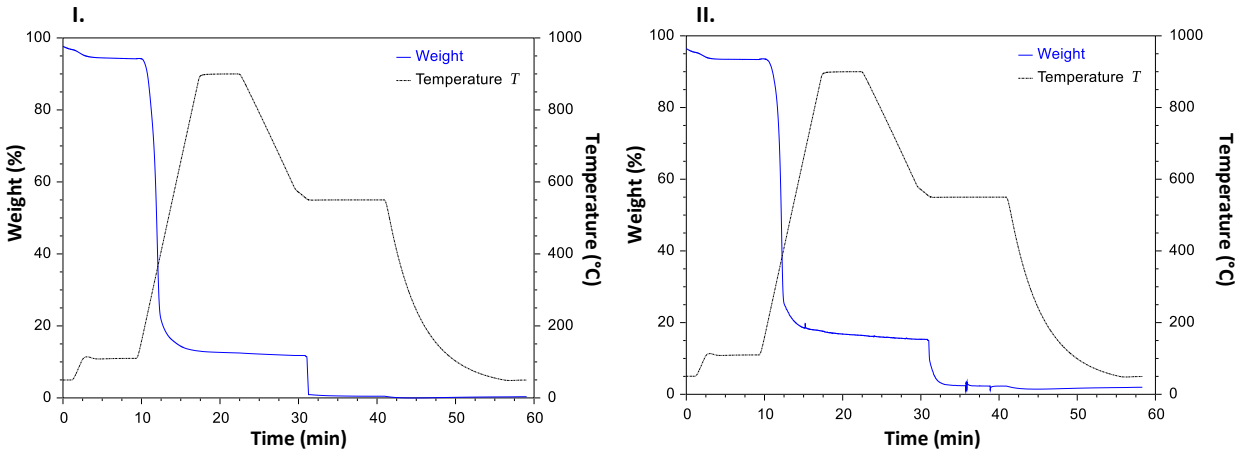

Figure 7.6 The Thermogravimetric Analyses of the **I.** *Green* Corncob Nanofibrillated Cellulose (NFC) Aerogels and **II.** *Green* Wheat Straw NFC Aerogels

The primary decrease in weight is accredited to the evaporation of moisture from the samples (Ceaser, 2019; Oun & Rhim, 2016). This water removal step occurs through physical desorption, as well as by elimination reactions (Borsoi, Zimmernnam, Zattera, Santana, & Ferreira, 2016). The decline was observed between 50 °C and 110 °C for both CC and WS NFC, during Step 1 – 3 of the TGA (Table 3.2, p. 31). The CC NFC aerogels experienced a 3.29 ± 0.09 % decrease in weight (Figure 7.6 I), while the WS NFC aerogels had a 2.90 ± 0.03 % reduction (Figure 7.6 II).

The second principal reduction in weight was observed during Step 4 – 6 of the TGA (Table 3.2, p. 31). The onset of thermal degradation ensued at 192.1 ± 2.8 °C for the CC NFC aerogels (Figure 7.6 I) and 193.7 ± 4.8 °C for the WS NFC aerogels (Figure 7.6 II). At this point, the degradation and decomposition of hemicellulose is initiated (Borsoi et al., 2016; Costa et al., 2015). This occurrence is followed by the degradation of the amorphous regions in cellulose, the crystalline regions in cellulose, and eventually, lignin (Ceaser, 2019; Costa et al., 2015). The samples were reduced to ash after complete pyrolysis during Step 7 (Table 3.2, p. 31). By the end of the TGA, CC and WS NFC exhibited ash contents of 0.50 ± 0.04 % and 1.32 ± 0.23 %, respectively. This assertion indicates that the CC and WS NFC aerogels are apt for applications in environments lower than approximately 190 °C. However, if the environmental temperature exceeds this value, the biosorbents will thermally degrade, and the oil will no longer be retained. Consequently, the sorbents developed in this study will not be suitable for application in burning oil slicks. The surface temperatures of these slicks are estimated at 300 °C (Opstad & Guénette, 2000).

7.1.5 Scale-up of Process

See Appendix I (p. 199) for the potential scale-up of the process. This study has found that the modified *green* NFC aerogels can achieve sorptions comparable to that of the currently implemented petrochemical-based sorbents. However, it is recommended that a techno-economic analyses be completed in order to establish whether the process of NFC isolation, modification and aerogel formation can realistically compete with commercially-available synthetic sorbents from a financial aspect.

Chapter 8 – Conclusions and Recommendations

8.1 Conclusions

The primary aim of this study entailed developing a process for the production of bio-based sorbents from corncob (CC) and wheat straw (WS), and their respective cellulose and NFC constituents which were functionalised via different *green* methods to increase the selective sorption of oil in contaminated water.

This aim was accomplished by optimising *green* surface acetylation reactions on CC, WS and their respective cellulose and NFC counterparts, in order to develop fibres that are hydrophobic and oleophilic. In order to compare the oil sorption (OS) capacities of *green* plant-based biosorbents to traditional *non-green* plant-based biosorbents, a *non-green* surface modification was furthermore applied to each source. The OS of the *green* biosorbents were, therefore, measured against the capacities that can be achieved by similar *non-green* alternatives. This investigation was directed by the Key Research Questions (KRQ) 1 – 4, as developed in Chapter 1, Section 1.4.

8.1.1 The Surface Modification of Corncob and Wheat Straw

The following KRQ were answered:

1. Can a *green* surface acetylation method be applied to the native biomass waste sources, CC and WS, in order to create a selective oleophilicity and hydrophobicity?
4. Can the *green* surface acetylation methods optimised in this study perform equally to traditional *non-green* surface acetylation reactions?

The molecular surface of WS and CC were tuned to become oleophilic via *green* and *non-green* molecular surface acetylation reactions. The *green* modifications were optimised on CC and WS by implementing a central composite design (CCD). The reaction involved applying acetic anhydride as an acetylating agent and specified amounts of iodine as a catalyst (Li et al., 2009; Nwabueze et al., 2016). The acetylation temperature was varied between 50 – 150 °C, the reaction time from 0.6 – 7.4 h and the catalyst concentration was varied from 0.7 – 7.4 % (w/w) iodine. The degree of substitution (DS) and homogeneous OS were maximised.

The optimal DS of 2.14 ± 0.19 and optimal homogeneous OS of 19.25 ± 0.23 g/g achieved by CC at 150.5 °C, 5.7 h and 0.6 % (w/w) iodine were not statistically different to the optimal DS of 2.38 ± 0.09 and optimal OS of 18.99 ± 1.50 g/g attained for WS at 150.5 °C, 7.4 h and 5.7 % (w/w) iodine. The different chemical compositions of the CC and WS caused the feedstocks to react differently to the chemical reaction, thereby achieving the optimal modifications at different conditions.

The performances of the modifications were compared to the acetylations reached by the *non-green* methodology, which replaced the *green* catalyst with *non-green* N-bromosuccinimide (NBS) (X. F. Sun et al., 2004). The highest performance of the *non-green* modification was achieved at 120 °C, 6 h and 1 % (w/v) NBS for both CC and WS. The highest DS of 2.76 ± 0.48 and highest homogeneous OS of 20.93 ± 0.81 g/g was attained by CC, while the WS reached a DS of 2.19 ± 0.05 and homogeneous OS of 18.12 ± 0.18 g/g.

Moreover, the *green* modification yielded hydrophobic CC and WS with a heterogeneous, selective OS of 18.37 ± 0.12 g/g and 16.91 ± 0.42 g/g. In conjunction, the *non-green* modified CC and WS yielded a heterogeneous OS of 20.46 ± 1.42 g/g and 17.12 ± 1.95 g/g. Consequently, the performances accomplished by these feedstocks via the *green* and *non-green* surface modifications were statistically similar, and the *green* sorbents thereby performed equally to the *non-green* sorbents on the *biomass level*.

However, the traditional petrochemical-based sorbents, such as polyurethane foam, polypropylene webs, nanoporous polystyrene fibres, and rubber gels are known to retain approximately 60 – 70 g/g motor oil (Nyankson, Rodene, & Gupta, 2016; She et al., 2010). The biosorbents developed from CC and WS on this level can, therefore, not compete with the performances achieved by the petrochemical-based sorbents. Subsequently, the study was shifted to the *cellulose level* in order to establish whether the CC and WS cellulose-based sorbents can exhibit increased sorption capacities in order to be considered as a worthy competitor for the *non-green* alternatives.

8.1.2 The Surface Modification of Corncob and Wheat Straw Cellulose

The following KRQ were answered:

2. Does an increased surface area lead to an increased capacity for OS when isolating cellulose from the native biomass, and can a selective affinity to OS be achieved by implementing *green* surface acetylation methodologies?
4. Can the *green* surface acetylation methods optimised in this study perform equally to traditional *non-green* surface acetylation reactions?

The surface area available for sorption was amplified by removing the lignin, hemicellulose and other extractives, thereby isolating the cellulose constituents from CC and WS for OS application (Wahi et al., 2013). These segregated fibres were thereafter modified via *green* and *non-green* surface modifications in order to accomplish hydrophobicity.

The *green* modification was optimised by implementing acetic anhydride as an acetylating agent and specified volumes of a 50 % (w/w) sodium hydroxide (NaOH) solution as catalyst (Koroskenyi & McCarthy, 2001). A CCD was applied to cotton, where the temperature was varied between 40 – 140 °C, the reaction time was fluctuated between 3.8 – 44.2 h, and the catalyst concentration was varied from 1.2 – 13.8 % (v/v) NaOH-solution. The DS and OS were maximised on cotton, and the optimised reaction conditions were applied to the isolated CC and WS cellulose. The DS of 0.89 ± 0.05 and homogeneous OS of 21.80 ± 1.44 g/g accomplished by CC cellulose at 115.2 °C, 34.1 h and 13.8 % (v/v) NaOH-solution were statistically similar to the DS of 0.91 ± 0.04 and OS of 21.04 ± 1.70 g/g attained by WS cellulose.

A *non-green* acetylation, which implements acetic anhydride as an acetylating agent and sulfuric acid as a catalyst (Huang et al., 2014), was applied to cellulose as a reference for the performance of acetylation. The highest performance of the *non-green* modification was achieved at 60 °C, 2 h and 5 % (v/w) sulfuric acid. The CC cellulose reached a DS of 1.54 ± 0.05 and a homogeneous OS of 30.79 ± 2.08 g/g, while the WS cellulose exhibited a DS of 1.55 ± 0.05 and a homogeneous OS of 29.51 ± 0.93 g/g.

Films were created from the cellulose samples by implementing konjac glucomannan as a binder. The *green* modification yielded hydrophobic CC and WS cellulose films with a heterogeneous OS of 12.09 ± 0.45 g/g and 12.77 ± 1.15 g/g, while the *non-green* modified CC and WS cellulose films had heterogeneous OS values of 20.39 ± 0.62 g/g and 21.03 ± 1.69 g/g. From these results, it was evident that the CC and WS cellulose fibres reacted correspondingly when subjected to the same type of modification (i.e. *green* or *non-green*). However, the *non-green* modifications outperformed the *green* modifications by approximately 65 – 69 % when comparing the heterogeneous OS.

Traditional petrochemical-based sorbents retain approximately 60 – 70 g/g motor oil (Nyankson, Rodene, & Gupta, 2016; She et al., 2010), and the biosorbents developed from CC and WS cellulose can, therefore, not compete with the performances achieved by these sorbents. Subsequently, the study was shifted to the *NFC level* in order to establish whether the CC and WS NFC-based sorbents can exhibit increased sorptions in order to be considered as a worthy competitor for the *non-green* alternatives.

Furthermore, it was discovered that the presence of the konjac glucomannan binding material in the cellulose films adversely affected the OS capabilities. In order to act as binding material, the konjac glucomannan cross-linked with some of the active chemical sites of the cellulose particles (Ibrahim & Mondal, 2019; Liu et al., 2017). These konjac glucomannan fibres have abundant surface hydroxyl groups (Koroskenyi & McCarthy, 2001), which render the fibres highly hydrophilic. Utilising this substance as binding material for the cellulose films essentially reverses some of the effects brought about by surface modification. It is necessary to apply additional surface acetylation reactions to the konjac glucomannan post-film formation, or an alternative, less-hydrophilic binding material needs to be implemented.

8.1.3 The Surface Modification of Corncob and Wheat Straw Nanofibrillated Cellulose

The following KRQ were answered:

3. When additionally increasing the surface area by isolating NFC, is the capacity for OS increased and can *green* surface acetylation establish oleophilicity and hydrophobicity?
4. Can the *green* surface acetylation methods optimised in this study perform equally to traditional *non-green* surface acetylation reactions?

The surface area of the fibres underwent an additional increase by fractionating the cellulose into NFC particles (Keplinger et al., 2019) through enzymatic hydrolyses with FibreCare®, followed by mechanical fibrillation. These samples were then also modified via *green* and *non-green* surface acetylation reactions.

NFC was enzymatically modified by applying acetic anhydride, dimethyl sulphoxide and Amano Lipase A from *Aspergillus niger*, as adapted from Bozic et al. (2015). A CCD was executed on commercial NFC procured from the University of Maine, where the reaction temperature was varied between 28 – 62 °C, reaction duration was ranged from 28 – 68 h, and the catalyst concentration was fluctuated between 199 – 2 301 units (U) of lipase. The DS was maximised on commercial NFC, and the optimised reaction conditions were applied to the isolated CC and WS NFC. The optimal DS of 1.01 ± 0.12 accomplished by CC NFC at 28.2 °C, 48.0 h and 724.4 U of lipase was statistically similar to the DS of 0.85 ± 0.15 reached by WS NFC.

The performances of the modifications were compared to the acetylations achieved by the *non-green* methodology, which implemented acetic anhydride, dimethylformamide and pyridine (Tingaut et al., 2009; Zepic et al., 2015). The highest performance of the *non-green* modification was attained at 105 °C, 24 h and 3 % (v/v) pyridine. A DS of 1.32 ± 0.06 and 1.15 ± 0.05 was reached by CC and WS NFC, respectively.

Aerogels were created from the NFC samples without the implementation of a binder material. The *green* modification yielded hydrophobic CC and WS NFC aerogels with a heterogeneous OS of 41.48 ± 3.25 g/g and 41.60 ± 2.32 g/g, respectively, while the *non-green* modified CC and WS NFC aerogels had heterogeneous OS values of 46.23 ± 0.45 g/g and 45.12 ± 0.90 g/g. From these results, it was clear that the CC and WS NFC reacted similarly to the *green* modification. Additionally, these feedstocks reacted analogously to the *non-green* modification, and statistically similar results were realised with the different feedstocks by each method. The performance achieved by the *green* CC and WS NFC aerogels compared favourably to the performance of the *non-green* aerogels. Moreover, it was established that these *green* NFC aerogels exhibited 71 – 74 g/g motor oil sorption, which indicated comparable performances to the industrial petrochemical-based sorbents that can retain approximately 60 – 70 g/g motor oil (Nyankson, Rodene, & Gupta, 2016; She et al., 2010).

8.1.4 The Selection of the Optimal Oil Sorbent

Due to anthropogenic activity, unplanned population growth and urbanisation, as well as a considerable increase in industrialisation and misuse of natural water resources, the water quality and quantity available for human consumption is deteriorating (De Gisi et al., 2016). Typical domestic wastewater in South Africa contains approximately 30 - 300 mg/L oil-based constituents, such as hydrocarbons and triglycerides (Mahlobo, 2008). In order to directly utilise domestic greywater for the watering of plants, these oil-based constituents need to be removed prior to application in order to avoid blocking the pores of the plant roots meant for nutrient- and water reception (Oniosun et al., 2019). Moreover, when entering the sewage system, the presence of fats, oil and grease (FOG) are infamous for causing rigorous damage in pipes and pumping stations of wastewater treatment plants, which in turn has an adverse impact on further wastewater processing (El-gawad, 2014). An essential aspect of wastewater management, therefore, constitutes removing the oil-based molecules from the water, prior to further treatment (Mahlobo, 2008). Additionally, hydrocarbon spills in the ocean drastically impact marine life. It influences the insulating ability of marine mammals, the water repellence of feathers, it can be harmful when ingested and affects the growth and physical attributes of exposed fish and plants (National Oceanic Atmospheric Administration, 2017).

The CC and WS biomass, cellulose films and NFC aerogels – modified via *green* and *non-green* surface acetylation reactions – were compared by using the set of key performance indicators identified in Chapter 1. It was determined that the *green* CC NFC aerogels and *green* WS NFC aerogels most adequately satisfied the criteria for acting as a *green*, plant-based biosorbent for the application in the abovementioned water-treatment scenarios.

These biosorbents were derived from CC and WS, and were therefore created from sustainable sources (Deschamps et al., 2003; Liu et al., 2017). *Green* surface modifications were applied to achieve highly oleophilic, hydrophobic products, with an optimal heterogeneous OS of 45 – 46 g/g (Deschamps et al., 2003; Liu et al., 2017). The products remained biodegradable after surface modification (Deschamps et al., 2003) and the stable acyl-enzyme complex

molecules that were found to occur in the final product were ascertained to be bound to the biosorbent. These molecules will, therefore, not be released during sorption applications, and will subsequently not cause harm to the environment. These acyl-enzyme bonds were additionally established to be acetylated, thereby contributing to the OS capacities of the aerogels.

The NFC aerogels exhibited low densities and high porosities, aiding in OS application. The densities of the *green* NFC aerogels were determined as 10 – 11 g/L, where the density of water is 1 000 g/L, and the density of seawater is approximately 1 025 g/L. The aerogels will consequently float on the surface of a water source, aiding in the application of sorption and retrieval. Moreover, the CC and WS NFC aerogels exhibited porosities of approximately 99 %, leading to high sorptions capacities (Liu et al., 2017).

The potential scale-up for the production and modification of hydrophobic, *green* CC and WS NFC aerogels were explored in Appendix I (p. 199). This study has found that the modified *green* NFC aerogels can achieve sorptions comparable to that of the currently implemented petrochemical-based sorbents. However, it is recommended that a techno-economic analyses be completed in order to establish whether the process of NFC isolation, modification and aerogel formation can realistically compete with commercially-available synthetic sorbents from a financial aspect. Moreover, the developed sorbents are currently single-use items since the three-dimensional aerogel matrix degenerates after the first usage cycle. The retrained oil cannot easily be extracted for re-use without the expensive separation of the oil from the loose NFC particles. More research is needed to provide the aerogels with tensile strength, thereby establishing reusability, while retaining the high sorption capacities.

8.2 Recommendations

Accurate Representation of Green Optimal Reactions on All Levels

The *green* surface modifications of the biomass, cellulose and NFC samples were optimised by response surface methodology. Statistical models were developed by implementing a CCD in order to study the interactions of temperature, time and catalyst concentration of each respective type of modification applied to the biomass, cellulose and NFC feedstocks. However, the statistical *Lack of Fit* of the developed models were only insignificant on the *biomass level*, indicating that the models on the *cellulose level* and *NFC level* did not fit the experimental data well. In addition, the model on the *biomass level* predicted extensive ranges for DS and OS. In order to develop more robust models for these responses, it is recommended that more experimental runs are completed. Other statistical optimisation methodologies, such as Box-Behnken or the Taguchi Method, need to be tested to establish whether it produces models with an improved fit.

Accurate Representation of Non-green Optimal Reactions on All Levels

The *non-green* reactions on all the levels were performed with one-factor optimisations, and were not statistically optimised. In order to obtain more accurate representations of the performances of these *non-green* reactions, it is recommended that a full CCD is completed for these acetylations. The effects of the interactions between temperature, time and catalyst concentration should be established.

Biomass for Ease of Application

The 425 to 600 µm biomass particles proved difficult for application. It is complex to retain the particles after sorption. Moreover, re-collecting the oil from the fibres correspondingly pose a physical challenge. It is recommended that a method be developed which can improve the ease of application of this form of biosorbent.

Additionally, different particle sizes need to be investigated on the *biomass level*. According to Nwabueze et al. (2016), a decreased particle size will lead to an increased surface area, which will have an inclined sorption capacity to effect.

Cellulose Film Binding Material Improvement

It was ascertained that the presence of the konjac glucomannan binding material in the cellulose films affected the OS abilities. These konjac glucomannan fibres have abundant surface hydroxyl groups (Koroskenyi & McCarthy, 2001), which render the fibres highly hydrophilic. It is recommended to apply additional surface acetylation methods to the konjac glucomannan, or an alternative less-hydrophilic binding material needs to be implemented.

Furthermore, cellulose aerogels should be created rather than producing cellulose films. This action will increase the porosity of the biosorbent, which will lead to a more significant OS. For cellulose fibres to form aerogels, chemical cross-linking is necessary. This phenomenon occurs if the three-dimensional network is formed by a chemical reaction between the cellulose particles and an additional cross-linking agent (Liu et al., 2017). In this case, a binding material is required to induce the hydrogel formation (Adebajo et al., 2003). A *green* cross-linking agent, therefore, needs to be investigated.

The Entrapment of Bioactive Substances

It is recommended that a study is completed in order to determine whether the biosorbents can be utilised for the controlled release of bioactive substances, such as lipase enzymes. These enzymes can aid the hydrolyses of oil particles into fatty acids and glycerol. This method can be applied when an oil spill is too significant to retrieve, which will cause the oil to deteriorate into less harmful substances through the bioremediation mechanism.

Techno-economic Analyses

A techno-economic analysis should be completed to determine if the process of biomass fractionation, NFC extraction, surface modification and aerogel creation is economically viable for application in wastewater treatment systems. The performance of the lignocellulosic biomass at each stage must be studied in aggregation with the processing cost necessary to achieve each sorption performance.

Reusability

High oil retention, in combination with a simple release of the absorbed or adsorbed particles, ensures reusability of the sorption material (Deschamps et al., 2003; She et al., 2010). Excellent physical and chemical resistance is desired in order to ensure a long life cycle of the product (She et al., 2010). High reusability or durability contributes to the product being more economically beneficial. Currently, these sorbents can only be utilised once, since the products are very sensitive to physical damage. A *green* strengthening agent needs to be implemented to provide these biosorbents with tensile strength. This modification should be executed in such a way that the sorption properties of the biosorbents are retained.

References

Adebajo, M. O., Frost, R. L., Kloprogge, J. T., Carmody, O., & Kokot, S. (2003). Porous Materials for Oil Spill Cleanup: A Review of Synthesis. *Journal of Porous Materials*, *10*(3), 159–170. https://doi.org/10.1023/A:1027484117065

Afsahi, G., Dimic-Misic, K., Gane, P., Budtova, T., Maloney, T., & Vuorinen, T. (2018). The investigation of rheological and strength properties of NFC hydrogels and aerogels from hardwood pulp by short catalytic bleaching (Hcat). *Cellulose*, *25*(3), 1637–1655. https://doi.org/10.1007/s10570-018-1678-6

Agency for Toxic Substances and Disease Registry. (2011). Toxicological profile for sulfur trioxide and sulfuric acid. Retrieved October 31, 2019, from https://www.atsdr.cdc.gov/substances/toxsubstance.asp?toxid=47

Agency for Toxic Substances and Disease Registry. (2014). Medical Management Guidelines for Sodium Hydroxide. Retrieved October 31, 2019, from https://www.atsdr.cdc.gov/MMG/MMG.asp?id=246&tid=45

Al Zubaidi, I. A. H., Al Tamimi, A. K., & Ahmed, H. (2016). Remediation of water from crude oil spill using a fibrous sorbent. *Environmental Technology and Innovation*, *6*, 105–114. https://doi.org/10.1016/j.eti.2016.08.002

Alaa El-Din, G., Amer, A. A., Malsh, G., & Hussein, M. (2018). Study on the use of banana peels for oil spill removal. *Alexandria Engineering Journal*, *57*(3), 2061–2068. https://doi.org/10.1016/j.aej.2017.05.020

Ali, Z., & Arshad, M. (2014). Saccharification of corn cobs an agro-industrial waste by sulphuric acid for the production of monomeric sugars. *International Journal of Biosciences*, *5*(3), 204–213. https://doi.org/10.12692/ijb/5.3.204-213

American Chemistry Society. (2020). 12 Principles of *Green* Chemistry. Retrieved November 8, 2020, from https://www.acs.org/content/acs/en/*green*chemistry/principles/12-principles-of-*green*-chemistry.html?_ga=2.199575789.232863237.1541622832-214832631.1541622832&gclid=Cj0KCQiAy579BRCPARIsAB6QoIaUcNztoFBoEg4Cl7Iw0-1mi28_JOYt3SaaZVnDytCybHaKZCWILpkaAi5eEALw_wcB

Amin, J. S., Abkenar, M. V., & Zendehboudi, S. (2015). Natural Sorbent for Oil Spill Cleanup from Water Surface: Environmental Implication. *Industrial and Engineering Chemistry Research*, *54*, 10615–10621. https://doi.org/10.1021/acs.iecr.5b01715

Arola, S. (2015). *Biochemical modification and functionalization of nanocellulose surface*. Aalto University School of Science.

Arumugam, N., & Anandakumar, S. (2016). Mini review on corncob biomass: A potential resource for value-added metabolites. *European Journal of Experimental Biology*, *6*(5), 9–13.

Asadpour, R., Sapari, N. B., Isa, M. H., & Kakooei, S. (2016). Acetylation of oil palm empty fruit bunch fiber as an adsorbent for removal of crude oil. *Environmental Science and Pollution Research*, *23*(12), 11740–11750. https://doi.org/10.1007/s11356-016-6349-2

Asadpour, R., Sapari, N. B., Isa, M. H., & Orji, K. U. (2014). Enhancing the hydrophobicity of mangrove bark by esterification for oil adsorption. *Water Science and Technology*, *70*(7), 1220–1228.

https://doi.org/10.2166/wst.2014.355

ASTM International. (2019). ASTM D871-96(2019) Standard Test Methods of Testing Cellulose Acetate. Retrieved September 2, 2019, from https://www.astm.org/Standards/D871.htm

Barnhardt Manufacturing Company Inc. (2020). Properties of Cotton - An Extensive Technical Guide. Retrieved November 8, 2020, from https://barnhardtcotton.net/technology/cotton-properties/

Bester, L. M. (2018). *Development and optimisation of a process for cellulose nanoparticle production from waste paper sludge with enzymatic hydrolysis as an integral part*. Stellenbosch University.

Bismarck, A., Aranberri-Askargorta, I., Springer, J., Lampke, T., Wielage, B., Stamboulis, A., … Limbach, H. (2004). Surface Characterization of Flax, Hemp and Water Uptake Behavior. *Polymer Composites*, *23*(5). https://doi.org/doi.org/10.1002/pc.10485

Bondi, C. A. M., Marks, J. L., Wroblewski, L. B., Raatikainen, H. S., Lenox, S. R., & Gebhardt, K. E. (2015). Human and Environmental Toxicity of Sodium Lauryl Sulfate: Evidence for Safe Use in Household Cleaning Products. *Environmental Health Insights*, *9*(9), 27–32. https://doi.org/10.4137/EHI.S31765

Borsoi, C., Zimmernnam, M. V. G., Zattera, A. J., Santana, R. M. C., & Ferreira, C. A. (2016). Thermal degradation behavior of cellulose nanofibers and nanowhiskers. *Journal of Thermal Analysis and Calorimetry*, *126*(3), 1867–1878. https://doi.org/10.1007/s10973-016-5653-x

Bozic, M., Vivod, V., Kavcic, S., Leitgeb, M., & Kokol, V. (2015). New findings about the lipase acetylation of nanofibrillated cellulose using acetic anhydride as acyl donor. *Carbohydrate Polymers*. https://doi.org/10.1016/j.carbpol.2015.02.061

Buranov, A. U., & Mazza, G. (2010). Extraction and characterization of hemicelluloses from flax shives by different methods. *Carbohydrate Polymers*, *79*(1), 17–25. https://doi.org/10.1016/j.carbpol.2009.06.014

Carrascoa, C., Baudela, H., Sendeliusa, J., Modiga, T., Roslandera, C., Galbea, M., … Lidén, G. (2010). SO2-catalyzed steam pretreatment and fermentation of enzymatically hydrolyzed sugarcane bagasse. *Enzyme and Microbial Technology*, *46*, 64–73. https://doi.org/10.1007/s12010-013-0097-2

Ceaser, R. (2019). *Comparative analysis of methods for producing nanocellulose from wheat straw and bran, with co-extraction of valuable products*. Stellenbosch University.

Chen, X., Qian, X., & An, X. (2011). Using calcium carbonate whiskers as papermaking filler. *BioResources*, *6*(3), 2435–2447. https://doi.org/10.15376/biores.6.3.2435-2447

Cheng, H., Gu, B., Pennefather, M. P., Nguyen, T. X., Phan-Thien, N., & Duong, H. M. (2017). Cotton aerogels and cotton-cellulose aerogels from environmental waste for oil spillage cleanup. *Materials & Design*, *130*, 452–458. https://doi.org/10.1016/j.matdes.2017.05.082

Cherian, B. M., Leão, A. L., Caldeira, M. D. S., Chiarelli, D., de Souza, S. F., Narine, S., & Chaves, M. R. D. M. (2012). Use of Saponins as an Effective Surface Modifier in Cellulose Nanocomposites. *Molecular Crystals and Liquid Crystals*, *556*(1), 233–245. https://doi.org/10.1080/15421406.2012.635969

Cherian, B. M., Leão, A. L., de Souza, S. F., Thomas, S., Pothan, L. A., & Kottaisamy, M. (2010). Isolation of nanocellulose from pineapple leaf fibres by steam explosion. *Carbohydrate Polymers*, *81*(3), 720–725.

https://doi.org/10.1016/j.carbpol.2010.03.046

Chimphango, A. F. A., Mugwagwa, L. R., & Swart, M. (2020). Extraction of Multiple Value-Added Compounds from Agricultural Biomass Waste: A Review. In M. Daramola & A. Ayeni (Eds.), *Valorization of Biomass to Value-Added Commodities* (1st ed., pp. 163–192). Springer. https://doi.org/https://doi.org/10.1007/978-3-030-38032-8_9

Chowdhury, Z. Z., & Hamid, S. B. A. (2016). Preparation and characterization of nanocrystalline cellulose using ultrasonication combined with a microwave-assisted pretreatment process. *BioResources*, *11*(2), 3397–3415. https://doi.org/10.15376/biores.11.2.3397-3415

Cintrón, M. S., & Hinchliffe, D. J. (2015). FT-IR examination of the development of secondary cell wall in cotton fibers. *Fibers*, *3*(1), 30–40. https://doi.org/10.3390/fib3010030

Costa, L. A. S., Assis, D. D. J., Gomes, G. V. P., Da Silva, J. B. A., Fonsêca, A. F., & Druzian, J. I. (2015). Extraction and Characterization of Nanocellulose from Corn Stover. *Materials Today: Proceedings*, *2*(1), 287–294. https://doi.org/10.1016/j.matpr.2015.04.045

De Gisi, S., Lofrano, G., Grassi, M., & Notarnicola, M. (2016). Characteristics and adsorption capacities of low-cost sorbents for wastewater treatment: A review. *Sustainable Materials and Technologies*, *9*, 10–40. https://doi.org/10.1016/j.susmat.2016.06.002

Deschamps, G., Caruel, H., Borredon, M. E., Bonnin, C., & Vignoles, C. (2003). Oil Removal from Water by Selective Sorption on Hydrophobic Cotton Fibers. 1. Study of Sorption Properties and Comparison with Other Cotton Fiber-Based Sorbents. *Environmental Science and Technology*, *37*(5), 1013–1015. https://doi.org/10.1021/es020061s

Dufresne, A. (2012). *Nanocellulose - From Nature to High Performance Tailored Materials* (1st ed.). Germany: Die Gruyter.

Egüés, I., Stepan, A. M., Eceiza, A., Toriz, G., Gatenholm, P., & Labidi, J. (2014). Corncob arabinoxylan for new materials. *Carbohydrate Polymers*, *102*(1), 12–20. https://doi.org/10.1016/j.carbpol.2013.11.011

El-gawad, H. S. A. (2014). Oil and Grease Removal from Industrial Wastewater Using New Utility Approach. *Advances in Environmental Chemistry*, *2014*, 1–6. Retrieved from https://doi.org/10.1155/2014/916878

Ermeng, L., Wuyang, X., Mingxiao, T., & Yuewu, P. (2017). Preparation of an Efficient Oil-Spill Adsorbent Based on Wheat Straw. *BioResources*, *12*(1), 296–315.

Espinosa, E., Sánchez, R., Otero, R., Domínguez-Robles, J., & Rodríguez, A. (2017). A comparative study of the suitability of different cereal straws for lignocellulose nanofibers isolation. *International Journal of Biological Macromolecules*, *103*, 990–999. https://doi.org/10.1016/j.ijbiomac.2017.05.156

Faik, A. (2013). Plant Cell Wall Structure-Pretreatment. The Critical Relationship in Biomass Conversion to Fermentable Sugars. In T. Gu (Ed.), *Green Biomass Pretreatment for Biodfuels* (pp. 1–30). Springer.

Fan, X., Li, M., Zhang, J., Tang, P., & Yuan, Q. (2014). Optimization of SO2-catalyzed hydrolysis of corncob for xylose and xylitol production. *Journal of Chemical Technology and Biotechnology*, *89*(11), 1720–1726. https://doi.org/10.1002/jctb.4250

Farhat, W., Venditti, R., Quick, A., Taha, M., Mignard, N., Becquart, F., & Ayoub, A. (2017). Hemicellulose extraction and characterization for applications in paper coatings and adhesives. *Industrial Crops and Products*, *107*, 370–377. https://doi.org/10.1016/j.indcrop.2017.05.055

Feng, J., Nguyen, S. T., Fan, Z., & Duong, H. M. (2015). Advanced fabrication and oil absorption properties of super-hydrophobic recycled cellulose aerogels. *Chemical Engineering Journal*, *270*, 168–175. https://doi.org/10.1016/j.cej.2015.02.034

Gaballah, I., Goy, D., Allain, E., Kilbertus, G., & Thauront, J. (1997). Recovery of Copper through Decontamination of Synthetic Solutions Using Modified Barks. *Metallurgical and Materials Transactions B*, *28B*(1), 13–23. https://doi.org/10.1007/s11663-997-0122-3

Halal, S. L. M. E., Colussi, R., Pinto, V. Z., Bartz, J., Radunz, M., Carreño, N. L. V, … Zavareze, E. D. R. (2015). Structure, morphology and functionality of acetylated and oxidised barley starches. *Food Chemistry*, *168*, 247–256. https://doi.org/10.1016/j.foodchem.2014.07.046

Hames, B., Ruiz, R., Scarlata, C., Sluiter, A., Sluiter, J., & Templeton, D. (2008). NREL/TP-510-42620 Technical Report: Preparation of Samples for Compositional Analysis. Retrieved from https://www.nrel.gov/docs/gen/fy08/42620.pdf

Hamid, S. B. A., Chowdhury, Z. Z., & Karim, Z. (2014). Catalytic extraction of microcrystalline cellulose (MCC) from Elaeis guineensis using central composite design (CCD). *BioResources*, *9*(4), 7403–7426. https://doi.org/10.15376/biores.9.4.7403-7426

Hatton, F. L., Malmstrom, E., & Carlmark, A. (2015). Tailor-made copolymers for the adsorption to cellulosic surfaces. *European Polymer Journal*, *65*, 325–339. https://doi.org/10.1016/j.eurpolymj.2015.01.026

Ho, Y. S., & McKay, G. (1999). Pseudo-second order model for sorption processes. *Process Biochemistry*, *34*, 451–465.

Hokkanen, S., Bhatnagar, A., & Sillanpää, M. (2016). A review on modification methods to cellulose-based adsorbents to improve adsorption capacity. *Water Research*, *91*, 156–173. https://doi.org/10.1016/j.watres.2016.01.008

Hoşgün, E. Z., & Bozan, B. (2019). Effect of Different Types of Thermochemical Pretreatment on the Enzymatic Hydrolysis and the Composition of Hazelnut Shells. *Waste and Biomass Valorization*, *11*(7), 3739–3748. https://doi.org/10.1007/s12649-019-00711-z

Hospodarova, V., Singovszka, E., & Stevulova, N. (2018). Characterization of Cellulosic Fibers by FTIR Spectroscopy for Their Further Implementation to Building Materials. *American Journal of Analytical Chemistry*, *9*(6), 303–310. https://doi.org/10.4236/ajac.2018.96023

Hossen, M. R., Talbot, M. W., Kennard, R., Bousfield, D. W., & Mason, M. D. (2020). A comparative study of methods for porosity determination of cellulose based porous materials. *Cellulose*, *27*(12), 6849–6860. https://doi.org/10.1007/s10570-020-03257-9

Hromádková, Z., & Ebringerová, A. (1995). Isolation and characterization of hemicelluloses from corn hulls. *Chem Papers*, *49*, 97–101.

Hsieh, Y.-L. (2007). Chemical structure and properties of cotton. In S. Gordon & Y.-L. Hsieh (Eds.), *Cotton: Science and technology* (p. 568). Woodhead Publishing.

Huang, K., Zhang, M., Zhang, G., Jiang, X., & Huang, D. (2014). Acetylation Modification of Rice Straw Fiber and Its Thermal Properties. *Cellulose Chemistry and Technology*, *48*(3–4), 199–207.

Hubbe, M. A., Ayoub, A., Daystar, J. S., Venditti, R. A., & Pawlak, J. J. (2013). Enhanced Absorbent Products Incorporating Cellulose and its Derivatives: A Review. *BioResources*, *8*(4), 6556–6629. https://doi.org/10.15376/biores.8.4.6556-6629

Hubbe, M. A., Rojas, O. J., Fingas, M., & Gupta, B. S. (2013). Cellulosic Substrates for Removal of Pollutants from Aqueous Systems: A review. 3. Spilled Oil and Emulsified Organic Liquids. *BioResources*, *8*(2), 3038–3097. https://doi.org/10.15376/biores.8.2.3038-3097

Hubbe, M. A., Rojas, O. J., & Lucia, L. A. (2015). *Green* Modification of Surface Characteristics of Cellulosic Materials at the Molecular or Nano Scale: A Review. *BioResources*, *10*(3), 6095–6206.

Huntley, C. J., Crews, K. D., & Curry, M. L. (2015). Chemical Functionalization and Characterization of Cellulose Extracted from Wheat Straw using Acid Hydrolysis Methodologies. *International Journal of Polymer Science*, *2015*, 1–9. https://doi.org/10.1155/2015/293981

Ibrahim, M., & Mondal, H. (Eds.). (2019). *Cellulose-Based Superabsorbent Hydrogels*. Springer. https://doi.org/https://doi.org/10.1007/978-3-319-77830-3

Ifelebuegu, A. O., & Johnson, A. (2017). Nonconventional low-cost cellulose- and keratin-based biopolymeric sorbents for oil/water separation and spill cleanup: A review. *Critical Reviews in Environmental Science and Technology*, *47*(11), 964–1001. https://doi.org/10.1080/10643389.2017.1318620

Impola, A. (2017). *Base-catalyzed Reformation of Kraft Lignin for Base-catalyzed Reformation of Kraft Lignin for Carbon Fiber Precursors*. University of Freiburg.

Jawaid, M., Salit, M. S., & Alothman, O. Y. (Eds.). (2017). *Green Biocomposites Design and Applications*. Springer. https://doi.org/10.1007/978-3-319-49382-4

Johnson, R. F., Manjreker, T. G., & Halligan, J. E. (1973). Removal of Oil from Water Surfaces by Sorption on Unstructured Fibers. *Environmental Science & Technology*, *7*(5), 439–443. https://doi.org/10.1021/es60077a003

Junka, K. (2014). *Modification of nanofibrillated cellulose in aqueous media*. Aalto University: School of Chemical Technology.

Kalia, S., Kaith, B. S., & Kaur, I. (2011). *Cellulose Fibers: Bio- and Nano- Polymer Composites, Green Chemistry and Technology*. London: Springer. https://doi.org/10.1007/978-3-642-17370-7

Kalia, S., Thakur, K., Celli, A., Kiechel, M. A., & Schauer, C. L. (2013). Surface modification of plant fibers using environment friendly methods for their application in polymer composites, textile industry and antimicrobial activities: A review. *Journal of Environmental Chemical Engineering*, *1*(3), 97–112. https://doi.org/10.1016/j.jece.2013.04.009

Kapoor, M., Panwar, D., & Kaira, G. S. (2016). Bioprocesses for Enzyme Production Using Agro-Industrial Wastes:

Technical Challenges and Commercialization Potential. In G. S. Dhillon & S. B. T. Kaur (Eds.), *Agro-Industrial Wastes as Feedstock for Enzyme Production* (pp. 61–93). San Diego: Academic Press. https://doi.org/https://doi.org/10.1016/B978-0-12-802392-1.00003-4

Kargarzadeh, H., Mariano, M., Gopakumar, D., Ahmad, I., Thomas, S., Dufresne, A., … Lin, N. (2018). Advances in cellulose nanomaterials. *Cellulose*, *25*(4), 2151–2189. https://doi.org/10.1007/s10570-018-1723-5

Keplinger, T., Wang, X., & Burgert, I. (2019). Nanofibrillated cellulose composites and wood derived scaffolds for functional materials. *Journal of Materials Chemistry A*, *7*(7), 2981–2992. https://doi.org/10.1039/C8TA10711D

Khalil, H. P. S. A., Bhat, A. H., & Yusra, A. F. A. (2012). *Green* composites from sustainable cellulose nanofibrils: A review. *Carbohydrate Polymers*, *87*(2), 963–979. https://doi.org/10.1016/j.carbpol.2011.08.078

Khalil, H. P. S. A., Davoudpour, Y., Islam, M. N., Mustapha, A., Sudesh, K., Dungani, R., & Jawaid, M. (2014). Production and modification of nanofibrillated cellulose using various mechanical processes: A review. *Carbohydrate Polymers*, *99*, 649–665. https://doi.org/10.1016/j.carbpol.2013.08.069

Kim, J. S., Lee, Y. Y., & Kim, T. H. (2016). A review on alkaline pretreatment technology for bioconversion of lignocellulosic biomass. *Bioresource Technology*, *199*, 42–48. https://doi.org/10.1016/j.biortech.2015.08.085

Kim, T. H., & Kim, S. G. (2011). Clinical outcomes of occupational exposure to N,N-dimethylformamide: Perspectives from experimental toxicology. *Safety and Health at Work*, *2*(2), 97–104. https://doi.org/10.5491/SHAW.2011.2.2.97

Korhonen, J. T., Kettunen, M., Ras, R. H. A., & Ikkala, O. (2011). Hydrophobic nanocellulose aerogels as floating, sustainable, reusable, and recyclable oil absorbents. *ACS Applied Materials and Interfaces*, *3*, 1813–1816. https://doi.org/10.1021/am200475b

Koroskenyi, B., & McCarthy, S. P. (2001). Synthesis of acetylated konjac glucomannan and effect of degree of acetylation on water absorbency. *Biomacromolecules*, *2*(3), 824–826. https://doi.org/10.1021/bm010014c

Kumar, A., Negi, Y. S., Choudhary, V., & Bhardwaj, N. K. (2014). Characterization of Cellulose Nanocrystals Produced by Acid-Hydrolysis from Sugarcane Bagasse as Agro-Waste. *Journal of Materials Physics and Chemistry*, *2*(1), 1–8. https://doi.org/10.12691/jmpc-2-1-1

Kumar, P., Barrett, D. M., Delwiche, M. J., & Stroeve, P. (2009). Methods for pretreatment of lignocellulosic biomass for efficient hydrolysis and biofuel production. *Industrial and Engineering Chemistry Research*, *48*(8), 3713–3729. https://doi.org/10.1021/ie801542g

Lavoine, N., Desloges, I., Dufresne, A., & Bras, J. (2012). Microfibrillated cellulose - Its barrier properties and applications in cellulosic materials: A review. *Carbohydrate Polymers*, *90*(2), 735–764. https://doi.org/10.1016/j.carbpol.2012.05.026

Li, J., Zhang, L. P., Peng, F., Bian, J., Yuan, T. Q., Xu, F., & Sun, R. C. (2009). Microwave-assisted solvent-free acetylation of cellulose with acetic anhydride in the presence of iodine as a catalyst. *Molecules*, *14*(9), 3551–3566. https://doi.org/10.3390/molecules14093551

Liu, H., Geng, B., Chen, Y., & Wang, H. (2017). Review on the Aerogel-Type Oil Sorbents Derived from Nanocellulose. *ACS Sustainable Chemistry and Engineering*, *5*(1), 49–66. https://doi.org/10.1021/acssuschemeng.6b02301

Long, L. Y., Weng, Y. X., & Wang, Y. Z. (2018). Cellulose aerogels: Synthesis, applications, and prospects. *Polymers*, *8*(6), 1–28. https://doi.org/10.3390/polym10060623

Lu, Y., Lu, Y. C., Hu, H. Q., Xie, F. J., Wei, X. Y., & Fan, X. (2017). Structural characterization of lignin and its degradation products with spectroscopic methods. *Journal of Spectroscopy*, *2017*, 1–15. https://doi.org/10.1155/2017/8951658

Luzi, F., Puglia, D., Sarasini, F., Tirillò, J., Maffei, G., Zuorro, A., … Torre, L. (2019). Valorization and extraction of cellulose nanocrystals from North African grass: Ampelodesmos mauritanicus. *Carbohydrate Polymers*, *209*, 328–337. https://doi.org/10.1016/j.carbpol.2019.01.048

Ma, L., Du, L., Cui, Y., Song, P., Jiang, F., Ma, Q., & Xiao, D. (2016). Isolation and structural analysis of hemicellulose from corncobs after a delignification pretreatment. *Analytical Methods*, *8*(41), 7500–7506. https://doi.org/10.1039/c6ay01863g

Mahlobo, M. (2008). *Reduction and Monitoring of Fat, Oil and Grease in the Hillcrest Area and the Greater eThekwini Municipality*. Durban. South Africa.

Malvern Instruments Ltd. (2004). Zetasizer Nano Series User Manual. Worcestershire: Malvern Instruments.

Marin, E., & Perry, G. (2015). *Carboxylated Cellulose Nanocrystals Extraction from Kraft Pulp Using Ammonium Persulfate as Low Cost Source & Sustainable Method for High Quality Flexible Packaging Bio-coating*. Lund University.

Matavire, T. O. (2018). *Bran to produce entrapment materials for the controlled release of chemicals and bioactive substances*. Stellenbosch University.

Matthews, J. F., Himmel, M. E., & Crowley, M. F. (2012). Conversion of cellulose Iα to Iβ via a high temperature intermediate (I-HT) and other cellulose phase transformations. *Cellulose*, *19*(1), 297–306. https://doi.org/10.1007/s10570-011-9608-x

McGeer, P. (2016). Medical uses of Sodium thiosulfate. *Journal of Neurology and Neuromedicine*, *1*(3), 28–30. https://doi.org/10.29245/2572.942x/2016/3.1032

Meakin, J. C. (1973). Trace-metal contaminants in filter paper. *Clinical Chemistry*, *19*(1), 141. https://doi.org/10.1093/clinchem/19.1.141

Merck KGa. (2020). 12 Principles of *Green* Chemistry. Retrieved November 8, 2020, from https://www.sigmaaldrich.com/chemistry/*green*er-alternatives/*green*-chemistry.html?gclid=Cj0KCQiAy579BRCPARIsAB6QoIb_GwQ9cEsSd9y3h54MtJvA-s0YjURYGgtVp5ePwi1p3oebFUR5QLoaAnYAEALw_wcB

Minnesota Pollution Control Agency. (2017). *Emulsifiers and Dispersants*. Retrieved from https://www.pca.state.mn.us/sites/default/files/c-er4-06.pdf

Missoum, K., Belgacem, M. N., & Bras, J. (2013). Nanofibrillated cellulose surface modification: A review.

Materials, *6*(5). https://doi.org/10.3390/ma6051745

Montgomery, D. C., & Runger, G. C. (1994). *Applied Statistics and Probability for Engineers*. *European Journal of Engineering Education* (Vol. 19). https://doi.org/10.1080/03043799408928333

Nagarajappa, G. B., Pandey, K. K., Shinde, A. S., & Vagdevi, H. M. (2016). N-Bromosuccinimide (NBS) - An efficient catalyst for acetylation of wood. *Holzforschung*, *70*(5), 421–427. https://doi.org/10.1515/hf-2015-0088

Nam, S., French, A. D., Condon, B. D., & Concha, M. (2016). Segal crystallinity index revisited by the simulation of X-ray diffraction patterns of cotton cellulose Iβ and cellulose II. *Carbohydrate Polymers*, *135*(January 2016), 1–9. https://doi.org/10.1016/j.carbpol.2015.08.035

National Oceanic Atmospheric Administration. (2017). What is eutrophication? National Ocean Service Website. Retrieved October 23, 2019, from https://oceanservice.noaa.gov/facts/eutrophication.html

Nechyporchuk, O. (2015). *Cellulose Nanofibers for the Production of Bionanocomposites*. University of Grenoble Alpes.

Nel, P. (2017). *Performance assessment of cellulose-based biocomposites prepared with natural polymers using 'green' solvents*. Stellenbosch University.

Ngah, W. S. W., & Hanafiah, M. A. K. M. (2008). Removal of heavy metal ions from wastewater by chemically modified plant wastes as adsorbents: A review. *Bioresource Technology*, *99*(10), 3935–3948. https://doi.org/10.1016/j.biortech.2007.06.011

Norrihan, B. S. (2008). *Isolation of Cellulose Fibers from Sugarcane Bagasse and Corn Cob and Preparation of Cellulose Nanocrystals from a Selected Pure Cellulose Source*. University of Malaysia Sarawak.

Nwabueze, H. O., Chiaha, P. N., Ezekannagha, B. C., & Okoani, O. E. (2016). Acetylation of Corn Cobs Using Iodine Catalyst, For Oil Spills Remediation. *The International Journal Of Engineering And Science*, *5*(9), 53–59.

Nwadiogbu, J. O., Ajiwe, V. I. E., & Okoye, P. A. C. (2016). Removal of crude oil from aqueous medium by sorption on hydrophobic corncobs: Equilibrium and kinetic studies. *Journal of Taibah University for Science*, *10*(1), 56–63. https://doi.org/10.1016/j.jtusci.2015.03.014

Nwadiogbu, J. O., Okoye, P. A. C., Ajiwe, V. I., & Nnaji, N. J. N. (2014). Hydrophobic treatment of corn cob by acetylation: Kinetics and thermodynamics studies. *Journal of Environmental Chemical Engineering*, *2*(3), 1699–1704. https://doi.org/10.1016/j.jece.2014.06.003

Nyankson, E., Rodene, D., & Gupta, R. B. (2016). Advancements in Crude Oil Spill Remediation Research after the Deepwater Horizon Oil Spill. *Water, Air, and Soil Pollution*, *227*(1). https://doi.org/10.1007/s11270-015-2727-5

Oniosun, S., Harbottle, M., Tripathy, S., & Cleall, P. (2019). Plant growth, root distribution and non-aqueous phase liquid phytoremediation at the pore-scale. *Journal of Environmental Management*, *249*(December 2018), 109378. https://doi.org/10.1016/j.jenvman.2019.109378

Onwuka, J. C., Agbaji, E. B., Ajibola, V., & Okibe, F. G. (2019). Thermodynamic pathway of lignocellulosic acetylation process. *BMC Chemistry*, *13*(1), 1–11. https://doi.org/10.1186/s13065-019-0593-8

Opstad, K., & Guénette, C. (2000). Fire on the sea surface, ignitability and sustainahility under various environmental conditions. In *Fire Safety Science* (pp. 741–752). https://doi.org/10.3801/IAFSS.FSS.6-741

Oun, A. A., & Rhim, J. W. (2016). Characterization of nanocelluloses isolated from Ushar (Calotropis procera) seed fiber: Effect of isolation method. *Materials Letters*, *168*, 146–150. https://doi.org/10.1016/j.matlet.2016.01.052

Pasha, I., Saeed, F., Waqas, K., Anjum, F. M., & Arshad, M. U. (2013). Nutraceutical and Functional Scenario of Wheat Straw. *Critical Reviews in Food Science and Nutrition*, *53*(3), 287–295. https://doi.org/10.1080/10408398.2010.528080

Peres de Paula, M., Lacerda, T. M., & Frollini, E. (2008). Sisal cellulose acetates obtained from heterogeneous reactions. *Express Polymer Letters*, *2*(6), 423–428. https://doi.org/10.3144/expresspolymlett.2008.51

Pirbazari, E. A. (2015). Surfactant-Modified Wheat Straw: Preparation, Characterization and its Application for Methylene Blue Adsorption from Aqueous Solution. *Journal of Chemical Engineering & Process Technology*, *6*(3). https://doi.org/10.4172/2157-7048.1000231

Potgieter, J. G. (2011). *Utilisation of Agricultural Residue in the Greater Gariep Agricultural Area as a Renewable Energy Resource*. Stellenbosch University.

Pruitt, S. (2017). United States Environmental Protection Agency. Retrieved June 8, 2017, from https://www.epa.gov/emergency-response/sorbents

Qian, Z., Wang, Z., Zhao, N., & Xu, J. (2018). Aerogels Derived from Polymer Nanofibers and Their Applications. *Macromolecular Rapid Communications*, *39*(14), 1–16. https://doi.org/10.1002/marc.201700724

Rabetafika, H. N., Bchir, B., Blecker, C., Paquot, M., & Wathelet, B. (2014). Comparative study of alkaline extraction process of hemicelluloses from pear pomace. *Biomass and Bioenergy*, *61*, 254–264. https://doi.org/10.1016/j.biombioe.2013.12.022

Reddy, K. O., Maheswari, C. U., Muzenda, E., Shukla, M., & Rajulu, A. V. (2016). Extraction and Characterization of Cellulose from Pretreated Ficus (Peepal Tree) Leaf Fibers. *Journal of Natural Fibers*, *13*(1), 54–64. https://doi.org/10.1080/15440478.2014.984055

Rehman, M. S. U., Kim, I., Chisti, Y., & Han, J. I. (2013). Use of ultrasound in the production of bioethanol from lignocellulosic biomass. *Energy Education Science and Technology*, *30*(2), 1391–1410.

Renuka, S., Rengasamy, R., & Das, D. (2016). Studies on needle-punched natural and polypropylene fiber nonwovens as oil sorbents. *Journal of Industrial Textiles*, *46*(4), 1121–1143. https://doi.org/10.1177/1528083715613630

Riva, G. H., García-estrada, J., Vega, B., López-dellamary, F., Hérnandez, M. E., & Silva, J. A. (2015). Cellulose-Chitosan Nanocomposites - Evaluation of Physical, Mechanical and Biological Properties. In *Cellulose - Fundamental Aspects and Current Trends*. Intech.

Robati, D. (2013). Pseudo-second-order kinetic equations for modeling adsorption systems for removal of lead ions using multi-walled carbon nanotube. *Journal Of Nanostructure in Chemistry*, *3*(55). https://doi.org/10.1080/1536383x.2013.787610

Rosa, S. M. L., Rehman, N., De Miranda, M. I. G., Nachtigall, S. M. B., & Bica, C. I. D. (2012). Chlorine-free extraction of cellulose from rice husk and whisker isolation. *Carbohydrate Polymers*, *87*(2), 1131–1138. https://doi.org/10.1016/j.carbpol.2011.08.084

Rowell, R. M. (2014). Acetylation of wood - A review. *International Journal of Lignocellulosic Products*, *1*(1), 1–27. https://doi.org/10.1021/bk-2014-1158.ch018

Rowell, R. M., Pettersen, R., & Tshabalala, M. (2012). Cell Wall Chemistry. In *Handbook of Wood Chemistry and Wood Composites* (2nd ed., pp. 33–72). https://doi.org/10.1201/b12487-5

Rowell, R. M., Simonson, R., Hess, S., Plackett, D., Cronshaw, D., & Dunningham, E. (1994). Acetyl distribution in acetylated whole wood and reactivity of isolated wood cell-wall components to acetic anhydride. *Wood and Fiber Science*, *26*(1), 11–18.

Salajkova, M. (2013). *Wood Nanocellulose Materials and Effects from Surface Modification of Nanoparticles*. KTH Royal Institute of Technology: School of Chemical Science and Engineering. Stockholm.

Scatolino, M. V, Silva, D. W., Mendes, R. F., & Mendes, L. M. (2013). Use of maize cob for production of particleboard. *Ciencia e Agrotecnologia*, *37*(4), 330–337. https://doi.org/10.1590/S1413-70542013000400006

Schmidt, A. A., Tenkanen, M., Thomsen, A. B., & Woidemann, A. (1998). *Hydrolysis of solubilized hemicellulose derived from wet-oxidized wheat straw by a mixture of commercial fungal enzyme preparations*.

Schwietzke, S., Kim, Y., Ximenes, E., Mosier, N., & Ladisch, M. (2009). Ethanol Production from Maize. In A. L. Kriz & B. A. Lardiks (Eds.), *Molecular Genetic Approaches to Maize Improvement* (pp. 173–195). Springer-Verlag. https://doi.org/10.1007/978-3-540-68922-5

Shamsabadi, M. A., Behzad, T., & Bagheri, R. (2015). Optimization of acid hydrolysis conditions to improve cellulose nanofibers extraction from wheat straw. *Fibers and Polymers*, *16*(3), 579–584. https://doi.org/10.1007/s12221-015-0579-7

She, D., Sun, R. C., & Jones, G. L. (2010). Chemical Modification of Straw as Novel Materials for Industries. In *Cereal Straw as a Resource for Sustainable Biomaterials and Biofuels* (1st ed., pp. 209–217). Elsevier. https://doi.org/10.1016/B978-0-444-53234-3.00007-9

Sigma-Aldrich. (2020). Amano Lipase A from Aspergillus niger. Retrieved November 1, 2020, from https://www.sigmaaldrich.com/catalog/product/aldrich/534781?lang=en&region=ZA

Smole, M. S., Hribernik, S., Kleinschek, K. S., & Kreze, T. (2012). Plant Fibres for Textile and Technical Applications. In S. Grundas & A. Stepniewski (Eds.), *Advances in Agrophysical Research*. IntechOpen. https://doi.org/http://dx.doi.org/10.5772/52372

Spinella, S., Maiorana, A., Qian, Q., Dawson, N. J., Hepworth, V., McCallum, S. A., … Gross, R. A. (2016). Concurrent Cellulose Hydrolysis and Esterification to Prepare a Surface-Modified Cellulose Nanocrystal Decorated with Carboxylic Acid Moieties. *ACS Sustainable Chemistry and Engineering*, *4*(3), 1538–1550. https://doi.org/10.1021/acssuschemeng.5b01489

Sun, J. X., Sun, X. F., Zhao, H., & Sun, R. C. (2004). Isolation and characterization of cellulose from sugarcane

bagasse. *Polymer Degradation and Stability*, *84*(2), 331–339. https://doi.org/10.1016/j.polymdegradstab.2004.02.008

Sun, R. C. (2010). *Cereal Straw as a Resource for Sustainable Biomaterials and Biofuels* (1st ed.). Elsevier.

Sun, R. C., Lawther, J. M., & Banks, W. B. (1996). Fractional and structural characterization of wheat straw hemicelluloses. *Carbohydrate Polymers*, *29*(4), 325–331. https://doi.org/10.1016/S0144-8617(96)00018-5

Sun, X. F., Sun, R. C., Fowler, P., & Baird, M. S. (2005). Extraction and characterization of original lignin and hemicelluloses from wheat straw. *Journal of Agricultural and Food Chemistry*, *53*(4), 860–870. https://doi.org/10.1021/jf040456q

Sun, X. F., Sun, R. C., & Sun, J. X. (2002). Acetylation of Rice Straw with or without Catalysts and Its Characterization as a Natural Sorbent in Oil Spill Cleanup. *Journal of Agricultural and Food Chemistry*, *50*(22). https://doi.org/10.1021/jf020392o

Sun, X. F., Sun, R. C., & Sun, J. X. (2004). Acetylation of sugarcane bagasse using NBS as a catalyst under mild reaction conditions for the production of oil sorption-active materials. *Bioresource Technology*, *95*(3), 343–350. https://doi.org/10.1016/j.biortech.2004.02.025

Tabil, L., Adapa, P., & Kashaninejad, M. (2011). Biomass Feedstock Pre-Processing – Part 1: Pre-Treatment. In *Biofuel's Engineering Process Technology* (p. 742). Intech. https://doi.org/10.5772/52807

Tarrés, Q., Oliver-Ortega, H., Llop, M., Pèlach, M. À., Delgado-Aguilar, M., & Mutjé, P. (2016). Effective and simple methodology to produce nanocellulose-based aerogels for selective oil removal. *Cellulose*, *23*(5), 3077–3088. https://doi.org/10.1007/s10570-016-1017-8

Teixeira, E. D. M., Corrêa, A. C., Manzoli, A., Leite, F. D. L., Oliveira, C. D. R., & Mattoso, L. H. C. (2010). Cellulose nanofibers from white and naturally colored cotton fibers. *Cellulose*, *17*(3), 595–606. https://doi.org/10.1007/s10570-010-9403-0

Teli, M. D., & Valia, S. P. (2013a). Acetylation of banana fibre to improve oil absorbency. *Carbohydrate Polymers*, *92*(1), 328–333. https://doi.org/10.1016/j.carbpol.2012.09.019

Teli, M. D., & Valia, S. P. (2013b). Acetylation of jute fiber to improve oil absorbency. *Fibers and Polymers*, *14*(6), 915–919. https://doi.org/10.1007/s12221-013-0915-8

Thakur, V. K. (Ed.). (2013). *Green Composites from Natural Resources*. CRC Press.

Tijani, M. M., Aqsha, A., & Mahinpey, N. (2016). Development of oil-spill sorbent from straw biomass waste: Experiments and modeling studies. *Journal of Environmental Management*, *171*, 166–176. https://doi.org/10.1016/j.jenvman.2016.02.010

Tingaut, P., Zimmermann, T., & Lopez-Suevos, F. (2009). Synthesis and Characterization of Bionanocomposites with Tunable Properties from Poly(lactic acid) and Acetylated Microfibrillated Cellulose. *Biomacromolecules*, *11*(2), 454–464.

Tozluoğlu, A., Özyurek, Ö., Çöpür, Y., & Özdemir, H. (2015). Integrated Production of Biofilm, Bioethanol, and Papermaking Pulp from Wheat Straw. *BioResources*, *10*(4). https://doi.org/10.15376/biores.10.4.7834-7853

Trimukhe, K. D., Mahadik, N. D., Gokhale, D. V, & Varma, A. J. (2008). Environment friendly crosslinked chitosan as a matrix for selective adsorption and purification of lipase of Aspergillus niger. *International Journal of Biological Macromolecules*, *43*(5), 422–425. https://doi.org/10.1016/j.ijbiomac.2008.08.005

Tupa, M. V., Ramírez, J. A. Á., Vázquez, A., & Foresti, M. L. (2015). Organocatalytic acetylation of starch: Effect of reaction conditions on DS and characterisation of esterified granules. *Food Chemistry*, *170*, 295–302. https://doi.org/10.1016/j.foodchem.2014.08.062

Tywabi, Z. (2015). *Processing of Dissolving Pulp in Ionic Liquids*. Durban University of Technology. South Africa.

U.S. National Library of Medicine. (2004). Calcium Carbonate Compound Summary. Retrieved June 9, 2020, from https://pubchem.ncbi.nlm.nih.gov/compound/Calcium-carbonate

U.S. National Library of Medicine. (2005a). Acetic Anhydride Compound Summary. Retrieved October 31, 2019, from https://pubchem.ncbi.nlm.nih.gov/compound/7918#section=Information-Sources

U.S. National Library of Medicine. (2005b). N-Bromosuccinimide Compound Summary. Retrieved October 31, 2019, from https://pubchem.ncbi.nlm.nih.gov/compound/N-Bromosuccinimide

University of Maine. (2020). Cellulose Nanofibers (CNF) Product Specification. Retrieved March 7, 2020, from https://umaine.edu/pdc/wp-content/uploads/sites/398/2016/03/Specs-CNF.pdf

Vázquez, G. B., Leos, A. G., Rodríguez-Duran, L. V, & de Los Santos, R. T. (2020). Characterization of Lignocellulosic Biomass and Processing for Second-Generation Sugars Production. In A. P. Ingle, A. K. Chandel, & S. S. da Silva (Eds.), *Lignocellulosic Biorefining Technologies* (1st ed., pp. 29–46). Wiley.

Vignes, R. (2000). Dimethyl Sulfoxide (DMSO) - A “New” Clean, Unique, Superior Solvent. *American Chemical Society*.

Wahi, R., Chuah, L. A., Choong, T. S. Y., Ngaini, Z., & Nourouzi, M. M. (2013). Oil removal from aqueous state by natural fibrous sorbent: An overview. *Separation and Purification Technology*, *113*, 51–63. https://doi.org/10.1016/j.seppur.2013.04.015

Wang, J., Geng, G., Wang, A., Liu, X., Du, J., Zou, Z., … Han, F. (2015). Double biomimetic fabrication of robustly superhydrophobic cotton fiber and its application in oil spill cleanup. *Industrial Crops and Products*, *77*, 36–43. https://doi.org/10.1016/j.indcrop.2015.08.044

Wang, J., Zheng, Y., & Wang, A. (2012). Effect of kapok fiber treated with various solvents on oil absorbency. *Industrial Crops and Products*, *40*(1), 178–184. https://doi.org/10.1016/j.indcrop.2012.03.002

Wang, J., Zheng, Y., & Wang, A. (2013). Coated kapok fiber for removal of spilled oil. *Marine Pollution Bulletin*, *69*(1–2), 91–96. https://doi.org/10.1016/j.marpolbul.2013.01.007

Wang, S.-Y. (2004). *Molecular iodine*. *Synlett Spotlight 103*. https://doi.org/10.1055/s-2004-834833

Wang, S., Qin, W., & Dai, Y. (2012). Separation of oil phase from dilute oil/water emulsion in confined space apparatus. *Chinese Journal of Chemical Engineering*, *20*(2), 239–245. https://doi.org/10.1016/S1004-9541(12)60384-X

Wang, Z., Barford, J. P., Hui, C. W., & McKay, G. (2015). Kinetic and equilibrium studies of hydrophilic and

hydrophobic rice husk cellulosic fibers used as oil spill sorbents. *Chemical Engineering Journal*, *281*, 961–969. https://doi.org/10.1016/j.cej.2015.07.002

Wei, Q. F., Mather, R. R., & Fotheringham, A. F. (2005). Oil removal from used sorbents using a biosurfactant. *Bioresource Technology*, *96*(3), 331–334. https://doi.org/10.1016/j.biortech.2004.04.005

Yang, K., & Wang, Y.-J. (2003). Lipase-catalyzed cellulose acetylation in aqueous and organic media. *Biotechnology Progress*, *19*(6), 1664–1671.

Yin, C., Li, J., Xu, Q., Peng, Q., Liu, Y., & Shen, X. (2007). Chemical modification of cotton cellulose in supercritical carbon dioxide: Synthesis and characterization of cellulose carbamate. *Carbohydrate Polymers*, *67*(2), 147–154. https://doi.org/10.1016/j.carbpol.2006.05.010

Yin, T., Zhang, X., Liu, X., & Wang, C. (2017). Resource recovery of Eichhornia crassipes as oil superabsorbent. *Marine Pollution Bulletin*, *118*(2017), 267–274. https://doi.org/10.1016/j.marpolbul.2017.01.064

Yoon, J. H., Seo, H. S., Lee, J., Moon, C., & Lee, K. (2016). Acute high-level toluene exposure decreases hippocampal neurogenesis in rats. *Toxicology and Industrial Health*, *32*(11), 1910–1920. https://doi.org/10.1177/0748233715599087

Zanini, M., Lavoratti, A., Lazzari, L. K., Galiotto, D., Pagnocelli, M., Baldasso, C., & Zattera, A. J. (2017). Producing aerogels from silanized cellulose nanofiber suspension. *Cellulose*, *24*(2), 769–779. https://doi.org/10.1007/s10570-016-1142-4

Zepic, V., Poljansek, I., Oven, P., Skapin, A. S., & Hancic, A. (2015). Effect of Drying Pretreatment on the Acetylation of Nanofibrillated Cellulose. *Bioresources*, *10*(4), 8148–8167.

Zhang, C., Li, M., Liu, G., Luo, H., & Zhang, R. (2009). Pyridine degradation in the microbial fuel cells. *Journal of Hazardous Materials*, *172*(1), 465–471. https://doi.org/10.1016/j.jhazmat.2009.07.027

Zheng, Q., Zhou, T., Wang, Y., Cao, X., Wu, S., Zhao, M., … Guan, X. (2018). Pretreatment of wheat straw leads to structural changes and improved enzymatic hydrolysis. *Scientific Reports*, *8*, 1–9. https://doi.org/10.1038/s41598-018-19517-5

Zhou, S., Liu, P., Wang, M., Zhao, H., Yang, J., & Xu, F. (2016). Sustainable, Reusable, and Superhydrophobic Aerogels from Microfibrillated Cellulose for Highly Effective Oil/Water Separation. *ACS Sustainable Chemistry and Engineering*, *4*(12), 6409–6416. https://doi.org/10.1021/acssuschemeng.6b01075

Appendix A – Reflux Experimental Setup

A.1 Reflux Experimental Setup

The following experimental setup was utilised during cellulose- and nanofibrillated cellulose (NFC) isolation, and for the *green*- and *non-green* modifications of the biomass, cellulose and NFC. This setup consisted of a 250 mL round bottom flask connected to a reflux condenser. The sample was added to the round bottom flask together with a magnetic stirring rod, which was then placed in a glycerol bath equipped with an underplate heater, complete with temperature control and magnetic stirring, as demonstrated in Figure A.1. The cooling in the condenser was achieved with recirculating water. A submersible pump (HJ741, 600 L/h, 8 Watt) was employed for water reticulation. The condenser outlet vapours were scrubbed by passing through distilled water prior to the outlet into the fume hood.

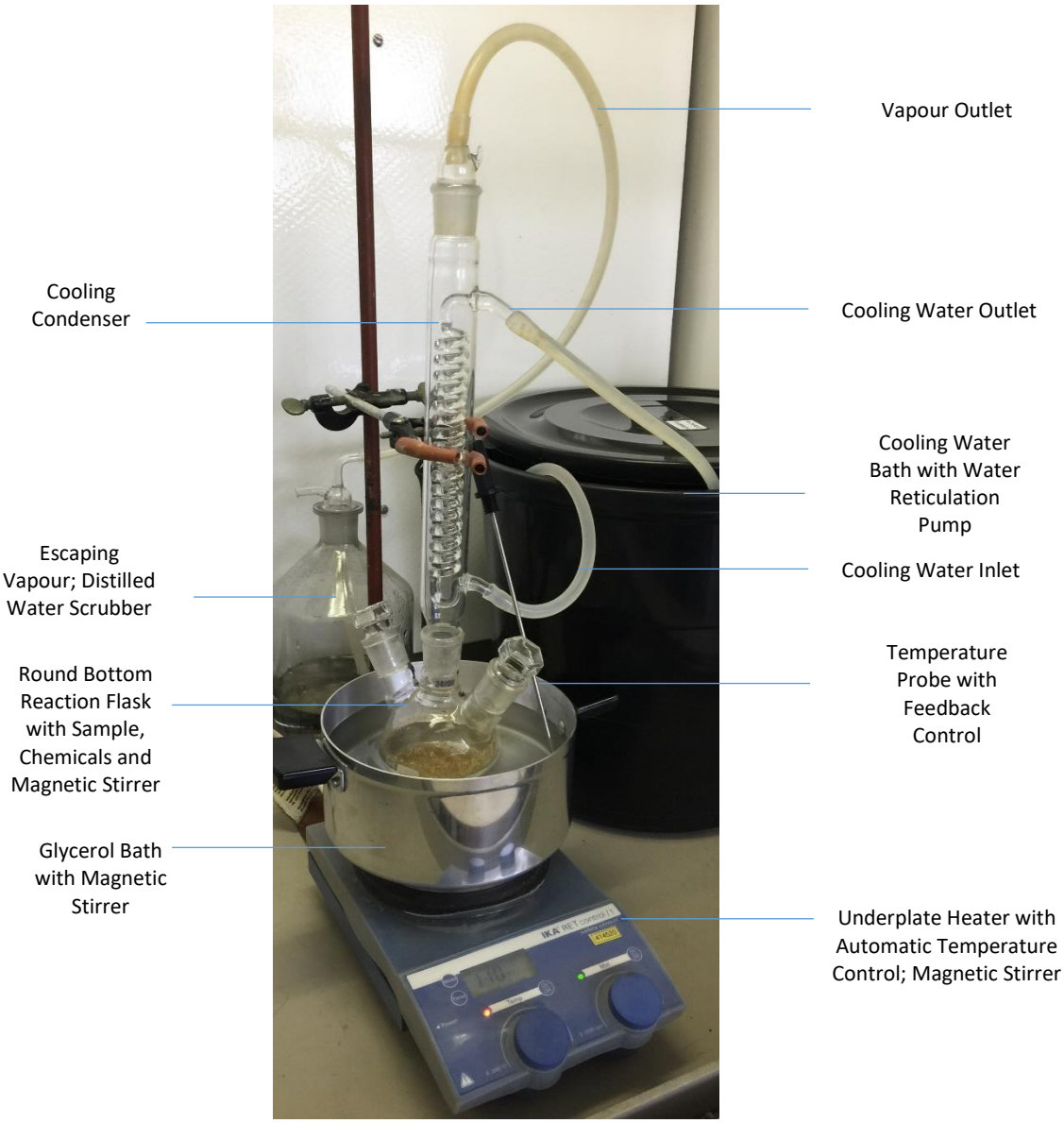

Figure A.1 A Photograph of the Reflux-condenser Experimental Setup

Appendix B – Fourier Transform Infrared Peak Assignments

B.1 Fourier Transform Infrared Spectroscopy Peak Assignments

Table B.1 The Peak Assignment, utilised in Fourier Transform Infrared Spectra Analyses

Wavenumber (cm^{-1})	Peak Assignment	Reference
896	β-glycosidic linkages (C–O bonds in cellulose), representing the amorphous regions	(Hospodarova et al., 2018; Reddy et al., 2016)
985	C–O stretching of arabinose side chains of hemicelluloses	(X. F. Sun et al., 2005)
1 027	–OH in cellulose	(Hospodarova et al., 2018)
1 034	C–O–C stretch of the hydroxyl group of xylan peak for hemicelluloses	(Ceaser, 2019)
1 159	Stretching of the C–O–C glycosidic linkages in cellulose	(Cintrón & Hinchliffe, 2015)
1 234	C–O stretching band of the acetyl group	(Zepic et al., 2015)
1 242	Linkages between hemicelluloses and lignin	(Luzi et al., 2019)
1 310; 1 337	–OH in-plane bending bands	(Zepic et al., 2015)
1 334	–CH in cellulose	(Hospodarova et al., 2018)
1 367	Bending vibrations of $–CH_2$ in cellulose	(Hospodarova et al., 2018)
1 369	C–H band in $–O(C=O)–CH_3$	(Zepic et al., 2015)
1 420 – 1 430	Stretching vibrations of $–CH_2$ in cellulose, representing the crystalline structure	(Hospodarova et al., 2018)
1 530	Amide II band	(Bozic et al., 2015)
1 595	Aromatic ring peak of lignin	(Ceaser, 2019)
1 633	Vibration of water in cellulose	(Hospodarova et al., 2018)
1 650	Amide I band	(Bozic et al., 2015)
1 700	Acetic anhydride	(Zepic et al., 2015)
1 731	Ester linkage of carboxylic group of the phenolic compounds (ferulic and *p*-coumaric acids)	(A. Kumar et al., 2014)
1 740	C=O stretching of the ester	(Zepic et al., 2015)
1 760; 1 840	Acetic acid	(Zepic et al., 2015)
2 919	C–H stretching of hemicelluloses and CH_2 stretching of lignin	(Farhat et al., 2017; Zheng et al., 2018)
3 316	OH-stretching of hemicelluloses	(Buranov & Mazza, 2010)
3 337	OH stretching band	(Hospodarova et al., 2018; Zepic et al., 2015).

Appendix C – The Isolation of Nanofibrillated Cellulose

C.1 Zeta Sizer® Nano-ZS90 Size Analyser Particle Distribution Graphs

A Zeta Sizer® Nano-ZS90 Size Analyser (Malvern) was used to determine the particle diameter distribution achieved after each step in the NFC isolation procedure. The obtained particle diameter distributions are displayed in Figure C.1.

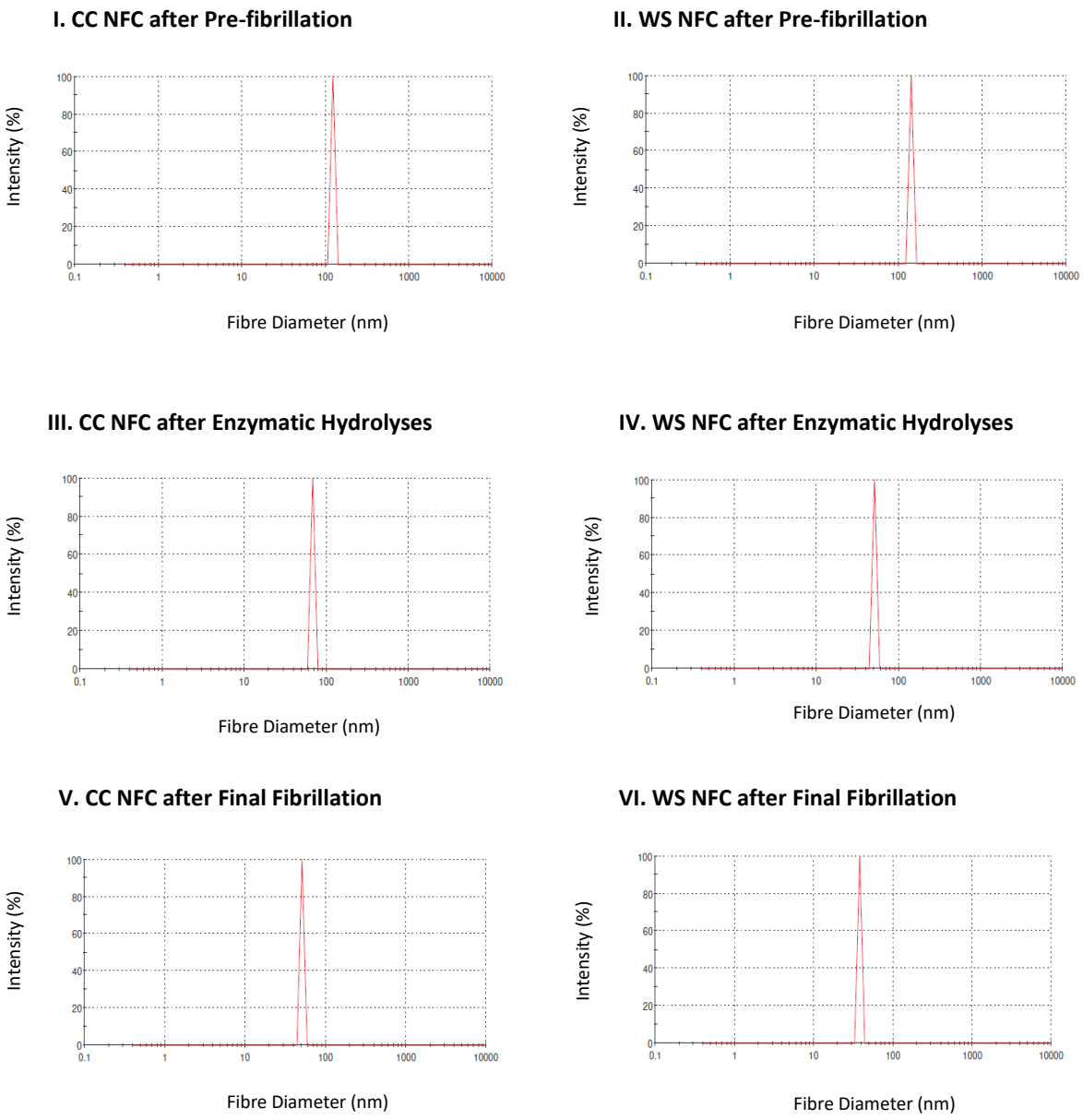

Figure C.1 The Fibre Diameter (nm) Distribution by Intensity (%) achieved by Nanofibrillated Cellulose (NFC) Isolation from Corncob (CC) Cellulose and Wheat Straw (WS) Cellulose, as determined with the Zeta Sizer® Nano-ZS90 Size Analyser

Appendix D – Biomass Sorbents Supplementary Results

D.1 Preliminary Experiments to Establish Scope for Central Composite Design of *Green* Biomass Modification

Preliminary experiments were conducted in order to establish the scope for the temperature, time and catalyst concentration inputs to the central composite design (CCD) of the *green* biomass modification. These preliminary experiments were accomplished with wheat straw (WS) by varying the reaction temperature between 50 and 150 °C, acetylation duration between 2 and 7.5 h and catalyst concentration between 2 and 7.5 % (w/w) iodine, in single-factor experiments. The experimental details of each run are depicted in Table D.1, and the degree of substitution (DS) achieved with each test is indicated.

Table D.1 Experimental Conditions and Degree of Substitution for the Preliminary *Green* Modification of Wheat Straw for the Scope Establishment of the Central Composite Design Matrix

Run ID [a]	Temperature (°C)	Time (h)	Catalyst Concentration [b, c] (%)	DS [d]
WS-B2-0 [e]	n/a	n/a	n/a	n/a
WS-B2-P1	50	2	5	1.04 ± 0.12
WS-B2-P2	100	2	5	1.56 ± 0.03
WS-B2-P3	130	2	5	2.01 ± 0.07
WS-B2-P4	130	2	2	1.50 ± 0.08
WS-B2-P5	130	6	5	2.31 ± 0.03
WS-B2-P6	130	2	7.5	1.55 ± 0.10
WS-B2-P7	150	2	5	1.69 ± 0.08
WS-B2-P8	130	7.5	5	1.85 ± 0.05

a – Run identification for the preliminary modification of wheat straw (WS), where B2 as suffix represents a *green* modification; **b** – Each run performed with a constant acetic anhydride loading of 25:1 (25 mL acetic anhydride to 1 g biomass); **c** – Target iodine as a weight percentage of biomass; **d** – Degree of Substitution abbreviated as DS; **e** – Unmodified WS sample for reference

Figure D.1 demonstrates the DS and Fourier Transform Infrared (FT-IR) spectra of each preliminary run. The runs WS-B2-P1, WS-B2-P2, WS-B2-P3 and WS-B2-P4 (Figure D.1 I) were utilised to study the effect of temperature at a constant time (2 h) and constant catalyst concentration (5 % (w/w) iodine). The FT-IR in Figure D.1 II illustrates intensifying ester peak intensities (1 740 cm^{-1}, 1 369 cm^{-1} and 1 234 cm^{-1}) when increasing the temperature from 50 °C to 100 °C and 130 °C. Analogously, a significant increase in DS occurred when elevating the reaction temperature from 50 °C to 100 °C ($p = 1.40 \times 10^{-4}$) and 100 °C to 130 °C ($p = 2.24 \times 10^{-5}$). A further escalation to 150 °C transpired in lowered ester peaks and a significantly reduced DS ($p = 6.90 \times 10^{-4}$). In order to study the interactions between temperature, time and catalyst concentration, a temperature range of 50 °C to 150 °C (with $\alpha = 2^{3/4}$) was selected for the CCD.

I. Effect of Temperature on DS

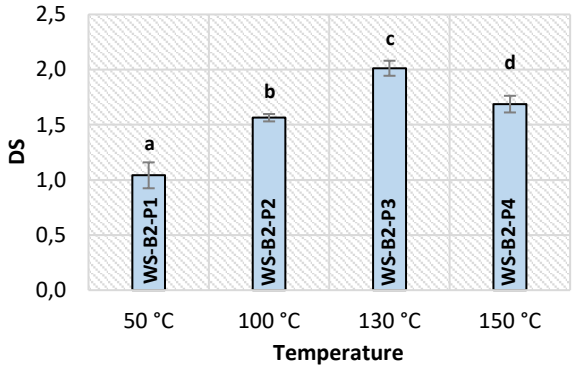

III. Effect of Time on DS

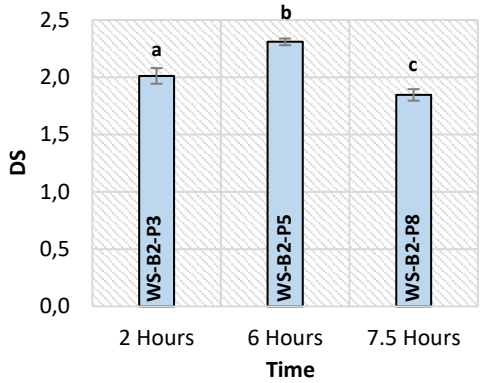

V. Effect of Catalyst Concentration on DS

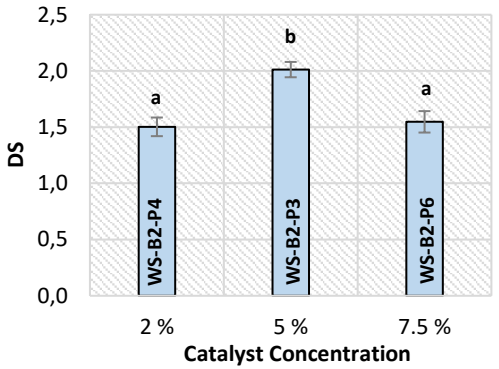

II. Effect of Temperature on FT-IR Peaks

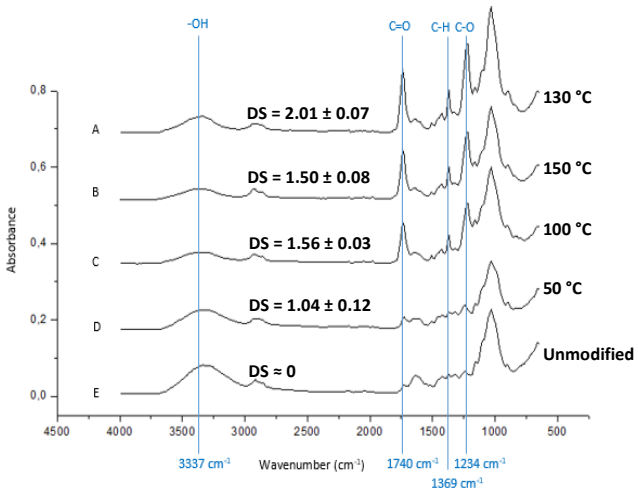

IV. Effect of Time on FT-IR Peaks

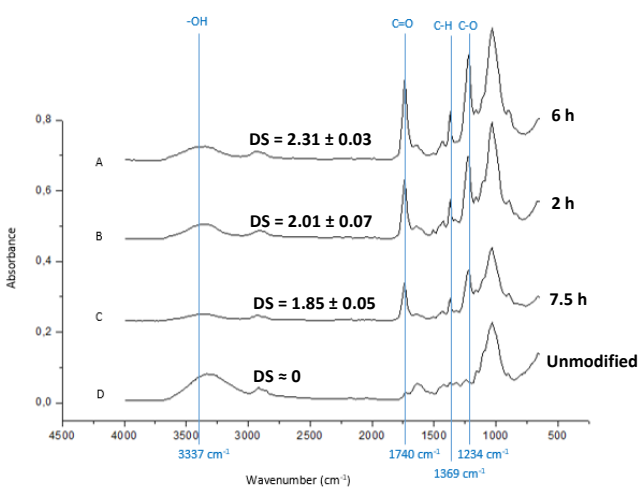

VI. Effect of Catalyst Concentration on FT-IR Peaks

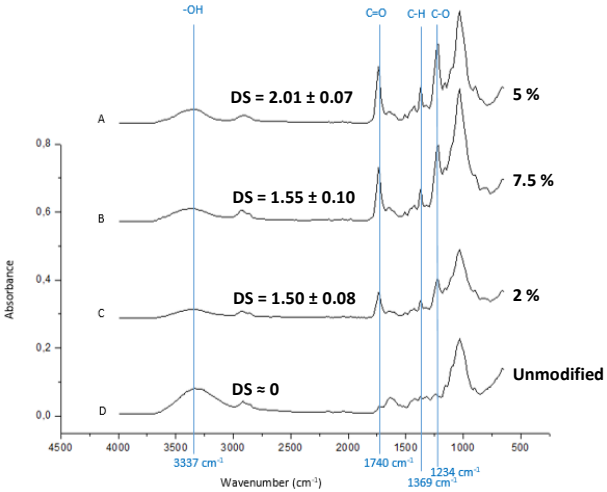

Figure D.1 The Effects of Temperature, Time and Catalyst Concentration on the Degree of Substitution (DS) and Fourier Transform Infrared (FT-IR) Spectra of the Preliminary *Green* Acetylated Wheat Straw at **I., II.** Constant Time and Catalyst Concentration (2 h, 5 % (w/w) Iodine); **III., IV.** Constant Temperature and Catalyst Concentration (130 °C, 5 % (w/w) Iodine); **V., VI.** Constant Temperature and Reaction Time (130 °C, 2 h)

The experiments WS-B2-P3, WS-B2-P5 and WS-B2-P8 (Figure D.1 III) were employed to study the effect of time at a constant temperature (130 °C) and constant catalyst concentration (5 % (w/w) iodine). A statistically significant increase in DS ($p = 2.00 \times 10^{-4}$) was perceived when increasing the reaction time from 2 to 6 h, which was also signified by higher acetylation peaks (Figure D.1 IV). The DS at 7.5 h was significantly decreased ($p = 3.94 \times 10^{-6}$). In order to study the interactions between input parameters, a time range of 0.6 to 7.4 h was selected for the CCD. This time range ensured the alpha values of $\alpha = 2^{3/4}$ to maintain the statistical rotatability of the experimental design.

Lastly, WS-B2-P3, WS-B2-P4 and WS-B2-P6 (Figure D.1 V) were implemented to establish the scope for catalyst concentration at a constant time (2 h) and constant temperature (130 °C). A statistically significant increase in DS ($p = 7.81 \times 10^{-5}$) and ester peak intensities (Figure D.1 VI) occurred when escalating the iodine concentration from 2 to 5 % (w/w). Although it is difficult to discern between the ester peak intensities at 5 % (w/w) and 7.5 % (w/w), a significantly higher DS was reached at 5 % (w/w) iodine ($p = 2.12 \times 10^{-4}$). A testing range of 0.6 to 7.4 % (w/w) iodine was therefore implemented for the CCD (with $\alpha = 2^{3/4}$).

The scope for the CCD is summarised as per Table D.2 and applied to CC and WS for optimisation.

Table D.2 Independent Variables Applied During the *Green* Modification of Wheat Straw and Corncob

Factor	Symbol	Range	Coded Levels				
			-α	**-1**	**0**	**1**	**α**
Temperature	X_1	50 – 150 °C	50	70	100	130	150
Time	X_2	0.6 – 7.4 h	0.6	2	4	6	7.4
Catalyst Concentration [a]	X_3	0.6 – 7.4 % (w/w)	0.6	2	4	6	7.4

a – Target iodine catalyst as a weight percentage of biomass

D.2 Validation of Models determined by Central Composite Design of the *Green* Biomass Modification of Corncob and Wheat Straw

The polynomial models predicted by Statistica 13.2 are presented in Table D.3. The degree of substitution (DS) and oil sorption (OS) were implemented as response variables.

Table D.3 The Mathematical Models, Developed to Describe the Response of Degree of Substitution and Oil Sorption to the Input Parameters – Temperature, Time, and Catalyst Concentration, for the *Green* Surface Modification of Corncob and Wheat Straw

Biomass [a]	Mathematical Model [b, c]	Equation
CC	$Y_1 = (-2.75078) + (0.05014)X_1 + (0.23577)X_2 + (0.24658)X_3 + (-0.00018)X_1^2 + (-0.02650)X_2^2 + (-0.01164)X_3^2 + (0.00081)X_1X_2 + (-0.00131)X_1X_3 + (-0.01537)X_2X_3$	[D.1]
	$Y_2 = (-27.1737) + (0.4713)X_1 + (1.8204)X_2 + (3.0979)X_3 + (-0.0017)X_1^2 + (-0.1957)X_2^2 + (-0.1870)X_3^2 + (0.0032)X_1X_2 + (-0.0130)X_1X_3 + (-0.1070)X_2X_3$	[D.2]
WS	$Y_1 = (-0.755423) + (0.037821)X_1 + (-0.022567)X_2 + (0.078398)X_3 + (-0.000171)X_1^2 + (-0.024136)X_2^2 + (-0.021383)X_3^2 + (0.001619)X_1X_2 + (-0.000022)X_1X_3 + (0.025023)X_2X_3$	[D.3]
	$Y_2 = (-10.9324) + (0.3738)X_1 + (-0.2611)X_2 + (1.5416)X_3 + (-0.0017)X_1^2 + (-0.2654)X_2^2 + (-0.2491)X_3^2 + (0.0186)X_1X_2 + (-0.0027)X_1X_3 + (0.1987)X_2X_3$	[D.4]

a – Corncob is abbreviated as CC, while wheat straw is abbreviated as WS; **b –** Temperature (X_1), Time (X_2) and Catalyst Concentration (X_3) as input variables; **c –** Degree of Substitution (Y_1) and Oil Sorption (Y_2) as model responses

ANOVA analyses (Table D.4 and Table D.5) were applied to the developed models to determine the regression coefficients and analyse the statistical fit to the experimental data. These analyses indicated a regression coefficient of $R^2 = 0.7004$ for the model predicting DS of CC (Equation D.1) and $R^2 = 0.6492$ for the model predicting OS of CC (Equation D.2). Additionally, $R^2 = 0.7684$ was accomplished for the model predicting DS of WS (Equation D.3) and $R^2 = 0.6998$ for the model predicting OS of WS (Equation D.4). Even though low regression coefficients were achieved, the models held an insignificant *Lack of Fit* (Table D.4 and Table D.5), indicating that the DS and OS can be accurately predicted by the developed models for both CC and WS.

Table D.4 and Table D.5 furthermore indicated that the linear and quadratic effects of temperature and time had statistically significant effects ($p < 0.05$) on the DS and OS of CC and WS. In contrast, the rest of the effects were negligible ($p > 0.05$).

Table D.4 The ANOVA Analyses of the Polynomial Models of Corncob with Degree of Substitution and Oil Sorption as Response Variables

Factor [a, b]	Degrees of Freedom	Sum of Squares	Mean Square	F-value	p	Statistical Significance
Model Predicting DS (Equation D.1; R^2 = 0.7004)						
X_1 (Temperature)	1	1.6705	1.6705	46.31	2.44×10^{-3}	Significant
X_1^2	1	0.3677	0.3677	10.19	3.31×10^{-2}	Significant
X_2 (Time)	1	0.1022	0.1022	2.83	0.17	Insignificant
X_2^2	1	0.1534	0.1534	4.25	0.11	Insignificant
X_3 (Catalyst Conc.)	1	0.0839	0.0839	2.33	0.20	Insignificant
X_3^2	1	0.0296	0.0296	0.82	0.42	Insignificant
X_1X_2	1	0.0189	0.0189	0.52	0.51	Insignificant
X_1X_3	1	0.0495	0.0495	1.37	0.31	Insignificant
X_2X_3	1	0.0302	0.0302	0.84	0.41	Insignificant
Lack of Fit	5	0.8904	0.1781	4.94	0.07	Insignificant
Pure Error	4	0.1443	0.0361	-	-	-
Total Sum of Squares	18	3.4533	-	-	-	-
Model Predicting OS (Equation D.2; R^2 = 0.6492)						
X_1 (Temperature)	1	97.3252	97.3252	34.33	4.24×10^{-3}	Significant
X_1^2	1	32.5798	32.5798	11.49	2.75×10^{-2}	Significant
X_2 (Time)	1	1.1785	1.1785	0.42	0.55	Insignificant
X_2^2	1	8.3672	8.3672	2.95	0.16	Insignificant
X_3 (Catalyst Conc.)	1	0.8032	0.8032	0.28	0.62	Insignificant
X_3^2	1	7.6350	7.6350	2.69	0.18	Insignificant
X_1X_2	1	0.2960	0.2960	0.10	0.76	Insignificant
X_1X_3	1	4.8312	4.8312	1.70	0.26	Insignificant
X_2X_3	1	1.4668	1.4668	0.52	0.51	Insignificant
Lack of Fit	5	67.3863	13.4773	4.75	0.08	Insignificant
Pure Error	4	11.3415	2.8354	-	-	-
Total Sum of Squares	18	224.3914	-	-	-	-

a – Temperature (X_1), Time (X_2) and Catalyst Concentration (X_3) as input variables; **b** – Degree of substitution is abbreviated as DS, and oil sorption is abbreviated as OS

Table D.5 The ANOVA Analyses of the Polynomial Models of Wheat Straw with Degree of Substitution and Oil Sorption as Response Variables

Factor [a]	Degrees of Freedom	Sum of Squares	Mean Square	F-value	p	Statistical Significance
Model Predicting DS (Equation D.3; R^2 = 0.7684)						
X_1 (Temperature)	1	1.2438	1.2438	58.16	1.59×10^{-3}	Significant
X_1^2	1	0.3224	0.3224	15.08	0.02	Significant
X_2 (Time)	1	0.1173	0.1173	5.48	0.08	Insignificant
X_2^2	1	0.1272	0.1272	5.95	0.07	Insignificant
X_3 (Catalyst Conc.)	1	0.0015	0.0015	0.07	0.80	Insignificant
X_3^2	1	0.0999	0.0999	4.67	0.10	Insignificant
X_1X_2	1	0.0755	0.0755	3.53	0.13	Insignificant
X_1X_3	1	0.0000	0.0000	0.00	0.98	Insignificant
X_2X_3	1	0.0801	0.0801	3.75	0.12	Insignificant
Lack of Fit	5	0.5044	0.1009	4.72	0.08	Insignificant
Pure Error	4	0.0855	0.0214	-	-	-
Total Sum of Squares	18	2.5475	-	-	-	-
Model Predicting OS (Equation D.4; R^2 = 0.6998)						
X_1 (Temperature)	1	95.6809	95.6809	47.27	2.35×10^{-3}	Significant
X_1^2	1	33.7502	33.7502	16.67	1.51×10^{-2}	Significant
X_2 (Time)	1	4.0713	4.0713	2.01	0.23	Insignificant
X_2^2	1	15.3874	15.3874	7.60	0.05	Insignificant
X_3 (Catalyst Conc.)	1	0.3254	0.3254	0.16	0.71	Insignificant
X_3^2	1	13.5478	13.5478	6.69	0.06	Insignificant
X_1X_2	1	9.9922	9.9922	4.94	0.09	Insignificant
X_1X_3	1	0.2052	0.2052	0.10	0.77	Insignificant
X_2X_3	1	5.0554	5.0554	2.50	0.19	Insignificant
Lack of Fit	5	62.6421	12.5284	6.19	0.05	Insignificant
Pure Error	4	8.0974	2.0243	-	-	-
Total Sum of Squares	18	235.6078	-	-	-	-

a – Temperature (X_1), Time (X_2) and Catalyst Concentration (X_3) as input variables; **b –** Degree of substitution is abbreviated as DS, and oil sorption is abbreviated as OS

In comparison to the statistical validation, the adjusted models were experimentally validated at three random conditions (CC-B2-V1, CC-B2-V2 and CC-B2-V3 in Table D.6 and WS-B2-V1, WS-B2-V2 and WS-B2-V3 in Table D.7). Even though the OS differs with the predicted values with more than 10 %, the obtained DS and OS values were within the 95 % confidence interval ($\alpha = 0.05$) for all validation runs. The developed models were therefore deemed acceptable to predict the DS and OS of CC and WS. The models were accepted for this purpose, but it is recommended that further tests are executed in order to improve the accuracy of the models. The OS prediction range needs to become narrower, and higher R^2 values are desired.

Table D.6 A Comparison of the Predicted and Experimental Values of Degree of Substitution and Oil Sorption for the Model Validation of the *Green* Corncob Surface Modification

Run [a]	Temperature (°C)	Time (h)	Catalyst Concentration [b, c] (%)	Model Prediction	Experimental Value	Error (%)
DS (Equation D.1)						
CC-B2-V1	80	2	3	0.82 [d]	0.76 ± 0.07	7.39
CC-B2-V2	100	8	5	0.95 [e]	0.93 ± 0.09	2.05
CC-B2-V3	130	5	1	1.72 [f]	1.56 ± 0.17	8.87
OS (g oil/g sorbent) (Equation D.2)						
CC-B2-V1	80	2	3	6.77 [g]	5.38 ± 0.48	20.58
CC-B2-V2	100	8	5	7.45 [h]	6.36 ± 0.20	14.58
CC-B2-V3	130	5	1	12.07 [i]	15.33 ± 0.45	27.03

a – Run identification for corncob (CC), where B2 as suffix represents a *green* modification
b – Each run performed with a constant acetic anhydride loading of 25:1 (25 mL acetic anhydride to 1 g biomass)
c – Target iodine as a weight percentage of biomass
d – Predicted that degree of substitution (DS) could range from 0.53 to 1.11 at these conditions with 95 % confidence
e – Predicted that DS could range from 0.36 to 1.54 at these conditions with 95 % confidence
f – Predicted that DS could range from 1.22 to 2.21 at these conditions with 95 % confidence
g – Predicted that oil sorption (OS) could range from 4.20 to 9.35 g oil/g sorbent at these conditions with 95 % confidence
h – Predicted that OS could range from 2.21 to 12.68 g oil/g sorbent at these conditions with 95 % confidence
i – Predicted that OS could range from 7.69 to 16.44 g oil/g sorbent at these conditions with 95 % confidence

Table D.7 A Comparison of the Predicted and Experimental Values of Degree of Substitution and Oil Sorption for the Model Validation of the *Green* Wheat Straw Surface Modification

Run [a]	Temperature (°C)	Time (h)	Catalyst Concentration [b, c] (%)	Model Prediction	Experimental Value	Error (%)
DS (Equation D.3)						
WS-B2-V1	40	2	2	0.64 [d]	0.62 ± 0.16	3.96
WS-B2-V2	95	1	1	1.48 [e]	1.45 ± 0.09	2.44
WS-B2-V3	100	2	1	1.61 [f]	1.47 ± 0.10	8.76
OS (g oil/g sorbent) (Equation D.4)						
WS-B2-V1	40	2	2	3.80 [g]	4.63 ± 0.36	21.93
WS-B2-V2	95	1	1	11.29 [h]	11.36 ± 0.15	0.57
WS-B2-V3	100	2	1	12.54 [i]	13.72 ± 0.66	9.34

a – Run identification for wheat straw (WS), where B2 as suffix represents a *green* modification
b – Each run performed with a constant acetic anhydride loading of 25:1 (25 mL acetic anhydride to 1 g biomass)
c – Target iodine as a weight percentage of biomass
d – Predicted that degree of substitution (DS) could range from 0.01 to 1.28 at these conditions with 95 % confidence
e – Predicted that DS could range from 1.00 to 1.97 at these conditions with 95 % confidence
f – Predicted that DS could range from 1.25 to 1.96 at these conditions with 95 % confidence
g – Predicted that oil sorption (OS) could range from 0 to 9.99 g oil/g sorbent at these conditions with 95 % confidence
h – Predicted that OS could range from 6.59 to 15.99 g oil/g sorbent at these conditions with 95 % confidence
i – Predicted that OS could range from 9.08 to 16.01 g oil/g sorbent at these conditions with 95 % confidence

The Normal Probability Plots of the responses are displayed in Figure D.2 in order to confirm that the data is normally distributed and therefore, reliable.

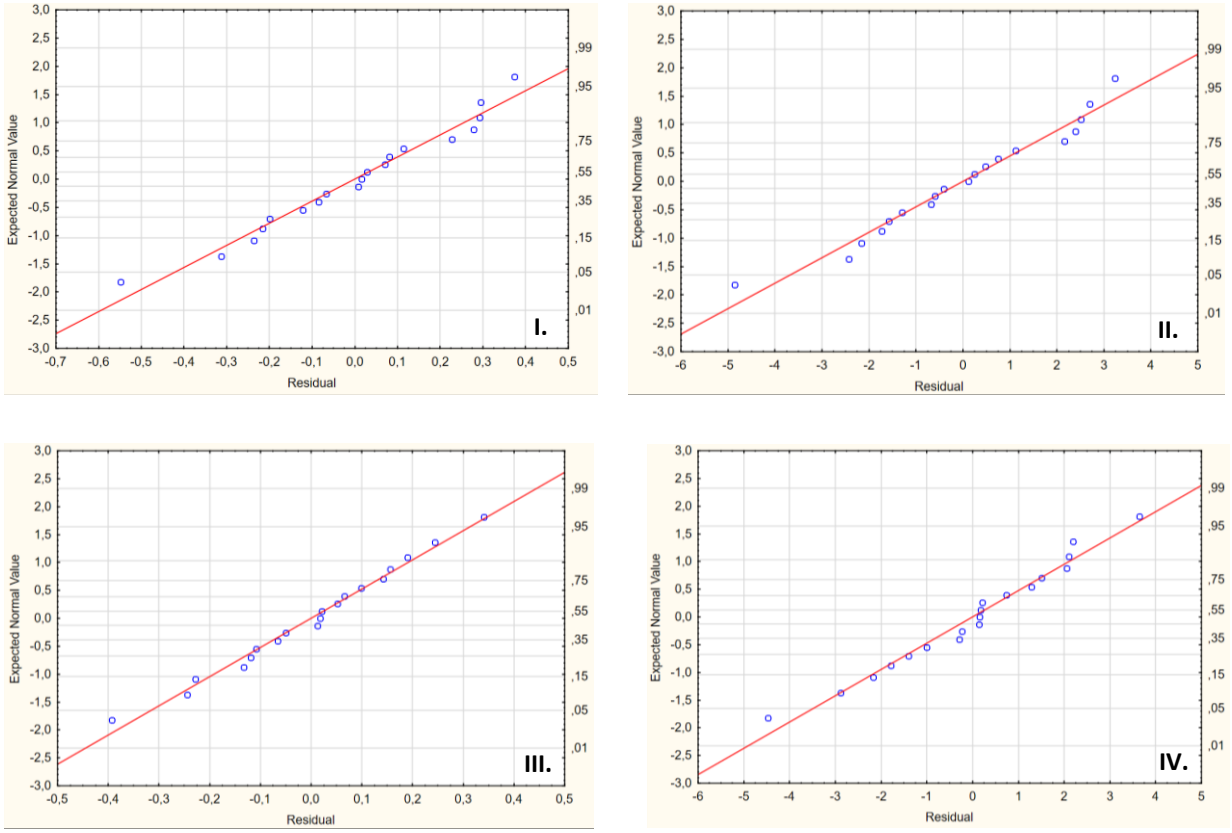

Figure D.2 The Normal Probability Plot of Raw Residuals for the Polynomial Models of **I.** Degree of Substitution of Corncob (Equation D.1); **II.** Oil Sorption of Corncob (Equation D.2); **III.** Degree of Substitution of Wheat Straw (Equation D.3) and **IV.** Oil Sorption of Wheat Straw (Equation D.4)

D.3 Chemical Structures for Lignocellulosic Biomass

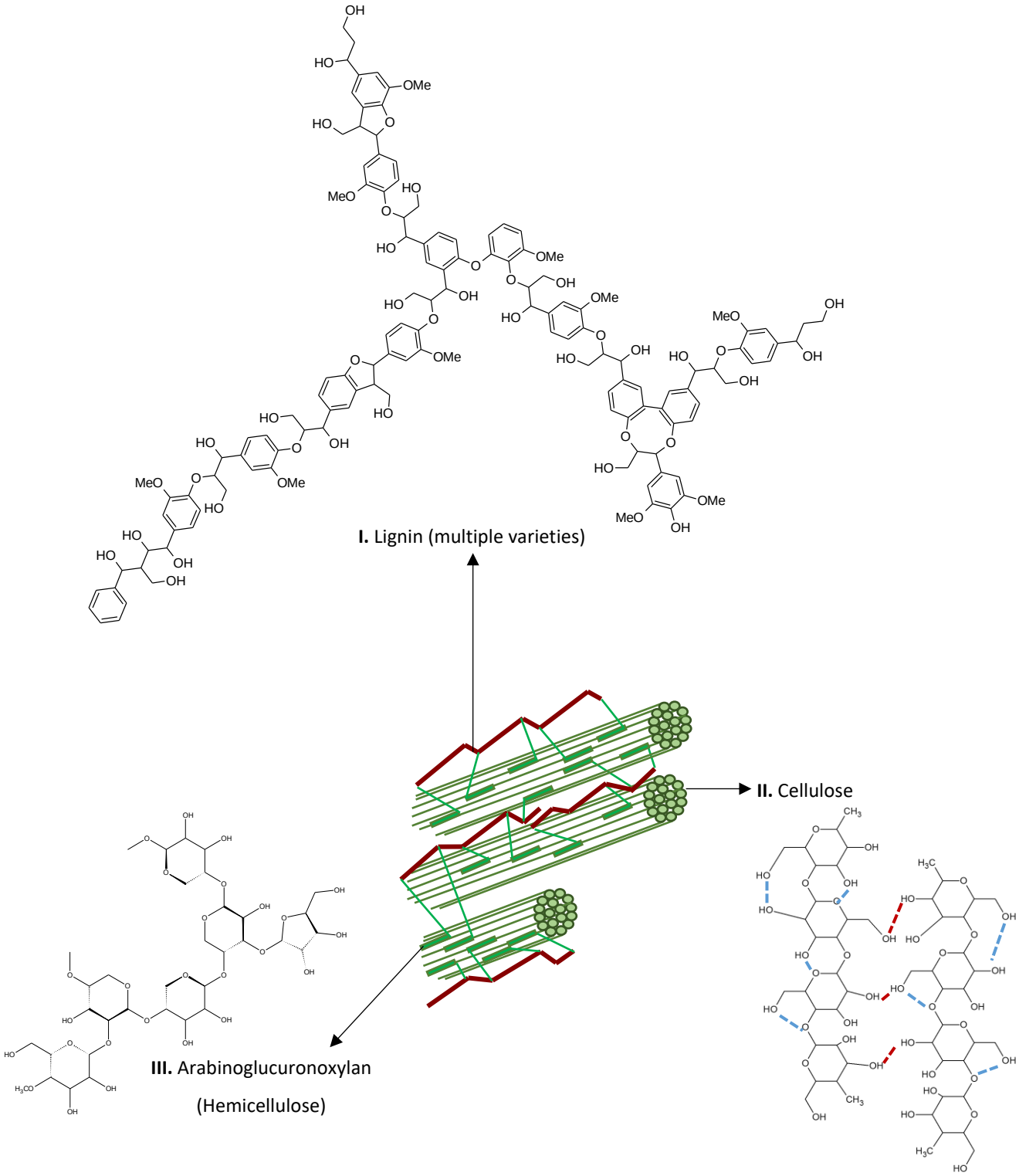

Figure D.3 The Typical Biomass Composition, redrawn from Salimi, Nejati, Karimi, & Tavasoli (2016), with **I.** Lignin, redrawn from Lu et al. (2017); **II.** Cellulose Chains (with Inter- (Red) and Intramolecular (Blue) Bonding), redrawn from Rowell et al. (2012); and **III.** Arabinoglucuronoxylan, redrawn from Impola (2017)

Appendix E – Cellulose Sorbents Supplementary Results

E.1 Preliminary Experiments to Establish Scope for Central Composite Design of the *Green* Cellulose Modification

Preliminary experiments were conducted in order to establish the scope for the temperature, time and catalyst concentration inputs to the central composite design (CCD) of the *green* cellulose modification. These preliminary experiments were accomplished by varying the reaction temperature between 40 and 120 °C, acetylation duration between 2 and 24 h and catalyst concentration between 0 and 14 % (v/v) NaOH-solution, in single-factor experiments. The experimental details of each run are depicted in Table E.1, and the degree of substitution (DS) attained with each test is indicated.

Table E.1 Experimental Conditions and Degree of Substitution for the Preliminary *Green* Modification on Cotton for the Scope Establishment of the Central Composite Design Matrix

Run ID [a]	Temperature (°C)	Time (h)	Catalyst Concentration [b, c] (%)	DS [d]
CO-C2-0 [e]	n/a	n/a	n/a	n/a
CO-C2-P1	40	2	7.5	0.59 ± 0.02
CO-C2-P2	90	2	7.5	0.79 ± 0.06
CO-C2-P3	120	2	7.5	0.90 ± 0.08
CO-C2-P4	90	24	7.5	1.34 ± 0.08
CO-C2-P5	90	2	3.75	0.83 ± 0.04
CO-C2-P6	90	2	14	0.45 ± 0.01
CO-C2-P7	90	2	0	0.40 ± 0.04

a – Run identification for the preliminary modification of cotton (CO), where C2 as suffix represents a *green* modification; **b** – Each run performed with a constant acetic anhydride loading of 30:1 (30 mL acetic anhydride to 1 g CO); **c** – Target sodium hydroxide (50 % (w/w) NaOH-solution) percentage, based on volume to volume ratio of acetic anhydride; **d** – Degree of Substitution abbreviated as DS; **e** – Unmodified CO sample for reference

Figure E.1 illustrates the DS and Fourier Transform Infrared (FT-IR) spectra of each preliminary run. The runs CO-C2-P1, CO-C2-P2 and CO-C2-P3 (Figure E.1 I) were utilised to study the effect of temperature at a constant time (2 h) and constant catalyst concentration (7.5 % (v/v) NaOH-solution). Increasing the temperature from 40 °C to 90 °C led to a significant incline in DS ($p = 5.47 \times 10^{-4}$), while a further increase to 120 °C had no significant effect ($p = 0.06$) on the acetylation. This occurrence in DS was reiterated by the FT-IR spectra (Figure E.1 II), where increased ester peak intensities (1 740 cm^{-1}, 1 369 cm^{-1} and 1 234 cm^{-1}) transpired at 90 °C when compared to 40 °C. In contrast, the responses at 90 °C and 120 °C indicated similar ester peaks. Nevertheless, the DS achieved at 120 °C were marginally higher (though not statistically significant) than reached at 90 °C, and the temperature range of 40 °C to 140 °C was selected for the CCD investigation (with $\alpha = 2^{3/4}$) in order to study the effects of interaction between the input parameters.

It is important to note that the temperature should not be escalated above 140 °C. A 50 % (w/w) NaOH-solution becomes volatile above 143 °C, and the current experimental setup cannot condense the vapours at these amplified temperatures, since a chemical coolant is not employed in the condenser.

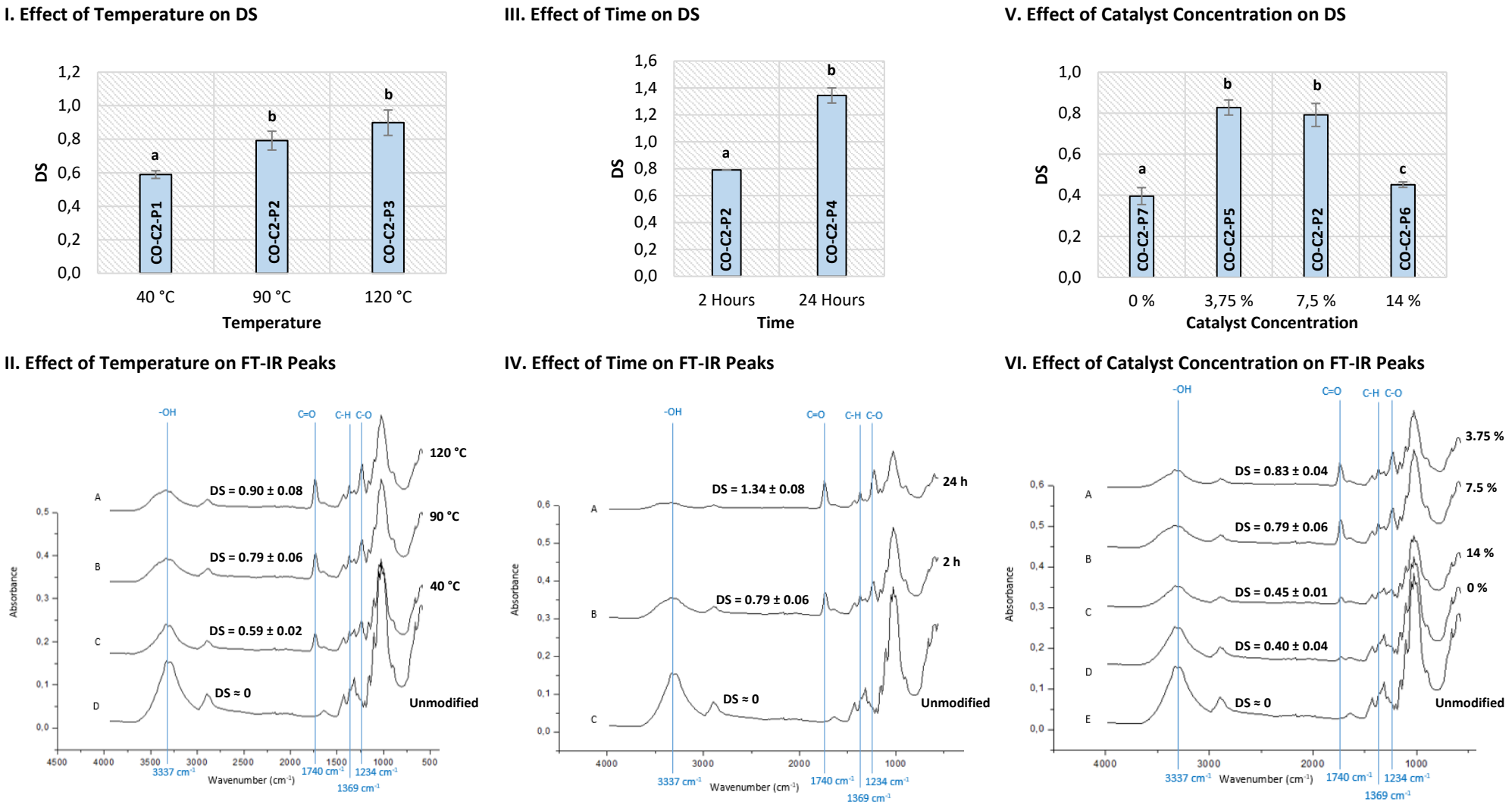

Figure E.1 The Effects of Temperature, Time and Catalyst Concentration on the Degree of Substitution (DS) and Fourier Transform Infrared (FT-IR) Spectra of the Preliminary *Green* Acetylated Cotton at **I., II.** Constant Time and Catalyst Concentration (2 h, 7.5 % (v/v) NaOH-solution); **III., IV.** Constant Temperature and Catalyst Concentration (90 °C, 7.5 % (v/v) NaOH-solution); **V., VI.** Constant Temperature and Reaction Time (90 °C, 2 h)

The runs CO-C2-P2 and CO-C2-P4 (Figure E.1 III) were employed to study the effect of time at a constant temperature (90 °C) and constant catalyst concentration (7.5 % (v/v) NaOH-solution). An increase in reaction time from 2 to 24 h leads to a significant escalation in acetylation ($p = 2.78 \times 10^{-5}$), which indicated that the optimal reaction duration might occur above 24 h. The experiment executed at 24 h presented intensified ester intensities (at 1 740 cm^{-1}, 1 369 cm^{-1} and 1 234 cm^{-1}) in Figure E.1 IV. Similar experiments were conducted with rice and wheat husks at room temperature for up to 48 h at different NaOH-concentrations (Thakur, 2013). In order for the experimental design to maintain rotatability, the alpha values of $\alpha = 2^{3/4}$ were selected, and the range of reaction time of 3.8 – 44.2 h was utilised for the CCD.

Furthermore, CO-C2-P2, CO-C2-P5, CO-C2-P6 and CO-C2-P7 (Figure E.1 V) were implemented to establish the scope for catalyst concentration at a constant time (2 h) and constant temperature (90 °C). Increasing the catalyst concentration from 0 % (v/v) NaOH-solution to 3.75 % (v/v) NaOH-solution had a significantly heightened (4.42×10^{-6}) DS to effect. The FT-IR spectra (Figure E.1 VI) depicted increased ester peaks at 3.75 % (v/v) NaOH-solution. However, a further increase to 7.5 % (v/v) NaOH-solution had no significant effect ($p = 0.32$) on the acetylation of cotton and visibly similar ester peaks were observed for these samples. A significantly reduced DS was accomplished at 14 % (v/v) NaOH-solution ($p = 2.26 \times 10^{-5}$), accompanied by considerably declined ester peaks. It was decided to test the entire range of catalyst concentration in the CCD (with $\alpha = 2^{3/4}$) in order to determine any interactions that it might have with temperature and time. The scope is therefore selected as per Table E.2.

Table E.2 Independent Variables Applied During the *Green* Modification of Cotton

Factor	Symbol	Range	Coded Levels				
			-α	**-1**	**0**	**1**	**α**
Temperature	X_1	40 – 140 °C	40	60	90	120	140
Time	X_2	3.8 – 44.2 h	3.8	12	24	36	44.2
Catalyst Concentration [a]	X_3	1.2 – 13.8 % (v/v)	1.2	3.75	7.5	11.25	13.8

a – Target sodium hydroxide (50 % (w/w) NaOH-solution) percentage, based on volume to volume ratio of acetic anhydride

E.2 Validation of Models determined by Central Composite Design of *Green* Cellulose Modification of Cotton

The polynomial models predicted by Statistica 13.2 are presented in Table E.3 (Equation E.1 and Equation E.2). The degree of substitution (DS) and oil sorption (OS) were implemented as response variables.

Table E.3 The Mathematical Models, Developed to Describe the Response of Degree of Substitution and Oil Sorption to the Input Parameters – Temperature, Time, and Catalyst Concentration, for the *Green* Surface Modification of Cotton

Model	Mathematical Model [a, b]	Equation
Original Prediction	$Y_1 = (0.011108) + (0.007908)X_1 + (0.011896)X_2 + (0.016003)X_3 + (-0.000043)X_1^2 + (-0.000222)X_2^2 + (-0.000941)X_3^2 + (0.000062)X_1X_2 + (0.000040)X_1X_3 + (-0.000227)X_2X_3$	[E.1]
	$Y_2 = (12.27558) + (0.09164)X_1 + (0.13447)X_2 + (0.19750)X_3 + (-0.00052)X_1^2 + (-0.00280)X_2^2 + (-0.01397)X_3^2 + (0.00087)X_1X_2 + (0.00075)X_1X_3 + (-0.00239)X_2X_3$	[E.2]
Adapted Prediction	$Y_1 = (-0.043582) + (0.009318)X_1 + (0.015160)X_2 + (-0.000041)X_1^2 + (-0.000209)X_2^2$	[E.3]
	$Y_2 = (11.29168) + (0.11229)X_1 + (0.18490)X_2 + (-0.00049)X_1^2 + (-0.00260)X_2^2$	[E.4]

a – Temperature (X_1), Time (X_2) and Catalyst Concentration (X_3) as input variables; **b** – Degree of Substitution (Y_1) and Oil Sorption (Y_2) as model responses

ANOVA analysis (Table E.4) were applied to the models to determine the regression coefficients and analyse the statistical fit to the experimental data. These analyses indicated a regression coefficient of $R^2 = 0.5061$ for the model predicting DS (Equation E.1) and $R^2 = 0.5045$ for the model predicting OS (Equation E.2). The significant *Lack of Fit* for both models designated that the DS and OS cannot be accurately predicted.

In an attempt to improve the statistical fit of the models, the negligible effects were pooled into the error-terms (b_0 in Equation 3.12, Section 3.5). These negligible effects included the linear and quadratic effects of the catalyst, as well as the interactions between the input parameters ($p > 0.05$, Table E.4). The adjusted models are signified by Equation E.3 and Equation E.4 (Table E.3).

Table E.4 The ANOVA Analyses of the Polynomial Models of Cotton with Degree of Substitution and Oil Sorption as Response Variables

Factor [a, b]	Degrees of Freedom	Sum of Squares	Mean Square	F-value	p	Statistical Significance
Model Predicting DS (Equation E.1, R^2 = 0.5061)						
X_1 (Temperature)	1	0.0460	0.0460	30.29	5.31×10^{-3}	Significant
X_1^2	1	0.0206	0.0206	13.59	2.11×10^{-2}	Significant
X_2 (Time)	1	0.0519	0.0519	34.21	4.26×10^{-3}	Significant
X_2^2	1	0.0140	0.0140	9.22	3.85×10^{-2}	Significant
X_3 (Catalyst Conc.)	1	0.0000	0.0000	0.00	0.98	Insignificant
X_3^2	1	0.0024	0.0024	1.58	0.28	Insignificant
X_1X_2	1	0.0040	0.0040	2.66	0.18	Insignificant
X_1X_3	1	0.0002	0.0002	0.11	0.76	Insignificant
X_2X_3	1	0.0008	0.0008	0.55	0.50	Insignificant
Lack of Fit	5	0.1242	0.0248	16.36	0.01	Significant
Pure Error	4	0.0061	0.0015	-	-	-
Total Sum of Squares	18	0.2636	-	-	-	-
Model Predicting OS (Equation E.2, R^2 = 0.5045)						
X_1 (Temperature)	1	7.2728	7.2728	27.34	6.39×10^{-3}	Significant
X_1^2	1	2.9985	2.9985	11.27	2.84×10^{-2}	Significant
X_2 (Time)	1	7.1530	7.1530	26.89	6.58×10^{-3}	Significant
X_2^2	1	2.2128	2.2128	8.32	4.48×10^{-2}	Significant
X_3 (Catalyst Conc.)	1	0.0008	0.0008	0.00	0.96	Insignificant
X_3^2	1	0.5272	0.5272	1.98	0.23	Insignificant
X_1X_2	1	0.7784	0.7784	2.93	0.16	Insignificant
X_1X_3	1	0.0569	0.0569	0.21	0.67	Insignificant
X_2X_3	1	0.0926	0.0926	0.35	0.59	Insignificant
Lack of Fit	5	18.5880	3.7176	13.97	0.01	Significant
Pure Error	4	10.0642	0.2660	-	-	-
Total Sum of Squares	18	39.6619	-	-	-	-

a – Temperature (X_1), Time (X_2) and Catalyst Concentration (X_3) as input variables; **b –** Degree of substitution is abbreviated as DS, and oil sorption is abbreviated as OS

The ANOVA analyses of the adapted models (Table E.5) indicated that the *Lack of Fit* was improved. However, the fit of the experimental data remained suboptimal, and marginally lower regression coefficients were obtained. These consisted of R^2 = 0.4779 for the model predicting DS (Equation E.3) and R^2 = 0.4678 for the model predicting OS (Equation E.4).

Table E.5 The ANOVA Analyses of the Adjusted Polynomial Models of Cotton with Degree of Substitution and Oil Sorption as Response Variables

Factor [a, b]	Degrees of Freedom	Sum of Squares	Mean Square	F-value	p	Statistical Significance
Adjusted Model Predicting DS (Equation E.3, R^2 = 0.4779)						
X_1 (Temperature)	1	0.0460	0.0460	30.29	5.31×10^{-3}	Significant
X_1^2	1	0.0190	0.0190	12.53	2.40×10^{-2}	Significant
X_2 (Time)	1	0.0519	0.0519	34.21	4.26×10^{-3}	Significant
X_2^2	1	0.0126	0.0126	8.31	4.49×10^{-2}	Significant
Lack of Fit	10	0.1316	0.1316	8.67	2.59×10^{-2}	Significant
Pure Error	4	0.0061	0.0015	-	-	-
Total Sum of Squares	18	0.2636	-	-	-	-
Adjusted Model Predicting OS (g oil/g sorbent) (Equation E.4, R^2 = 0.4678)						
X_1 (Temperature)	1	7.2728	7.2728	27.34	6.39×10^{-3}	Significant
X_1^2	1	2.6988	2.6988	10.14	3.34×10^{-2}	Significant
X_2 (Time)	1	7.1530	7.1530	26.89	6.58×10^{-3}	Significant
X_2^2	1	1.9490	1.9490	7.33	5.37×10^{-2}	Insignificant
Lack of Fit	10	20.0439	2.0044	7.53	3.33×10^{-2}	Significant
Pure Error	4	1.0642	0.2660	-	-	-
Total Sum of Squares	18	39.6619	-	-	-	-

a – Temperature (X_1) and Time (X_2) as input variables; **b** – Degree of substitution is abbreviated as DS, and oil sorption is abbreviated as OS

In comparison to the statistical validation, the adjusted models were experimentally validated at three random conditions (CO-C2-V1, CO-C2-V2 and CO-C2-V3 in Table E.6). Even though the DS values differ from the predicted values with more than 10 %, the obtained DS and OS values were within the 95 % confidence interval ($\alpha = 0.05$) for all three validation runs. The developed models were therefore deemed acceptable for predicting the DS and OS of cellulose. The models were accepted for this purpose, but it is recommended that further tests are executed in order to improve the accuracy of the models.

Table E.6 A Comparison of the Predicted and Experimental Values of Degree of Substitution and Oil Sorption for the Model Validations of the *Green* Cotton Surface Modification

Run [a]	Temperature (°C)	Time (h)	Catalyst Concentration [b, c] (%)	Model Prediction	Experimental Value	Error (%)
DS (Equation E.3)						
CO-C2-V1	60	14	7.5	0.54 [d]	0.63 ± 0.02	16.49
CO-C2-V2	100	36	5	0.75 [e]	0.83 ± 0.06	10.63
CO-C2-V3	120	24	3.75	0.73 [f]	0.83 ± 0.04	13.49
OS (g oil/g sorbent) (Equation E.4)						
CO-C2-V1	60	14	7.5	18.35 [g]	16.57 ± 0.39	9.71
CO-C2-V2	100	36	5	20.93 [h]	20.31 ± 0.56	2.95
CO-C2-V3	120	24	3.75	20.67 [i]	21.94 ± 0.80	6.14

a – Run identification for cotton (CO), where C2 as suffix represents a *green* modification
b – Each run performed with a constant acetic anhydride loading of 30:1 (30 mL acetic anhydride to 1 g CO)
c – Target sodium hydroxide (50 % (w/w) NaOH-solution) percentage, based on volume to volume ratio of acetic anhydride
d – Predicted that degree of substitution (DS) could range from 0.42 to 0.66 at these conditions with 95 % confidence
e – Predicted that DS could range from 0.64 to 0.87 at these conditions with 95 % confidence
f – Predicted that DS could range from 0.61 to 0.84 at these conditions with 95 % confidence
g – Predicted that oil sorption (OS) could range from 16.79 to 19.91 g oil/g sorbent at these conditions with 95 % confidence
h – Predicted that OS could range from 19.38 to 22.47 g oil/g sorbent at these conditions with 95 % confidence
i – Predicted that OS could range from 19.13 to 22.22 g oil/g sorbent at these conditions with 95 % confidence

The Normal Probability Plots of the responses are displayed in Figure E.2 in order to confirm that the data is normally distributed and therefore, reliable.

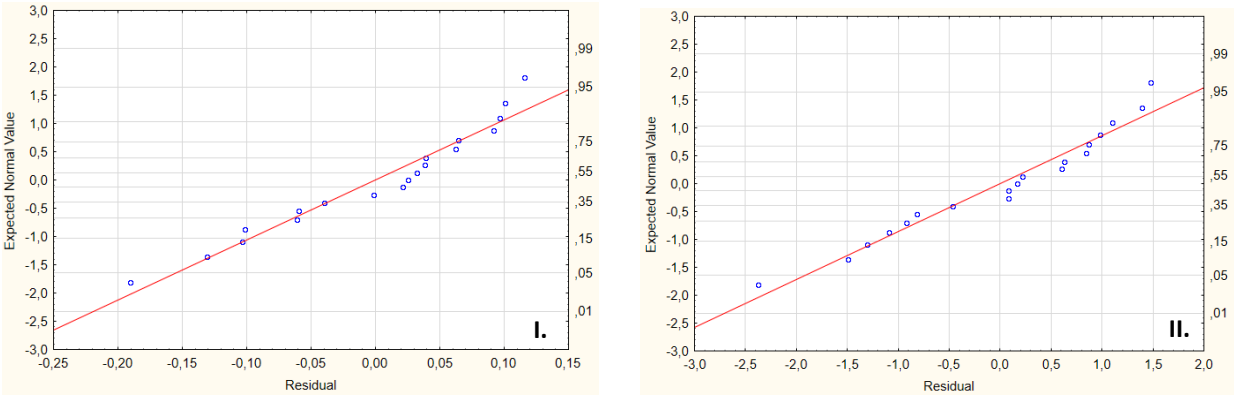

Figure E.2 The Normal Probability Plot of Raw Residuals for the Adjusted Polynomial Models of Cotton with **I.** Degree of Substitution (Equation E.3) and **II.** Oil Sorption (Equation E.4)

E.3 Additional Experimental Results on the *Cellulose level*

E.3.1 The Crystallinity of Cellulose

From the methodology explained in Section 3.4, it is known that the amorphous regions of the chemical structure are represented at the peak at approximately 2θ = 18 °, while the crystalline peak occurs at 2θ = 22.5 °. The crystallinities of the samples are then determined by incorporating the intensity of these peaks into a mathematical model, as executed in Section 5.3.1.

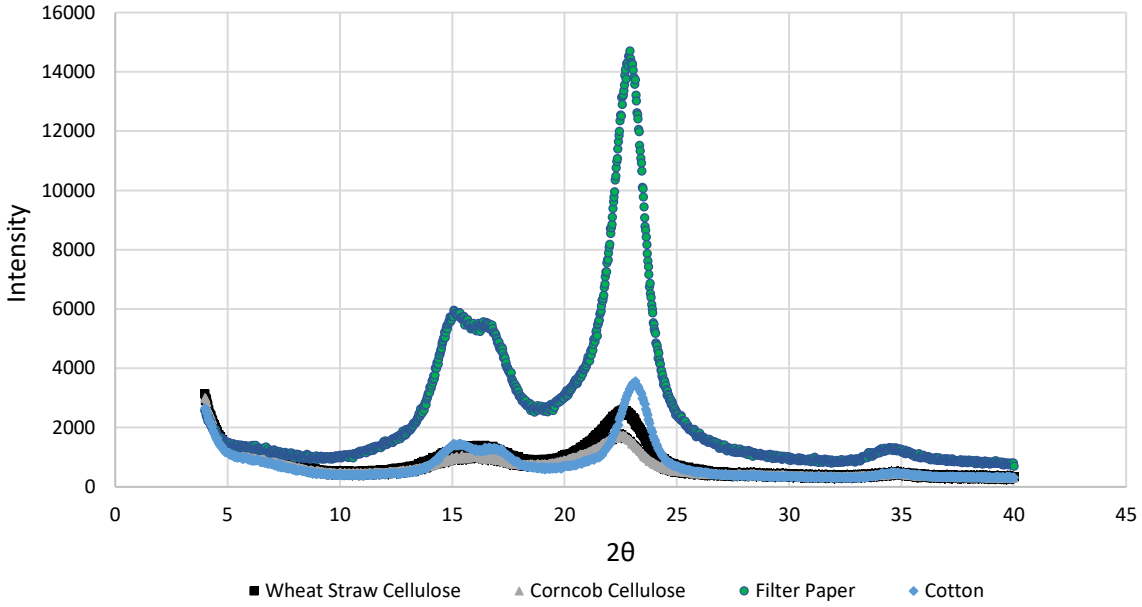

Figure E.3 The X-ray Diffraction Spectra of Wheat Straw Cellulose, Corncob Cellulose, Cotton and Filter Paper, as determined with a Bruker D2 Phaser X-ray Diffractometer

Appendix F – Nanofibrillated Cellulose Sorbent Supplementary Results

F.1 Preliminary Experiments to Establish Scope for Central Composite Design of the *Green* Nanofibrillated Cellulose Modification

Preliminary experiments were conducted in order to establish the scope for the temperature, time and catalyst concentration inputs to the central composite design (CCD) of the *green* nanofibrillated cellulose (NFC) modification. These preliminary experiments were accomplished by varying the reaction temperature between 25 and 60 °C, acetylation duration between 12 and 72 h and catalyst concentration between 200 and 2 250 U of lipase, in single-factor experiments. The experimental details of each run are depicted in Table F.1, and the degree of substitution (DS) achieved with each test is indicated.

Table F.1 Experimental Conditions and Degree of Substitution for the Preliminary *Green* Modification of Commercial Nanofibrillated Cellulose for the Scope Establishment of the Central Composite Design Matrix

Run ID [a]	Temperature (°C)	Time (h)	Catalyst Concentration [b, c] (U)	DS [d]
CN-N2-0 [e]	n/a	n/a	n/a	n/a
CN-N2-P1	25	24	1 250	0.62 ± 0.05
CN-N2-P2	30	24	1 250	0.67 ± 0.08
CN-N2-P3	45	24	1 250	0.67 ± 0.05
CN-N2-P4	60	24	1 250	0.52 ± 0.06
CN-N2-P5	45	12	1 250	0.55 ± 0.02
CN-N2-P6	45	48	1 250	0.85 ± 0.18
CN-N2-P7	45	72	1 250	0.55 ± 0.04
CN-N2-P8	45	24	200	0.60 ± 0.05
CN-N2-P9	45	24	2 250	0.59 ± 0.04

a – Run identification for the modification of commercial nanofibrillated cellulose (CN), where N2 as suffix represents a *green* modification; **b** – Each run is performed with a constant acetic anhydride loading of 6.1 M; **c** – Target concentration of Amano Lipase A from *Aspergillus niger* based on the Units (U) of enzyme added; **d** – Degree of Substitution abbreviated as DS; **e** – Unmodified CN sample for reference

Figure F.1 describes the DS and Fourier Transform Infrared (FT-IR) spectra of each preliminary run. The runs CN-N2-P1, CN-N2-P2, CN-N2-P3 and CN-N2-P4 (Figure F.1 I) were utilised to study the effect of temperature at a constant time (24 h) and constant catalyst concentration (1 250 U). The optimal operating conditions of the lipase is typically 45 °C at pH 6.5 (Sigma-Aldrich, 2020), while this enzyme deactivates at approximately 60 °C (Bozic et al., 2015). The FT-IR (Figure F.1 II) show similar ester peak intensities (at 1 740 cm^{-1}, 1 369 cm^{-1} and 1 234 cm^{-1}) for 25 °C, 30 °C and 45 °C. Marginally lower ester peaks are perceived at 60 °C. No significant increase in DS transpired when increasing the temperature from 25 °C to 30 °C ($p = 0.31$) or 30 °C to 45 °C ($p = 0.93$). However, a significant decrease in DS occurred when increasing the temperature from 45 °C to 60 °C ($p = 6.70 \times 10^{-3}$). In order for the experimental design to maintain rotatability, the alpha values of $\alpha = 2^{3/4}$ were transcribed, and the range of temperature tested was selected as 28 °C to 62 °C.

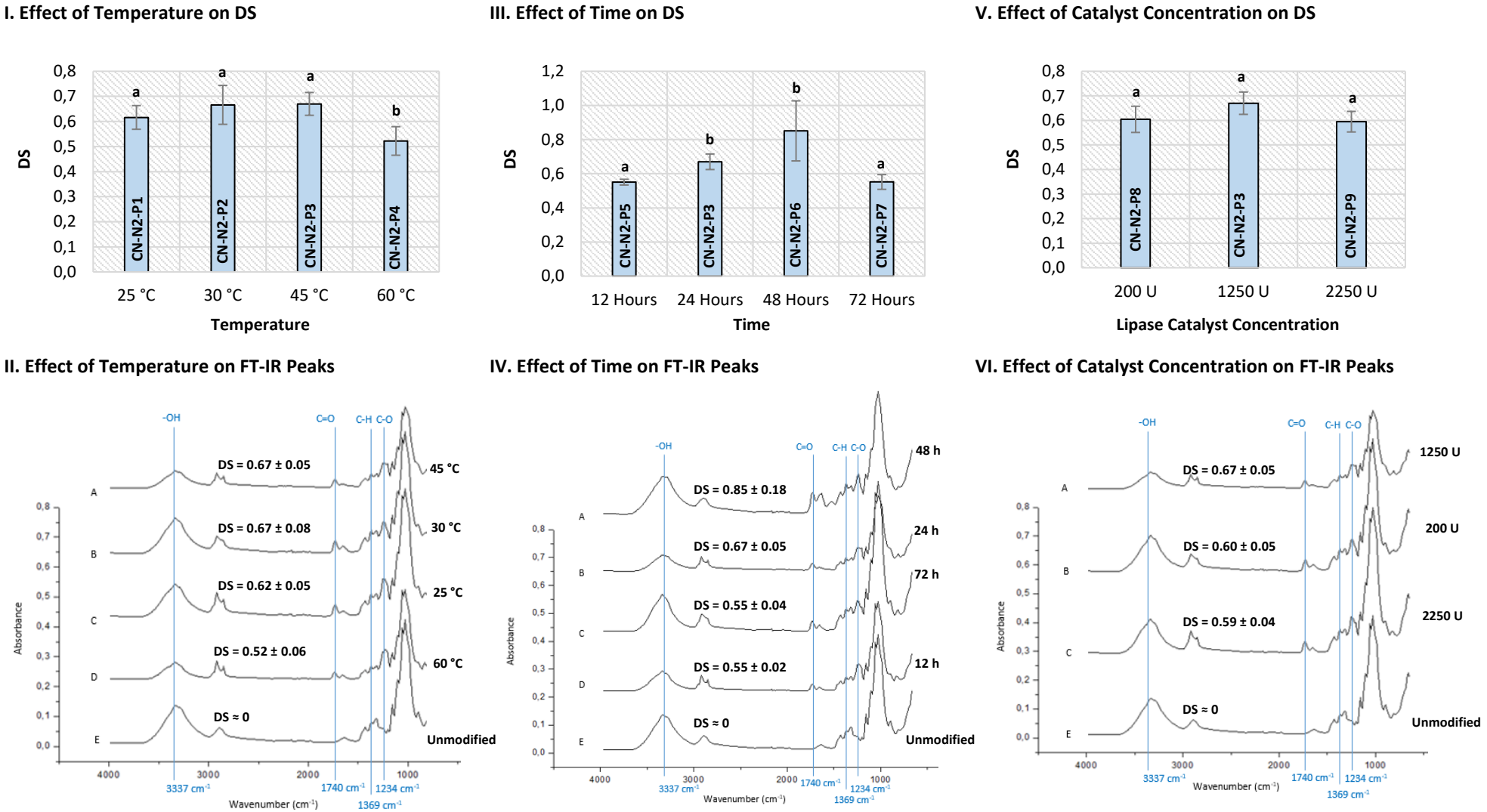

Figure F.1 The Effects of Temperature, Time and Catalyst Concentration on the Degree of Substitution (DS) and Fourier Transform Infrared (FT-IR) Spectra of the Preliminary *Green* Acetylated Commercial Nanofibrillated Cellulose (CN) at **I., II.** Constant Time and Catalyst Concentration (24 h, 1 250 U Lipase); **III., IV.** Constant Temperature and Catalyst Concentration (45 °C, 1 250 U Lipase); **V., VI.** Constant Temperature and Reaction Time (45 °C, 24 h)

The runs CN-N2-P3, CN-N2-P5, CN-N2-P6 and CN-N2-P7 (Figure F.1 III) were employed to study the effect of time at a constant temperature (45 °C), and catalyst concentration (1 250 U). A prolonged duration of 24 h led to a significant increase in acetylation ($p = 2.64 \times 10^{-3}$). In contrast, a further escalation to 48 h had no significant influence ($p = 0.09$). A significant decline in DS occurred when increasing the reaction time to 72 h ($p = 0.02$).

When studying Figure F.1 IV, it was difficult to discern between the ester peaks (1 740 cm^{-1}, 1 369 cm^{-1} and 1 234 cm^{-1}) at 24 h and 72 h. However, the ester peak intensities at 12 h were marginally declined, while the peaks at 48 h were considerably amplified in comparison. In contrast, the hydroxyl stretching peak at 3 337 cm^{-1} was lower at 24 h than at 48 h. Erosion during the chemical reaction can cause internal hydroxyl groups to become exposed, which can lead to a slight increase in the intensity of the hydroxyl stretching band (Zepic et al., 2015). A testing range of 28 – 68 h was therefore used for the CCD (with $\alpha = 2^{3/4}$) in order to study the effects of interaction between the input parameters.

The runs CN-N2-P3, CN-N2-P8 and CN-N2-P9 (Figure F.1 V) were implemented to establish the scope for catalyst concentration at a constant time (24 h) and constant temperature (45 °C). Increasing the lipase concentration from 200 U to 2 250 U had no significant influence ($p = 0.10$) on the DS at the specified temperature and reaction time (45 °C and 24 h). The ester peak intensities (Figure F.1 VI) were also visibly similar. It was decided to test the entire range of catalyst concentration in the CCD (with $\alpha = 2^{3/4}$) in order to determine any interactions that might occur with temperature and time. The scope for the CCD is therefore defined as per Table F.2.

Table F.2 Independent Variables Applied During the *Green* Modification of Commercial Nanofibrillated Cellulose

Factor	Symbol	Range	Coded Levels				
			-α	**-1**	**0**	**1**	**α**
Temperature	X_1	28 – 62 °C	28	35	45	55	62
Time	X_2	28 – 68 h	28	36	48	60	68
Catalyst Concentration [a]	X_3	199 – 2 301 U	199	625	1 250	1 875	2 301

a – Catalyst concentration expressed as activity of lipase (U, Units)

F.2 Validation of Models determined by Central Composite Design of *Green* Commercial Nanofibrillated Cellulose Modification

The polynomial model predicted by Statistica 13.2 is depicted as Equation F.1 in Table F.3. ANOVA analysis was applied to the developed model in order to determine the regression coefficients and analyse the statistical fit to the experimental data.

Table F.3 The Mathematical Models, Developed to Describe the Response of Degree of Substitution to the Input Parameters – Temperature, Time, and Catalyst Concentration, for the *Green* Surface Modification of Commercial Nanofibrillated Cellulose

Model	Mathematical Model [a, b]	Equation
Original Prediction	$Y_1 = (0.227015) + (-0.006184)X_1 + (0.028245)X_2 + (0.000477)X_3 + (0.000128)X_1^2 + (-0.000238)X_2^2 + (-0.0000001)X_3^2 + (-0.000252)X_1X_2 + (-0.000005)X_1X_3 + (0.000001)X_2X_3$	[F.1]
Adapted Prediction	$Y_1 = (0.833545) + (-0.019002)X_1 + (0.026718)X_2 + (0.000164)X_1^2 + (-0.000213)X_2^2 + (0.000000)X_3^2 + (-0.000252)X_1X_2 + (0.000002)X_1X_3$	[F.2]

a – Temperature (X_1), Time (X_2) and Catalyst Concentration (X_3) as input variables; **b** – Degree of Substitution (Y_1) as model response

The ANOVA analysis (Table F.4) indicated a regression coefficient of R^2 = 0.8437. The significant *Lack of Fit* designated that the experimental data cannot be accurately predicted by the model. However, the fit of the model could be improved by pooling the negligible effects into the error-term of the model (b_0 in Equation 3.12, Section 3.5). This ANOVA analysis indicates that the catalyst concentration (p = 0.65) and the interaction between catalyst concentration and time (p = 0.37) had insignificant effects on the DS accomplished by the modification. The adjusted model is signified by Equation F.2 (Table F.3), and the ANOVA analysis of this adjusted model is shown in Table F.5.

Table F.4 The ANOVA Analysis of the Polynomial Model of Commercial Nanofibrillated Cellulose with Degree of Substitution as Response Variable

Factor [a, b]	Degrees of Freedom	Sum of Squares	Mean Square	F-value	p	Statistical Significance
Model Predicting DS (Equation F.1; R^2 = 0.8437)						
X_1 (Temperature)	1	0.2467	0.2467	1070.39	5.00×10^{-6}	Significant
X_1^2	1	0.0022	0.0022	9.69	3.58×10^{-2}	Significant
X_2 (Time)	1	0.0505	0.0505	219.29	1.21×10^{-4}	Significant
X_2^2	1	0.0161	0.0161	69.82	1.12×10^{-3}	Significant
X_3 (Catalyst Conc.)	1	0.0001	0.0001	0.23	0.65	Insignificant
X_3^2	1	0.0240	0.0240	104.15	5.19×10^{-4}	Significant
X_1X_2	1	0.0073	0.0073	31.68	4.90×10^{-3}	Significant
X_1X_3	1	0.0089	0.0089	38.77	3.39×10^{-3}	Significant
X_2X_3	1	0.0002	0.0002	1.02	0.37	Insignificant
Lack of Fit	5	0.0650	0.0130	56.42	8.43×10^{-4}	Significant
Pure Error	4	0.0009	0.0002	-	-	-
Total Sum of Squares	18	0.4220	-	-	-	-

a – Temperature (X_1), Time (X_2) and Catalyst Concentration (X_3) as input variables; **b** – Degree of Substitution is abbreviated as DS

Table F.5 The ANOVA Analysis of the Adjusted Polynomial Model of Commercial Nanofibrillated Cellulose with Degree of Substitution as Response Variable

Factor [a, b]	Degrees of Freedom	Sum of Squares	Mean Square	F-value	p	Statistical Significance
Model Predicting DS (Equation F.2; R^2 = 0.8431)						
X_1 (Temperature)	1	0.2467	0.2467	1070.39	5.00×10^{-6}	Significant
X_1^2	1	0.0022	0.0022	9.69	3.58×10^{-2}	Significant
X_2 (Time)	1	0.0505	0.0505	219.29	1.21×10^{-4}	Significant
X_2^2	1	0.0161	0.0161	69.82	1.12×10^{-3}	Significant
X_3^2	1	0.0240	0.0240	104.15	5.19×10^{-4}	Significant
X_1X_2	1	0.0073	0.0073	31.68	4.90×10^{-3}	Significant
X_1X_3	1	0.0089	0.0089	38.77	3.39×10^{-3}	Significant
Lack of Fit	7	0.0653	0.0093	40.48	1.49×10^{-3}	Significant
Pure Error	4	0.0009		-	-	-
Total Sum of Squares	18	0.4220	-	-	-	-

a – Temperature (X_1), Time (X_2) and Catalyst Concentration (X_3) as input variables; **b** – Degree of Substitution is abbreviated as DS

Although the *Lack of Fit* was improved with the adjusted model, with a similar regression coefficient of R^2 = 0.8431, the fit of the experimental data remained suboptimal. In comparison to the statistical validation, the adjusted model was experimentally validated at three random conditions (Table F.6).

Table F.6 A Comparison of the Predicted and Experimental Values of Degree of Substitution for the Model Validation of the *Green* Commercial Nanofibrillated Cellulose Surface Modification

Run [a, b]	Temperature (°C)	Time (h)	Catalyst Concentration [c] (U)	DS		
				Model Prediction	Experimental Value	Error (%)
CN-N2-V1	35	35	1 000	0.77 [d]	0.81 ± 0.16	5.35
CN-N2-V2	35	25	600	0.72 [e]	0.75 ± 0.15	4.52
CN-N2-V3	40	60	1 500	0.61 [f]	0.64 ± 0.11	5.47

a – Run identification for commercial nanofibrillated cellulose (CN), where N2 as suffix represents a *green* modification
b – Each run performed with a constant acetic anhydride loading of 6.1 M
c – Target concentration of Amano Lipase A from *Aspergillus niger* based on the Units (U) of enzyme added
d – Predicted that degree of substitution (DS) could range from 0.72 to 0.82 at these conditions with 95 % confidence
e – Predicted that DS could range from 0.65 to 0.78 at these conditions with 95 % confidence
f – Predicted that DS could range from 0.56 to 0.65 at these conditions with 95 % confidence

From the three runs that were completed to validate the model (CN-N2-V1, CN-N2-V2 and CN-N2-V3), it is depicted that the experimental results are within the 95 % confidence interval (α = 0.05) of the values predicted by the model. The adjusted model was therefore deemed acceptable to predict the DS of NFC. The model is accepted for this purpose, but it is recommended that further tests are executed in order to improve the accuracy of the model.

The Normal Probability Plot of the response is displayed in Figure F.2 in order to confirm that the data is normally distributed and therefore, reliable.

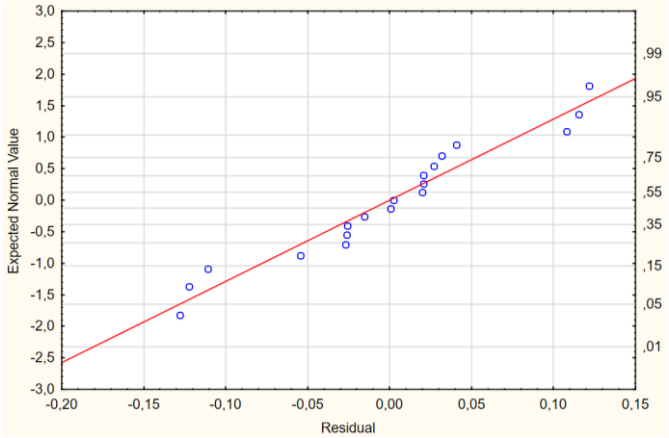

Figure F.2 The Normal Probability Plot of Raw Residuals for the Adjusted Polynomial Model of Degree of Substitution of Commercial Nanofibrillated Cellulose (Equation F.2)

F.3 Additional Experimental Results on the *Nanofibrillated cellulose level*

F.3.1 The Crystallinity of Nanofibrillated Cellulose

From the methodology discussed in Section 3.4, it is known that the amorphous regions of the chemical structure are represented at the peak at approximately 2θ = 18 °, while the crystalline peak occurs at 2θ = 22.5 °. The crystallinities of the samples are then determined by incorporating the intensities of these peaks into a mathematical model, as executed in Section 6.3.1.

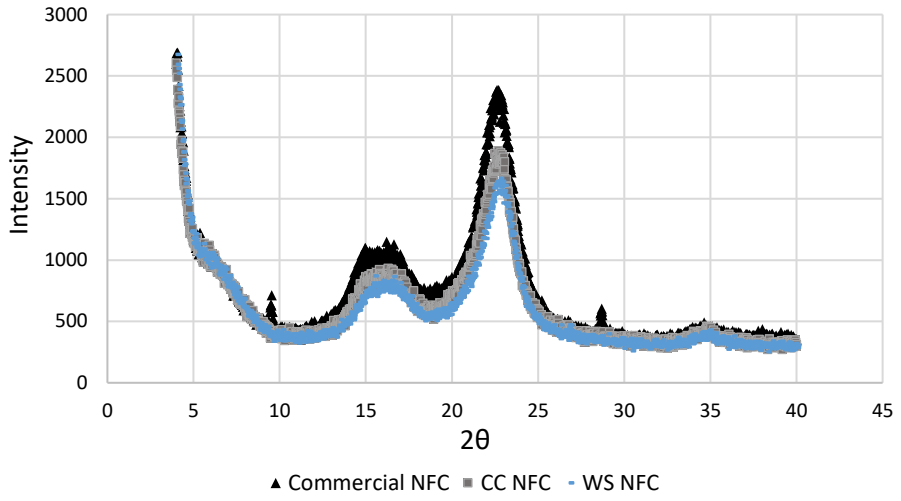

Figure F.3 The X-ray Diffraction Spectra of Commercial Nanofibrillated Cellulose (NFC), Corncob (CC) NFC and Wheat Straw (WS), as determined with a Bruker D2 Phaser X-ray Diffractometer

F.3.2 The Sorption Achieved by Aerogels compared to Nanofibrillated Cellulose Particles

The homogeneous OS of the samples were quantitatively measured at room temperature under static conditions with sunflower oil, as depicted in Figure F.4. This measurement was completed for the NFC particles prior to the formation of aerogels, as well as for the NFC samples in their aerogel form.

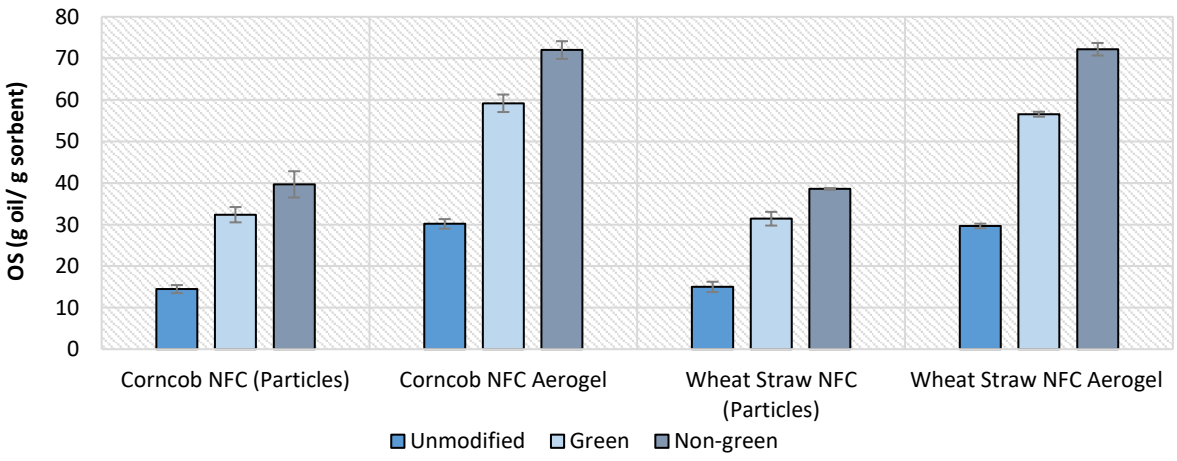

Figure F.4 The Homogeneous Oil Sorption (OS) of Sunflower Oil at Room Temperature (± 20 °C) for Modified and Unmodified Nanofibrillated Cellulose (NFC) as Particles, compared to the OS achieved by NFC Aerogels

It is evident that the performance of the aerogels exceeded the performance of the particles. The escalated OS occurred due to the increased porosity and lower density provided by the formation of the three-dimensional structure with aerogel development.

F.3.3 The Effect of Viscosity and Temperature on the Oil Sorption of the *Green* Nanofibrillated Cellulose Aerogels

Sorption experiments were concluded with oils of different viscosity at 20 °C (Figure F.5). A significant increase in sorption is depicted when comparing the sorption of sunflower oil, with a dynamic viscosity of 64.1 cP, to the canola oil with a marginally increased viscosity of 71 cP, for both CC NFC ($p = 0.03$) and WS NFC ($p = 5.21 \times 10^{-3}$).

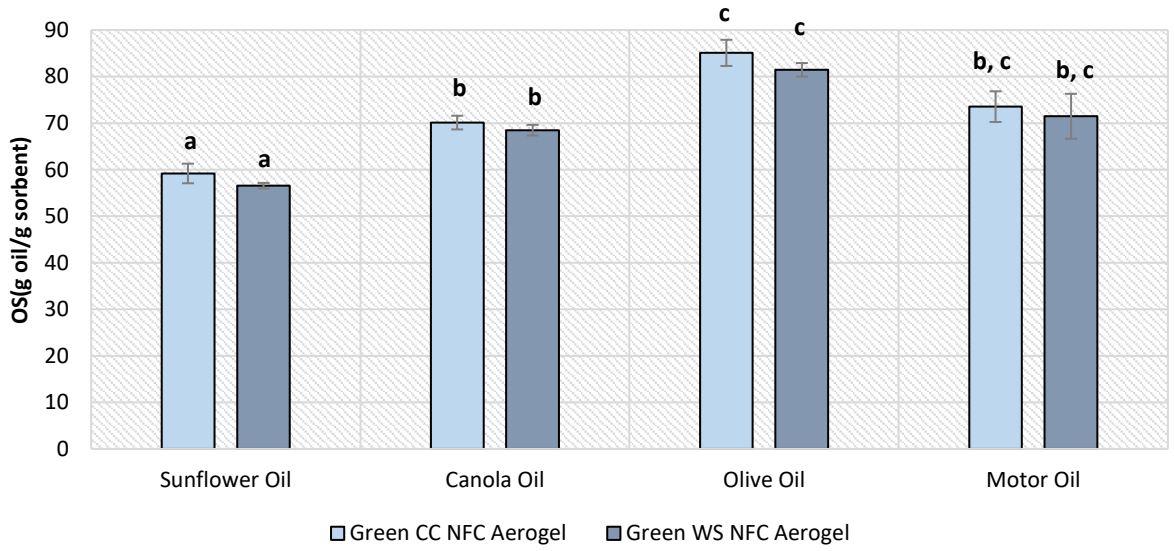

Figure F.5 The Homogeneous Oil Sorption (OS) of Corncob (CC) and Wheat Straw (WS) Nanofibrillated Cellulose (NFC) Aerogels with Sunflower Oil (64 cP), Canola Oil (71 cP), Olive Oil (92 cP) and Motor Oil (140 cP) at 20 °C

The sorption with olive oil, with an increased viscosity of 91.5 cP, was additionally significantly increased for CC NFC ($p = 0.02$) and WS NFC ($p = 0.01$). However, a further increase in viscosity to 140 cP with motor oil, led to sorption that was not statistically different to the sorptions attained for CC NFC ($p = 0.31$) and WS NFC ($p = 0.49$). The sorptions for CC and WS NFC are statistically similar ($p = 0.23$ to $p = 0.67$) at each respective oil.

The rheological properties of the oil have an influence on the capacity for OS. According to Lv et al. (2017), a higher viscosity can cause an initial increase in adherence of oil to the surface of the sorbent. However, penetration into the fibrous pores can be inhibited by heightened viscosities, when the stronger intermolecular forces of the oil particles constrain the absorption mechanism.

A – *Green* CC NFC Aerogel

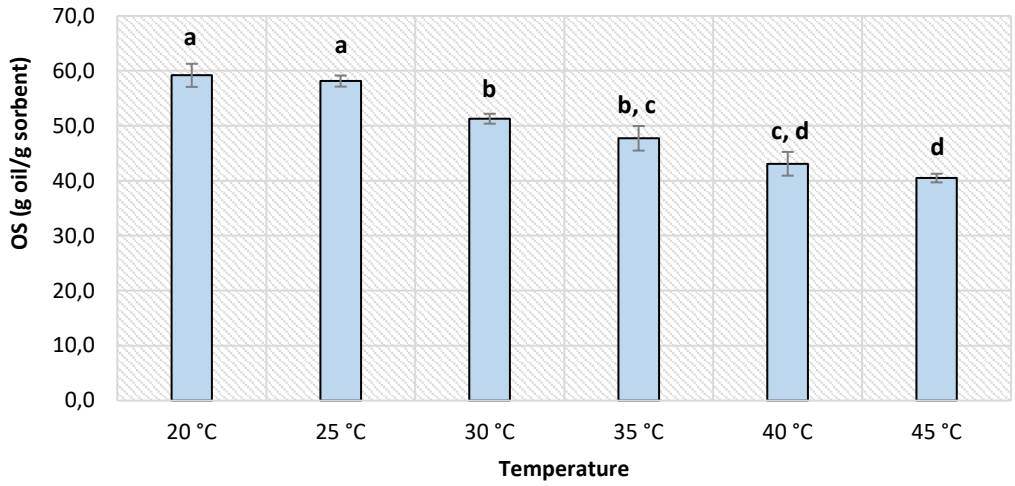

B – *Green* WS NFC Aerogel

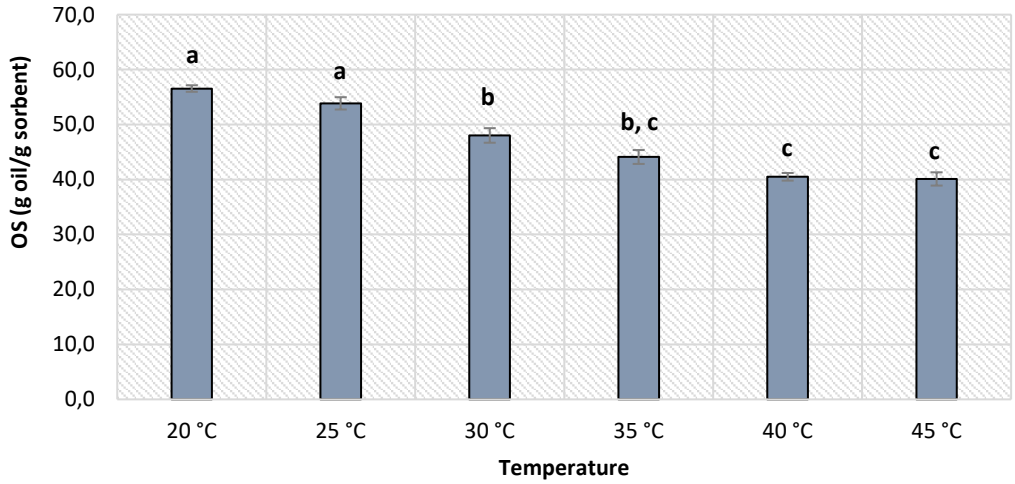

Figure F.6 The Homogeneous Oil Sorption (OS) of Corncob (CC) and Wheat Straw (WS) Nanofibrillated Cellulose (NFC) Aerogels with Sunflower Oil (64 cP) at Different Temperatures

The effect of the oil temperature on sorption was studied with sunflower oil (Figure F.6). An increase in temperature can lead to a decrease in viscosity. Lower viscosities can cause the oil to drain from the fibrous surface, resulting in a lower OS (Alaa El-Din et al., 2018).

In comparison, increased temperatures provide the oil particles with heightened molecular energy, which causes the Brownian motion of the oil particles to increase (J. Wang et al., 2015). This mechanism instigates that more energy is necessary for the oil particles to attach to the sorbent surface on the molecular level.

Appendix G – Calibrations for Determining the Degree of Substitution

G.1 Wheat Straw Calibration Curves

Calibration curves for the degree of substitution (DS) of wheat straw (WS) were developed by utilising five samples from the *green* WS biomass modification. The samples selected for calibration curve development are summarised in Table G.1.

Table G.1 Selected Samples for Degree of Substitution Calibration Curves of Wheat Straw

Calibration Sample Identification	Modification Sample [a]	Expected DS [b] Quality
WS-DS-0	Unmodified WS	≈ 0 [c]
WS-DS-1	WS-B2-9	Low
WS-DS-2	WS-B2-3	Medium
WS-DS-3	WS-B2-8	High
WS-DS-4	WS-B2-7	Very High

a – See Section 4.2.2 individual sample details; **b** – Degree of substitution abbreviated as DS; **c** – Assume unmodified samples contain negligible acetyl groups

Titrations were completed for the unmodified WS sample ("*blank* sample", Table G.2) and each calibration sample (Table G.3 and Table G.4).

Table G.2 Titration of *Blank* Sample for Degree of Substitution Calibration Curves of Wheat Straw

Calibration Sample Identification	Repeat	Mass (g)	HCl Titration Volume (mL)	NaOH Titration Volume (mL)
WS-DS-0	a	0.5062	10.3	1.1
	b	0.5019	11.9	1.0
	c	0.5013	9.0	1.0
	Average	0.5031 ± 0.0027	10.4 ± 1.5	1.0 ± 0.1

Table G.3 Experimental Titration of Samples for the Degree of Substitution Calibration Curves of Wheat Straw

Calibration Sample Identification	Repeat	Mass (g)	HCl Titration Volume (mL)	NaOH Titration Volume (mL)
WS-DS-1	a	0.5126	5.5	1.1
	b	0.5035	5.8	1.0
	c	0.5112	5.9	1.0
WS-DS-2	a	0.5024	4.6	1.1
	b	0.5006	4.8	1.1
	c	0.5041	4.5	1.0
WS-DS-3	a	0.5079	1.9	1.0
	b	0.5010	1.8	1.0
	c	0.5005	1.5	1.0
WS-DS-4	a	0.5001	1.2	1.0
	b	0.5049	1.3	1.0
	c	0.5078	1.5	1.0

Table G.4 Average Acetyl Content and Degree of Substitution for Calibration Curves of Wheat Straw

Calibration Sample Identification	Repeat	Acetyl Content (%)	Average Acetyl Content (%)	DS [a]	Average DS [a]
WS-DS-1	a	20.86	19.73 ± 1.04	0.99	0.92 ± 0.06
	b	19.52		0.91	
	c	18.81		0.87	
WS-DS-2	a	25.14	24.85 ± 0.42	1.26	1.24 ± 0.03
	b	24.37		1.20	
	c	25.05		1.25	
WS-DS-3	a	35.88	36.94 ± 1.13	2.08	2.18 ± 0.10
	b	36.81		2.16	
	c	38.13		2.29	
WS-DS-4	a	39.45	38.56 ± 0.94	2.42	2.33 ± 0.09
	b	38.65		2.34	
	c	37.58		2.24	

a – Degree of substitution abbreviated as DS

The FT-IR spectra of each sample were analysed with the relevant baselines to determine the necessary peak heights and areas under the curve (Table G.5). The calibration parameters (Table G.6) were then calculated to determine the four calibration curves illustrated in Figure G.1.

Table G.5 Peak Height and Areas under the Curve from Fourier Transform Infrared Spectra for developing Calibration Curves of Degree of Substitution of Wheat Straw

Calibration Sample Identification	H_{1370}	H_{1060}	H_{1740}	A_{1740}	A_{1370}
WS-DS-1	0.029	0.226	0.060	1.798	0.407
WS-DS-2	0.039	0.217	0.078	2.707	0.572
WS-DS-3	0.077	0.182	0.164	5.958	1.404
WS-DS-4	0.104	0.210	0.238	8.479	2.032

Table G.6 Calculated Parameters for the Calibration Curves of Degree of Substitution of Wheat Straw

Calibration Sample Identification	Average Acetyl Content (%)	A_{1740}/H_{1060}	H_{1740}/H_{1060}	A_{1370}/H_{1060}	H_{1370}/H_{1060}
WS-DS-1	19.73 ± 1.04	7.956	0.265	1.801	0.128
WS-DS-2	24.85 ± 0.42	12.475	0.359	2.636	0.180
WS-DS-3	36.94 ± 1.13	32.736	0.901	7.714	0.423
WS-DS-4	38.56 ± 0.94	40.376	1.133	9.676	0.495

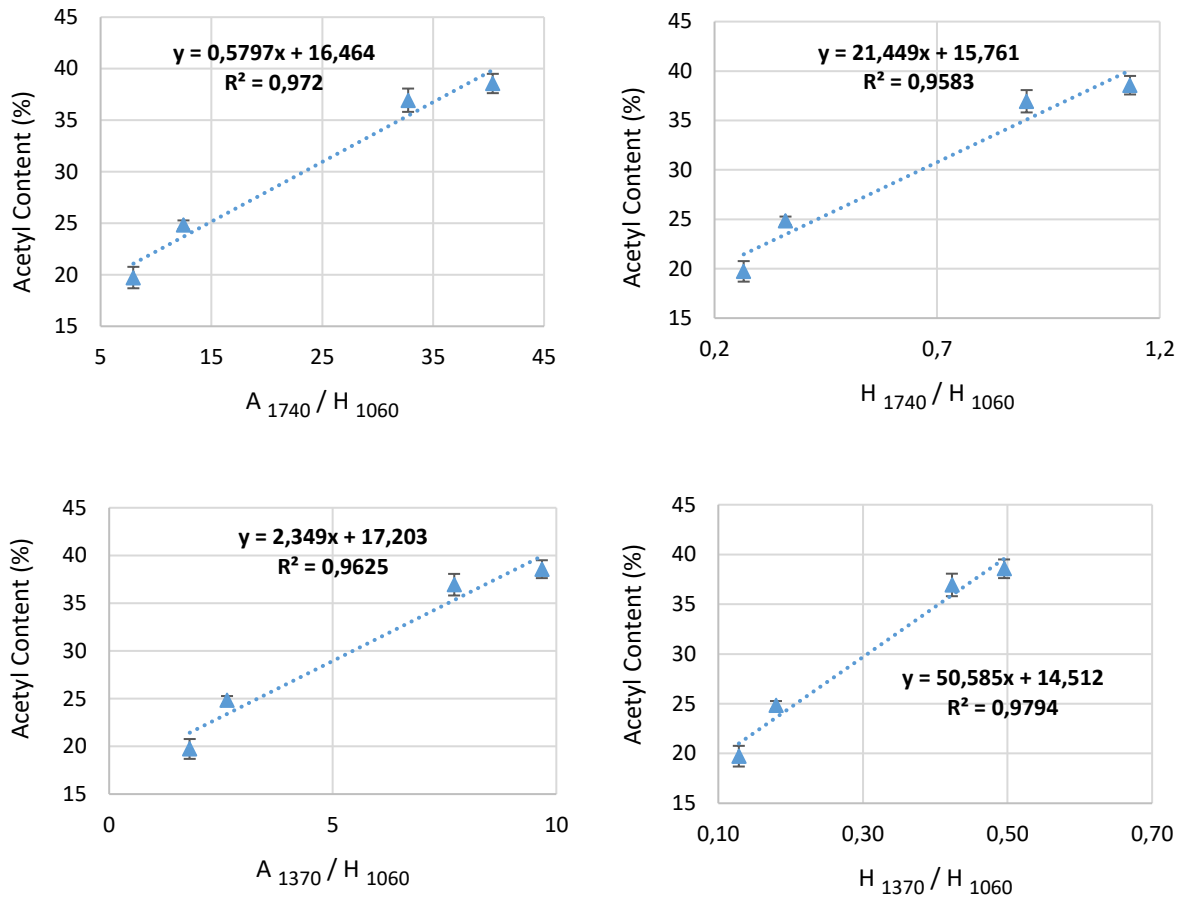

Figure G.1 Calibration Curves for Degree of Substitution of Wheat Straw

In order to validate the DS calibration curves of WS, the following two randomly selected samples were utilised from the *green* WS biomass modification (Table G.7). The titrations were completed for each validation sample (Table G.8 and Table G.9).

Table G.7 Selected Samples for Validation of Degree of Substitution Calibration Curves of Wheat Straw

Validation Sample Identification	Modification Sample ID [a]
WS-DS Validation 1	WS-B2-5
WS-DS Validation 2	WS-B2-15

a – See Section 4.2.2 for details of individual samples

Table G.8 Experimental Titration of Samples for Validation of Degree of Substitution Calibration Curves of Wheat Straw

Validation Sample Identification	Repeat	Mass (g)	HCl Titration Volume (mL)	NaOH Titration Volume (mL)
WS-DS Validation 1	a	0.5011	2.3	1.0
	b	0.5032	2.1	1.1
	c	0.5005	1.9	1.0
WS-DS Validation 2	a	0.5028	2.5	1.1
	b	0.5036	2.8	1.0
	c	0.5007	2.7	1.0

Table G.9 Experimental Validation of the Average Acetyl Content and Degree of Substitution for Wheat Straw Calibration Curves

Validation Sample Identification	Repeat	Acetyl Content (%)	Average Acetyl Content (%)	DS [a]	Average DS [a]
WS-DS Validation 1	a	34.65	35.62 ± 0.89	1.97	2.06 ± 0.08
	b	35.79		2.07	
	c	36.41		2.13	
WS-DS Validation 2	a	34.11	33.14 ± 0.90	1.93	1.85 ± 0.07
	b	32.34		1.78	
	c	32.96		1.83	

a – Degree of substitution abbreviated as DS

The FT-IR spectra of each sample were analysed with the relevant baselines to determine the necessary peak heights and areas under the curve (Table G.10). The calibration parameters (Table G.11) were then calculated to compare the theoretical and experimental values (Table G.12 and Table G.13).

Table G.10 Peak Height and Areas under the Curve from Fourier Transform Infrared Spectra for Validating Calibration Curves of Degree of Substitution of Wheat Straw

Validation Sample Identification	H_{1370}	H_{1060}	H_{1740}	A_{1740}	A_{1370}
WS-DS Validation 1	0.048	0.137	0.116	4.286	1.029
WS-DS Validation 2	0.066	0.187	0.142	5.008	1.110

Table G.11 Calculated Parameters for the Validation of Calibration Curves of Degree of Substitution of Wheat Straw

Validation Sample Identification	A_{1740}/H_{1060}	H_{1740}/H_{1060}	A_{1370}/H_{1060}	H_{1370}/H_{1060}
WS-DS Validation 1	31.285	0.847	7.511	0.350
WS-DS Validation 2	26.781	0.759	5.936	0.353

Table G.12 A Comparison between the Theoretical and Experimental Degree of Substitution for WS-DS Validation 1

Validation Sample Identification	Experimental [a]	Theoretical [b]	Error [c] (%)
Acetyl Content (%)	35.62 ± 0.89	33.90 ± 1.18	5.06
DS [d]	2.06 ± 0.08	1.91 ± 0.10	7.73

a – Determined by titration; **b** – Determined with calibration curves; **c** – Percentage error based on average values; **d** – Degree of substitution abbreviated as DS

Table G.13 A Comparison between the Theoretical and Experimental Degree of Substitution for WS-DS Validation 2

Validation Sample Identification	Experimental [a]	Theoretical [b]	Error [c] (%)
Acetyl Content (%)	33.14 ± 0.90	31.89 ± 0.52	3.91
DS [d]	1.85 ± 0.07	1.74 ± 0.04	5.81

a – Determined by titration; **b** – Determined with calibration curves; **c** – Percentage error based on average values; **d** – Degree of substitution abbreviated as DS

Since the errors (Table G.12 and Table G.13) are less than 10 %, the models are accepted. The acetyl contents of the samples can thus be calculated by the following equations, with H_{1060}, H_{1370}, H_{1740}, A_{1740} and A_{1370} as the relevant peak heights and areas under the curve, as obtained from the FT-IR with the respective baselines. An average of the four results is used as the acetyl content of each sample.

$$Acetyl\ Content\ (\%) = 0.58\left(\frac{A_{1740}}{H_{1060}}\right) + 16.46\ ;R^2 = 0.97 \quad [G.1]$$

$$Acetyl\ Content\ (\%) = 21.45\left(\frac{H_{1740}}{H_{1060}}\right) + 15.76\ ;R^2 = 0.96 \quad [G.2]$$

$$Acetyl\ Content\ (\%) = 2.35\left(\frac{A_{1370}}{H_{1060}}\right) + 17.20\ ;R^2 = 0.96 \quad [G.3]$$

$$Acetyl\ Content\ (\%) = 50.59\left(\frac{H_{1370}}{H_{1060}}\right) + 14.51\ ;R^2 = 0.98 \quad [G.4]$$

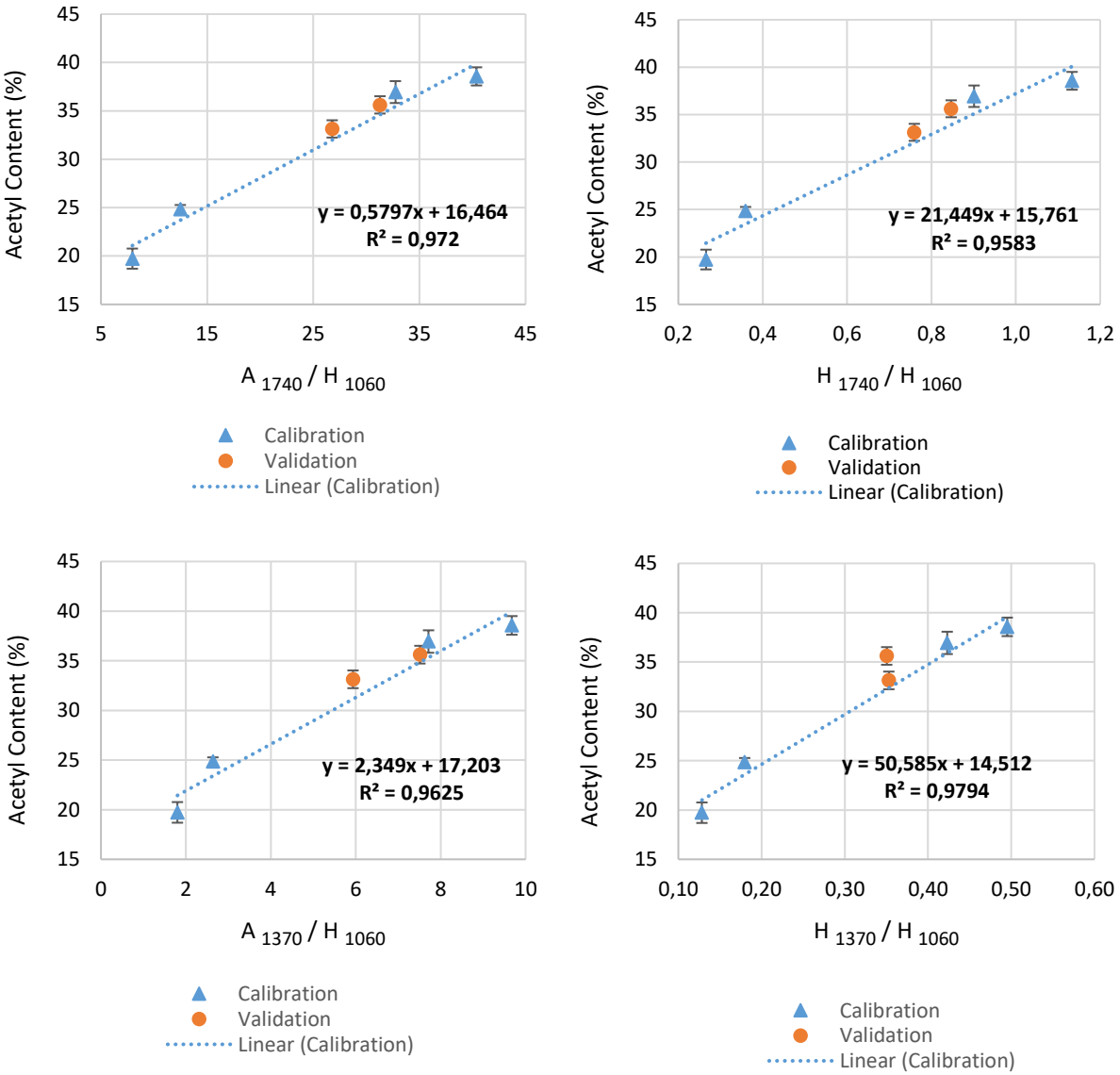

Figure G.2 Calibration Curves and Validation Points for Degree of Substitution of Wheat Straw

G.2 Corncob Calibration Curves

Calibration curves for the DS of corncob (CC) were developed by utilising five samples from the *green* CC biomass modification. The samples selected for calibration curve development are summarised in Table G.14.

Table G.14 Selected Samples for Degree of Substitution Calibration Curves of Corncob

Calibration Sample Identification	Modification Sample [a]	Expected DS [b] Quality
CC-DS-0	Unmodified CC	≈ 0 [c]
CC-DS-1	CC-B2-9	Low
CC-DS-2	CC-B2-15	Medium
CC-DS-3	CC-B2-6	High
CC-DS-4	CC-B2-10	Very High

a – See Section 4.2.2 individual sample details; **b** – Degree of substitution abbreviated as DS; **c** – Assume unmodified samples contain negligible acetyl groups

Titrations were completed for the unmodified CC sample ("*blank* sample", Table G.15) and each calibration sample (Table G.16 and Table G.17).

Table G.15 Titrations of *Blank* Sample for Degree of Substitution Calibration Curves of Corncob

Calibration Sample Identification	Repeat	Mass (g)	HCl Titration Volume (mL)	NaOH Titration Volume (mL)
CC-DS-0	a	0.5015	11.1	1.1
	b	0.4999	10.8	1.0
	c	0.4999	9.9	1.0
	Average	0.5004 ± 0.0009	10.6 ± 0.62	1.0 ± 0.1

Table G.16 Experimental Titration of Samples for the Degree of Substitution Calibration Curves of Corncob

Calibration Sample Identification	Repeat	Mass (g)	HCl Titration Volume (mL)	NaOH Titration Volume (mL)
CC-DS-1	a	0.5023	8.5	1.0
	b	0.5015	8.4	1.0
	c	0.5032	8.5	1.0
CC-DS-2	a	0.5087	4.1	1.0
	b	0.5059	4.3	1.0
	c	0.5002	4.1	1.0
CC-DS-3	a	0.5036	3.4	1.0
	b	0.5011	3.5	1.0
	c	0.5098	3.4	1.0
CC-DS-4	a	0.5041	2.4	1.0
	b	0.5073	2.5	1.0
	c	0.5035	2.5	1.0

Table G.17 Average Acetyl Content and Degree of Substitution for Calibration Curves of Corncob

Calibration Sample Identification	Repeat	Acetyl Content (%)	Average Acetyl Content (%)	DS [a]	Average DS [a]
CC-DS-1	a	8.86	9.00 ± 0.26	0.37	0.37 ± 0.01
	b	9.30		0.39	
	c	8.84		0.36	
CC-DS-2	a	27.36	27.28 ± 0.59	1.41	1.40 ± 0.04
	b	26.66		1.36	
	c	27.83		1.44	
CC-DS-3	a	30.63	30.42 ± 0.19	1.65	1.63 ± 0.01
	b	30.36		1.63	
	c	30.26		1.62	
CC-DS-4	a	34.87	34.53 ± 0.32	1.99	1.96 ± 0.03
	b	34.23		1.94	
	c	34.49		1.96	

a – Degree of substitution abbreviated as DS

The FT-IR spectra of each sample were analysed with the relevant baselines to determine the necessary peak heights and areas under the curve (Table G.18). The calibration parameters (Table G.19) were then calculated to determine the four calibration curves illustrated in Figure G.3.

Table G.18 Peak Height and Areas under the Curve from Fourier Transform Infrared Spectra for developing Calibration Curves of Degree of Substitution of Corncob

Calibration Sample Identification	H_{1370}	H_{1060}	H_{1740}	A_{1740}	A_{1370}
CC-DS-1	0.039	0.229	0.047	2.482	0.763
CC-DS-2	0.066	0.132	0.140	5.019	1.166
CC-DS-3	0.077	0.168	0.163	6.074	1.487
CC-DS-4	0.145	0.274	0.329	11.839	2.759

Table G.19 Calculated Parameters for the Calibration Curves of Degree of Substitution of Corncob

Calibration Sample Identification	Average Acetyl Content (%)	A_{1740}/H_{1060}	H_{1740}/H_{1060}	A_{1370}/H_{1060}	H_{1370}/H_{1060}
CC-DS-1	9.00 ± 0.26	10.838	0.205	3.332	0.170
CC-DS-2	27.28 ± 0.59	38.023	1.061	8.833	0.500
CC-DS-3	30.42 ± 0.19	36.155	0.970	8.851	0.458
CC-DS-4	34.53 ± 0.32	43.208	1.201	10.069	0.529

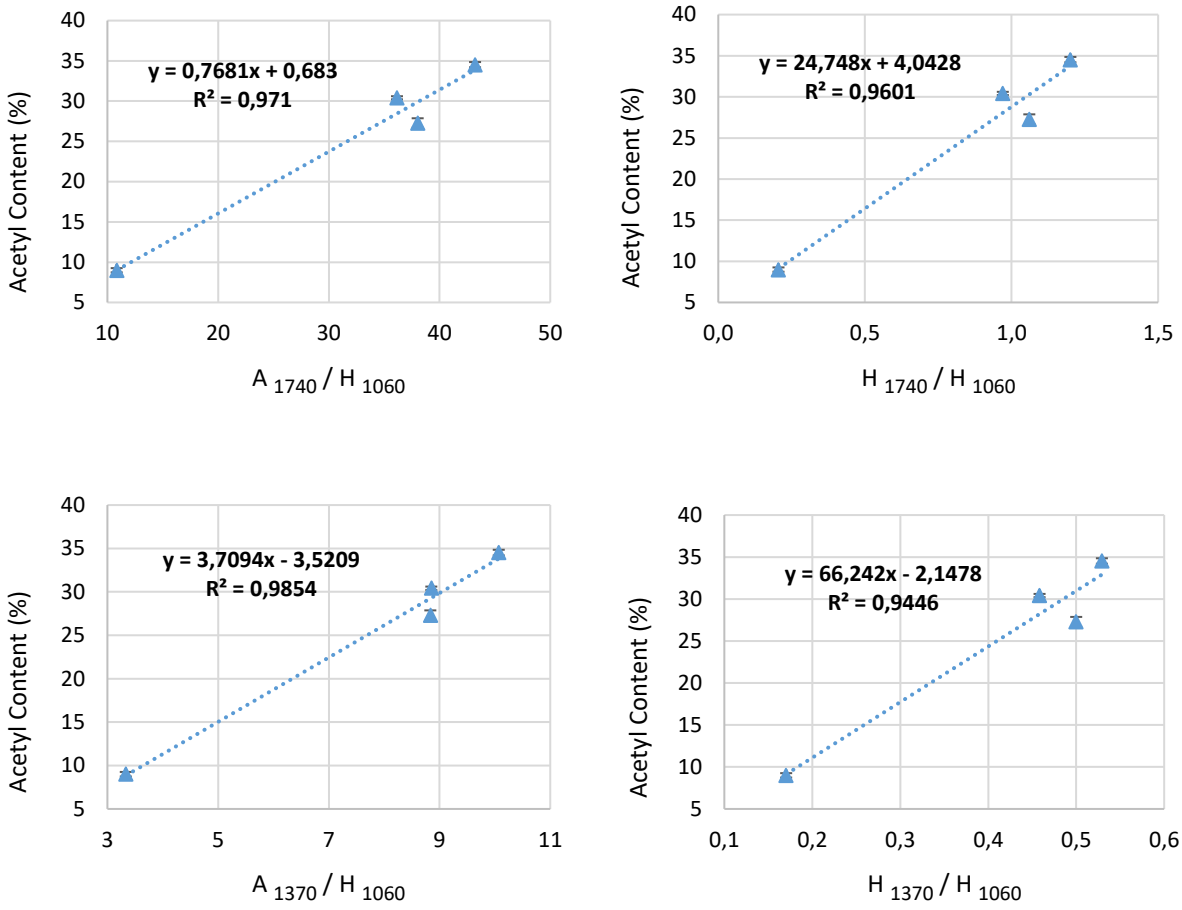

Figure G.3 Calibration Curves for Degree of Substitution of Corncob

In order to validate the DS calibration curves for CC, the following two randomly selected samples were utilised from the *green* CC biomass modification (Table G.20). The titrations were completed for each validation sample (Table G.21 and Table G.22).

Table G.20 Selected Samples for Validation of Degree of Substitution Calibration Curves of Corncob

Validation Sample Identification	Modification Sample ID [a]
CC-DS Validation 1	CC-B2-4
CC-DS Validation 2	CC-B2-12

a – See Section 4.2.2 for details of individual samples

Table G.21 Experimental Titration of Samples for Validation of Degree of Substitution Calibration Curves of Corncob

Validation Sample Identification	Repeat	Mass (g)	HCl Titration Volume (mL)	NaOH Titration Volume (mL)
CC-DS Validation 1	a	0.5021	6.4	1.0
	b	0.4999	6.9	1.0
	c	0.5002	6.6	1.0
CC-DS Validation 2	a	0.5017	3.9	1.0
	b	0.5088	3.8	1.1
	c	0.5039	3.6	1.0

Table G.22 Experimental Validation of the Average Acetyl Content and Degree of Substitution for Corncob Calibration Curves

Validation Sample Identification	Repeat	Acetyl Content (%)	Average Acetyl Content (%)	DS [a]	Average DS [a]
CC-DS Validation 1	a	17.86	16.91 ± 1.05	0.82	0.76 ± 0.06
	b	15.79		0.70	
	c	17.07		0.77	
CC-DS Validation 2	a	28.60	29.14 ± 0.58	1.50	1.53 ± 0.04
	b	29.05		1.53	
	c	29.76		1.58	

a – Degree of substitution abbreviated as DS

The FT-IR spectra of each sample were analysed with the relevant baselines to determine the necessary peak heights and areas under the curve (Table G.23). The calibration parameters (Table G.24) were then calculated to compare the theoretical and experimental values (Table G.25 and Table G.26).

Table G.23 Peak Height and Areas under the Curve from Fourier Transform Infrared Spectra for Validating Calibration Curves of Degree of Substitution of Corncob

Validation Sample Identification	H_{1370}	H_{1060}	H_{1740}	A_{1740}	A_{1370}
CC-DS Validation 1	0.055	0.186	0.093	3.437	0.895
CC-DS Validation 2	0.091	0.213	0.187	7.470	1.935

Table G.24 Calculated Parameters for the Validation of Calibration Curves of Degree of Substitution of Corncob

Validation Sample Identification	A_{1740}/H_{1060}	H_{1740}/H_{1060}	A_{1370}/H_{1060}	H_{1370}/H_{1060}
CC-DS Validation 1	18.4785	0.5000	4.8118	0.2957
CC-DS Validation 2	35.0704	0.8779	9.0845	0.4272

Table G.25 A Comparison between the Theoretical and Experimental Degree of Substitution for CC-DS Validation 1

Validation Sample Identification	Experimental [a]	Theoretical [b]	Error [c] (%)
Acetyl Content (%)	16.91 ± 1.05	15.77 ± 1.42	7.24
DS [d]	0.76 ± 0.06	0.70 ± 0.08	8.59

a – Determined by titration; **b** – Determined with calibration curves; **c** – Percentage error based on average values; **d** – Degree of substitution abbreviated as DS

Table G.26 A Comparison between the Theoretical and Experimental Degree of Substitution for CC-DS Validation 2

Validation Sample	Experimental [a]	Theoretical [b]	Error [c] (%)
Acetyl Content (%)	29.14 ± 0.58	27.43 ± 2.00	6.22
DS [d]	1.53 ± 0.04	1.41 ± 0.14	8.50

a – Determined by titration; **b** – Determined with calibration curves; **c** – Percentage error based on average values; **d** – Degree of substitution abbreviated as DS

Since these errors (Table G.25 and Table G.26) are less than 10 %, the models are accepted. The acetyl contents of the samples can thus be calculated by the following equations, with H_{1060}, H_{1370}, H_{1740}, A_{1740} and A_{1370} as the relevant peak heights and areas under the curve, as obtained from the FT-IR with the respective baselines. An average of the four results is used as the acetyl content of each sample.

$$Acetyl\ Content\ (\%) = 0.77\left(\frac{A_{1740}}{H_{1060}}\right) + 0.68\ ;R^2 = 0.97 \quad [G.5]$$

$$Acetyl\ Content\ (\%) = 24.75\left(\frac{H_{1740}}{H_{1060}}\right) + 4.04\ ;R^2 = 0.96 \quad [G.6]$$

$$Acetyl\ Content\ (\%) = 3.71\left(\frac{A_{1370}}{H_{1060}}\right) - 3.52\ ;R^2 = 0.99 \quad [G.7]$$

$$Acetyl\ Content\ (\%) = 66.24\left(\frac{H_{1370}}{H_{1060}}\right) - 2.15\ ;R^2 = 0.94 \quad [G.8]$$

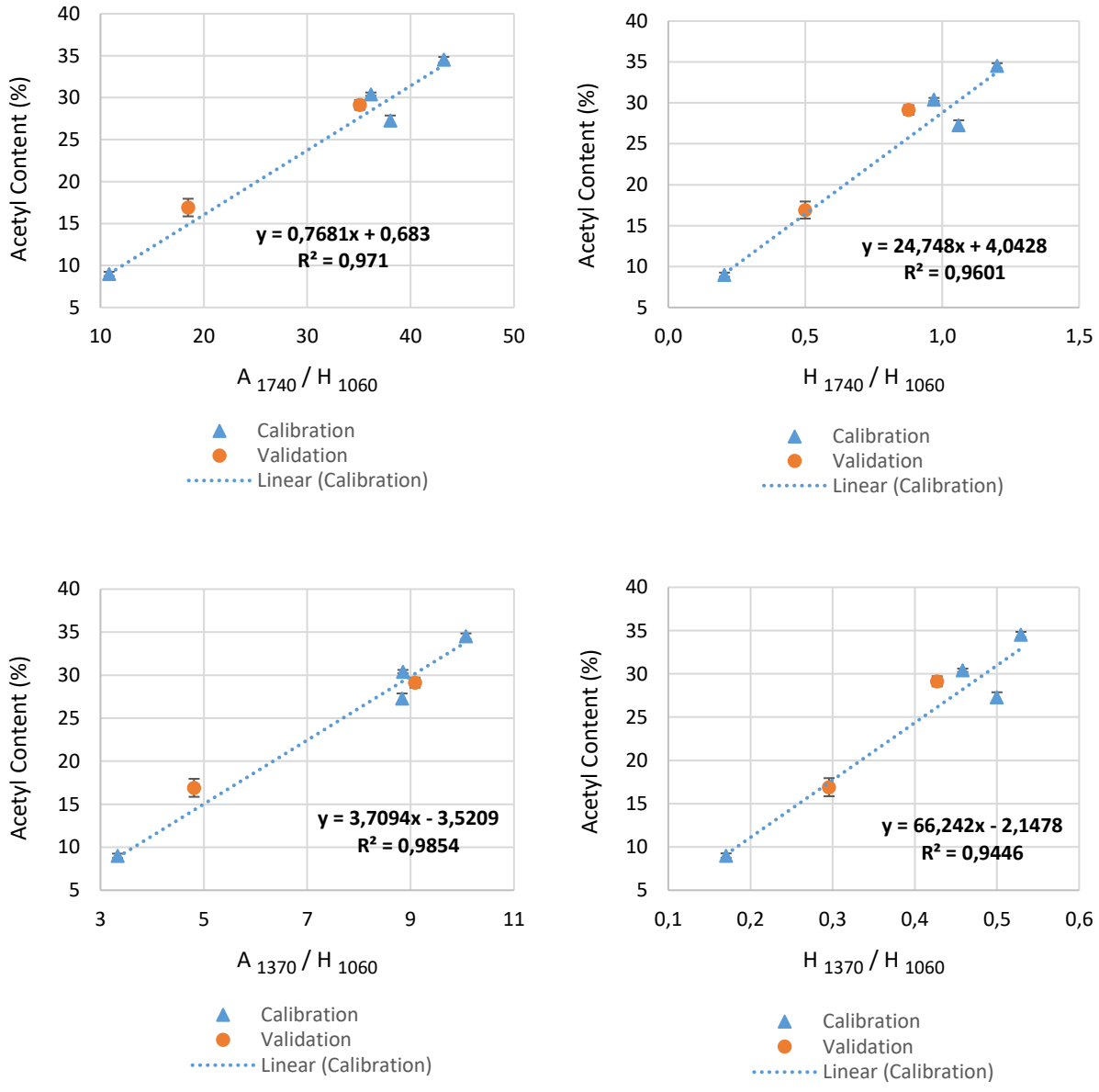

Figure G.4 Calibration Curves and Validation Points for Degree of Substitution of Corncob

G.3 Cellulose Calibration Curves

Calibration curves for the DS of cellulose were developed by utilising five samples from the *non-green* cotton modification. The samples selected for calibration curve development are summarised in Table G.27. These calibration curves were also applied to calculate the DS attained with filter paper, corncob (CC) cellulose and wheat straw (WS) cellulose.

Table G.27 Selected Samples for Degree of Substitution Calibration Curves of Cotton

Calibration Sample Identification	Modification Sample [a]	Expected DS [b] Quality
COT-DS-0	Unmodified Cotton	≈ 0 [c]
COT-DS-1	CO-C1-6	Low
COT-DS-2	CO-C1-1	Medium
COT-DS-3	CO-C1-7	High
COT-DS-4	CO-C1-2	Very High

a – See Section 5.2.4 individual sample details; **b** – Degree of substitution abbreviated as DS; **c** – Assume unmodified samples contain negligible acetyl groups

Titrations were completed for the unmodified cotton sample ("*blank* sample", Table G.28) and each calibration sample (Table G.29 and Table G.30).

Table G.28 Titrations of *Blank* Sample for Degree of Substitution Calibration Curves of Cotton

Calibration Sample Identification	Repeat	Mass (g)	HCl Titration Volume (mL)	NaOH Titration Volume (mL)
COT-DS-0	a	0.5001	13.8	1.9
	b	0.5023	14.2	2.0
	c	0.5059	12.8	2.1
	Average	0.5028 ± 0.0029	13.6 ± 0.7	2.0 ± 0.1

Table G.29 Experimental Titration of Samples for the Degree of Substitution Calibration Curves of Cotton

Calibration Sample Identification	Repeat	Mass (g)	HCl Titration Volume (mL)	NaOH Titration Volume (mL)
COT-DS-1	a	0.5012	11.9	2.1
	b	0.5004	11.6	1.7
	c	0.5026	11.3	1.9
COT-DS-2	a	0.5011	8.1	1.9
	b	0.5026	7.5	2.1
	c	0.5008	8.1	1.8
COT-DS-3	a	0.5014	6.6	1.7
	b	0.5032	6.2	1.8
	c	0.5066	6.1	1.6
COT-DS-4	a	0.5042	4.4	1.4
	b	0.5029	4.1	1.2
	c	0.5017	4.2	1.1

Table G.30 Average Acetyl Content and Degree of Substitution for Calibration Curves of Cotton

Calibration Sample Identification	Repeat	Acetyl Content (%)	Average Acetyl Content (%)	DS [a]	Average DS [a]
COT-DS-1	a	7.73	8.16 ± 1.12	0.32	0.33 ± 0.05
	b	7.31		0.30	
	c	9.42		0.39	
COT-DS-2	a	23.20	24.18 ± 2.07	1.13	1.19 ± 0.14
	b	26.55		1.35	
	c	22.78		1.10	
COT-DS-3	a	28.76	29.91 ± 1.04	1.51	1.59 ± 0.08
	b	30.80		1.66	
	c	30.17		1.61	
COT-DS-4	a	36.71	36.81 ± 0.39	2.16	2.17 ± 0.04
	b	37.24		2.20	
	c	36.47		2.13	

a – Degree of substitution abbreviated as DS

The FT-IR spectra of each sample were analysed with the relevant baselines to determine the necessary peak heights and areas under the curve (Table G.31). The calibration parameters (Table G.32) were then calculated to determine the four calibration curves illustrated in Figure G.5.

Table G.31 Peak Height and Areas under the Curve from Fourier Transform Infrared Spectra for developing Calibration Curves of Degree of Substitution of Cotton

Calibration Sample Identification	H_{1370}	H_{1060}	H_{1740}	A_{1740}	A_{1370}
COT-DS-1	0.017	0.083	0.017	0.258	0.166
COT-DS-2	0.027	0.082	0.061	2.032	0.489
COT-DS-3	0.091	0.184	0.214	7.84	1.970
COT-DS-4	0.027	0.048	0.070	2.494	0.658

Table G.32 Calculated Parameters for the Calibration Curves of Degree of Substitution of Cotton

Calibration Sample Identification	Average Acetyl Content (%)	A_{1740}/H_{1060}	H_{1740}/H_{1060}	A_{1370}/H_{1060}	H_{1370}/H_{1060}
COT-DS-1	8.16 ± 1.12	3.108	0.205	2.000	0.205
COT-DS-2	24.18 ± 2.07	24.780	0.744	5.963	0.329
COT-DS-3	29.91 ± 1.04	42.609	1.163	10.707	0.495
COT-DS-4	36.81 ± 0.39	51.958	1.458	13.708	0.563

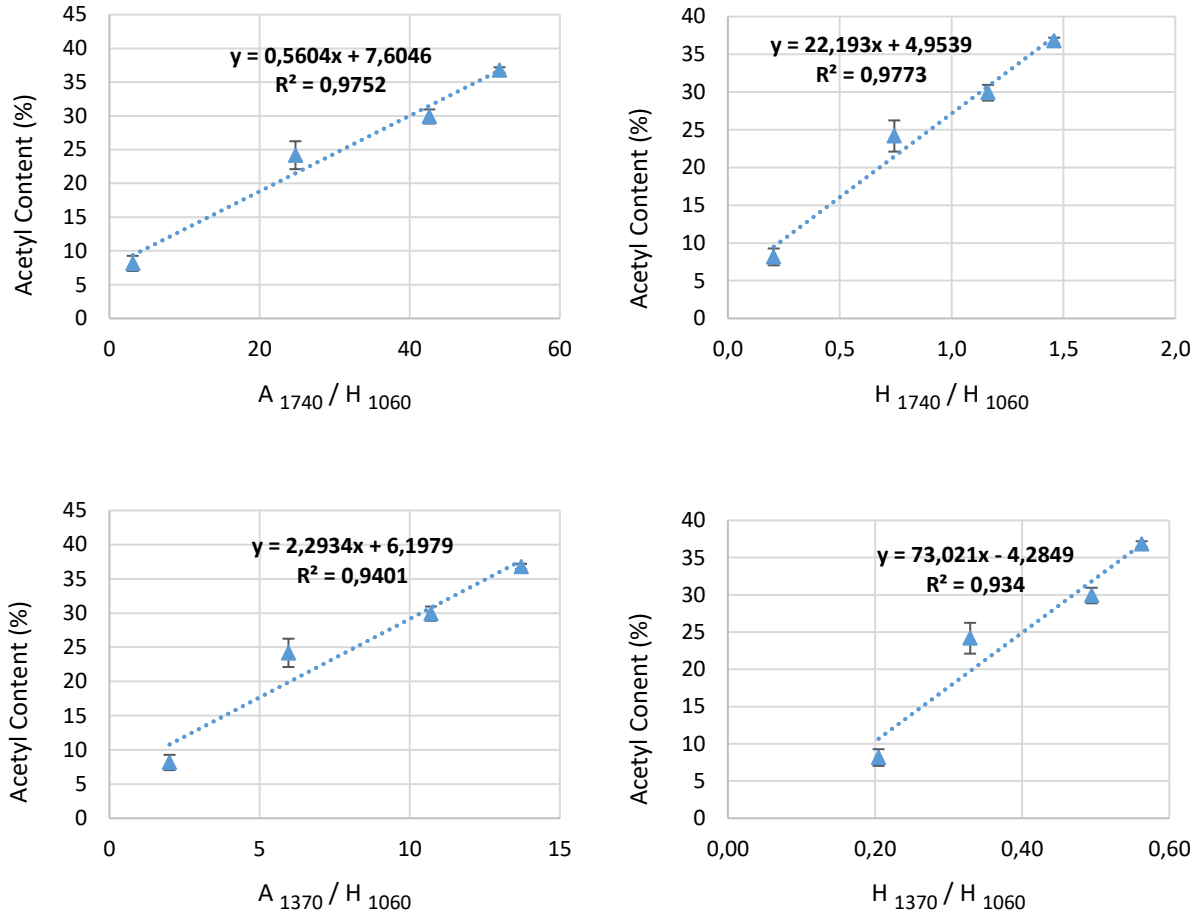

Figure G.5 Calibration Curves for Degree of Substitution of Cotton

In order to validate the DS calibration curves for cotton, the following two randomly selected samples were utilised from the *non-green* cotton modification (Table G.33). The titrations were completed for each validation sample (Table G.34 and Table G.35).

Table G.33 Selected Samples for Validation of Degree of Substitution Calibration Curves of Cotton

Validation Sample Identification	Modification Sample ID [a]
COT-DS Validation 1	CO-C1-4
COT-DS Validation 2	CO-C1-5

a – See Section 5.2.4 individual sample details

Table G.34 Experimental Titration of Samples for Validation of Degree of Substitution Calibration Curves of Cotton

Validation Sample Identification	Repeat	Mass (g)	HCl Titration Volume (mL)	NaOH Titration Volume (mL)
COT-DS Validation 1	a	0.5012	5.6	2.5
	b	0.5036	6.1	2.6
	c	0.5002	5.7	2.5
COT-DS Validation 2	a	0.5081	8.1	1.9
	b	0.5003	7.7	1.8
	c	0.5024	7.6	1.6

Table G.35 Experimental Validation of the Average Acetyl Content and Degree of Substitution for Cotton Calibration Curves

Validation Sample Identification	Repeat	Acetyl Content (%)	Average Acetyl Content (%)	DS [a]	Average DS a
COT-DS Validation 1	a	36.50	35.76 ± 1.00	2.14	2.07 ± 0.09
	b	34.62		1.97	
	c	36.15		2.11	
COT-DS Validation 2	a	22.88	23.80 ± 0.84	1.11	1.17 ± 0.05
	b	24.52		1.21	
	c	23.99		1.18	

a – Degree of substitution abbreviated as DS

The FT-IR spectra of each sample were analysed with the relevant baselines to determine the necessary peak heights and areas under the curve (Table G.36). The calibration parameters (Table G.37) were then calculated to compare the theoretical and experimental values (Table G.38 and Table G.39).

Table G.36 Peak Height and Areas under the Curve from Fourier Transform Infrared Spectra for Validating Calibration Curves of Degree of Substitution of Cotton

Validation Sample Identification	H_{1370}	H_{1060}	H_{1740}	A_{1740}	A_{1370}
COT-DS Validation 1	0.024	0.044	0.066	2.246	0.585
COT-DS Validation 2	0.055	0.134	0.127	4.464	1.08

Table G.37 Calculated Parameters for the Validation of Calibration Curves of Degree of Substitution of Cotton

Validation Sample Identification	A_{1740}/H_{1060}	H_{1740}/H_{1060}	A_{1370}/H_{1060}	H_{1370}/H_{1060}
COT-DS Validation 1	51.045	1.500	13.295	0.545
COT-DS Validation 2	33.313	0.948	8.060	0.410

Table G.38 Comparison between the Theoretical and Experimental Degree of Substitution for COT-DS Validation 1

Validation Sample Identification	Experimental [a]	Theoretical [b]	Error [c] (%)
Acetyl Content (%)	35.76 ± 1.00	36.67 ± 1.15	2.49
DS [d]	2.07 ± 0.09	2.15 ± 0.11	3.85

a – Determined by titration; **b** – Determined with calibration curves; **c** – Percentage error based on average values; **d** – Degree of substitution abbreviated as DS

Table G.39 Comparison between the Theoretical and Experimental Degree of Substitution for COT-DS Validation 2

Validation Sample Identification	Experimental [a]	Theoretical [b]	Error [c] (%)
Acetyl Content (%)	23.80 ± 0.84	25.66 ± 0.69	7.25
DS [d]	1.17 ± 0.05	1.29 ± 0.05	9.44

a – Determined by titration; **b** – Determined with calibration curves; **c** – Percentage error based on average values; **d** – Degree of substitution abbreviated as DS

Since these errors (Table G.38 and Table G.39) are less than 10 %, the models are accepted. The acetyl contents of the samples can thus be calculated by the following equations, with H_{1060}, H_{1370}, H_{1740}, A_{1740} and A_{1370} as the relevant peak heights and areas under the curve, as obtained from the FT-IR with the respective baselines. An average of the four results is used as the acetyl content of each sample.

$$Acetyl\ Content\ (\%) = 0.56\left(\frac{A_{1740}}{H_{1060}}\right) + 7.60\ ; R^2 = 0.98 \quad [G.9]$$

$$Acetyl\ Content\ (\%) = 22.19\left(\frac{H_{1740}}{H_{1060}}\right) + 4.95\ ; R^2 = 0.98 \quad [G.10]$$

$$Acetyl\ Content\ (\%) = 2.29\left(\frac{A_{1370}}{H_{1060}}\right) + 6.20\ ; R^2 = 0.94 \quad [G.11]$$

$$Acetyl\ Content\ (\%) = 73.02\left(\frac{H_{1370}}{H_{1060}}\right) - 4.28\ ; R^2 = 0.93 \quad [G.12]$$

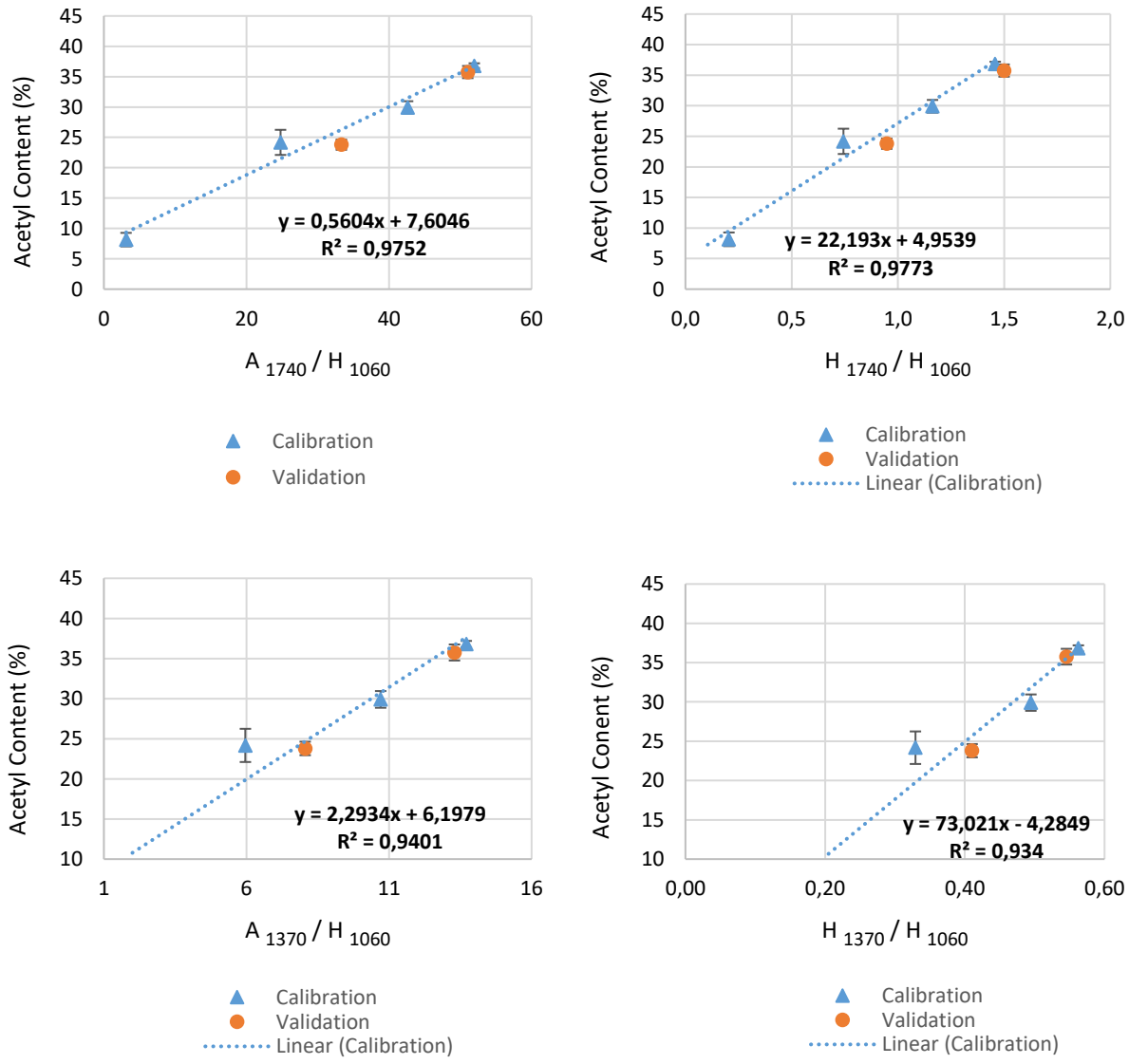

Figure G.6 Calibration Curves and Validation Points for Degree of Substitution of Cotton

G.4 Nanofibrillated Cellulose Calibration Curves

Calibration curves for the DS of nanofibrillated cellulose (NFC) were developed by utilising five samples from the *non-green* commercial NFC modification. The samples selected for calibration curve development are summarised in Table G.40. These calibration curves were also applied to calculate the DS achieved on corncob (CC) NFC and wheat straw (WS) NFC.

Table G.40 Selected Samples for Degree of Substitution Calibration Curves of Commercial Nanofibrillated Cellulose

Calibration Sample Identification	Modification Sample [a]	Expected DS [b] Quality
NFC-DS-0	Unmodified CN NFC	≈ 0 [c]
NFC-DS-1	CN-N1-9	Low
NFC-DS-2	CN-N1-3	Medium
NFC-DS-3	CN-N1-5	High
NFC-DS-4	CN-N1-1	Very High

a – See Section 6.2.4 individual sample details; **b** – Degree of substitution abbreviated as DS; **c** – Assume unmodified samples contain negligible acetyl groups

Titrations were completed for the unmodified NFC sample ("*blank* sample", Table G.41) and each calibration sample (Table G.42 and Table G.43).

Table G.41 Titrations of *Blank* Sample for Degree of Substitution Calibration Curves of Commercial Nanofibrillated Cellulose

Calibration Sample Identification	Repeat	Mass (g)	HCl Titration Volume (mL)	NaOH Titration Volume (mL)
NFC-DS-0	a	0.1025	5.5	1
	b	0.1032	5.6	1.1
	c	0.1029	5.1	1
	Average	0.1029 ± 0.0004	5.40 ± 0.26	1.03 ± 0.06

Table G.42 Experimental Titration of Samples for the Degree of Substitution Calibration Curves of Commercial Nanofibrillated Cellulose

Calibration Sample Identification	Repeat	Mass (g)	HCl Titration Volume (mL)	NaOH Titration Volume (mL)
NFC-DS-1	a	0.1055	4.8	1
	b	0.1003	4.9	1.1
	c	0.1056	5.0	1
NFC-DS-2	a	0.1025	4.7	1
	b	0.1014	4.6	1
	c	0.1079	4.6	1.1
NFC-DS-3	a	0.1039	4.5	1
	b	0.1011	4.4	1
	c	0.1009	4.6	1.1
NFC-DS-4	a	0.1027	4.3	1.1
	b	0.1099	4.4	1
	c	0.1003	4.2	1

Table G.43 Average Acetyl Content and Degree of Substitution for Calibration Curves of Commercial Nanofibrillated Cellulose

Calibration Sample Identification	Repeat	Acetyl Content (%)	Average Acetyl Content (%)	DS [a]	Average DS [a]
NFC-DS-1	a	11.56	10.40 ± 2.55	0.49	0.44 ± 0.12
	b	12.16		0.52	
	c	7.47		0.30	
NFC-DS-2	a	14.00	15.85 ± 1.68	0.61	0.71 ± 0.09
	b	16.27		0.73	
	c	17.29		0.78	
NFC-DS-3	a	17.95	19.01 ± 1.39	0.82	0.88 ± 0.08
	b	20.58		0.97	
	c	18.49		0.85	
NFC-DS-4	a	24.45	22.81 ± 3.37	1.21	1.11 ± 0.21
	b	18.93		0.88	
	c	25.04		1.25	

a – Degree of substitution abbreviated as DS

The FT-IR spectra of each sample were analysed with the relevant baselines to determine the necessary peak heights and areas under the curve (Table G.44). The calibration parameters (Table G.45) were then calculated to determine the four calibration curves illustrated in Figure G.7.

Table G.44 Peak Height and Areas under the Curve from Fourier Transform Infrared Spectra for developing Calibration Curves of Degree of Substitution of Commercial Nanofibrillated Cellulose

Calibration Sample Identification	H_{1370}	H_{1060}	H_{1740}	A_{1740}	A_{1370}
NFC-DS-1	0.049	0.341	0.031	0.906	0.460
NFC-DS-2	0.076	0.458	0.068	2.259	0.738
NFC-DS-3	0.069	0.335	0.084	2.759	0.848
NFC-DS-4	0.032	0.137	0.050	1.707	0.459

Table G.45 Calculated Parameters for the Calibration Curves of Degree of Substitution of Commercial Nanofibrillated Cellulose

Calibration Sample Identification	Average Acetyl Content (%)	A_{1740}/H_{1060}	H_{1740}/H_{1060}	A_{1370}/H_{1060}	H_{1370}/H_{1060}
NFC-DS-1	10.40 ± 2.55	2.657	0.091	1.349	0.144
NFC-DS-2	15.85 ± 1.68	4.932	0.148	1.611	0.166
NFC-DS-3	19.01 ± 1.39	8.236	0.251	2.531	0.206
NFC-DS-4	22.81 ± 3.37	12.460	0.365	3.350	0.234

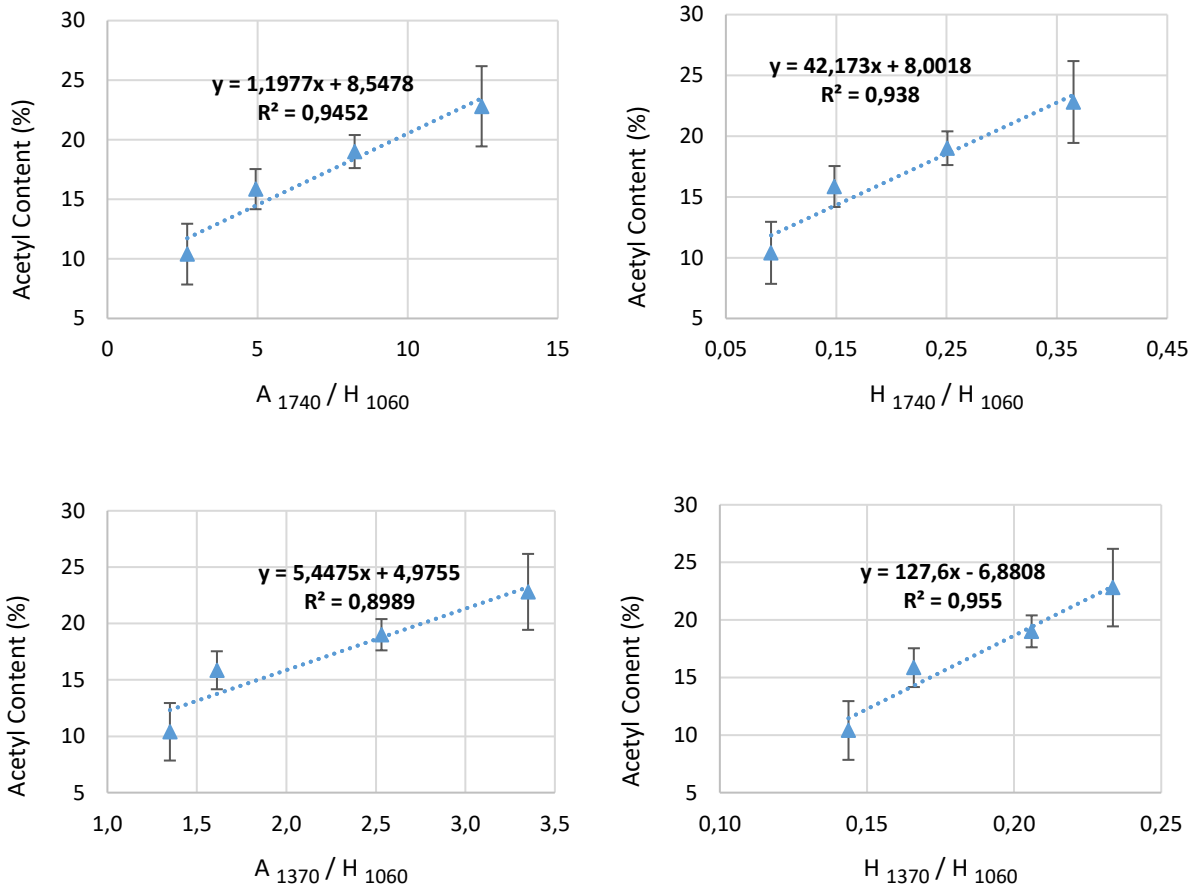

Figure G.7 Calibration Curves for Degree of Substitution of Commercial Nanofibrillated Cellulose

In order to validate the DS calibration curves for commercial NFC, the following two randomly selected samples are utilised from the *non-green* commercial NFC modification (Table G.46). The titrations were completed for each validation sample (Table G.47 and Table G.48).

Table G.46 Selected Samples for Validation of Degree of Substitution Calibration Curves of Commercial Nanofibrillated Cellulose

Validation Sample Identification	Modification Sample ID [a]
NFC-DS Validation 1	CN-N1-6
NFC-DS Validation 2	CN-N1-2

a – See Section 6.2.4 individual sample details

Table G.47 Experimental Titration of Samples for Validation of Degree of Substitution Calibration Curves of Commercial Nanofibrillated Cellulose

Validation Sample Identification	Repeat	Mass (g)	HCl Titration Volume (mL)	NaOH Titration Volume (mL)
NFC-DS Validation 1	a	0.1054	4.7	1.0
	b	0.1009	4.8	1.1
	c	0.1026	4.7	1.1
NFC-DS Validation 2	a	0.1031	4.5	1.0
	b	0.1004	4.5	1.0
	c	0.1025	4.6	1.1

Table G.48 Experimental Validation of the Average Acetyl Content and Degree of Substitution for Commercial Nanofibrillated Cellulose Calibration Curves

Validation Sample Identification	Repeat	Acetyl Content (%)	Average Acetyl Content (%)	DS [a]	Average DS [a]
NFC-DS Validation 1	a	13.61	14.64 ± 1.29	0.59	0.64 ± 0.07
	b	14.22		0.62	
	c	16.08		0.72	
NFC-DS Validation 2	a	18.09	18.29 ± 0.26	0.83	0.84 ± 0.01
	b	18.58		0.86	
	c	18.20		0.83	

a – Degree of substitution abbreviated as DS

The FT-IR spectra of each sample were analysed with the relevant baselines to determine the necessary peak heights and areas under the curve (Table G.49). The calibration parameters (Table G.50) were then calculated to compare the theoretical and experimental values (Table G.51 and Table G.52).

Table G.49 Peak Heights and Areas under the Curve from Fourier Transform Infrared Spectra for Validating Calibration Curves of Degree of Substitution of Commercial Nanofibrillated Cellulose

Validation Sample Identification	H_{1370}	H_{1060}	H_{1740}	A_{1740}	A_{1370}
NFC-DS Validation 1	0.042	0.241	0.045	1.244	0.466
NFC-DS Validation 2	0.060	0.288	0.078	2.722	0.718

Table G.50 Calculated Parameters for the Validation of Calibration Curves of Degree of Substitution of Commercial Nanofibrillated Cellulose

Validation Sample Identification	A_{1740}/H_{1060}	H_{1740}/H_{1060}	A_{1370}/H_{1060}	H_{1370}/H_{1060}
NFC-DS Validation 1	5.162	0.187	1.934	0.174
NFC-DS Validation 2	9.451	0.271	2.493	0.208

Table G.51 Comparison between the Theoretical and Experimental Degree of Substitution for NFC-DS Validation 1

Validation Sample Identification	Experimental [a]	Theoretical [b]	Error [c] (%)
Acetyl Content (%)	14.64 ± 1.29	15.37 ± 0.48	4.73
DS [d]	0.64 ± 0.07	0.68 ± 0.02	5.44

a – Determined by titration; **b** – Determined with calibration curves; **c** – Percentage error based on average values; **d** – Degree of substitution abbreviated as DS

Table G.52 Comparison between the Theoretical and Experimental Degree of Substitution for NFC-DS Validation 2

Validation Sample Identification	Experimental [a]	Theoretical [b]	Error [c] (%)
Acetyl Content (%)	18.29 ± 0.26	19.39 ± 0.58	5.65
DS [d]	0.84 ± 0.01	0.90 ± 0.03	6.90

a – Determined by titration; **b** – Determined with calibration curves; **c** – Percentage error based on average values; **d** – Degree of substitution abbreviated as DS

Since these errors (Table G.51 and Table G.52) are less than 10 %, the models are accepted. The acetyl contents of the samples can thus be calculated by the following equations, with H_{1060}, H_{1370}, H_{1740}, A_{1740} and A_{1370} as the relevant peak heights and areas under the curve, as obtained from the FT-IR with the respective baselines. An average of the four results is used as the acetyl content of each sample.

$$Acetyl\ Content\ (\%) = 1.20\left(\frac{A_{1740}}{H_{1060}}\right) + 8.55\ ;R^2 = 0.95 \quad [G.13]$$

$$Acetyl\ Content\ (\%) = 42.17\left(\frac{H_{1740}}{H_{1060}}\right) + 8.00\ ;R^2 = 0.94 \quad [G.14]$$

$$Acetyl\ Content\ (\%) = 5.45\left(\frac{A_{1370}}{H_{1060}}\right) + 4.98\ ;R^2 = 0.90 \quad [G.15]$$

$$Acetyl\ Content\ (\%) = 127.6\left(\frac{H_{1370}}{H_{1060}}\right) - 6.88\ ;R^2 = 0.96 \quad [G.16]$$

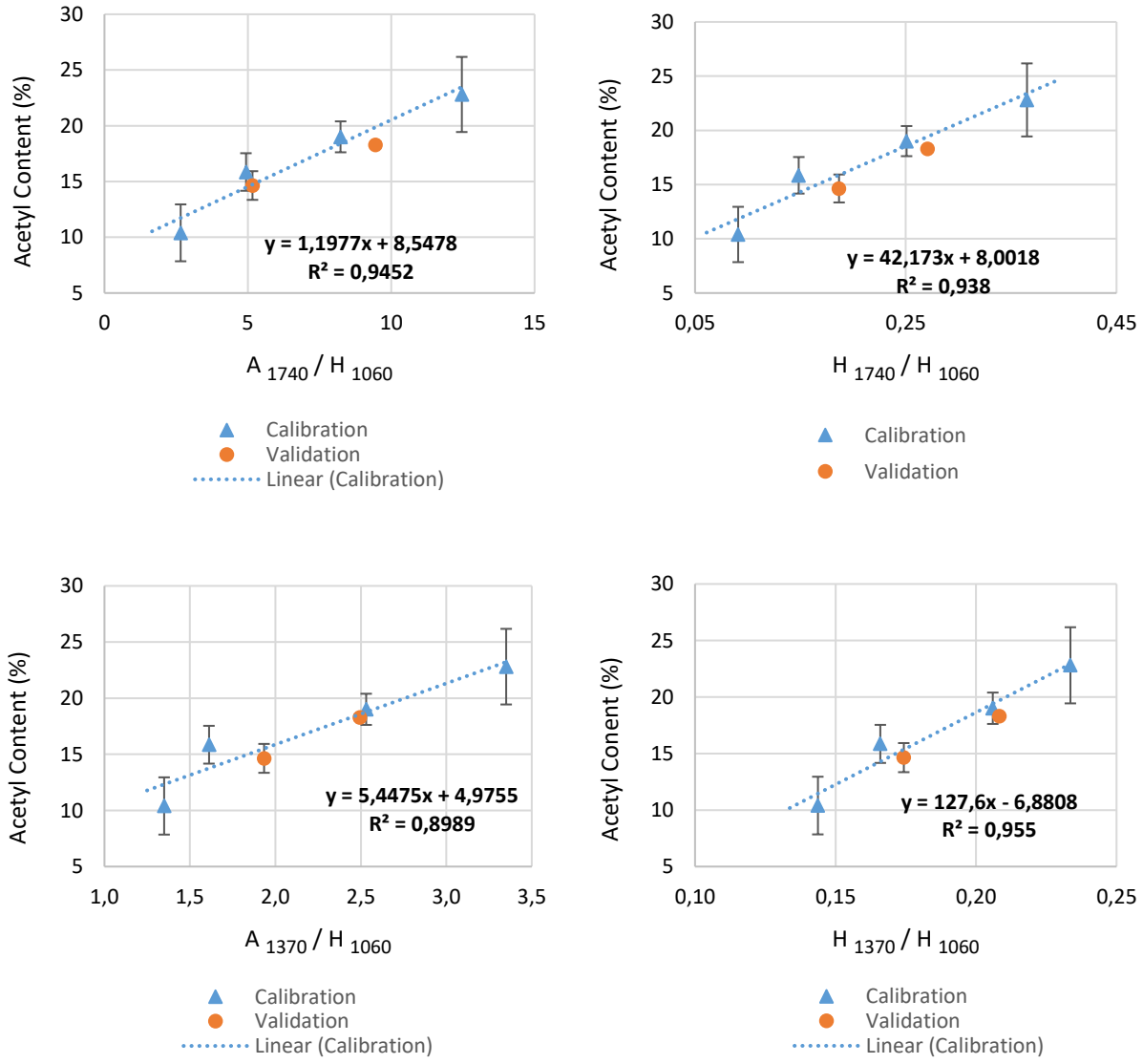

Figure G.8 Calibration Curves and Validation Points for Degree of Substitution of Commercial Nanofibrillated Cellulose

Appendix H – Selection of Optimal Oil Sorbent

The primary aim of this study entailed developing a process for the production of bio-based sorbents from corncob (CC) and wheat straw (WS), and their respective cellulose and nanofibrillated cellulose (NFC) constituents which are functionalised via different *green* methods to increase the selective sorption of oil in contaminated water. In order for these biosorbents to qualify as materials that successfully remove oil from water in a *green* way, a defined list of key performance indicators needed to be met:

1. Sustainable, abundantly available, biodegradable sources (Deschamps et al., 2003; Liu et al., 2017) such as the agricultural waste crops, CC and WS, needs to be implemented.

2. The fibres need to be modified to have a selective affinity towards oil particles rather than water particles (Deschamps et al., 2003; Liu et al., 2017).

3. This modification needs to be conducted in a way that does not make use of toxic chemicals and does not contribute to environmental pollution or increased carbon dioxide emissions.

4. A low density is favoured since a buoyant sorbent allows simpler application in water treatment systems (Deschamps et al., 2003; Liu et al., 2017).

5. A higher porosity leads to a higher possible sorption capacity (Liu et al., 2017) since the oil particles can be retained in the material matrix structure (Deschamps et al., 2003).

6. The product should be biodegradable (Deschamps et al., 2003), and the implementation of the biosorbent should not adversely affect the living organisms that it comes into contact with.

All samples satisfied the criterion of a sustainable, abundant, biodegradable source material since CC and WS were utilised for biosorbent production. No synthetic polymers or other chemicals were present in the products.

The modified products (*green* and *non-green*) correspondingly remained biodegradable (Deschamps et al., 2003) and the biosorbents were adequately washed with distilled water until a filtrate pH of 7 was reached, indicating that all acetic anhydride reactants and acetic acid by-products were removed from the samples after modification. All chemicals were washed out of the biosorbents, with the exception of the *green* NFC modification (Section 6.3.2). The enzyme could not be adequately removed from the final sample, and it was determined that the lipase proteins had formed a stable bond with the NFC during the reaction (Bozic et al., 2015). However, Bozic et al. (2015) additionally proved that these stable acyl-enzyme complex molecules were acetylated and therefore contributed to the OS capacities of the particles. Since these protein molecules are bound to the biosorbent, these constituents will not be released during OS applications and thus pose no threat to the environment.

The biosorbents, therefore, needed to be compared based on Criteria 2 – 5. The following ratings in Table H.1 were assigned in order to compare their attributes directly.

Table H.1 Ratings Assigned to Different Critical Quality Attributes for Application as Sufficient, Sustainable Biosorbents

Criteria	Attribute	Favoured Quality	Ratings Assigned
2	Selective affinity towards OS [a]	Higher value favoured	Use heterogeneous OS; Convert to a percentage, based on the highest value in modification group
3	Environmentally Friendly Modification	*Green* favoured	100 % = *Green* Modification 0 % = *Non-green* Modification
4	Density	Low density favoured	Use density measurements; Convert to a percentage, based on the highest value in modification group
5	Porosity	High porosity favoured	Use porosity measurements; Convert to a percentage, based on the highest value in modification group

a – OS represents Oil Sorption

The ratings in Table H.1 were assigned to the *green* and *non-green* modified CC and WS biomass, cellulose and NFC samples. Figure H.1 I and II were utilised to compare the modified and unmodified CC and WS biomass biosorbents, and the summary of these ratings are displayed in Table H.2. The unmodified samples were classified as environmentally friendly, but lacked a selective affinity for OS.

Table H.2 Summary of Ratings Assigned to Modified and Unmodified Corncob and Wheat Straw Biosorbents by Comparison of Radar Graphs

Source [a]	Sample	Environmentally Friendly Modification	Highest Selective Affinity towards OS [b]	Rating
CC	Unmodified	✓	×	1/2
	***Green* Modified**	✓	×	**1/2**
	Non-green Modified	×	✓	1/2
WS	Unmodified	✓	×	1/2
	***Green* Modified**	✓	✓	**2/2**
	Non-green Modified	×	✓	1/2

a – Corncob is abbreviated as CC, while wheat straw is abbreviated as WS; **b –** OS represents Oil Sorption

The *non-green* CC exhibited a higher selective OS (20.46 ± 1.42 g/g) when compared to the OS (6.82 ± 2.30 g/g and 18.39 ± 0.12 g/g) of the unmodified and *green* CC samples. However, since toxic chemicals were employed in the modification, the biosorbent can not be classified as *green*. Moreover, the *green* WS biosorbents had comparable selective OS (16.91 ± 0.42 g/g) to the *non-green* WS sorbents (17.12 ± 1.95 g/g). These samples demonstrated an increased OS selectivity when compared to the unmodified WS (8.52 ± 0.12 g/g). Since an environmentally friendly modification is favoured above a non-environmentally friendly method, the *green* CC and WS biosorbents are classified as the best sorbents in the biomass category.

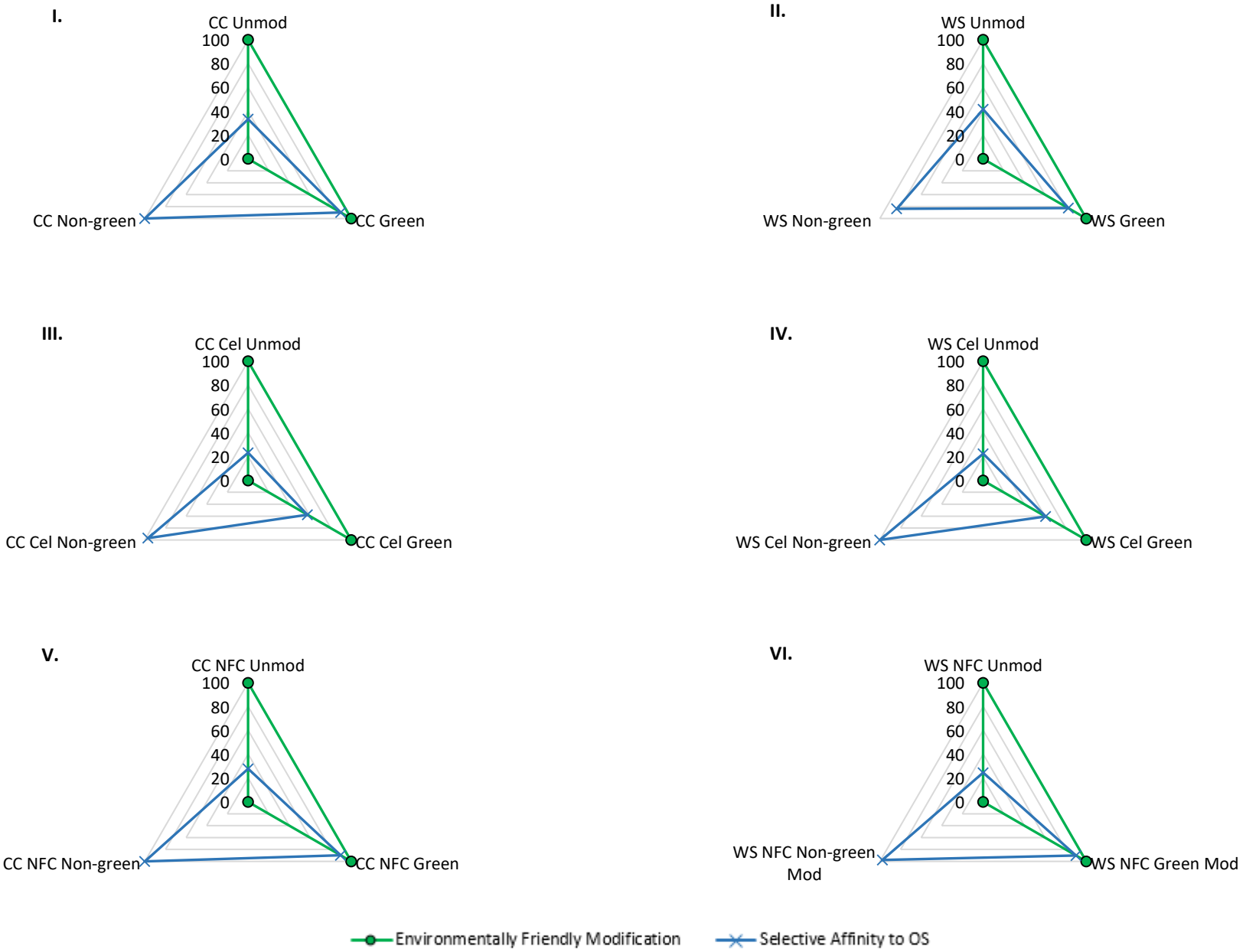

Figure H.1 The Radar Graphs of **I.** Corncob (CC) Biomass; **II.** Wheat Straw (WS) Biomass; **III.** CC Cellulose; **IV.** WS Cellulose; **V.** CC Nanofibrillated Cellulose (NFC), and **VI.** WS NFC

Figure H.1 III and IV were utilised to compare the modified and unmodified CC and WS cellulose films, and the summary of these ratings are displayed in Table H.3. The unmodified samples were classified as environmentally friendly, but lacked a selective affinity for OS. The *non-green* CC cellulose films showed a higher selective OS (20.39 ± 0.62 g/g) than the *green* (12.09 ± 0.45 g/g) and unmodified (4.88 ± 0.77 g/g) CC cellulose films. Additionally, the *non-green* WS films demonstrated higher OS (21.03 ± 1.69 g/g) than the *green* (12.77 ± 1.15 g/g) and unmodified (4.72 ± 0.43 g/g) WS cellulose films. Since an environmentally friendly modification is favoured above a non-environmentally friendly method, the *green* CC and WS films are classified as the best sorbents in the cellulose category.

Table H.3 Summary of Ratings Assigned to Modified and Unmodified Corncob and Wheat Straw Cellulose Films by Comparison of Radar Graphs

Source [a]	Sample	Environmentally Friendly Modification	Highest Selective Affinity towards OS [b]	Rating
CC Cellulose Films	Unmodified	✓	×	1/2
	***Green* Modified**	✓	×	**1/2**
	Non-green Modified	×	✓	1/2
WS Cellulose Films	Unmodified	✓	×	1/2
	***Green* Modified**	✓	×	**1/2**
	Non-green Modified	×	✓	1/2

a – Corncob is abbreviated as CC, while wheat straw is abbreviated as WS; **b –** OS represents Oil Sorption

Table H.4 Summary of Ratings Assigned to Modified and Unmodified Corncob and Wheat Straw Nanofibrillated Cellulose Aerogels by Comparison of Radar Graphs

Source [a, b]	Sample	Environmentally Friendly Modification	Highest Selective Affinity towards OS [c]	Rating
CC NFC Aerogels	Unmodified	✓	×	1/2
	***Green* Modified**	✓	✓	**2/2**
	Non-green Modified	×	✓	1/2
WS NFC Aerogels	Unmodified	✓	×	1/2
	***Green* Modified**	✓	✓	**2/2**
	Non-green Modified	×	✓	1/2

a – Corncob is abbreviated as CC, while wheat straw is abbreviated as WS; **b –** NFC represents nanofibrillated cellulose; **c –** OS represents Oil Sorption

Figure H.1 V and VI were utilised to compare the modified and unmodified CC and WS NFC, and the summary of these ratings are displayed in Table H.4. The OS accomplished by the *green* (41.48 ± 3.25 g/g) and *non-green* (46.23 ± 0.45 g/g) CC NFC aerogels were statistically comparable ($p = 0.18$). However, the modified samples attained improved selective OS when compared to the unmodified CC NFC aerogels (12.85 ± 0.93 g/g). Moreover, comparable OS ($p = 0.17$) values were attained by the *green* (41.60 ± 2.32 g/g) and *non-green* (45.12 ± 0.90 g/g) WS NFC aerogels. These magnitudes were higher than the OS (11.35 ± 0.95 g/g) achieved by the unmodified aerogels. Thee *green* CC and WS aerogels are classified as the best sorbents in the NFC category.

Table H.2, Table H.3 and Table H.4 were considered, and the modified samples with the highest ratings were selected within each category. These samples are compared in Figure H.2 and Table H.5 based on selective OS, environmentally friednliness and porosity.

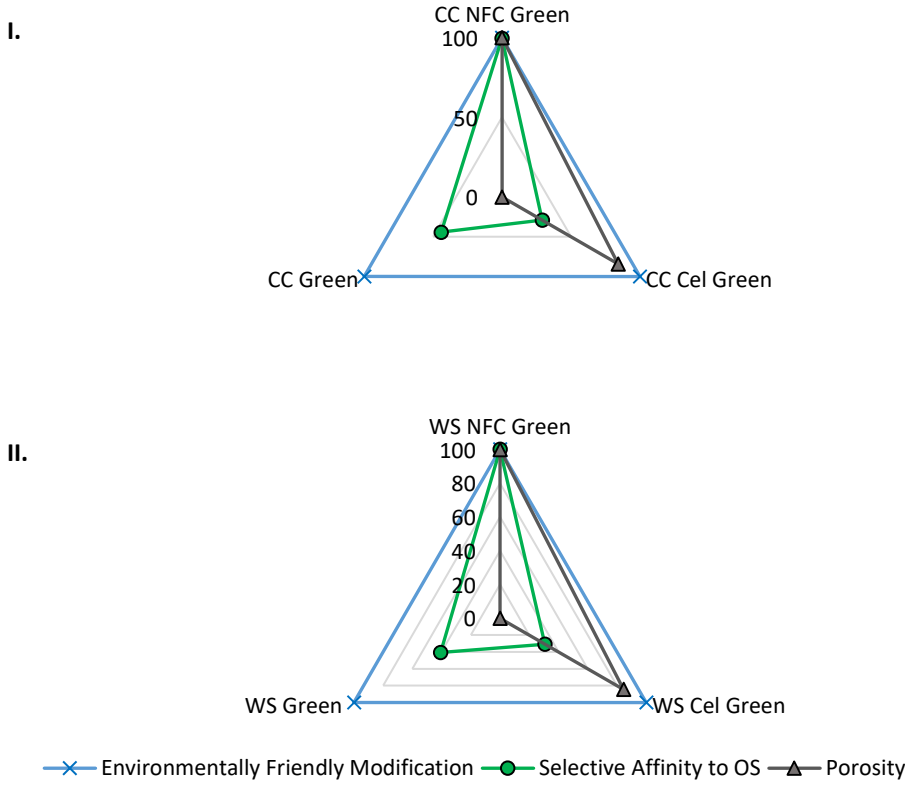

Figure H.2 The Radar Graphs of the Highest Rated Modified Samples on the *Biomass level*, *Cellulose (Cel) level* and *Nanofibrillated Cellulose (NFC) Level* for **I.** Corncob (CC) and **II.** Wheat Straw (WS)

Table H.5 Summary of Ratings Assigned to Highest Performing Modified Corncob and Wheat Straw Biomass, Cellulose Films and Nanofibrillated Cellulose Aerogels

Source [a, b]		Sample	Environmentally Friendly Modification	Highest Selective Affinity towards OS [c]	Highest Porosity	Lowest Bulk Densities	Rating
CC	*Biomass level*	*Green* CC Modified Biomass	✓	×	×	- [d]	1/4
	Cellulose level	*Green* CC Cellulose Film	✓	×	×	×	1/4
	NFC Level	***Green* CC NFC Aerogel**	✓	✓	✓	✓	**4/4**
WS	*Biomass level*	*Green* WS Modified Biomass	✓	×	×	- [d]	1/4
	Cellulose level	*Green* WS Cellulose Film	✓	×	×	×	1/4
	NFC Level	***Green* WS NFC Aerogel**	✓	✓	✓	✓	**4/4**

a – Corncob is abbreviated as CC, while wheat straw is abbreviated as WS; **b** – NFC represents nanofibrillated cellulose; **c** – OS represents Oil Sorption; **d** – Biomass bulk density not determined

The *green* CC biomass (Table H.2), *green* CC cellulose films (Table H.3) and *green* CC NFC aerogels (Table H.4) were selected for comparison in the CC category, while the *green* WS biomass (Table H.2), *non-green* WS cellulose films (Table H.3) and *green* WS NFC aerogels (Table H.4) were selected for comparison in the WS category. All these modificationwere based on the *green* chemistry pronciples, and were thus classified as environmentally friendly.

The CC and WS NFC aerogels demonstrated the highest porosities, lowest densities and highest selective oil sorptions (Table 7.1). The *green* CC and WS NFC aerogels were, therefore, selected as the optimal, lignocellulosic-based, environmentally friendly biosorbent for selective OS application in this study.

Appendix I – Potential Scale-up of Process

The following process description should be read in conjunction with the conceptual process flow diagrams (PFD), attached at the end of this discussion:

- PFD-001: Biomass Washing and Milling
- PFD-002: Reagent Mixing
- PFD-003: Cellulose Extraction – Part 1
- PFD-004: Cellulose Extraction – Part 2
- PFD-005: NFC Isolation and Modification
- Legend Sheet

I.1 Process Flow Diagram 001: Biomass Washing and Milling

A load of corncob (CC) or wheat straw (WS) is tipped onto a conveyor (CNV-001), which transports the biomass into a hopper (HOP-001). This hopper is manually transferred and tipped onto a second conveyor (CNV-002), which transmits the biomass onto a single deck vibrating screen (SCN-001). The screen is fitted with high-pressure nozzles for washing the biomass with potable water. The filtrate will consist of soiled water, which can potentially be recovered for purification and re-use. After washing has commenced, compressed air is implemented for drying the samples.

The washed and dried biomass is transported (CNV-003) to an industrial mill (MLL-001), where the particle size is reduced to a target of 200 – 425 µm. Size classification is established by the implementation of a double-deck screen (SCN-002). The oversize fraction (> 425 µm) is conveyed (CNV-004) to be re-ground (MLL-001), while the undersize fraction (< 200 µm) is stored on a stockpile for alternative usages, such as Research- and Development Studies. The biomass with the desired particle size of 200 – 425 µm commences to the Cellulose Extraction Plant (PFD-003).

I.2 Process Flow Diagram 002: Reagent Mixing

Five reagent mixing tanks are each fitted with the following instruments to successfully and safely create the necessary solutions: a temperature transmitter, a level transmitter and high-level switch, a rupture disk for safety in overpressure situations, and an agitator for mixing. Even though this is a PFD and not a piping- and instrumentation diagram (P&ID), these instruments are indicated for special mention. Valves and instruments will only be indicated when it is imperative for distinction in the explanation of the process.

The following reagents are created:

- Tank 1 (TNK-001): 2:1 (v/v) toluene-ethanol solution
- Tank 2 (TNK-002): 90 % (v/v) acetic acid solution
- Tank 3 (TNK-003): 5 % (w/w) sodium hydroxide solution
- Tank 4 (TNK-004): 32 % (v/v) sulfuric acid solution
- Tank 5 (TNK-005): 90 % (v/v) dimethyl sulphoxide solution

I.3 Process Flow Diagram 003: Cellulose Extraction – Part 1

The biomass with the desired particle size of 200 – 425 µm is conveyed (CNV-005) into an industrial Soxhlet extraction set-up (SOX-001), complete with a condenser, steam for heating and chilled water for cooling. The other details of the Soxhlet extraction device, such as instruments and mixing mechanisms, will be subject to the specific instrument procured and are not shown here.

The biomass is de-waxed with the toluene-ethanol (2:1, v/v) solution for 6 h (J. X. Sun et al., 2004). Hereafter it is filtered on a single deck screen (SCN-003) and washed with hot potable water until the filtrate attains a neutral pH (Chowdhury & Hamid, 2016). The filtrate, containing water, ethanol, toluene and wax, is pumped to a potential waste recovery plant.

The de-waxed biomass is transported (CNV-006) through a diverter chute (DIV-001) into the cellulose extraction vessel (EXT-001). This vessel has a condenser, steam for heating and chilled water for cooling. It is also fitted with a temperature transmitter, a level transmitter and high-level switch, a rupture disk, and an agitator. Phenolic- and hemicellulose hydrolysis is facilitated with the 90 % (v/v) acetic acid solution. The samples are refluxed at 120 °C for 2 h (Huntley et al., 2015). The product is then pumped back to the washing screen (SCN-003), washed until the filtrate achieves a neutral pH, and diverted (DIV-001) and conveyed (CNV-007) to the industrial autoclave (ATC-001) for delignification (PFD-004). The filtrate contains the phenolic components and hemicellulose, which can potentially be recovered.

I.4 Process Flow Diagram 004: Cellulose Extraction – Part 2

Delignification is accomplished by placing the biomass and the 5 % (w/w) aqueous NaOH-solution into the autoclave (ATC-001) with a 1:30 biomass to liquid ratio at 121 °C for 30 minutes (Rosa et al., 2012). The samples are allowed to cool for 1 hour, after which it is pumped to an industrial homogeniser (HOM-001). The details of the industrial autoclave and homogeniser, such as instruments and mixing mechanisms, will be subject to the instruments procured. These aspects are not shown here.

After homogenisation (HOM-001), the samples are diverted (DIV-002) to a single deck washing screen (SCN-004), where the retentate is washed with hot distilled water until the filtrate achieves a neutral pH. Drying is subsequently established with compressed air.

The dried biomass is diverted (DIV-003) to the settling tank (TNK-006), where acid hydrolyses is performed for 24 h with a 32 % (v/v) sulfuric acid solution (Huntley et al., 2015). The samples are then transferred back to the washing screen (SCN-004). The washing and drying steps are repeated, and cellulose is obtained.

The NFC isolation is initiated by dispersing the isolated cellulose at 5 % (w/w) in potable water in the industrial homogeniser (HOM-001). Pre-fibrillation is established, and the samples are diverted (DIV-002) to the NFC Isolation and Modification Plant (PFD-005).

I.5 Process Flow Diagram 005: NFC Isolation and Modification

The pre-fibrillated cellulose is added to the enzymatic hydrolyses tank (TNK-007). This tank is fitted with a steam jacket for heating and a chilled water jacket for cooling. Thereafter, 0.1 N HCl is added until a pH of 5 is reached. The tank is subsequently heated to 50 °C, and the FibreCare® is added through the manway. The solution is kept at 50 °C for 4 h. After 4 h, the temperature is raised to 100 °C for 15 minutes in order to stop the activity of the enzyme.

The hydrolysed sample is pumped to an industrial centrifuge (CEN-001). Centrifugation is completed, and the supernatant is drained. Hereafter, potable water is added to the sample and subsequent centrifugation is applied. NFC is consequently obtained.

The isolated NFC is pumped to an industrial homogeniser (HOM-002). A 0.5 % (w/v) NFC suspension is created in the homogeniser with the 90 % (v/v) dimethyl sulphoxide solution. The suspension is homogenised, settled for 24 h, and homogenised again. Moreover, the suspension is pumped to the NFC modification tank (TNK-008).

Lipase (724.4 U) is diluted in a 0.1 M phosphate buffer solution and manually added to the NFC-DMSO mixture in the NFC modification tank (TNK-008). Thereafter, the acetic anhydride is pumped into the tank. The mixture is heated to 28 °C for 48 h, after which the temperature is increased to 100 °C for 15 minutes in order to stop any residual enzyme activity. Cooling of the sample is established, and the solution is pumped to the centrifuge (CEN-001). Moreover, the washing steps are completed in the centrifuge with potable water, acetone and sodium dodecyl sulphate, respectively.

The acetylated NFC samples are dispersed at 0.25 % (w/w) in the mixing tank (TNK-009), mechanically poured into moulds (MLD-001) and pre-freezed at -80 °C (ULF-001). Lastly, the hydrogels are freeze-dried (FD-001), and hydrophobic aerogels are obtained.

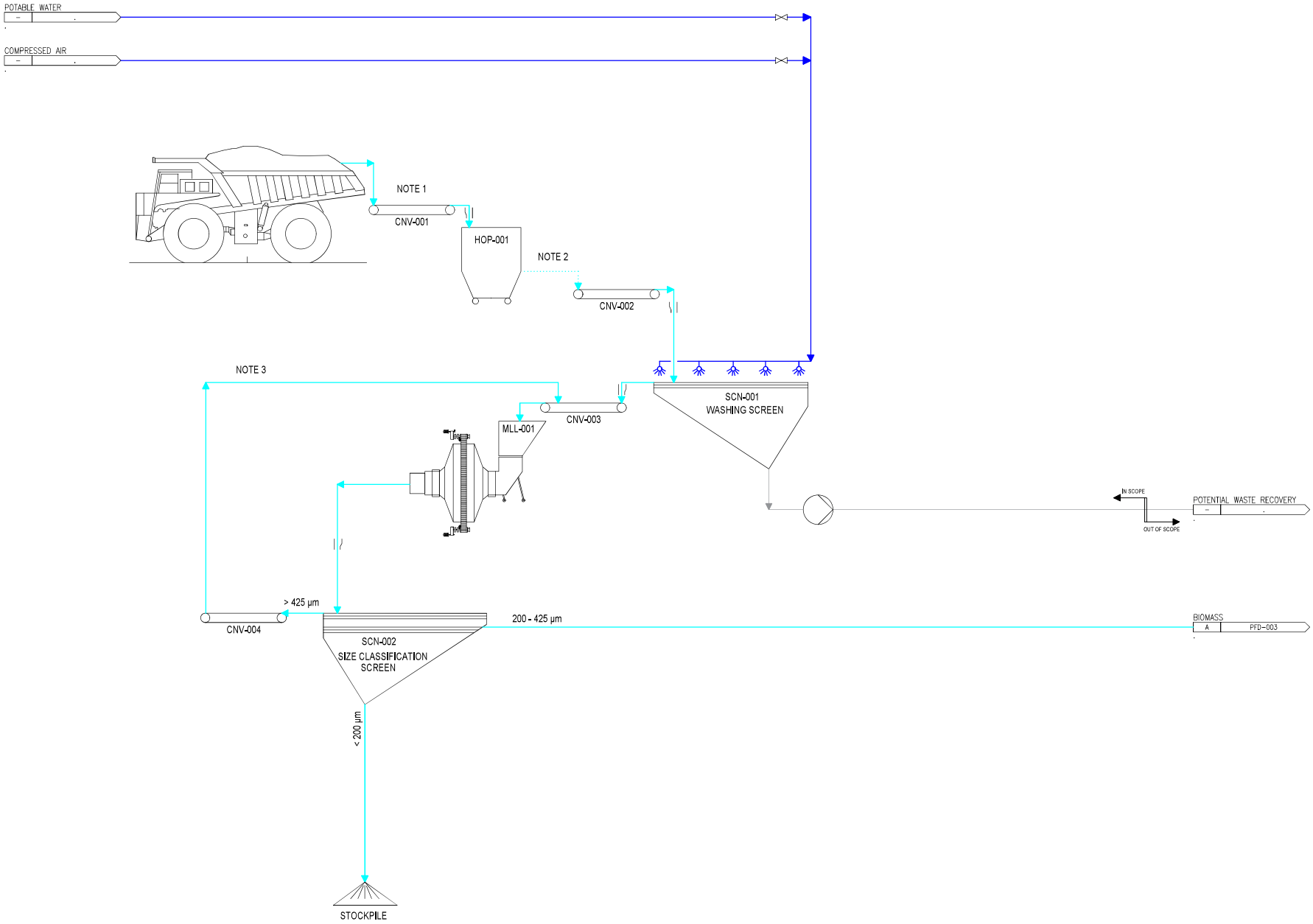

NOTES

1. A LOAD OF CORNCOB OR WHEAT STRAW IS TIPPED ONTO A CONVEYOR (CNV-001), WHICH TRANSPORTS THE BIOMASS INTO A HOPPER (HOP-001)
2. THE HOPPER IS MANUALLY TRANSFERRED AND TIPPED ONTO A SECOND CONVEYOR (CNV-002), WHICH TRANSMITS THE BIOMASS ONTO A SINGLE DECK VIBRATING SCREEN (SCN-001)
3. THE OVERSIZE FRACTION (> 425 µM) IS CONVEYED (CNV-004) TO BE RE-GROUND (MLL-001)

REV	DESCRIPTION	DRAWN	CHKD	ISSUED
00	FIRST REVISION	MS	-	-

REVISIONS

DRG No	TITLE

REFERENCE DRAWINGS

THE DEVELOPMENT OF NFC BIOSORBENTS

TITLE:

BIOMASS WASHING AND MILLING

SCALE:	DATE:	STATUS:
NTS @ A1	2020	CONCEPTUAL

DRG No.	REV.
PFD-001	00

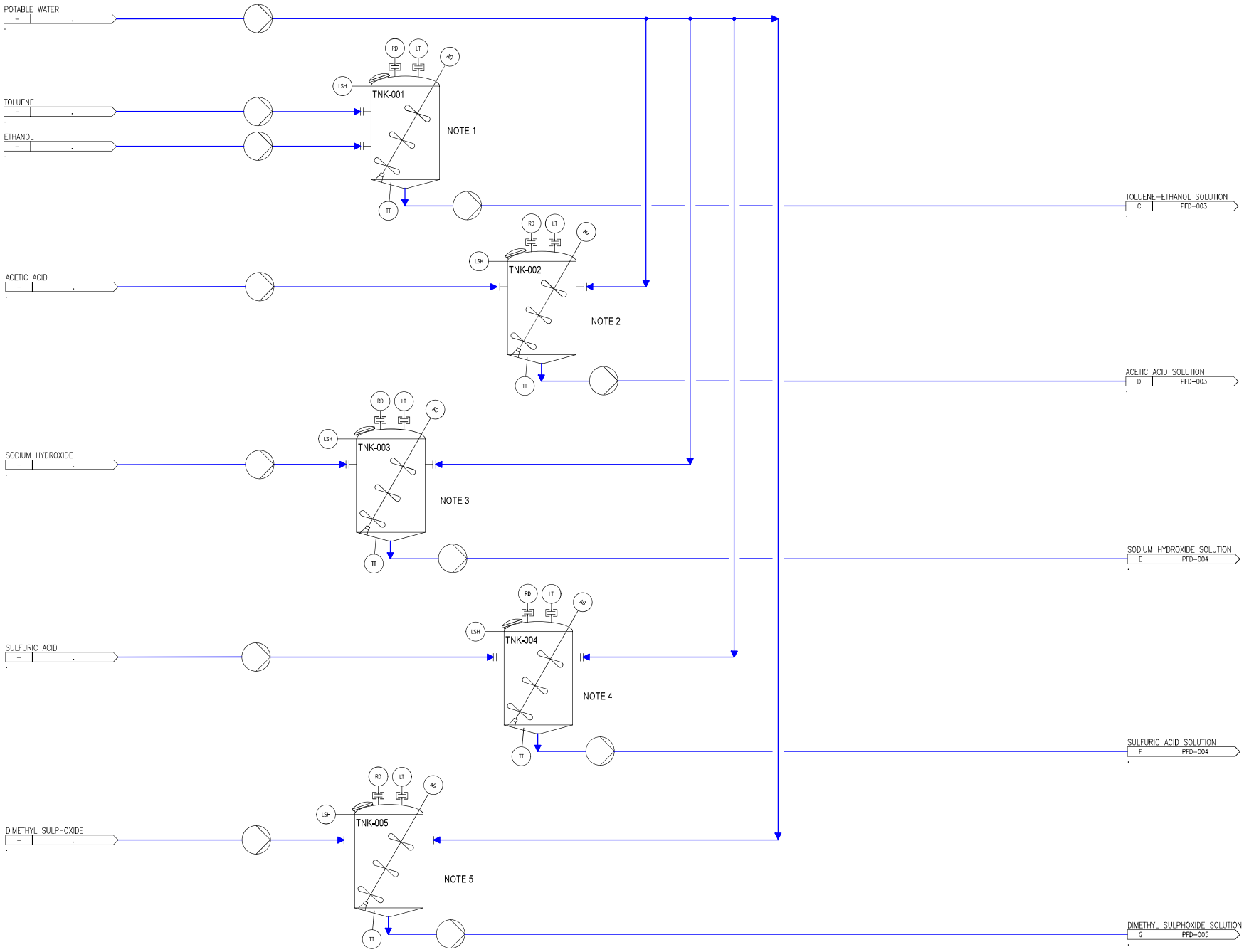

NOTES

1. 2:1 (V/V) TOLUENE-ETHANOL SOLUTION
2. 90 % (V/V) ACETIC ACID SOLUTION
3. 5 % (W/W) SODIUM HYDROXIDE SOLUTION
4. 32 % (V/V) SULFURIC ACID SOLUTION
5. 90 % (V/V) DIMETHYL SULPHOXIDE SOLUTION

REV	DESCRIPTION	DRAWN	CHKD	ISSUED
00	FIRST REVISION	MS	-	-

REVISIONS

DRG No	TITLE

REFERENCE DRAWINGS

THE DEVELOPMENT OF NFC BIOSORBENTS

TITLE:

REAGENT MIXING

SCALE:	DATE:	STATUS:
NTS @ A1	2020	CONCEPTUAL

DRG. No.	REV.
PFD-002	00

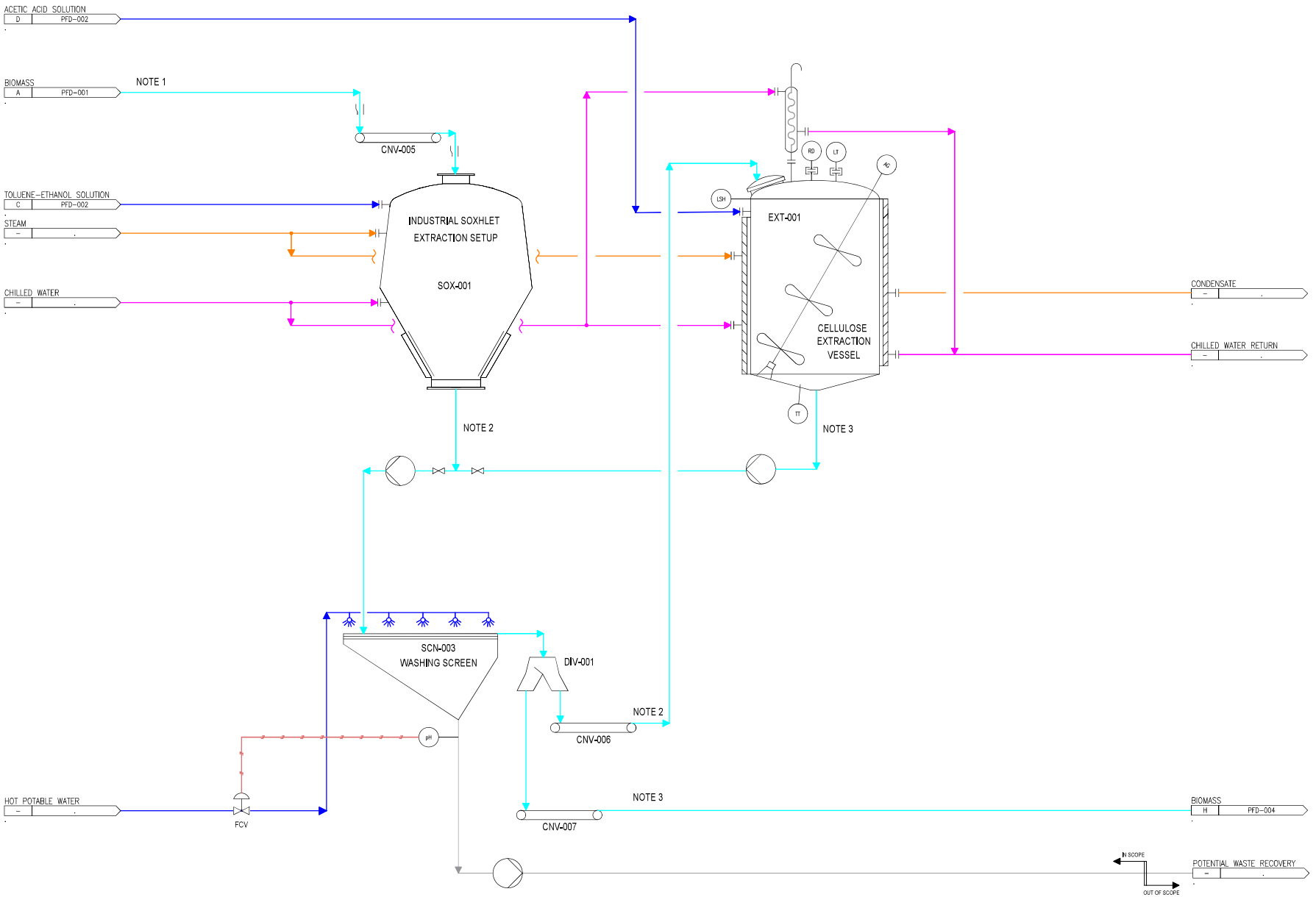

NOTES

1. BIOMASS WITH THE DESIRED PARTICLE SIZE OF 200 - 425 µM
2. DE-WAXED BIOMASS
3. BIOMASS THAT HAD UNDERDONE PHENOLIC- AND HEMICELLULOSE HYDROLYSIS

REV	DESCRIPTION	DRAWN	CHKD	ISSUED
00	FIRST REVISION	MS	-	-

REVISIONS

DRG No	TITLE

REFERENCE DRAWINGS

THE DEVELOPMENT OF NFC BIOSORBENTS

TITLE:

CELLULOSE EXTRACTION - PART 1

SCALE:	DATE:	STATUS:
NTS @ A1	2020	CONCEPTUAL

DRG. No.	REV.
PFD-003	00

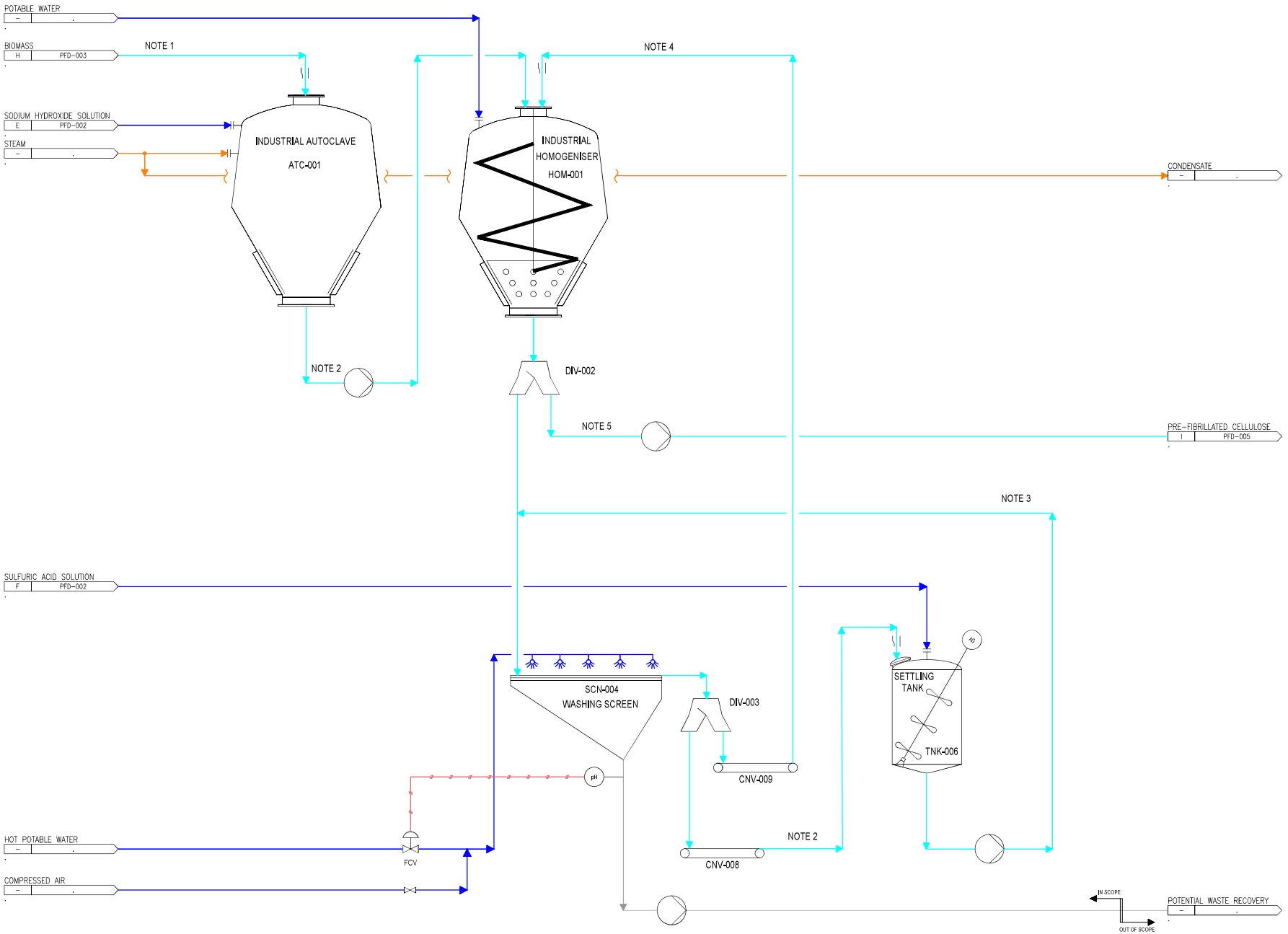

NOTES

1. BIOMASS THAT HAD UNDERDONE PHENOLIC- AND HEMICELLULOSE HYDROLYSIS
2. DELIGNIFIED BIOMASS
3. SOLUTION CONTAINING SEPARATED CELLULOSE, HEMICELLULOSE AND LIGNIN WHICH NEEDS TO BE FILTERED AND WASHED TO OBTAIN THE CELLULOSE (THE SOLID PHASE)
4. CELLULOSE
5. PRE-FIBRILLATED CELLULOSE

REV	DESCRIPTION	DRAWN	CHKD	ISSUED
00	FIRST REVISION	MS	-	-

REVISIONS

DRG No	TITLE

REFERENCE DRAWINGS

THE DEVELOPMENT OF NFC BIOSORBENTS

TITLE: CELLULOSE EXTRACTION - PART 2

SCALE:	DATE:	STATUS:
NTS @ A1	2020	CONCEPTUAL

DRG. No. PFD-004 REV. 00

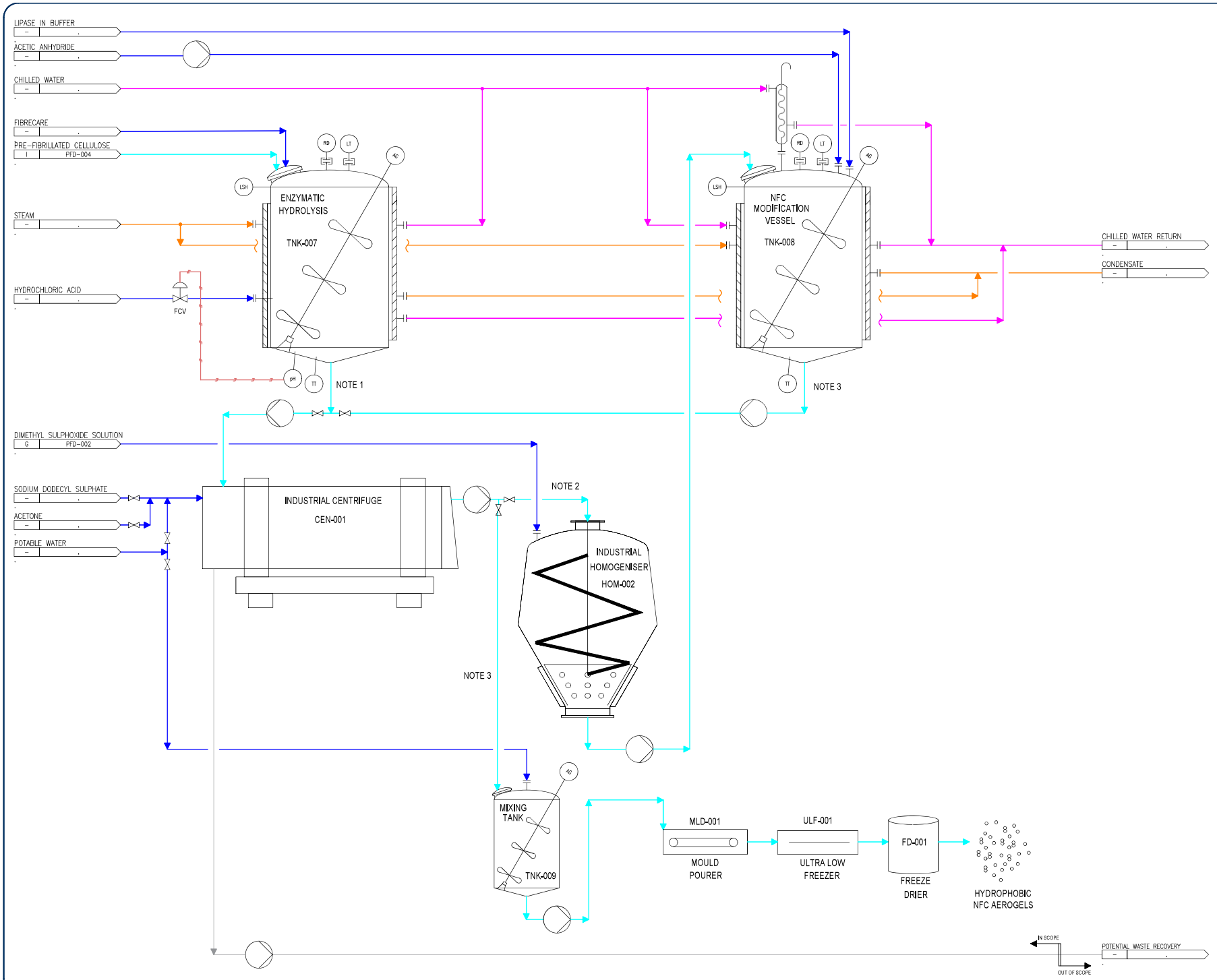

NOTES

1. ENZYMATIC HYDROLYSES WAS APPLIED TO DISRUPT THE INTRAMOLECULAR BONDS IN THE CELLULOSE CHAINS, THEREBY CREATING NFC (WHICH NFC NEEDS TO BE FILTERED BY THE SUBSEQUENT STEPS)
2. ISOLATED NFC
3. ACETYLATED NFC

REV	DESCRIPTION	DRAWN	CHKD	ISSUED
00	FIRST REVISION	MS	-	-

REVISIONS

DRG No	TITLE

REFERENCE DRAWINGS

THE DEVELOPMENT OF NFC BIOSORBENTS

TITLE:

NFC ISOLATION AND MODIFICATION

SCALE:	DATE:	STATUS:
NTS @ A1	2020	CONCEPTUAL

DRG. No.	REV.
PFD-005	00

TRK = TRUCK

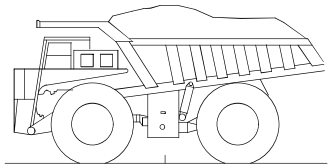

EXT = EXTRACTION VESSEL

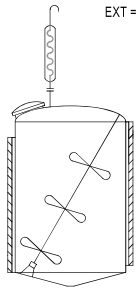

FD = FREEZE DRIER

DIV = DIVERTER CHUTE

FCV = FLOW CONTROL VALVE

MLL = MILL

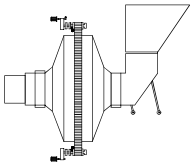

TNK = TANK

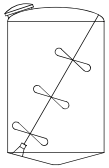

CNV = CONVEYOR

HYDROPHOBIC NFC AEROGELS

LT = LEVEL TRANSMITTER

SCN = SCREEN

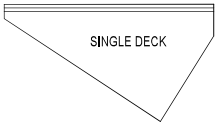

HOM = HOMOGENISER

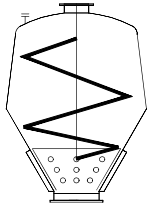

PMP = PUMP

CHT = CHUTE

RD = RUPTURE DISK

SCN = SCREEN

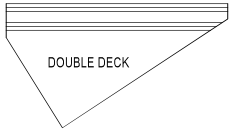

ATC = AUTOCLAVE

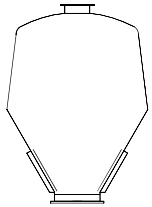

MLD = MOULD POURER

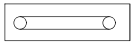

pH = pH PROBE

AG = AGITATOR

CEN = CENTRIFUGE

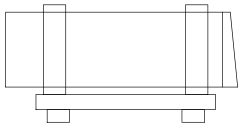

HOP = HOPPER

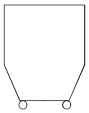

ULF = ULTRA LOW FREEZER

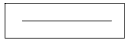

LSH = LEVEL SWITCH HIGH

TT = TEMPERATURE TRANSMITTER

NOTES

REV	DESCRIPTION	DRAWN	CHKD	ISSUED
00	FIRST REVISION	MS	-	-

REVISIONS

DRG No	TITLE

REFERENCE DRAWINGS

THE DEVELOPMENT OF NFC BIOSORBENTS

TITLE:

LEGEND SHEET

SCALE:	DATE:	STATUS:
NTS @ A1	2020	CONCEPTUAL

DRG. No.	REV.
-	00